Exploring Chirality of Unnatural Amino Acids and Peptides on Water Sorption and *Stratum Corneum* Uptake

PhD in Pharmacy

School of Chemistry, Food and Pharmacy

Ermelinda Cidália Silva Pereira

January 2019

DECLARATION

I confirm that this is my own work and the use of all material from other sources has been properly and fully acknowledged.

To my Father and my Brother

ABSTRACT

Skin is the largest organ in the human body and acts as a protective barrier against exterior chemical and pathogenic agents. Because of the large surface area and easy accessibility, drug delivery through skin has numerous potential applications. The *stratum corneum*, SC (the outermost layer of the skin), forms the main barrier to diffusion of permeants through the skin; circumventing this barrier is challenging and it is difficult to deliver "large" molecules such as proteins and peptides across the skin. The physicochemical properties of a permeant affect its transport into and through the skin and well characterised diffusional determinants include the octanol/water partition coefficient, molecular weight, solubility and hydrogen bonding groups of a drug. Less well understood is the role of chirality. The enantioselectivity of the skin during epidermal permeation has been poorly researched with few investigations focussing on the effect of drug chirality.

In this project, three libraries of unnatural amino acids were synthesised in their racemic and enantiomerically pure forms; a saturated series, an unsaturated series and a hydroxylated series of β-amino acids. The monomers were assembled into peptides of different dimensions, specifically dimers, tetramers and in some cases hexamers and octamers. This library was used to probe and seek to understand the effects of increasing molecular weight and chirality on permeant uptake into *stratum corneum* membranes. In addition, the ability of these materials to hold water, and so act as potential moisturising agents in dry skin conditions was explored.

To meet these objectives, the physical properties of these materials were measured and assessed ranging from analytical characterisation (Nuclear Magnetic Resonance - NMR, Mass Spectrometry - MS, Infra-Red - IR) to water uptake assays (Thermal Gravimeric Analysis - TGA, Dynamic Sorption Vapou - DVS). The materials tended to form intramolecular hydrogen bonds as the peptide length increased. Thus, their foldameric structures were also explored using circular dichroism and for some materials with unusual properties X-ray diffraction was performed. Selected compounds were applied to isolated sheets of stratum corneum to assess their uptake. The influence of chirality, molecular weight, chemical composition (saturated, unsaturated and hydroxylated), water holding capacity and secondary structure on the uptake of the material into the tissue were explored and the results illustrated that complex relationships existed between structure and uptake but chiral selectivity of drug uptake into the *stratum corneum* was demonstrated.

ACKNOWLEDGMENTS

TABLE OF CONTENTS

Chapter 1

Chapter 2

Chapter 3

Chapter 4

Chapter 7

LIST OF FIGURES

LIST OF TABLES

LIST OF ABBREVIATIONS AND ACRONYMS

^{13}C NMR	Carbon 13 Nuclear Magnetic Resonance
^{1}H NMR	Proton Nuclear Magnetic Resonance
δ	Chemical Shift
ε	Ellipticity
μg	Microgram
μL	Microliter
N_w	Number of Waters
AHA	α-Hydroxy-Acids
Au	Absorbance units
BnOH	Benzyl Alcohol
Boc$_2$O	Di-*tert*-butyl-dicarbonate
br.s	Broad singlet
c	Concentration
CC	Column Chromatography
CD	Circular Dichroism
CLE	Corneocyte Lipid Envelope
cm	Centimetre
COSY	Correlation Spectroscopy
CPD	Cyclopentadiene
CPP	Cell Penetrating Peptide
CSI	Chlorosulfonyl Isocyanate
d	Doublet

D/A	Donor/Acceptor
Da	Dalton
DCC	Dicyclohexylcarbodiimide
DCDH	Dimer *Cis* Down Hydroxylated
DCDS	Dimer *Cis* Down Saturated
DCDU	Dimer *Cis* Down Unsaturated
DCM	Dichloromethane
DCU	Dicyclohexylurea
DCUH	Dimer *Cis* Up Hydroxylated
DCUS	Dimer *Cis* Up Saturated
DCUU	Dimer *Cis* Up Unsaturated
dd	Doublet of doublets
ddd	Doublet of doublet of doublets
dddd	Doublet of doublet of doublet of doublets
DIPEA	*N*,*N*-Diisopropylethylamine
dm	Decimetre
DMAP	4-(Dimethylamino)Pyridine
DMF	Dimethyl Formamide
DMH	Dimer Mixture Hydroxylated
DMS	Dimer Mixture Saturated
DMSO	Dimethyl Sulfoxide
DMU	Dimer Mixture Unsaturated
dt	Doublet of triplets
DVS	Dynamic Vapour Sorption

ee	Enantiomeric Excess
EIC	Extracted Ion Chromatogram
ESI	Electrospray Ionisation
Et$_2$O	Diethyl Ether
EtOAc	Ethyl Acetate
EtOH	Ethanol
FAA	Free Amino Acids
FDA	Food and Drug Administration
g	Gram
GFP	Green Fluorescent Protein
Gly	Glycine
h	Hour
HCDH	Hexamer *Cis* Down Hydroxylated
HCUH	Hexamer *Cis* Up Hydroxylated
HCUS	Hexamer *Cis* Up Saturated
HMBC	Heteronuclear Multiple-Bond Correlation Spectroscopy
HPLC	High Performance Liquid Chromatography
HRMS	High resolution mass spectroscopy
HSQC	Heteronuclear Single-Quantum Correlation Spectroscopy
Im	Imidazole
IR	Infrared
J	Coupling constant
K	Kelvin
KDa	Kilo Dalton

K_{scw}	Partition coefficient between *stratum corneum* and water
L	Litre
L-Ala	L-Alanine
LC	Liquid Chromatography
LOD	Limit of Detection
LOQ	Limit of Quantification
M	Molar
m	Multiplet
MCDH	Monomer *cis* Down Hydroxylated
MCDS	Monomer *cis* Down Saturated
MCDU	Monomer *cis* Down Unsaturated
MCUH	Monomer *cis* Up Hydroxylated
MCUS	Monomer *cis* Up Saturated
MCUU	Monomer *cis* Up Unsaturated
MeOH	Methanol
mg	Milligram
min	Minute
mL	Millilitre
MMH	Monomer Mixture Hydroxylated
MMS	Monomer Mixture Saturated
MMU	Monomer Mixture Unsaturated
mol	Mole
MS	Mass Spectrometry
MTBE	*tert*-Butyl Methyl Ether

Mw	Molecular Weight
n_c	Number of moles of compound
ng	Nanogram
nm	Nanometre
NMF	Natural Moisturising Factor
NMO	4-Methylmorpholine *N*-Oxide
NMR	Nuclear Magnetic Resonance
NOESY	Nuclear Overhauser Effect Spectroscopy
n_w	Number of moles of water
ºC	Degrees Centigrade
OCUS	Octamer *cis* Up Saturated
PCA	Pyrrolidone Carboxylic Acid
Pd/C	Palladium on Carbon
PMBCl	*p*-Methoxybenzyl Chloride
ppm	Part Per Million
PyBop	Benzotriazol-1-yl-oxytripyrrolidinophosphonium hexafluorophosphate
q	Quartet
r.t	Room Temperature
R_f	Retention Factor
R_t	Retention Time
S	Solubility
s	Singlet
SAR	Structure/Activity Relationship
S_{asc}	Uptake of the analyte into the *stratum corneum*

SC	*Stratum Corneum*
SD	Standard Deviation
SPP	Skin Penetrating Peptide
T	Temperature
t	Triplet
TBSCl	*tert*-Butyldimethylsilyl Chloride
TCDH	Tetramer *cis* Down Hydroxylated
TCDS	Tetramer *cis* Down Saturated
TCDU	Tetramer *cis* Down Unsaturated
TCUH	Tetramer *cis* Up Hydroxylated
TCUS	Tetramer *cis* Up Saturated
TCUU	Tetramer *cis* Up Unsaturated
td	Triplet of doublets
TDD	Transdermal Drug Delivery
TFA	Trifluoro Acetic Acid
TGA	Thermal Gravimetric Analysis
TIPDSiCl$_2$	1,3-Dichloro-1,1,3,3-tetraisopropylsiloxane
TLC	Thin Layer Chromatography
TMH	Tetramer Mixture Hydroxylated
TMS	Tetramer Mixture Saturated
TMU	Tetramer Mixture Unsaturated
TNBSA	2,4,6-Trinitrobenzene Sulfonic Acid
UFH	Unfractioned Heparin
UV	Ultra Violet

v/v   Volume per Volume

VT NMR   Variable Temperature Nuclear Magnetic Resonance

w/v   Weight per Volume

CHAPTER 1

1. INTRODUCTION

Human skin is an impressive physical, immunological, and sensory barrier to the surrounding environment. It has long been used as a portal for drug delivery and it is a formidable barrier that usually requires appropriate technology for successful delivery. It is also a heterogeneous organ, with several delivery routes and sites that could be targeted for desirable pharmacological and immune responses. While the skin acts as a barrier, it is not a complete barrier. Many chemicals do penetrate the skin, either intentionally or unintentionally, and cutaneous metabolism does occur. Because of its large surface area, the skin may be a major route of entry into the body for drug administration. This may require the design of a specific chemical or physical delivery system to enhance the permeation of an active substance. In this chapter, a brief overview of the structure and function of the skin is presented along with aspects regarding physical chemistry and drug delivery that are of relevance to the present study.

1.1 SKIN STRUCTURE AND FUNCTION

Skin is a tegument that wraps human tissues, organs and fluids. Its thickness, colour, presence of hair, glands and nails varies depending on the body region. Despite these variations, all types of skin possess the same basic structure. It is the largest organ in the human body and provides a sturdy, flexible and self-repairing barrier to the exterior environment, protecting the internal organs and fluids from external influences. It prevents loss of endogenous water (humans are approximately 70% water) and nutrients, and protects against many unwanted toxic substances and pathogenic

microorganisms. The skin also responds to mechanical forces (elasticity and cushioning). It is organized in three distinct layers[1] (Figure 1.1): the epidermis, the dermis and the hypodermis. The external surface, epidermis, is stratified and its thickness varies depending on function and hydration. Thicker skin is mainly found in palmar areas such as hands and feet, where mechanical resistance is needed.
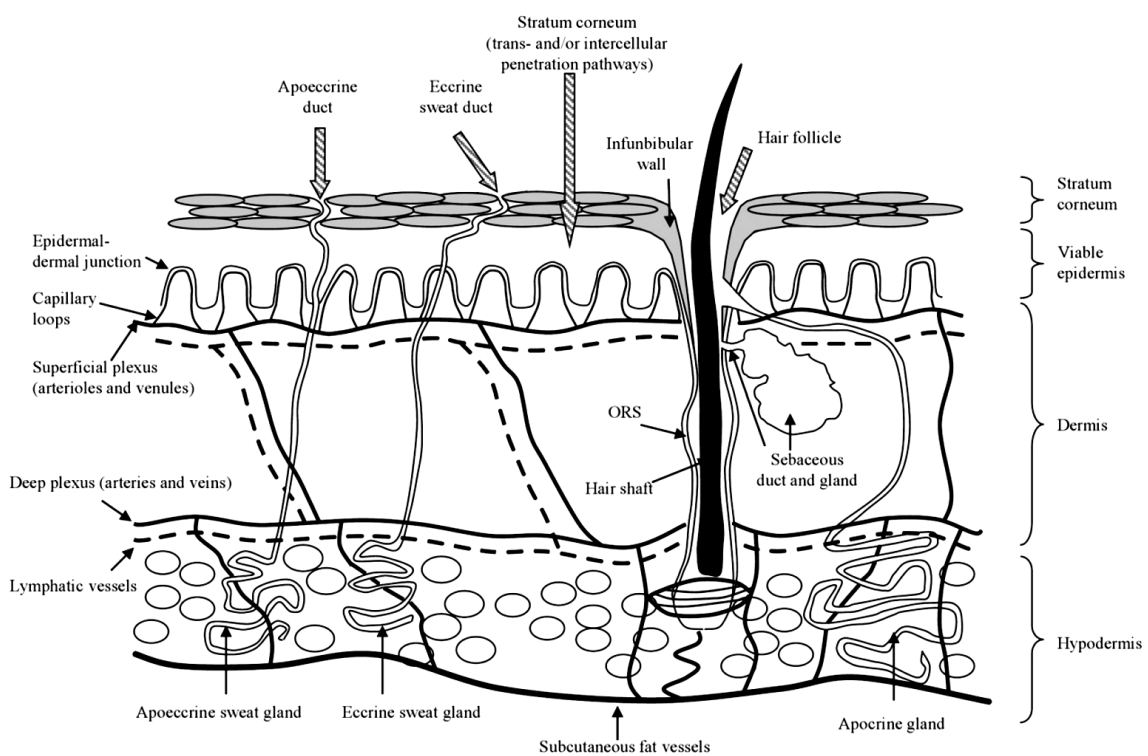
Figure 1.1 Schematic overview of the skin layers, appendages, blood and lymphatic vessels.[1]

1.1.1 HYPODERMIS

The hypodermis, or subcutaneous fat tissue, is the superficial membrane of the macroscopic anatomy of the skin from the inside to the outside. It is a relatively thick

layer (millimetre magnitude) in most areas but it is not present at all body sites (e.g., absent in the eyelids).[2] Its limits are difficult to define because it merges with the dermis and its principal function is to insulate the body and protect it against physical shock. Its adipose tissue is an important energy reservoir, mainly as triglycerides.

1.1.2 DERMIS

The dermis, or *corium*, composed of connective tissues as collagen fibrils, elastic tissue and a few reticular fibres; is the largest of the layers. It supports blood and lymphatic vessels, nerve endings, hair follicles and sebaceous and sweat glands. The vascular system and sweat glands are essential for the body's thermoregulation; skin's resting blood flow increases in response to an increase in temperature gradient between skin and core temperatures, caused by water elimination through sweat glands. The vasculature is also important for wound repair and removal of toxins; small molecules are removed from near the dermo-epidermal layer. The lymphatic flow has been shown to have an influence in the clearance of molecules with higher molecular weights.[3] Typically 3-5 mm thick, the dermis provides nutritional support for the avascular epidermis and comprises a fibrous protein matrix, mainly collagen, elastin, and reticulum, embedded in an amorphous colloidal polysaccharide gel. The physical behaviour of the dermis, including elasticity and support, is determined by the fibre bundles and the colloidal gel. The dermis provides flexibility with strength, serves as a barrier to infection, and functions as a water storage organ.[4]

1.1.3 EPIDERMIS

The epidermis is divided into two strata, the non-viable epidermis (*stratum corneum*, SC) and the viable epidermis. The viable epidermis is itself, a stratified layer (Figure 1.2) and its thickness varies from around 0.06 mm on the eyelids to around 0.8 mm on the palms of the hands and soles of the feet.[2] The epidermis of the soles and palms is thicker even in the embryo, the more prominent curvature lines are recognisable in twelve week old human embryo.[5] Over a period of 2-3 weeks, the SC is regenerated by keratinised cells that migrate from the *stratum basale*.

a)   b)
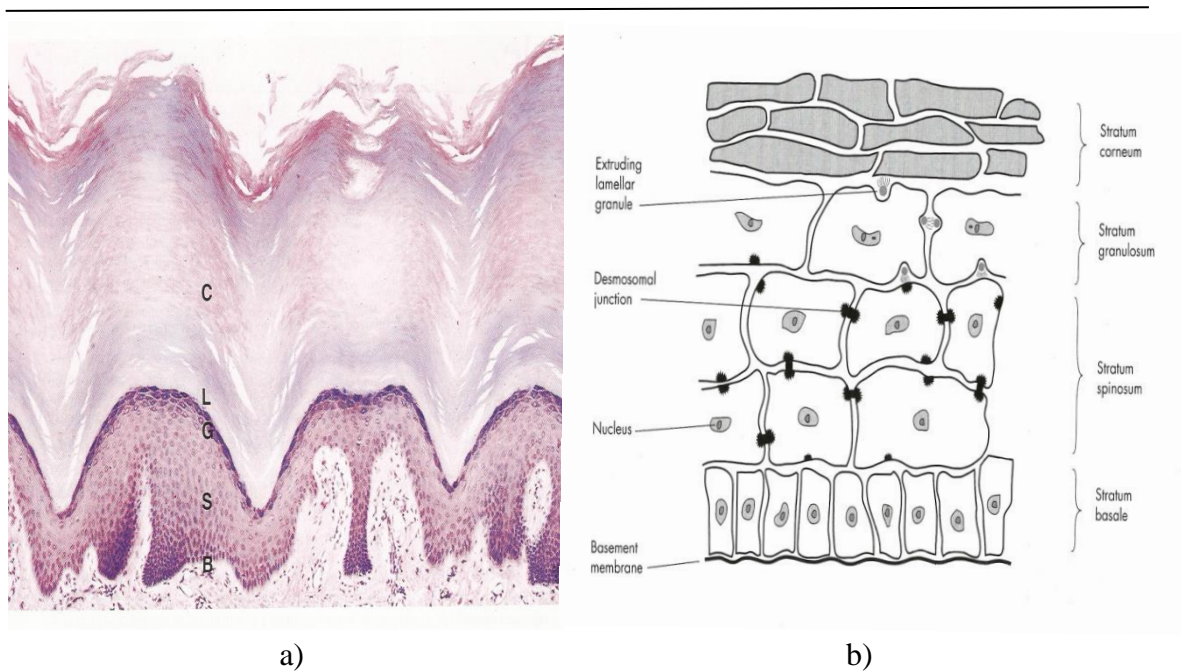
Figure 1.2 a) Histological preparation of human epidermis,[6] stratum corneum (C), *stratum lucidum* (L), *stratum granulosum* (G), *stratum spinosum* (S), *stratum basale* (B). b) Schematic representation of human epidermal cell differentiation.[2]

1.1.3.1 *Stratum Basale*

Also identified as *stratum germinativum* or, more commonly, the basal layer, its cells are similar to those of other tissues in the human body. The cells in the basal layer are cubic and form a unique layer separated from the dermis by a very thin membrane (basement membrane) by hemidesmosomes (involving one cytoplasmic plaque). Within the *stratum basale* and the *stratum spinosum* there are keratinocytes linked through desmosomes (involving two cytoplasmic plaques). Keratinocytes are the only cells within the epidermis that can divide *via* mitosis. After replication, one of the cells migrates towards the skin surface and the other remains in the basal layer; the cellular division happens, on average, once every 200 to 400 h.[2] The *stratum basale* also contains other specialised cell types such as melanocytes; these synthesise the pigment melanin (eumelanin and phaeomelanin – less common) from tyrosine *via* tyrosine hydroxylase enzymatic activity. The ratio between keratinocytes and melanocytes varies from 5:1 to 20:1 according to body site and it appears that melanocytes presence is light exposure inducible.[2] Melanin absorbs ultra violet (UV) radiation and is a free-radical scavenger. Melanocytes are in contact with keratinocytes by dendritic connections as well as the Langerhans cells, also found within the *stratum basale*. Langerhans cells derive from bone marrow and take up and process microbial antigens, they play an important role in some skin conditions. Merkel cells are also found in the basal layer, these cells are related to nerve endings having a role in cutaneous sensation and are found in large number in the lips and fingertips.

1.1.3.2 *Stratum Spinosum*

The *stratum spinosum* together with the *stratum basale* are often termed the Malpighian layer. The spinous cells from this layer are relatively large keratinocytes that change morphology from columnar to polygonal.[2] The keratinocytes are also connected to adjacent cells by desmosomes derived from the condensation of the synthetic product of cellular differentiation (keratins). Keratins agglomerate to form tonofilaments, these are also found, in small number, in the cells of the *stratum basale*.

1.1.3.3 *Stratum Granulosum*

The *stratum granulosum* (or granular layer) is the last layer of the viable epidermis. Its name is related to the fact that cells are characterised by numerous dense cytoplasmic granules. The chemical nature of these keratohyalin granules is distinct from that of the tonofilaments. It is believed that the keratinisation process involves a combination of tonofilaments and keratohyalin to form the mature keratin complex.[6] It is at the granular layer that the terminal cell differentiation process starts and cells undergo a number of structural and composition changes. The keratinocytes lose their organelles *via* enzymatic degradation and become corneocytes – chemical and physical resistant cells.[7] Membrane-coating granules are also synthesised in the Golgi complex (an organelle found in eukaryotic cells) and they contain the responsible precursors for the intercellular lipid lamellae found in the *stratum corneum*.[2] These granules are extruded into the intercellular spaces as they approach the *stratum lucidum*. The *stratum lucidum* is a transition layer between the *stratum granulosum* and the *stratum corneum*, well observed in thicker skin (as in palms and soles). Some dermatologists disagree on the

real existence of this layer claiming that it could be a tissue preparation artefact and thus, is often described as part of the *stratum corneum*.

1.1.3.4 *Stratum Corneum*

The *stratum corneum*, the outermost layer of the skin, is the result of the dynamic cell differentiation migrating process from the *stratum basale* to the upper *stratum granulosum*, a journey that takes approximately 14 days.[2] It is composed of dead, keratin-rich cells (corneocytes) embedded in a complex intercellular lipid mixture, particularly rich in ceramides, fatty acids, cholesterol and cholesterol sulphate, organised in bilayer arrays. The barrier function of the mammalian skin is mainly due to the SC, which is also responsible for the poor penetration of drugs into the skin.[8] It contains no blood vessels and therefore diffusion is the physical process that governs molecule transport into and out of the human body.[9] The SC has the ability to swell from a thickness of 10-15 μm (when dry)[10,11] up to a thickness of about 40 μm (when hydrated).[12] Though it is an epidermal layer, about 50 years ago the SC was not considered to be important in the permeability barrier;[13] nowadays it is often studied as a separate membrane in topical and transdermal drug delivery. It is often represented as a "brick and mortar" model (Figure 1.3), its keratinocytes are polygonal, elongated and relatively flat, approximately 0.2 to 1.5 μm thick with a diameter of 34 to 46 μm.[2]
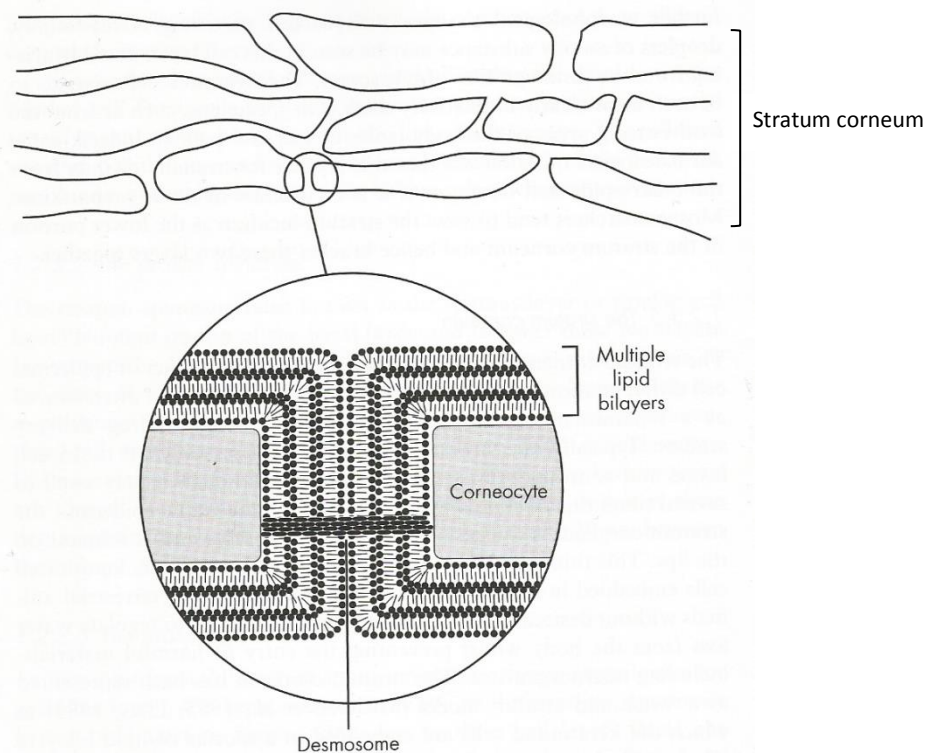
Figure 1.3 A representation of the "brick and mortar" model of human *stratum corneum*.[2]

At the deeper side of this layer, the cornified cells maintain desmosomic connections and intracellular keratin possesses an ordered pattern. Near the surface, the desmosomes and internal structure of the cells are destroyed in a process leading to desquamation. Together, this organised structure provides mechanical resistance and insulation to prevent water loss from the body. This barrier nature is due to its constituents, 75-80% is protein of which, about 70% is α-keratin and 10% is β-keratin and a proteinaceous cell envelope.[2] Corneocytes are surrounded by a monolayer of ω-OH-ceramides that form the corneocyte lipid envelope (CLE).[14] The cell envelope is a thick layer ($\cong$ 10nm) of highly cross-linked ceramides and fatty acids covalently bound to glutamate residues in the involucrum of the corneocytes. The CLE role in the SC barrier function can be

9

viewed as a scaffold for the organisation of the extracellular lamellar bilayers which are a mixture of the lipid matrix, fatty acids, cholesterol and cholesterol sulphate. Exhaustive lipid solvent extractions induce the collapse of the corneocytes and so the CLE has also been suggested to contribute to the cohesion of the SC.[14] Finally, the CLE can also function as a semi-permeable membrane that can allow the passage of water while restricting the loss of larger hygroscopic molecules, such as filaggrin (<u>fil</u>ament <u>aggr</u>egation prote<u>in</u>) breakdown products (smaller peptides and free amino acids), out of the corneocyte. Filaggrin is a crucial component of the keratinocyte mesh in the outer layer of epidermis; it helps keratin filaments to aggregate and it is synthesised initially as profilaggrin, an approximately 500 KDa highly phosphorylated, histidine-rich polypeptide.[15]

1.1.4 NATURAL MOISTURISING FACTOR

The SC barrier is continually disturbed by both external forces (UV, low relative humidity (RH), cold temperatures, and surfactants), and internal factors (cutaneous disease, psychological stress, and diabetic complications) which can lead to conditions such as dry skin and decreased performance of the barrier. In order to maintain its flexibility, integrity, and critical catabolic activity the SC must remain hydrated, and in healthy skin the tissue contains greater than 10% water. In the absence of water, the SC is an intrinsically fragile structure, which readily becomes cracked, brittle and rigid. Water plays a key role in maintaining the SC barrier integrity. This water would easily evaporate without the presence of inherent skin moisturising agents, leaving the skin dry and tight. Water supply from the innermost skin layers and normal sweating maintain the skin moisture level which mediates the activity of some hydrolytic enzymes, for

example those involved in the degradation of filaggrin that generate the Natural Moisturising Factor (NMF). Filaggrin, within the keratinocytes is a cohesive protein that integrates the keratin mesh; its degradation releases a number of amino acids which are partially metabolised into hygroscopic molecules. An analysis of the chemical composition of the SC[16] led to the conclusion that, the NMF components (Table 1.1) were breakdown products from the proteolysis of the filaggrin protein (Figure 1.4). NMF is a natural skin protector against dehydration and has also been referred to as "naturally occurring humectants" or "hygroscopic water soluble substances".[17]

Table 1.1 Chemical composition of NMF.[18]

Compound	%
Free amino acids and urocanic acid	40.0
Pyrrolidone carboxylic acid	12.0
Lactate	12.0
Sugars, organic acids, peptides, unidentified materials	8.5
Urea	7.0
Chlorine	6.0
Sodium	5.0
Potassium	4.0
Ammonia, uric acid, glucosamine, creatine	1.5
Calcium	1.5
Magnesium	1.5
Phosphate, citrate, formate	1.0

The presence of sugars in the SC represents primarily the activity of the enzyme *D*-glucocerebrosidase as it catalyses the removal of glucose from glucosylceramides to initiate lipid lamellae organization in the deep SC. In addition, the degradation of corneodesmosomes also releases sugars from these glycosylated proteins. Historically the main focus of interest has been the origin of the free amino acids (FAA) and their derivatives within the SC, which together represent over 50% of the NMF.

Being a complex mixture of low molecular weight water-soluble compounds, which is present within the corneocytes, the NMF components have the ability to bind water against the desiccating action of the environment and thereby maintain tissue hydration. This ability is mainly due to pyrrolidone carboxylic acid (PCA) and lactic acid salts; they absorb atmospheric water and dissolve in their own water of hydration, thereby acting as very efficient humectants. In essence, the amount of NMF in the SC determines how much water it can hold for any given relative humidity and the highly structured intercellular lipid lamellae is responsible for preventing the NMF components "escaping" from the surface layers of the skin.[19]

The contributions of the individual components of the NMF have been studied extensively, but their synergistic behaviour to the overall properties of the SC remains relatively poorly researched.
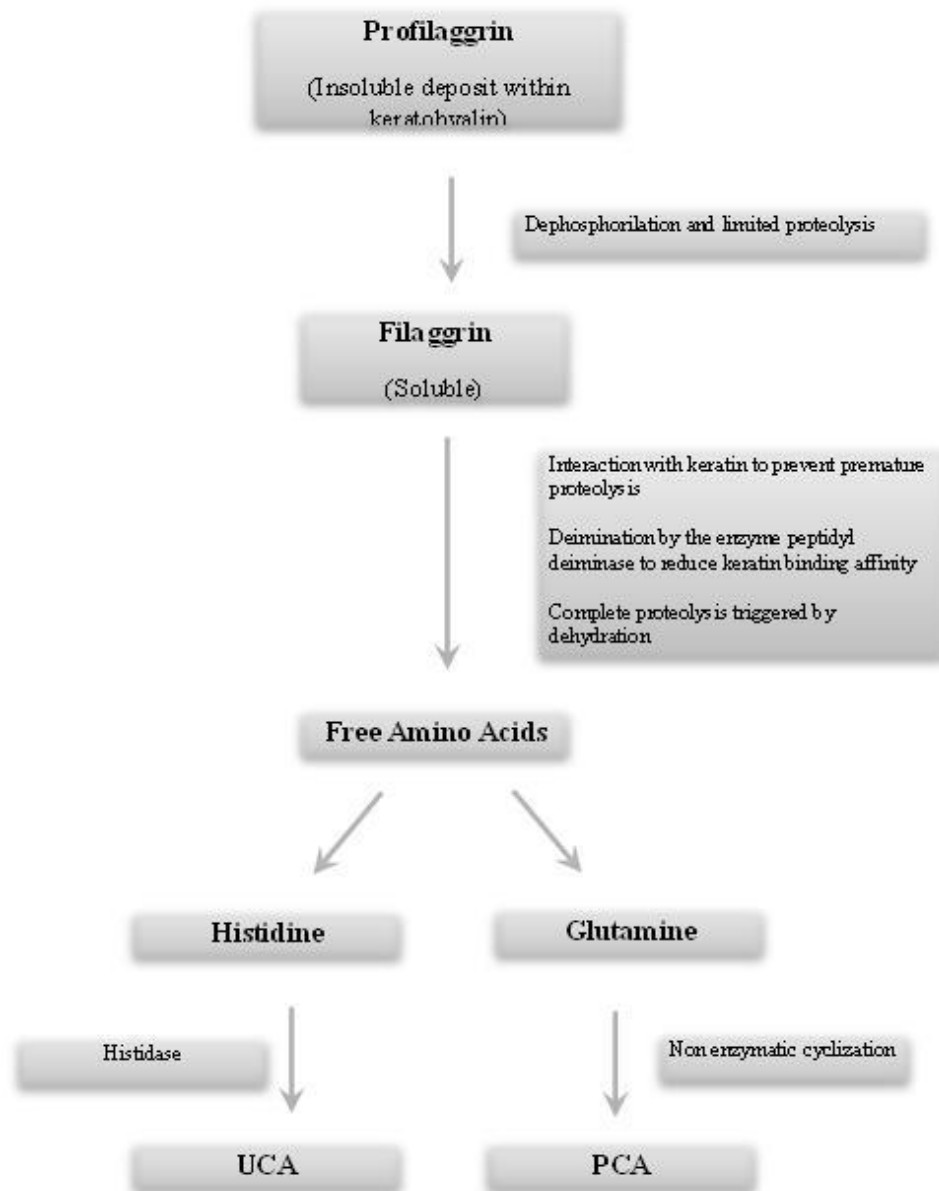
Figure 1.4 Schematic representation of profilaggrin transdermal differentiation.

Recently, the potent water biding molecule hyaluronic acid has been shown to be naturally present in the SC,[20] and the importance of glycerol, present at low concentrations, has been emphasised by the studies of Verkman and co-workers,[21] Previously, these two molecules have been ignored and the NMF composition and

function has focused on four major intrinsic components: lactate, free amino acids (FAA), PCA, and urea. PCA is produced in the skin through the arginine-citruline-ornitine-glutamic pathway, the free amino acid is not hygroscopic; however, the sodium salts of this acid are more hygroscopic than glycerine. The proportion of urea/other NMF component is 7%; it comes from the degradation of arginine or from sebaceous glands. This substance is a major skin hygroscopic agent and, because of its small size, urea penetrates to the deepest layers of the SC, where it breaks keratin hydrogen bonds and retains water molecules because of its osmotic properties.[18]

The chemical structure of α-hydroxy-acids (AHA) has an alcohol group on the alpha position (the carbon adjacent to the acid group); it is this proximity between functional groups that gives these molecules their ability for higher water retention and absorption. Thus, these highly hygroscopic compounds boost skin moisturising and strengthen the skin barrier function. AHAs have regulatory properties on keratinisation. The sodium salts of these acids are also highly hygroscopic and enhance the SC layer flexibility.[18]

A recent study reports the potential use of unnatural amino acid derivatives with enhanced ability of water retention as replacement NMF constituents.[22] Within this current project, two of those amino acids were also synthesised (see Appendix A1), namely *N*-hydroxyglycine and *N*-hydroxyserine.

The NMF is essential for the normal functioning of the SC. In combination with the SC lipids, this pool of low molecular weight compounds assists in the retention of water within the corneocytes, a capability that is vital for the integrity of this barrier, and its mechanical properties. Hydration of the SC is also essential for the normal functioning

of numerous enzymatic processes that are essential, not only for desquamation, but also for the generation of the NMF itself.

1.1.5 METABOLIC FUNCTION OF THE SKIN

Although one of the skin's functions is to prevent the entry of xenobiotics - a chemical substance that is not naturally produced, the barrier may be overcome to become an entry point. It is commonly believed that skin is an inert tissue but in reality, it is a living organ with its own biological system where chemical reactions (e.g. oxidation, reductions, hydrolysis and methylation) occur. The extent of cutaneous metabolism is modest compared to other organs such as the liver, the kidney, the lung and the intestine. Though modest, drug metabolism can be significant considering the large surface area of the skin.[2] There is growing evidence that most common drug-metabolising enzymes are expressed in the skin.[23] In 2007, Oesch and co-workers summarise the knowledge on drug metabolising enzymes in the skin of human, rat and pig[24] (often used as a model for human skin because of its similarities) and factors influencing the metabolic activity of skin enzymes have been studied by Zhang and co-workers.[25] In many case studies, the keratinocytes were shown to be the major site of drug metabolism in the skin.[26,27] An example of the occurrence of drug metabolism was reported by Nacht *et al.* where topically applied benzoyl peroxide was recovered on the dermal side as benzoic acid.[28] Another interesting study is reported by Slominski *et al.*, where the authors report the metabolism of melatonin in skin.[29] In addition to inherent drug metabolising enzymes, microorganisms present on the skin surface, such as *Staphylococcus epidermidis*, may also metabolise topically applied drugs.[2]

1.2 PERMEATION PROCESS THROUGH THE SKIN

There is a long tradition of delivering drugs through skin; records of the husk of castor oil plant in water being placed on an aching head date from the 16th century BC. From ointments, pastes and poultices, more sophisticated dosage forms have become significant commercial successes following the launch of the first transdermal patch, for scopolamine,[30] in 1979. Transdermal drug delivery (TDD) through the skin is controlled by a physical process – diffusion. Due to its characteristics, the SC is the main obstacle for this process to occur and there are essentially three pathways (not mutually exclusive) by which a molecule can traverse the SC (Figure 1.5): the shunt routes, the transcellular routes and the intercellular lipid domains. The individual contribution of each potential pathway is a function of the nature of the permeant (molecular species that moves through or into the tissue).[2]
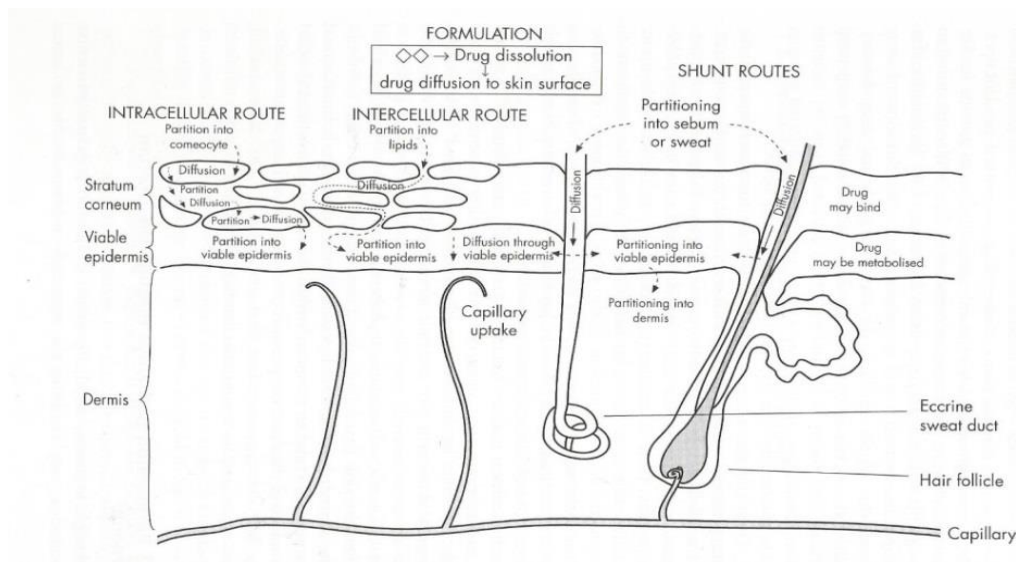
Figure 1.5 A representation of the principal mechanisms and pathways operating during transdermal and topical drug delivery.[2]

1.2.1 TRANSAPPENDAGEAL ROUTE

Representing a bypass through the SC barrier, the appendages (hair follicles, sweat ducts) account for about 0.1% of the total surface of the skin.[12] Although their contribution is generally neglected it should not be considered insignificant. Studies have demonstrated that the shunt routes can be either significant[31] or minor contributors[32] to the permeation/penetration of a drug. This behaviour is largely dependent on the nature of the permeant and the experimental design. For example, as described above, water can have a significant effect on the SC; full hydration of the tissue leads to skin swelling and so the shunt routes openings are likely to close down.

On the other hand, the shunt routes may be a quicker access to a drug in contrast to the longer path to traverse *via* other routes. The typical example of a clove of garlic rubbed on the soles of the feet and rapidly tasted in the mouth can be explained by penetration through the shunt routes avoiding the bulk of the SC. It also becomes of relevance in the transport of larger polar molecules and ions that would have lower affinity to traverse the bulk of the SC. The importance of the shunt routes has also been highlighted for the delivery of vesicular structures, as they offer lower resistance than the SC bulk.[2]

1.2.2 TRANSCELLULAR ROUTE

This route offers a highly hydrated moiety and one can conclude that the essentially aqueous environment is an optimum media for hydrophilic molecules. However, the polar route is essentially hydrated keratin-filled cells bound to the CLE and thus, a molecule crossing the SC encounters repeated obstacles. In other words, the path is complex; first the partitioning into the keratinocyte, then diffusion through the hydrated

keratin, followed by partition into the bilayer lipids and finally diffusing across the lipid bilayer to start the same path across the next keratinocyte. In addition there are between 4 and 20 layers of hydrophobic chains and hydrophilic head groups of the lipid domains between each keratinocyte.[2] Heisig *et al.*[33] demonstrated that the transcellular route should not be ignored and Sznitowska and co-workers showed that this route is the main barrier to a hydrophilic zwitterion (baclofen);[34] clearly the nature of the permeant influences the "chosen" path to traverse the SC.

1.2.3 INTERCELLULAR ROUTE

Representing 1% of the SC diffusional area,[2] the intercellular route may be considered the only continuous phase within the SC and it provides the path by which most small, uncharged molecules traverse the SC.[35]

A mosaic model domain was proposed by Forslind[36] for the SC lipids taking in account the lipid packing heterogeneity. This arrangement allows for water loss regulation whilst permitting sufficient water to enter the tissue to maintain keratinocyte hydration; inferring that fluid liquid crystalline domains could provide the pathway by which permeants traverse the SC. This model does not exclude the possibility of preferential paths, meaning that there would be alternative routes of lower resistance to permeation. More tortuous than the transcellular route, a molecule travels through the continuous 150 to 500 μm thick[2] lipid domains in between the keratinocytes, dependent on their physico-chemical properties. The real path dimension that molecules have to cross is unknown and thus various permeation parameters must be taken in account including pathlength, permeability and diffusion coefficients.

Though the skin is a complex biological system, a mathematical model can be applied to describe the behaviour of a molecule traveling through the skin. Fick's first law (Equations 1) has successfully been applied to analyse experimental data. This relatively simple mathematical model allows insight to the path of a drug traversing the skin, considering simple diffusion in a pseudo-steady-state.[2] The applicability of Fick's law, post excision low permeability of the skin and strong evidence that the diffusional resistance is in the SC, represent the three reasons that lead to believe that the movement of molecules across the skin is by passive diffusion.[37]

$$J = -D\frac{dc}{dx} \qquad\qquad \text{Equation 1.1}$$

Where, J is the flux of the permeant defining the amount of material that passes through a unit area per unit time, D is the diffusion coefficient of the permeant and $\frac{dc}{dx}$ is the concentration gradient (c is the concentration and x is the space coordinate measured normal to the section). Fick's second law (Equation 2) is derived from equation 1.

$$\frac{\partial c}{\partial t} = D\frac{\partial^2 c}{\partial x^2} \qquad\qquad \text{Equation 1.2}$$

Where, t is time. The solution of this equation (with the appropriate geometry, initial and boundary conditions) gives the permeation profile of a drug through skin.

1.2.4 PROPERTIES OF PERMEANTS AND UPTAKE

From the above, one can infer that the permeation pathways are not mutually exclusive, and that the nature of the permeant has great influence in the permeation process. It is well known that the physicochemical properties of a permeant affect its transport into and through the skin, including its octanol/water partition coefficient, molecular weight and hydrogen bonding groups. The partition coefficient may be the rate-limiting step as, in a very simplified fashion, a hydrophilic molecule will partition preferentially into hydrated keratinocytes (intracellular route) and a more lipophilic molecule will prefer the lipid bilayers. In 1992, Moriguchi and co-workers[38] developed a mathematical method to predict the octanol/water partition coefficient that involves several variables including number of carbon, nitrogen and oxygen atoms, their proximity, number of intramolecular hydrogen bonds, among other parameters. The size and shape of a molecule, in an isotropic medium, influences the diffusion coefficient; the bulkier the molecules the smaller its diffusivity. Despite this not so unexpected relationship, large and bulky molecules (aptamers) have recently been reported to traverse the skin as shown by Lenn *et al.*[39]

Normal ambient temperature and atmospheric pressure are the typical conditions for TDD. At these conditions, most organic molecules have low aqueous solubility and hence, the solubility/melting point is another parameter to take into account when predicting the permeability of a candidate through skin. Lipophilic molecules would naturally permeate at a higher rate than hydrophilic molecules, but it is also necessary that a candidate would exhibit some hydrophilic characteristics. Computational methods have been employed to estimate the solubility and permeability of drugs.[40] In addition

to its solubility, ionisation is another property that may influence the permeation process. The ionised form of a drug permeates through the lipid barrier at lower rates than the unionised drug.

Less well understood is the role of chirality. The enantioselectivity of the skin during epidermal permeation has been subject of study in some cases, for example nicorandil,[41] flurbiprofen,[42] and propranolol.[43] To date, however, only a few investigations have focused on the effect of chirality with respect to binding or metabolism in the skin, and their transdermal delivery.[44]

1.3 PERMEANT SELECTIVITY AND CHIRALITY

Biologists have been looking back through the evolutionary chain to understand what early life forms all species are descended from – since the publication of Charles Darwin's book "On the Origin of Species" in 1859. There are many questions yet to be answered about the origin of life and one of them is: why is it that the building blocks of life are all homochiral - that is, why are their molecules all structured in the same way, and not a mixture of the different possible ways? The answer remains unclear, but almost all amino acids are L-type and sugars are D-type. Researchers exploring the origin of life are keen to answer this question, and why the particular forms we see today – L-amino acids and D-sugars – were favoured, rather than their stereoisomers.

Many of the molecules that organisms produce exhibit a specific handedness. This is important because the response of an organism to a particular molecule often depends on how that molecule fits a particular site on a receptor molecule. Therefore, in

designing pharmaceuticals, chemists must be concerned about which enantiomer is the active one. Ideally, the pharmaceutical should consist of the pure active isomer.

The importance of stereochemistry in drug research and development as well as pharmacotherapy is well acknowledged. This is mainly due to a collective understanding that stereochemically pure drugs may provide safer and more efficient alternatives to racemates. Many chiral drugs are used as their racemic mixtures in clinical practice. In fact, two decades ago, 25% of therapeutic agents were commercialised as racemic mixtures.[45] Two enantiomers of a chiral drug generally differ in pharmacodynamic and/or pharmacokinetic properties as a consequence of the stereoselective interaction with optically active biological macromolecules. Stereoselective metabolism of drugs is most commonly the major contributing factor to stereoselectivity in pharmacokinetics.[46] Chiral substances possess a unique architecture such that, despite sharing identical molecular formulas, atom-to-atom linkages, and bonding distances, they cannot be superimposed. Thus, in the environment of living systems, where specific structure-activity relationships may be required for effect (e.g., enzymes, receptors, transporters, and DNA), the physiochemical and biochemical properties of racemic mixtures and individual stereoisomers can differ significantly. In drug development, enantiomeric selection to maximize clinical effects or mitigate drug toxicity has yielded both success and failure.[47]

The SC, the rate-limiting barrier in transdermal drug delivery is chiral in nature and enantiomers behave differently with respect to their transport across the skin. The role of the skin as a portal of entry for chiral molecules is becoming an increasingly active and exciting field of research. To date, however, only a few investigations have focused

on the effect of enantiomeric differences of chiral drugs with respect to binding or metabolism in the skin on their transdermal delivery.

Physicochemical properties of a racemate may be drastically different from the enantiomers. Chirality may also influence drug delivery because a single enantiomer or a non-racemic blend may have improved solubility, dissolution, and stability. In addition, many pharmaceutical excipients (e.g. cellulose and its derivatives) either naturally occur as single enantiomers or are derivatives.

Similar to the solid dosage forms containing chiral excipients, biological membranes may provide chiral environments. Most drugs cross the gastrointestinal membrane through passive diffusion; thus, no stereoselectivity in the process is expected. It appears, however, that stratum corneum possesses chiral discrimination properties. A mathematical model has been reported as being able to predict enantioselective permeation of chiral drugs across human skin, based on the interdependence of certain physicochemical characteristics.[48] Indeed, Kommuru *et al.* reported that *in vitro* data indicate significant stereoselectivity in skin penetration of ketoprofen[49] (Figure 1.6 a). Suedee *et al.* proposed a transdermal patch for selective controlled drug delivery of the active *S*-enantiomer from racemic propranolol.[50] The same author had previously reported a formulation containing a chiral cellulose derivative excipient for the enantioselective delivery of propranolol[51] (Figure 1.6 b). Heard and co-workers, in 1995, discussed the *stratum corneum* as a potential source of chiral discrimination that could result in differential diffusion rates of propranolol.[52] Their findings did not lead to the hypothesis of chiral discrimination during diffusion; they stated that definitive evidence for intrinsic stereoselectivity in skin permeation has yet to be obtained.

a)   b)
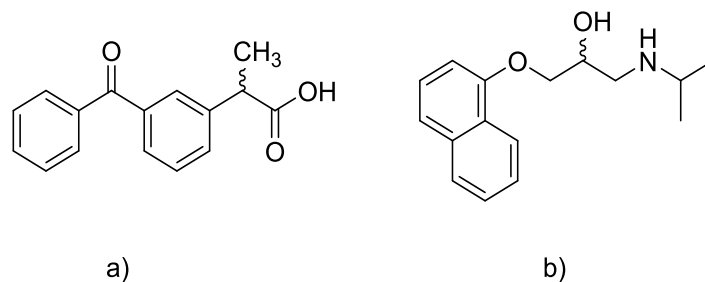
Figure 1.6 Chemical structures of a) ketoprofen and b) propranolol.

A majority of the chiral excipients in pharmaceutical dosage forms are from natural sources and therefore exist in the optically pure form. A selected list of commonly used excipients along with their major applications is shown in table 1.2.

The interaction of chiral excipients with drugs and their influence on the therapeutic outcomes have not been thoroughly investigated. This may be due to the misconception that excipients are "inactive" materials and are not expected to affect the performance of dosage forms.[44]

The rational development of products for transdermal drug delivery requires a thorough understanding of both the biological composition of the skin barrier and the physicochemical properties of drug molecules. For chiral drugs, whose biological activity is associated with one enantiomer, enantioselective permeation would affect the pharmacodynamics profile of the racemate. In such cases, development of a transdermal delivery system based on a single enantiomer, rather than racemate, could reduce the therapeutic dose required to achieve the desired pharmacological effect, which in turn can minimize or eliminate the adverse effects associated with chiral drugs.

Table 1.2 Examples of chiral excipients and their pharmaceutical applications.[44]

Excipients	Major applications
Celluloses	Disintegrants, suspending agents, stabilizers, coating agents, binders, viscosity builders, film formers, dissolution modifiers, enteric coating agents, taste masking, diluents.
Starch, Sugars and Derivatives	Binders, disintegrants, viscosity builders, sustained release matrix, suspending agents, diluents, sweeteners, dissolution enhancer binders, bulking agents for lyophilized products.
Cyclodextrins	Complexing agents, dissolution enhancers, stabilizers
Acids	Antioxidants, acidifying agents, acidulants, flavours, buffering agents, effervescent agents, diluents.
Amino acids, peptides and Derivatives	Stabilizers, sweeteners, solubility enhancers
Fats, Oils, Essential Oils	Emulsifying agents, suspending agents in emulsion systems, absorption enhancers, dissolution modifiers, flavours, penetration enhancers, antioxidants.

Physicochemical properties of chiral ibuprofen were evaluated and considered significant in the permeation process by Yuan *et al.*[53] The pure enantiomers of ibuprofen have lower melting points than racemic ibuprofen, and therefore have higher solubility in skin lipids and greater percutaneous absorption. In this study, the eutectic emulsion showed the highest permeation rates among all test preparations.

High melting points mean that the forces holding the molecule are strong hence low solubility[54] and a clear relationship was established between melting point and passive transport of poorly soluble drugs.[55]

Krishnaiah *et al.* investigated enantioselective penetration enhancing effect of carvone on the permeation of nicorandil[41] (Figure 1.7). Their findings showed that *R*-carvone exhibited a higher penetration enhancing activity when compared with *S*-carvone and *RS*-carvone.
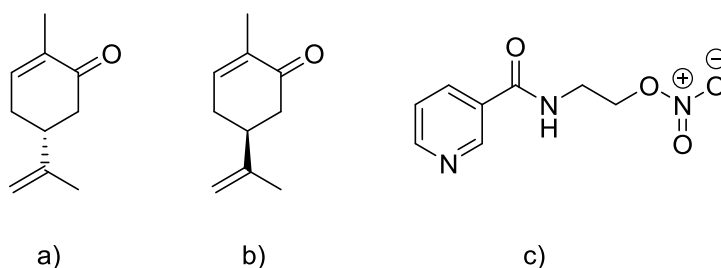
Figure 1.7 Chemical structures of carvone a) *R*, b) *S* and c) nicorandil.

A study conducted by Zeng *et al.* evaluated the possible relationship between the physical properties and the permeation of *S*-amlodipine and *RS*-amlodipine as well as the possible enantioselectivity of permeation of amlodipine in the presence and absence of enhancers, such as terpene enhancers and ethanol[56]. *S*-amlodipine was found to have

a higher flux than *RS*-amlodipine in the transdermal permeation study *in vitro*. However, the difference of amlodipine enantiomers in permeation was not found in the absence and presence of enhancers, such as linalool, (**-**)-menthol, (**-**)-limonene, and ethanol (Figure 1.8), and indicated that there was no enantioselectivity in the permeation of amlodipine across rat skin.
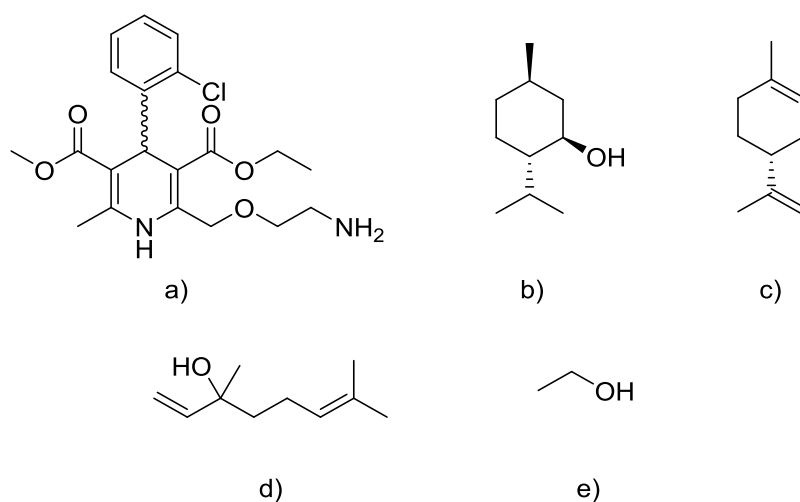
Figure 1.8 Chemical structure of a) amlodipine, b) (-) menthol, c) (-) limonene d) linalool and e) ethanol.

Another *beta* blocker (metoprolol, Figure 1.9) was evaluated by Kommuru *et al.* as well as the influence of chiral permeation enhancers. Kommuru found that the use of permeation enhancers was significant to the flux values when the formulation contains only one of the enantiomers.[57]
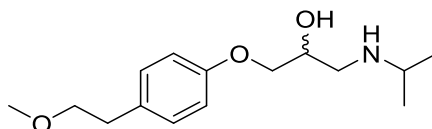
Figure 1.9 Chemical structure of metoprolol.

Flurbiprofen (Figure 1.10) is a chiral anti-inflammatory drug, Valentova *et al.* observed marked differences in the permeation profiles of enantiomers (*R*)- and (*S*)-flurbiprofen from a donor solution containing racemic (*RS*)-flurbiprofen.[42] Cilurzo *et al.*[58] found that, depending on the vehicle and the use of racemate or enantiomer, the ibuprofen fluxes followed the rank order: *S*-IB vehicled in a saturated solution > *S*-IB vehicled in a plaster ≅ *RS*-IB vehicled in a plaster > *RS*-IB vehicled in a saturated solution.
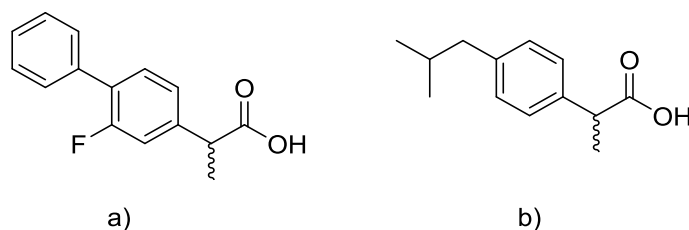
Figure 1.10 Chemical structures of a) flurbiprofen and b) ibuprofen.

A different approach was used by Suedee *et al.*,[59] to deliver *S*-omeprazole (Figure 1.11). They developed a pH-responsive drug delivery system for enantioselective delivery of racemic drugs.
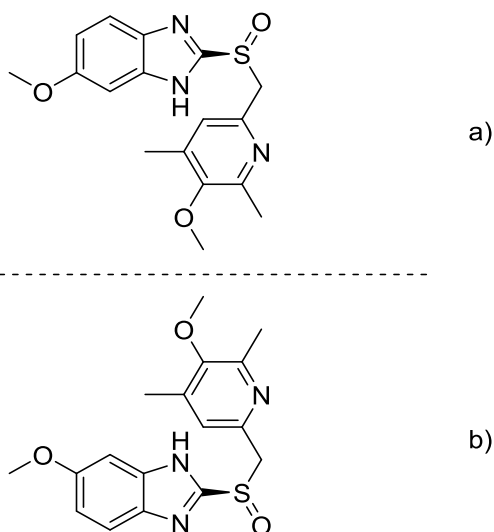
Figure 1.11 Chemical structure of omeprazole (a) *S* and (b) *R*, sold under the brand names of Prilosec and Losec.

All the above specified structures are molecules with low molecular weight (<500 Da), no more than five hydrogen bond donors, no more than ten hydrogen bond acceptors and calculated lipophilicity lower than five. That means that these compounds obey to the Lipinski's rule of 5 (note that lipophilicity lower than five is an assumption from oral drug delivery observations). Though generally successful, deviations do occur but the rule of 5 does identify key physicochemical parameters that are important for passive diffusion.

Whilst the above considers drug molecules, in light of the discussion of NMF, it is of interest to explore chirality and delivery of amino acids and their assembly into peptides. They initially comply with Lipinski's rule but, as the size of the peptide increases so does the molecular weight and number of hydrogen bond donor/acceptors; also, the side chain motifs may add extra properties and finally, naturally occurring

amino acids and peptides have an extra feature to their structure in that they are all chiral.

1.4 AMINO ACIDS AND PEPTIDES

A molecule is termed "chiral" when its mirror image is non-superimposable. Nature has a distinct preference for one of these mirror images. Amino acids, for example − the building blocks of proteins − are all of the same configuration, with very few exceptions. The chemical connection between two amino acids (-CONH-) is called the amide or peptide bond, and is generally represented as a single bond yet, it possesses characteristics that resemble a double bond due to an electronic resonance effect due to the atoms involved being in the same plane. This mesomeric effect is responsible for the high stability of the amide bond. The intermediate character "single-double" bond results in a shorter bonding length than the one observed in a single bond and consequently a significant reduction on the ability to rotate. Rotation is permitted about the N-Cα and the Cα-C bonds (Figure 1.12).
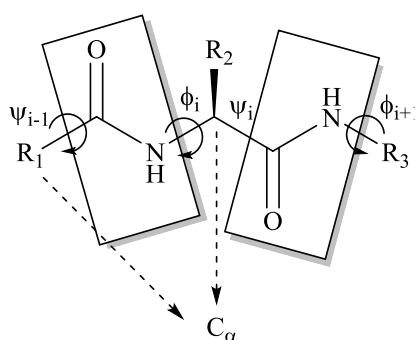
Figure 1.12 Illustration of a dipeptide and its dihedral angles. Adapted from Nelson et al.[60]

The backbone of a polypeptide chain can be pictured as a series of rigid planes with consecutive planes sharing a common point of rotation at Cα. These rigid peptide bonds limit the range of conformations that can be assumed by a polypeptide chain. The mesomeric effect enables the oxygen and nitrogen atoms to participate in hydrogen bonds and this property makes a remarkable contribution to the three-dimensional structure of peptides and proteins. By convention, the bond angles resulting from rotation at Cα are labelled φ for the N-Cα bond and ψ for the Cα-C bond.

The specific sequence of amino acids is known as the primary structure of a protein (Figure 1.13), and the term secondary structure refers to the local conformation of some part of a polypeptide commonly as a sequence of hydrogen bonding between non-adjacent amino acids. One of the most common secondary structures found in proteins is the α-helix because this conformation makes optimal use of internal hydrogen bonds. Helices are right or left-handed and so it is usual to refer to chirality of helices in terms of **P** (plus) or **M** (minus) if the axial chirality is right or left-handed, respectively.
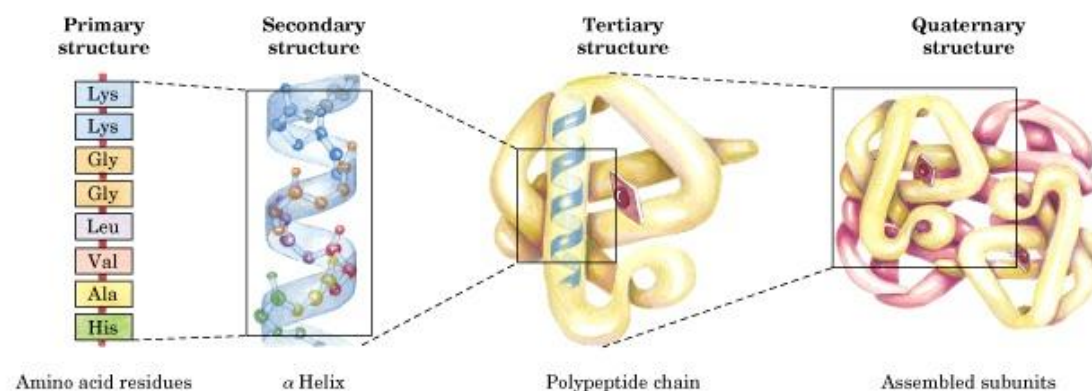
Figure 1.13 Levels of structure in proteins, showing the primary, secondary, tertiary and quaternary structures.[60]

The remarkable diversity of protein structure has inspired chemists to design their own oligomers which have unique secondary structures. The word "foldamer" was introduced in the scientific community in 1998 by Gellman[61] to describe these structures and ever since, it gained an important role in research.

1.5 DRUG DELIVERY

In 2008, Prausnitz[62] elaborated a list of the Food & Drug Administration (FDA) approved drugs for passive transdermal delivery and six years later (2014) Guy[63] updated that list with two more actives. A total of 17 drugs reflect the difficulty in compromising between skin permeability and pharmacological potency.

Numerous strategies have been explored to overcome the barrier of the SC and expand the administration of drugs through the skin including active and passive methods. The development of chemical enhancers is broadly reported in the literature and is increasingly being refined.[64,65] In recent years, studies have been conducted reporting the use of amino acid derivatives as carriers,[66,67] as transdermal permeation enhancers,[68] and as cell-penetrating peptides (CPP) to enhance topical delivery of proteins and peptides.[69,70] When applied to transdermal systems the common designation of CPP becomes SPP (skin-penetrating peptides). In 2006 Chen *et al.*,[71] described the delivery of insulin through skin using a peptide (11 residues) as facilitator. Kummar *et al.*,[72] identified a 6 residue peptide that altered the lipid organisation of the skin and enhanced the delivery of 5-fluoruracil. The same authors showed that peptides can enhance the delivery of cyclosporine,[73] through the skin and also provided some insight on the mechanism of action of 5 different peptides as mediators between cyclosporine and

keratin. In 2016 Menegatti *et al.*[74] developed a computational process for screening libraries of peptides to identify SPPs capable of enhancing transdermal delivery of cyclosporine. Cyclosporine is a cyclic peptide with a molecular weight over 1200 Da – i.e. significantly larger than the upper limit of 500 Da often cited. Gennari and co-workers,[75] delivered UFH (unfractioned heparin, Mw 12000-15000 Da), an anticoagulant and antithrombotic drug through human skin. The permeability of UFH increased about 30-fold after conjugation with a peptide. The molecular weight challenge was taken further by Gautam *et al.*,[76] they reported the delivery of GFP (green fluorescent protein, Mw 26.9 KDa) using a peptide as carrier.

The field is in expansion and Lipinski's rule of 5 seems not applicable when considering large biomolecules such as peptides, proteins or aptamers.

1.6 HYPOTHESIS TO BE TESTED. AIMS, OBJECTIVES AND WORK PLAN

From the above it is clear that further work is merited in terms of disruption of the skin's barrier for drug delivery. A specific aspect that has not received a lot of attention is the role of chirality in the permeation process. This project has the ambition of making a contribution in this field, by analysing the influence of the physical properties of enantiomerically pure compounds and establishing structure-activity relationships. The ultimate desire of this study is to obtain foldamers to use as peptidomimetics within the realm of therapeutics and even catalysis.[77,78]

Previous studies in our research group demonstrated that an unnatural five membered ring amino acid had high water holding capacity. This observation drove the design of a synthetic route to fulfil the premise stated above and the following objectives were set:

1. To synthesise a racemic and enantiomerically pure unnatural β amino acid;

2. Make structural changes to the synthesised β amino acid (derivatising into a saturated and a doubly hydroxylated β amino acid) and evaluate the effects of these changes;

3. Build on the molecular weight of the unnatural amino acid into peptic dimers, tetramers and hexamers and evaluate the effects of those changes;

4. To observe if the synthesised oligomers form a helix as a secondary structure;

5. To characterise all new compounds (structure and physical properties including hygroscopicity) and test them for skin uptake.

In order to fulfil the proposed objectives a route to the unnatural amino acid (**MMU**) was designed, as illustrated in Figure 1.14.
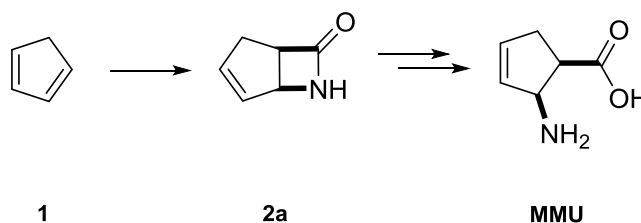
Figure 1.14 Synthetic route to achieve the desired unnatural amino acid.

Once the unnatural cyclic unsaturated amino acid was obtained and derivatised into the saturated and hydroxylated five membered ring amino acid, three series of peptides were generated following the synthetic route shown in Figure 1.15.
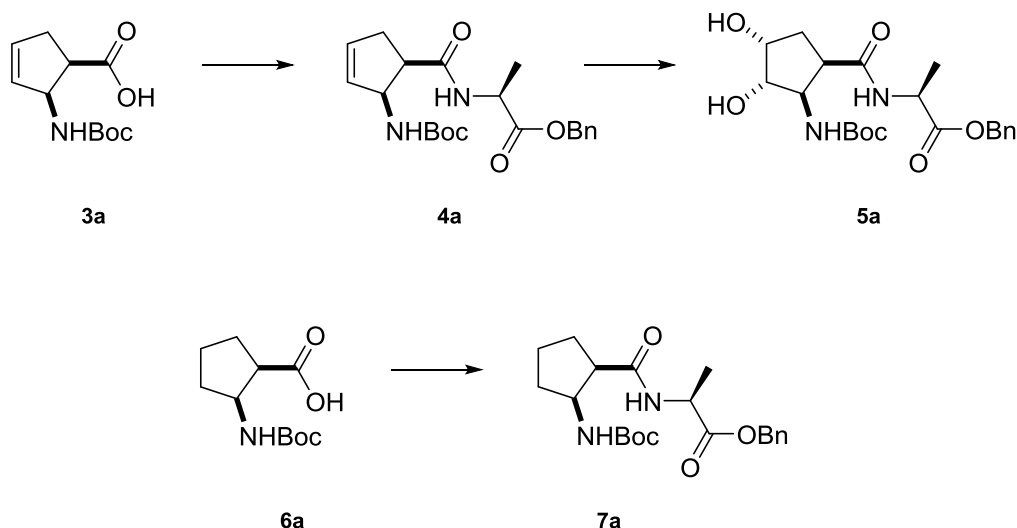
Figure 1.15 Synthetic route to achieve the desired starting materials to access foldamers.

The resulting dipeptides (**4a**, **5a** and **7a**) provided the starting materials to obtain the desired oligomers with a repetition of once, twice, three or even four times the dipeptide structure.

The following chapters describe the materials and general methods employed (Chapter 2), whilst Chapter 3, 4 and 5 provide experimental details, results and discussion of the synthesis, characterisation and water uptake of the unnatural amino acids (Chapter 3), dipeptides (Chapter 4) and peptides with higher molecular weights (Chapter 5) in their racemic and enantiomerically pure forms. Chapter 6 is dedicated to the analysis of the water and compound uptake regarding chirality and Chapter 7 includes a general discussion of the results obtained.

CHAPTER 2

2. MATERIALS AND METHODS

In this chapter an overview of the equipment, materials and methods used throughout this project is provided. Specific details about each method can be found in chapters 3, 4 and 5.

2.1 CHEMICALS

All chemicals were purchased from Sigma Aldrich and Fisher Scientific. A table of all chemicals used along this project with batch number, manufacturers, catalogue number and purity can be found in Appendix A2. Multiple orders of the same compound were made over the time course of this project; where the batch numbers were the same, the compound was entered only once.

2.2 SYNTHESIS

Classical methods of synthesis were used to obtain the desired compounds. The main reactions involved were a [2+2] cycloaddition to assess the main precursor, classic peptide chemistry (protection, deprotection and coupling) and an enzymatic resolution to assess enantiomerically pure compounds. The synthesis details are discussed in chapters 3, 4 and 5.

2.3 NUCLEAR MAGNETIC RESONANCE (NMR)

^{1}H NMR and ^{13}C NMR spectra were recorded on a Bruker Nanobay 400 (at 400 MHz or 100 MHz) spectrometer in the deuterated solvent stated or a Bruker DPX 400 (at 400MHz or 100 MHz), ^{1}H-^{1}H COSY, ^{1}H-^{13}C HQSC and ^{1}H-^{13}C HMBC spectra were

used for the assignment of the chemical shifts when necessary. A Bruker Avance III 500 MHz, or on a Bruker Avance III 700 MHz was used to record NOESY, ROESY and TOCSY spectra. The field was locked by referencing to the relevant deuteron resonance and all characteristic peaks are reported in parts per million (ppm) using the following abbreviation for splitting patterns: s (singlet), brs (broad singlet), d (doublet), dd (doublet of doublets), ddd (doublet of doublet of doublets), t (triplet), dt (doublet of triplets), ddt (doublet of doublet of triplets), q (quartet); m (multiplet). Coupling constants (J) are quoted in Hz.

2.4 INFRA-RED SPECTROSCOPY (IR)

IR spectra were recorded on a Thermo Scientific Nicolet iS5 FT-IR spectrophotometer equipped with a Thermo Scientific iD5 ATR Accessory. A small amount of sample (<10 mg) was placed as a solid and the spectra were typically collected between 400 and 4000 cm^{-1} with a mean of 16 scans recorded at a resolution of 4 cm^{-1}. All characteristic peaks are reported in wavenumbers (cm^{-1}).

2.5 MASS SPECTROMETRY (MS)

Mass spectra were recorded on a Thermo Scientific LQT-Orbitrap-XL at 100K resolution equipped with a Thermo Scientific Accela LC, with a 2.1x50 mm C18 column, particle size 1.9 μm, pore size 175 Å. The buffers used were typically water:acetonitrile (9:1, v/v) both with 0.1% formic acid. Samples were dissolved in water or methanol as appropriate and diluted to a final concentration of 30 μg/mL and a

5 μL injection was run. When that failed to deliver results a direct infusion into the Orbitrap in positive and negative mode was run.

2.6 MELTING POINT (MP)

Melting points were measured on a Stuart SMP10 digital melting point apparatus and are compared to literature values when available.

2.7 CHROMATOGRAPHY (THIN LAYER AND COLUMN)

Reactions were monitored by thin layer chromatography (TLC) on silica gel pre-coated aluminium sheets (TLC Silica Gel 60 F_{254}, Merck). Visualisation, when possible, was accomplished by irradiation by UV light at 254 nm and potassium permanganate stain. Column chromatography was performed on Merck silica gel (60 Å, 230 - 400 mesh, 40 - 63 μm).

2.8 HIGH PERFORMANCE LIQUID CHROMATOGRAPHY (HPLC)

An Agilent Technologies 1200 Series HPLC was used, with a ratio of HPLC grade hexane:propan-1-ol (95:5, v:v) as eluent, a Chiralpak AD-H column (0.46 cm x 25 cm), an injection volume of 5 μL at 1 mL/min, 30 min runs and UV detection at 210 nm.

2.9 X-RAY

Single-crystal X-ray diffraction data were collected for compounds **2b**, **MCUH**, **DCUH** and **DCDH**, on an Oxford Diffraction Gemini diffractometer, using Cu Kα incident radiation, with the crystal held at a temperature of 150 K using an Oxford Instruments

Cryojet device. The crystal structure was solved[79] and refined[80] using the Olex2[81] system and crystal data are summarised in Tables 1, to 4 respectively (Appendix A3).

Powder X-ray diffraction data were collected for N-hydroxyglycine on a Bruker D8 Advance (Cu Kα1, λ = 1.54056 Å) in capillary mode. The data collected was performed at room temperature (ca. 293 K) in the rage 3 - 65° 2Θ for a total of 15 minutes.

DICVOL06[82] as implemented in DASH[83] was utilised to index the data to a monoclinic cell and the simulated annealing procedure in DASH was employed to solve the crystal structure.

The unit cell and structure solution parameters are given in Tables 5 and 6 (Appendix A3).

2.10 POLARIMETRY

Specific optical rotations were obtained using a Perkin Elmer Polarimeter 341 with reference to the sodium D line (λ=589 nm) in HPLC grade water or chloroform. The results are shown as $[\alpha]_D^T$ in deg.dm^{-1}.g^{-1}.mL, given by equation 2.1

$$[\alpha]_\lambda^T = \frac{\alpha}{l \times c}$$

Equation 2.1

Where, α is the measured rotation, l is the path length in dm, T is the temperature in ºC and c is the concentration in g.mL^{-1}

2.11 DYNAMIC VAPOUR SORPTION (DVS)

The DVS experiments were outsourced to M2M facilities.

The experiment was carried out using ca. 10-20 mg of material loaded into a DVS Advantage System (Surface Measurement Systems, UK) held at $25 \pm 0.1°C$. The sample was then subjected to a step profile from 0% RH to 90% RH[a] (P/Po, whereby P = Partial pressure of water vapour and Po = Equilibrium vapour pressure of water) at 10% RH increments; followed by desorption from 90% RH to 0% RH at 10% RH decrements maintaining the sample at drying step at 25°C. The weight change during the sorption cycle was then monitored, allowing for the hygroscopic nature of the sample to be determined. The % RH was maintained by a mixture of DI water and nitrogen (flow rate of 200 sccm[b]) which acted as a wet purge and dry purge respectively. The percentage of mass change per minute (dm/dt) was set as 0.002 with a dm/dt window set as 5 minutes, minimum stability for 10 minutes and maximum stage time was 240 minutes at each % RH. The experiment was set with a sampling rate of 1 sec and save data set at 1 min.

---

[a] The RH is normally expressed as a percentage; a higher percentage means that the gas (nitrogen)-water mixture is more humid.

[b] Standard cubic centimetres per minute.

41

2.12 CIRCULAR DICHROISM (CD)

CD spectra were recorded using a Chirascan spectropolarimeter (Applied Photophysics, UK). Spectra are presented with absorbance (A) < 2 at any measured point with a 0.5 nm step, 1 nm bandwidth, and a 1 s collection time per step. The CD signal from the background was subtracted from the CD signal of the sample solution. The sample solutions were measured using a 0.1 mm quartz plate sample holder with water as the background. All CD spectra were measured at 20 ºC, which was controlled by an external temperature controller and water reservoir. Results are presented in molar ellipticity and it was calculated according to equation 2.2.

$$\varepsilon = \frac{Sample - Background}{10 \times c \times l}$$

Equation 2.2

Where, ε is molar ellipticity in deg.cm^2.dmol^{-1}, c is concentration in mol.L^{-1} and l is the pathlength in cm.

2.13 WATER UPTAKE DETERMINATION

Water uptake was determined using thermogravimetric analysis (TGA) on a TGA Q50 instrument from TA instruments, UK, with nitrogen purge. The experiments were conducted as follows: approximately 10 mg of each compound were kept under a controlled environment of 100% RH at 32ºC, over one week. The 100% RH was achieved using a desiccator containing water, equipped with a thermo-hygrometer and sealed (Figure 2.1). Each experiment was run in triplicate and the results are shown as mean ± SD. The samples were then heated at a constant rate of 5ºC/min from room temperature to 250-300ºC.
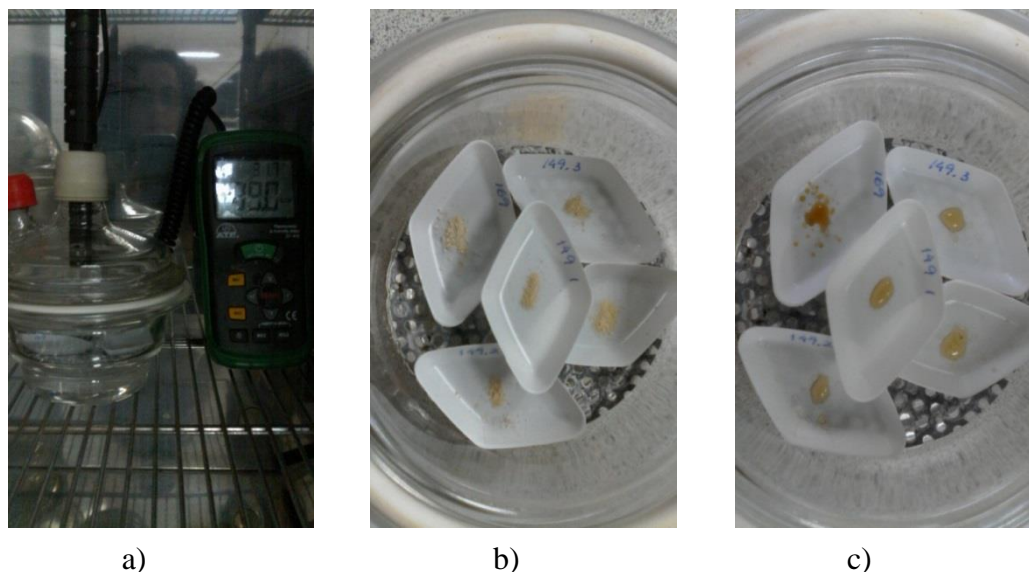
Figure 2.1 a) Desiccator equipped with a thermo-hygrometer in an incubator at 32ºC. b) Samples at time 0h. c) Samples with one week exposure to 100% RH.

The curves obtained allowed discrimination between surface water (up to about 100ºC) and crystallization water. The weight loss was measured between temperatures varying from 110-160ºC (each compound has its interval of temperature for water loss). The number of waters, N_w, that bind to the compound is calculated according to the following equation:

$$N_w = \frac{n_w}{n_c}$$ Equation 2.3

Where, n_w is the number of moles of water and n_c is the number of moles of compound.

2.14 SATURATED COMPOUND SOLUTIONS PREPARATION

Small amounts of compound were added to 1 mL of water. After each addition the solution was left stirring at room temperature until complete dissolution of solute. The addition was stopped once a visible suspension of the solute was observed. Each solution was then filtered and used in the compound uptake studies. The solubility was determined using method B described in Section 2.16.

2.15 STRATUM CORNEUM PREPARATION

SC was isolated following the classical procedure by Kligman and Christophers.[84] Pig skin samples from the flank were kindly donated by Pirbright Institute and stored at -20 ºC. When needed, the skin was defrosted and left to equilibrate at room temperature for about 2 hours, the bristles were shaved with a razor and the samples were then dipped in water at 60ºC for 1 min to allow the separation of the viable epidermis (Figure 2.2) by rolling it over itself (or by gentle pushing). The samples were then placed, viable epidermis down, in a Petri dish equipped with a bed of filter paper (six filter papers) embedded in 0.0001% (w/v) solution of trypsin in 0.5% (w/v) aqueous solution of sodium bicarbonate and left to digest overnight in an incubator at 37ºC. The digested viable epidermis was gently swabbed with a cotton tip embedded in water. The isolated SC was then rinsed with water several times and placed in a desiccator to dry. Once dried, the membrane was cut into approximately 2 cm^2 pieces and used in the compound uptake experiments.
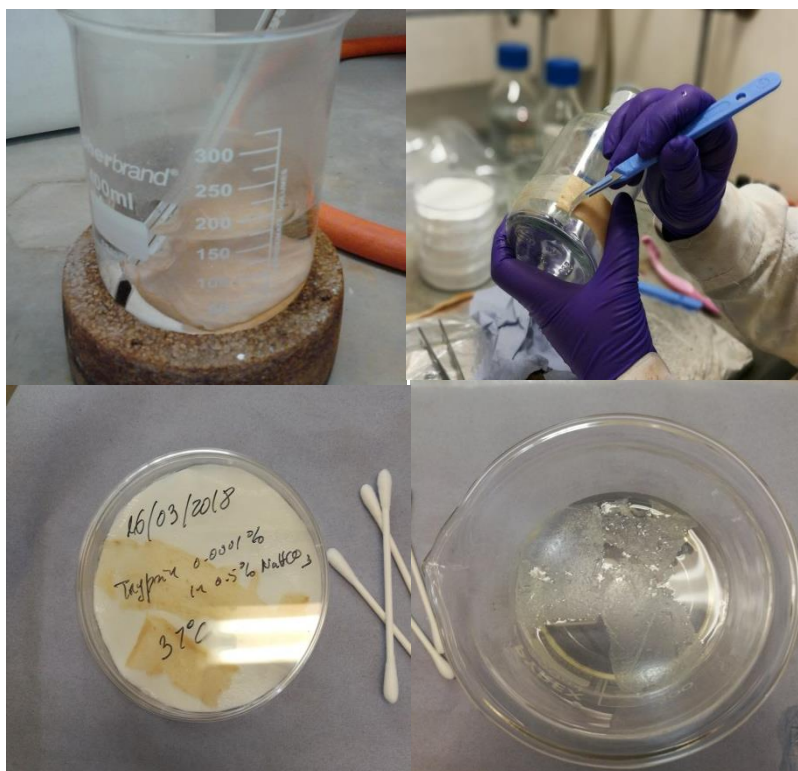
Figure 2.2 Illustration of the procedure for the SC isolation.

2.16 COMPOUND UPTAKE

A sample of dried SC was weighed (3-6 mg), dipped into a saturated solution of each compound and left at 32ºC, over a 24 hours period. The tissue was then removed, blotted dry on a filter paper and dipped into 1 mL of water for 24 hours, at room temperature to extract the water soluble compound. A second wash (1 mL of water) was done to evaluate residual compound within the SC. The SC was then removed and left to dry.

2.16.1 ASSESSMENT OF COMPOUND UPTAKE

Method A - TNBSA

The resulting solution was freeze dried for 48 h and the solid obtained was dissolved in 1mL of $NaHCO_3/Na_2CO_3$ buffer (pH 9.3). Standard solutions of the compound to be assessed were prepared ranging from 1.5-100 µM in buffer, with increments of 5 µM for 10-100 µM and 0.5 µM for 1.5-10 µM. 25 µL of 0.03 M TNBSA (2,4,6-trinitrobenzene sulfonic acid) in buffer solution were added to the sample solution, to the blank solution (buffer) and to each standard solution. The samples were left reacting for 30 minutes and their absorbance was read ($\lambda = 420$ nm) using a Jenway 7315 spectrophotometer. The concentration of the sample was determined using the calibration curve.

Method B - LC/MS

Standard solutions of the compound to were prepared ranging from 3-100 µg/mL in water. The resulting solutions were analysed by LC/MS (mass spectra were recorded on a Bruker micrOTOF-QII with electrospray ionisation (ESI) in positive mode, equipped with an Agilent 1100 Series LC with a 150x2.1 mm ACE 5 C18 column, particle size 5 µm, pore size 100 Å. The buffers used were water:acetonitrile (95:5, v/v) both with 0.1% formic acid for all compounds except **TCUU**, **TCUS** and **HCUS** which was water:acetonitrile (90:10, v/v) and **OCUS** with a ratio of 85:15 (v/v). Samples were run with a 10 µL injection at 200 µL/min) and the concentration of compound determined using a calibration curve of the same compound. Each experiment was repeated in triplicate and each analysis was run three times. The results are shown as a mean $\pm$ SD.

2.17 MOLECULAR MODELLING

The dimeric structures were energy minimised using Chemdraw's Chem3D package. The structure that generated the lowest energy was used for the addition of water molecules (10 or more water molecules were added to each dimer). Molecular dynamics was then performed at 300 K until equilibrium was reached and then the energy minimised.

CHAPTER 3

3. SYNTHESIS AND WATER UPTAKE OF UNNATURAL AMINO ACIDS

3.1 INTRODUCTION

This chapter is divided in four sections. The current section gives an overview of the final compounds synthesised and their synthetic routes whilst Section 3.2 describes, in detail, the synthetic procedures involved in obtaining and confirming the library of unnatural amino acids, termed "monomers" herein (Figure 3.1), and their characterisation. In this section, the procedures are described for library **a** (racemic library). Section 3.3 discusses the synthetic approaches and the results obtained when assessing the water uptake ability of the monomers and finally, Section 3.4 provides conclusions and the context for the work described in Chapter 4. Spectral data for the described compounds can be found in Appendix A4.

Schemes 3.1 and 3.2 provide a summary of the structures and synthetic strategies used to assess the desired compounds. The structural changes to the β amino acid (reduction and hydroxylation) have an impact on the molecule's lipophilicity/hydrophilicity and it is expected that this will have an influence on the properties of the synthesised compounds.

For ease of discussion throughout this thesis, compounds have been coded with a three or four letter code (chemical names for each compound are given below, section 3.2.9, where the compounds are confirmed through spectroscopic methods) according to the following:

First letter (for 3 and 4 letters code) – here **M** – refers to **M**onomer. In subsequent chapters, a **D**imer will be denoted as **D**, **T**etramer as **T**, **H**examer as **H** and **O**ctamer as **O**.

Second letter (for 3 letters code) – refers to the number of isomers, therefor **M** denotes a **M**ixture of the possible isomers;

Second and third letters (for 4 letters code) – refer to the stereochemistry of the amino and acid groups with respect to one another, therefor **CD** and **CU** denote the stereochemistry of the amine and acid groups (*Cis* **D**own and *C*is **U**p).

Third/fourth letter (3 letters/4 letters code) – refers to the derivatisation on the five membered ring. Therefor **U** denotes **U**nsaturation (double bond), **S** denotes **S**aturation (single bonds) and **H** denotes the presence of **H**ydroxyl groups (–OH).
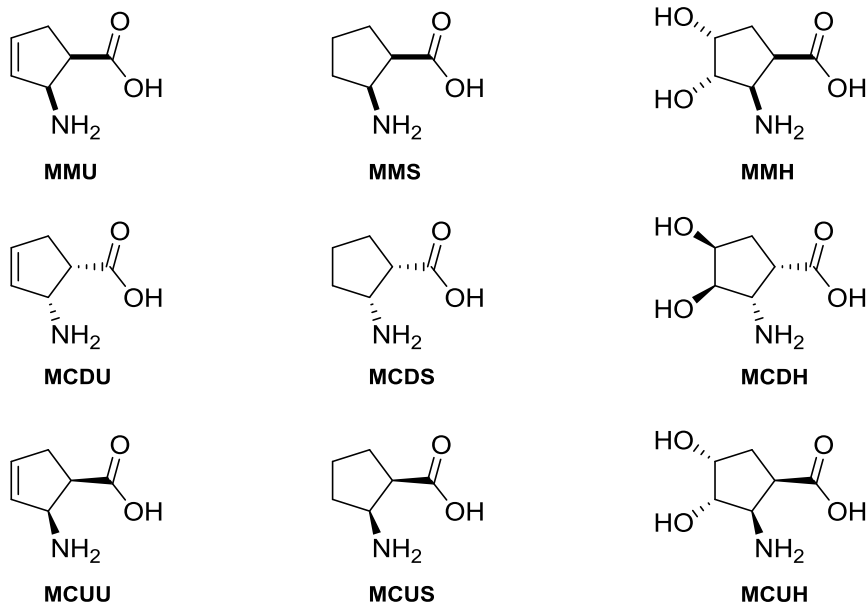
Figure 3.1 Summary of the synthesised monomeric structures.

50

For clarity with schemes, the letter "**a**" refers to mixtures (full and dash bonds, relative stereochemistry), the letter "**b**" denotes enantiomerically pure compound going to the back of the plane (dash bonds) and the letter "**c**" denotes enantiomerically pure compound going up the plane (full bonds). The series of compounds **a**, is drawn using relative stereochemistry; they should always be interpreted as a mixture of the possible isomers.
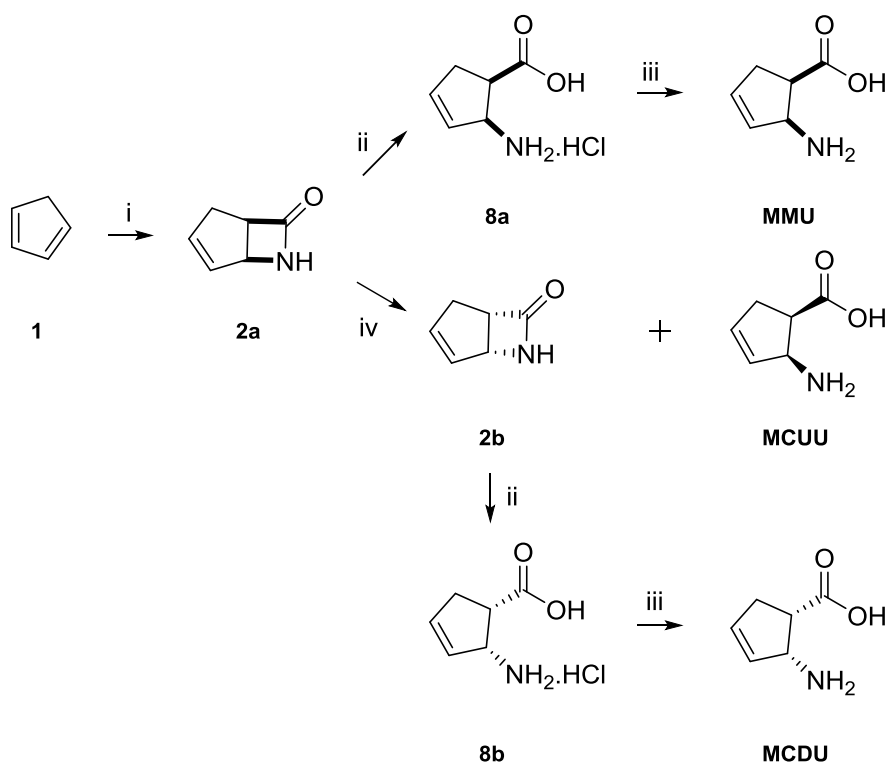
Scheme 3.1 Synthetic route to obtain monomers MMU, MCUU and MCDU. i) Cycloaddition: CSI, Et$_2$O, -20°C; ii) Lactam ring opening: 10% HCl, r.t.; iii) Ion exchange: Dowex®, 2M NH$_4$OH; iv) Enzymatic resolution: Lipase, H$_2$O, MTBE.
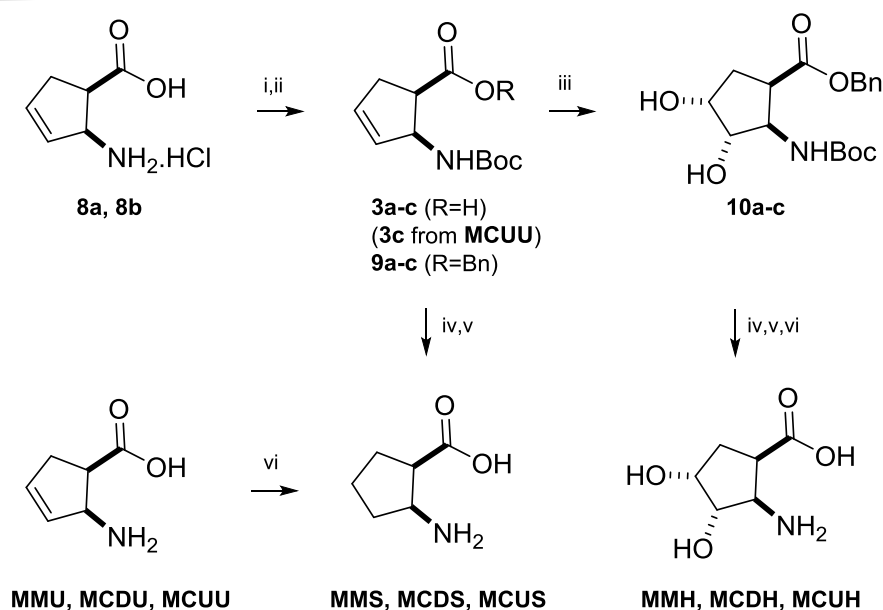
Scheme 3.2 Synthetic route to obtain monomers MMS, MCDS, MCUS, MMH, MCDH and MCUH. i) Protection of the amino group: Boc_2O, Dioxane, Water, 0°C; ii) Protection of the acid group: BnOH, PyBop, DIPEA, DCM, r.t.; iii) Hydroxylation: OsO_4, NMO, Acetone, r.t.; iv) Hydrogenation: H_2, Pd/C, MeOH; v) Amino group deprotection: TFA, DCM, r.t.; vi) Ion exchange: Dowex®, 2M NH_4OH, H_2O.

Note: In addition to the above depicted compounds, L-Alanine is also included in section 3.2 due to its use in Chapter 4 as part of the compounds therein prepared.

3.2 EXPERIMENTAL

3.2.1 CYCLOADDITION

Procedure to synthesise **2a**. A solution of chlorosulfonyl isocyanate (CSI) (6.46 mL, 74.0 mmol) in diethyl ether (Et_2O) was added dropwise to a solution of freshly doubly distilled 1,3-cyclopentadiene (CPD, **1**) (8.74 mL, 104 mmol) in dry Et_2O (150 mL) at -20°C (methanol (MeOH) bath cooled with a cryocooler). After complete addition, the

mixture was left stirring for 40 min. The mixture was then slowly poured into a cold solution (0ºC, ice bath) of Na_2SO_3 (7.60 g, 60.8 mmol) in water (100 mL) and 20% KOH (100mL). After stirring for 45 min at 0ºC, the organic layer was separated, and the aqueous layer extracted with ethyl acetate (EtOAc) (4×150 mL). The combined organic layers were dried over anhydrous Na_2SO_4 and concentrated under reduced pressure. The residue was purified by column chromatography (*n*-hexane: EtOAc, 1:3, R_f = 0.25) to afford 7.66 g (95%) of a light yellow oil, compound **2a** (white waxy solid when frozen).

3.2.2 ENZYMATIC RESOLUTION

Procedure to synthesise **2b** and **MCUU**. Lactam **2a** (5.17 g, 47.4 mmol) was dissolved in methyl *tert*-butyl ether (MTBE) (200 mL) and H_2O (0.85 mL, 47.4 mmol) was added followed by Lipase (10.3 g, 2g/g of substrate) and the mixture was left stirring at room temperature. Monitoring of enzymatic activity was carried out by HPLC. After 72 hours there was no evidence of the presence of (1*R*,5*S*)-6-azabicyclo[3.2.0]hept-3-ene-7-one (**2c**) and the enzyme was filtered and washed with MTBE. The filtrate was concentrated under reduced pressure and the product recrystallized from Et_2O. A crystalline yellowish solid, **2b** (2.53 g, 98%) was obtained. The filtered solid was thoroughly washed with water to separate the enzyme from the free β amino acid (**MCUU**). The water was eliminated under reduced pressure and the obtained solid was recrystallized from water with acetone to afford a light creamy solid, **MCUU** (2.95 g, 98%).

3.2.3 LACTAM RING OPENING

Procedure to synthesise **8a** and **8b**. A solution of **2a** (1.77 g, 12.6 mmol) in 10% HCl (20.0 mL) was stirred at room temperature for 2 hours. The mixture was concentrated to

dryness, dissolved in the minimum amount of hot ethanol (EtOH) and the product was precipitated adding Et$_2$O. The suspension was filtered and dried under suction to afford 2.53 g (95%) of a white shiny powder (**8a**).

3.2.4 PROTECTION OF THE AMINO AND ACID GROUPS

3.2.4.1 Amino Group Protection

Procedure to synthesise **3a-c**. To a solution of 2-aminocyclopent-3-ene-1-carboxylic acid hydrochloride (**8a**) (0.97 g, 5.91 mmol) in dioxane:water (18.0 mL, 2:1), 1M NaOH was added (6.00 mL) at 0°C. Di-*tert*-butyl dicarbonate (Boc$_2$O) (1.42 g, 6.50 mmol) was then added in portions followed by dropwise addition of 1M NaOH until pH 8-9. The mixture was stirred at room temperature for 4 hours. The mixture was then diluted in EtOAc (30 mL) and the layers separated. The aqueous layer was acidified with 10% HCl until the pH dropped to 3-4 and then extracted with EtOAc. The combined organic layers were dried over anhydrous Na$_2$SO4, filtered and concentrated under reduced pressure. A pale-brown solid, **3a**, was obtained and recrystallized using EtOAc/Hexane (1.27g, 94%)

3.2.4.2 Acid Group Protection

Procedure to synthesise **9a-c**. *N,N*-diisopropylethylamine (DIPEA) (1.18 mL, 6.80 mmol) followed by (benzotriazol-1-yloxy)tripyrrolidinophosphonium hexafluorophosphate (PyBop) (1.42 g, 2.72 mmol) were added to a solution of 2-((*tert*-butoxycarbonyl)amino)cyclopent-3-ene-1-carboxylic acid, **3a** (0.52 g, 2.27 mmol) in DCM and left stirring for 15 minutes at room temperature. Benzyl alcohol (BnOH) was added (0.24 mL, 2.27 mmol) and the mixture left stirring for 24 hours. Water was added

and the layers separated. The organic layer was washed with saturated $NaHCO_3$, H_2O and 1M HCl in repetitive cycles until almost or complete elimination of 1-hydroxybenzotriazole (HOBt, a by-product from PyBOP). The organic layer was then dried over anhydrous Na_2SO_4, filtered and concentrated under reduced pressure. The crude was purified by column chromatography (CC) and eluted with Hexane:EtOAc (1:1, v/v) to afford 0.46 g (64%), Rf = 0.6 (Hexane:EtOAc, 3:1), of a white solid, **9a**.

3.2.5 HYDROXYLATION

Procedure to synthesise **10a-c**. 0.45g (1.42 mmol) of **9a** were dissolved in acetone (10 mL), *N*-methylmorpholine *N*-oxide (NMO) (0.50 g, 4.25 mmol) and OsO_4 (0.14 mL, 2.5 wt% in ^{t}BuOH) were added and left stirring at room temperature for 2 hours. The reaction was monitored by TLC (product's Rf = 0.42 in Hexane:EtOAc, 1:3). The mixture was filtered over celite and silica and washed with acetone. After reduced pressure concentration, the resulting crude was taken into EtOAc and crystallized in hexane to obtain 0.32 g (64%) of a white solid, **10a**.

3.2.6 ORTHOGONAL DEPROTECTION OF THE AMINO AND ACID GROUPS

Procedure to synthesise monomers **MMU**, **MCDU**, **MMH**, **MCDH** and **MCUH**

3.2.6.1 Acid group deprotection

Benzyl 2-((*tert*-butoxycarbonyl)amino)cyclopent-3-ene-1-carboxylate, **10a**, (0.47 g, 1.48 mmol) was dissolved in MeOH (10 mL) and Palladium on Carbon (Pd/C) was added (catalytic amount). The flask was sealed with a septum and H_2 (1 atm) was attached in a balloon. The mixture was left stirring at room temperature and controlled

by TLC. After 4 hours, the mixture was filtered over celite and silica, concentrated under reduced pressure and the resulting crude was used in the next step with no further purification.

3.2.6.2 Amino group deprotection

Trifluoroacetic acid (TFA) (30.0 eq) was slowly added to a solution of Boc protected compound (from previous step – acid group deprotection) in DCM at 0ºC. The mixture was left stirring at room temperature for up to 8h. The excess of acid was eliminated under reduced pressure and the product precipitated with Et_2O. The product was analysed by NMR to confirm the absence of the Boc group and then taken to the next step.

3.2.7 ION EXCHANGE

2-aminocyclopent-3-ene-1-carboxylic acid hydrochloride[c], **8a**, (0.51 g, 3.12 mmol) was dissolved in the minimum amount of 0.1M HCl solution and loaded into a column packed with Dowex® 50WX8 hydrogen form (previously rinsed with water) and eluted with 2M ammonia solution. The column was then rinsed with water to dissolve any remaining product. The solvent was eliminated under reduced pressure and the residue dissolved in the minimum amount of water. Acetone was added to precipitate the product (**MMU**) as a white solid; after filtration 0.36 g (90%) were obtained.

---

[c] For compound **MCDU**, the starting material was the trifluoroacetate salt.

3.2.8 PRECURSORS CHARACTERISATION
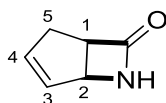
6-azabicyclo[3.2.0]hept-3-en-7-one (2a). **Yield** 95%. **^{1}H NMR** (400 MHz, CDCl$_3$): δ 2.44 (dd, J = 18.0 Hz, J = 10.4 Hz, 1H, H$_5$), 2.71 (dt, J = 18.4 Hz, J = 2.4 Hz, 1H, H$_5$), 3.82 (d, J = 10.4 Hz, 1H, H$_1$), 4.39-4.45 (m, 1H, H$_2$), 5.83-5.88 (m, 1H, H$_4$), 5.90-5.97 (m, 1H, H$_3$), 6.94 (br.s, 1H, NH). **^{13}C NMR** (100 MHz, CDCl$_3$): 30.9 (C$_5$), 53.4 (C$_1$), 59.4 (C$_2$), 130.9 (C$_4$), 137.2 (C$_3$), 172.5 (C=O). **IR** (ν, cm^{-1}): 3211, 2975, 2924, 2907, 2842, 1726, 1602, 1437, 1353, 1315, 1256, 1183, 1128, 1054, 1012. **HRMS** (ESI, MeOH) calculated for C$_9$H$_9$NO: 109.0528, found M+H: 110.0603.

(1S,5R)-6-azabicyclo[3.2.0]hept-3-ene-7-one (2b). **Yield** 98%. **mp** 74-76°C (lit.[85] 76-77°C). **^{1}H NMR** (400 MHz, CDCl$_3$): δ 2.42 (dd, J = 18.4 Hz, J = 10.4 Hz ,1H, H$_5$), 2.67 (dt, J = 18.4 Hz, J = 2.4 Hz, 1H, H$_5$), 3.79 (d, J = 10.4 Hz, 1H, H$_1$), 4.47 (s, 1H, H$_2$), 5.87-5.94 (m, 1H, H$_4$), 5.95-6.02 (m, 1H, H$_3$), 6.64 (br.s, 1H, NH). **^{13}C NMR** (100 MHz, CDCl$_3$): 30.9 (C$_2$), 53.3 (C$_1$), 59.4 (C$_5$), 130.7 (C$_3$), 137.1 (C$_4$), 172.6 (C=O). **HPLC** trace: 15 min (^{i}PA:Hexane, 5:95, v/v). $[\alpha]_D^{20}$ - 31.4, c = 0.01 g.mL^{-1} in CHCl$_3$ (lit.[85] $[\alpha]_D^{25}$ - 34.8, c = 0.45, CHCl$_3$). **IR** (ν, cm^{-1}): 3270, 3057, 2922, 2846, 1725, 1645, 1552, 1435, 1377, 1349, 1312, 1270, 1228, 1180, 1128, 1087, 1054, 1014. **HRMS** (ESI, MeOH) calculated for C$_6$H$_7$NO: 109.0528, found M$^+$: 110.0600.
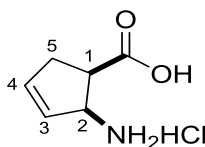
2-aminocyclopent-3-ene-1-carboxylic acid hydrochloride (8a). **Yield** 95%. **mp** 165-168°C (lit.[86] 178-180°C). **^{1}H NMR** (400 MHz, D_2O): δ 2.71-2.85 (m, 2H, H_5), 3.54 (q, J = 8.4 Hz, 1H, H_1), 4.46 (d, J = 7.6 Hz, 1H, H_2), 5.83 (dd, J = 8.0 Hz, J = 2.2 Hz, 1H, H_4), 6.24-6.32 (m, 1H, H_3). **^{13}C NMR** (100 MHz, D_2O): 34.2 (C_5), 43.5 (C_2), 55.9 (C_1), 125.9 (C_4), 138.7 (C_3), 175.3 (C=O). **IR** (ν, cm^{-1}): 3331, 3234, 2903, 1703, 1699, 1651, 1615, 1568, 1488, 1440, 1407, 1378, 1337, 1291, 1260, 1166, 1132, 1113, 1100, 1071, 1017. **HRMS** (ESI, H_2O) calculated for $C_9H_9NO_2$: 127.0633, found M+H: 128.0702.
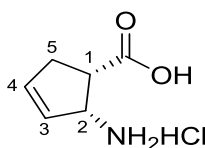
(1S,2R)-2-aminocyclopent-3-ene-1-carboxylic acid hydrochloride (8b). **Yield** 83%. **mp** 169-171°C. **^{1}H NMR** (400 MHz, D_2O): δ 2.64-2.89 (m, 2H, H_5), 3.54 (q, J = 8.4 Hz, 1H, H_1), 4.46 (d, J = 7.2 Hz, 1H, H_2), 5.77-5.86 (m, 1H, H_4), 6.26 (t, J = 2.8 Hz, 1H, H_3). **^{13}C NMR** (100 MHz, D_2O): 34.2 (C_5), 43.5 (C_1), 55.9 (C_2), 125.9 (C_4), 138.7 (C_3), 175.3 (C=O). $[\alpha]_D^{20}$ - 80.6, c = 0.01 g.mL^{-1} in H_2O (lit.[85] $[\alpha]_D^{25}$ - 80.2, c = 0.30, H_2O). **IR** (ν, cm^{-1}): 3351, 2974, 2936, 2898, 1798, 1739, 1711, 1686, 1517, 1443, 1388, 1364, 1342, 1326, 1274, 1241, 1166, 1065, 1039, 1022, 1011. **HRMS** (ESI, H_2O) calculated for $C_6H_{10}NO_2$: 127.0633, found M+H: 128.0706.
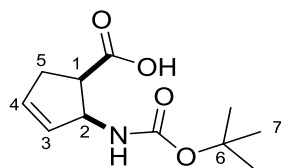
2-((*tert*-butoxycarbonyl)amino)cyclopent-3-ene-1-carboxylic acid (3a). **Yield** 94%.

mp 107-114ºC (lit.[86]134-137ºC). **^{1}H NMR** (400 MHz, DMSO): δ 1.35 (s, 9H, H_7),

2.25-2.36 (m, 1H, H_5), 2.65-2.75 (m, 1H, H_5), 3.14 (q, J = 8.0, 1H, H_1), 4.79-4.87 (m,

1H,H_2), 5.52 (d, J = 3.1, 1H, H_3), 5.80-5.86 (m, 1H, H_4), 6.61 (d, J = 9.5, 1H, NH),

12.02 (s, 1H, COOH). **^{13}C NMR** (100 MHz, DMSO): 28.3 (3xC_7), 33.5 (C_5), 46.2 (C_2),

56.7 (C_1), 77.6 (C_6)), 129.7 (C_4), 132.6 (C_3), 154.7 (C=O, NHCO), 173.4 (C=O). **IR** (ν,

cm^{-1}): 3301, 2977, 2522, 1708, 1699, 1682, 1651, 1644, 1634, 1475, 1450, 1397, 1366,

1284, 1241, 1233, 1208, 1160, 1126, 1107, 1041, 1024. **HRMS** (ESI, MeOH)

calculated for $C_{11}H_{17}NO_4$: 227.1158, found M+Na: 250.1050.
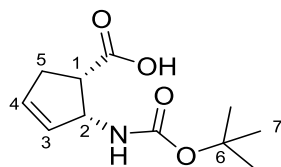
(1*S*,2*R*)-2-((*tert*-butoxycarbonyl)amino)cyclopent-3-ene-1-carboxylic acid (3b).

Yield 95%. **mp** 128-132ºC. **^{1}H NMR** (400 MHz, DMSO): δ 1.32 (s, 9H, H_7), 2.15-2.39

(m, 1H, H_5), 2.62-2.83 (m, 1H, H_5), 3.29 (q, J = 8.4 Hz, 1H, H_1), 4.96 (t, J = 8.8 Hz, 1H,

H_2), 5.46-5.63 (m, 1H, H_3), 5.78-5.92 (m, 1H, H_4), 7.02 (d, J = 9.6 Hz, 1H, NH), 12.03

(s, 1H, COOH). **^{13}C NMR** (100 MHz, DMSO): 28.1 (C_7), 33.5 (C_5), 47.3 (C_2), 56.7

(C_1), 77.6 (C_6), 129.7 (C_4), 132.6 (C_3), 154.7 (C=O, NHCO), 173.4 (C=O). $[\alpha]_D^{20}$ -

42.0, c = 0.01 g.mL^{-1} in CHCl$_3$. **IR** (ν, cm^{-1}): 3351, 3071, 2975, 2936, 2998, 2839,

2160, 1798, 1739, 1687, 1516, 1466, 1443, 1387, 1364, 1342, 1325, 1274, 1241, 1165,

1064, 1039, 1021, 1011. **HRMS** (ESI, MeOH) calculated for $C_{11}H_{17}NO_4$: 227.1158, found M+Na: 250.1048.
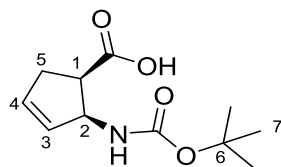
(1R,2S)-2-((*tert*-butoxycarbonyl)amino)cyclopent-3-ene-1-carboxylic acid (3c).

Yield 93%. **mp** 146-150ºC. **¹H NMR** (400 MHz, DMSO): δ 1.36 (s, 9H, H_7), 2.26-2.37 (m, 1H, $H_{5, anti}$), 3.63-2.77 (m, 1H, $H_{5, syn}$), 3.08-3.19 (m, 1H, H_1), 4.77-4.89 (m, 1H, H_2), 5.47-5.59 (d, J = 3.2 Hz, 1H, H_3), 5.78-5.88 (m, 1H, H_2), 6.61 (d, J = 9.6 Hz, 1H, NH), 12.02 (s, 1H, COOH). **¹³C NMR** (100 MHz, DMSO): 28.3 (3xC_7), 33.5 (C_5), 46.2 (C_2), 56.7 (C_1), 77.6 (C_6), 129.8 (C_4), 132.6 (C_3), 154.8 (C=O, NHCO), 173.4 (C=O). $[\alpha]_D^{20}$ + 109, c = 0.01 g.mL⁻¹ in CHCl₃. **IR** (ν, cm⁻¹): 3345, 2974, 2928, 1732, 1687, 1645, 1515, 1449, 1390, 1365, 1332, 1313, 1285, 1241, 1210, 1164, 1046, 1025. **HRMS** (ESI, MeOH) calculated for $C_{11}H_{17}NO_4$: 227.1158, found M+Na: 250.1048.
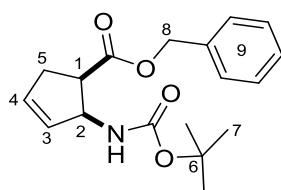
Benzyl 2-((*tert*-butoxycarbonyl)amino)-3-ene-1-carboxylate (9a). **Yield** 56%, **Rf** 0.60 (Hex:EtOAc, 3:1). **¹H NMR** (400 MHz, CDCl₃): δ 1.41 (s, 9H, H_7), 2.45-2.55 (m, 1H, H_5), 2.77-2.88 (m, 1H, H_5), 3.32-3.48 (m, 1H, H_1), 4.71 (d, J = 9.2 Hz, 1H, NH), 4.98 (d, J = 12.4 Hz, 1H, H_8), 5.04-5.16 (m, 1H, H_2), 5.22 (d, J = 12.4 Hz, 1H, H_8), 5.56-5.69 (m, 1H, H_4), 5.84-5.96 (m, 1H, H_3), 7.30-7.44 (m, 5H, H_9). **¹³C NMR** (100

MHz, CDCl$_3$): 28.5 (C$_7$), 34.6 (C$_5$), 46.3 (C$_1$), 57.8 (C$_2$), 66.8 (C$_8$), 79.6 (C$_6$), 128.3 (C$_7$), 128.4 (C$_9$), 128.7 (C$_9$) 130.1 (C$_4$), 133.2 (C$_3$), 155.0 (C=O, NHCO), 173.1 (C=O). **IR** (ν, cm^{-1}): 3365, 2919, 2850, 1719, 1703, 1498, 1453, 1390, 1365, 1356, 1333, 1287, 1250, 1155, 1070, 1047, 1025. **HRMS** (ESI, MeOH) calculated for C$_{18}$H$_{23}$NO$_4$: 317.1627, found M+Na: 340.1515.
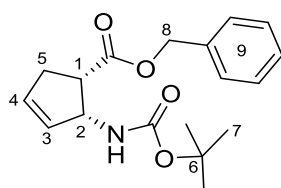
Benzyl (1*S*,2*R*)-2-((*tert*-butoxycarbonyl)amino)cyclopent-3-ene-1-carboxylate (9b).

Yield 94%. **Rf** 0.60 (Hex:EtOAc, 3:1). **^{1}H NMR** (400 MHz, CDCl$_3$): δ 1.41 (s, 9H, H$_7$), 2.42-2.57 (m, 1H, H$_5$), 2.73-2.91 (m, 1H, H$_5$), 3.40 (q, *J* = 8.0 Hz, 1H, H$_1$), 4.70 (d, *J* = 8.4 Hz, 1H, NH), 4.98 (d, *J* = 12.4 Hz, 1H, H$_8$), 5.03-5.14 (m, 1H, H$_2$), 5.22 (d, *J* = 12.4, 1H, H$_8$), 5.57-5.67 (m, 1H, H$_4$), 5.85-5.95 (m, 1H, H$_3$), 7.28-7.43 (m, 5H, H$_9$). **^{13}C NMR** (100 MHz, CDCl$_3$): 28.5 (C$_7$), 34.6 (C$_5$), 46.3 (C$_1$), 57.8 (C$_2$), 66.8 (C$_8$), 79.6 (C$_6$), 128.3 (C$_9$), 128.4 (C$_9$), 128.7 (C$_9$) 130.0 (C$_9$), 133.2 (C$_4$), 135.9 (C$_3$), 155.0 (C=O, NH*C*O), 173.2 (C=O). **IR** (ν, cm^{-1}): 3367, 2972, 1704, 1618, 1497, 1454, 1309, 1365, 1355, 1333, 1287, 1248, 1153, 1046, 1025. **HRMS** (ESI, MeOH) calculated for C$_{18}$H$_{23}$NO$_4$: 317.1627, found M+Na: 340.1510.
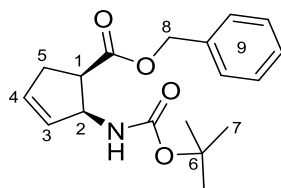
Benzyl (1*R*,2*S*)-2-((*tert*-butoxycarbonyl)amino)cyclopent-3-ene-1-carboxylate (9c).

Yield 67%. **Rf** 0.60 (Hex:EtOAc, 3:1). **mp** 200-208°C. **^{1}H NMR** (400 MHz, CDCl$_3$): δ

1.41 (s, 9H, H$_8$), 2.47-2.54 (m, 1H, H$_{5anti}$), 2.78-2.86 (m, 1H, H$_{5syn}$), 3.37-3.43 (m, 1H,

H$_1$), 4.71 (d, *J* = 9.2 Hz, 1H, N*H*), 4.98 (d, *J*=12.4, 1H, H$_8$), 5.07-5.14 (m, 1H, H$_2$), 5.21

(d, *J* = 12.4 Hz, 1H, H$_8$), 5.61-5.64 (m, 1H, H$_4$), 5.88-5.91 (m, 1H, H$_3$), 7.33-7.39 (m,

5H, H$_9$). **^{13}C NMR** (100 MHz, CDCl$_3$): 28.5 (C$_7$), 34.6 (C$_5$), 46.3 (C$_1$), 57.8 (C$_2$), 66.8

(C$_8$), 79.6 (C$_6$), 128.4 (C$_9$), 128.7 (C$_9$) 130.0 (C$_9$), 133.2 (C$_4$), 135.9 (C$_3$), 155.0 (C=O,

NH*C*O), 173.2 (C=O). $[\alpha]_D^{20}$ + 32.8, *c* = 0.01 g.mL^{-1} in CHCl$_3$. **IR** (ν, cm^{-1}): 3366,

2975, 1709, 1495, 1454, 1389, 1365, 1352, 1238, 1153, 1045, 1024. **HRMS** (ESI,

MeOH) calculated for C$_{18}$H$_{23}$NO$_4$: 317.1627, found M+Na: 340.1522.
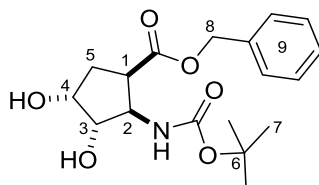
Benzyl 2-((*tert*-butoxycarbonyl)amino)-3,4-dihydroxycyclopentane-1-carboxylate

(10a). Yield 65%. **mp** 182-187°C. **^{1}H NMR** (400 MHz, CDCl$_3$): δ 1.42 (s, 9H, H$_7$),

1.53-1.74 (br.s, 1H, OH), 2.01-2.30 (m, 2H, H$_5$), 2.80 (br.s, 1H, OH), 3.23-3.49 (m, 1H,

H$_1$), 3.92-4.06 (m, 1H, H$_4$), 4.09-4.34 (m, 2H, H$_3$ and H$_2$), 5.14 (s, 2H, H$_8$), 5.51 (br.s,

1H, NH), 7.29-7.41 (m, 5H, H$_9$). **^{13}C NMR** (100 MHz, CDCl$_3$): 28.4 (C$_7$), 34.1 (C$_5$),

41.8 (C$_1$), 56.9 (C$_4$), 67.1 (C$_8$), 70.2 (C$_3$), 80.7 (C$_2$), 84.5 (C$_6$), 128.4 (C$_9$), 128.8 (C$_9$),

156.1 (C=O, NHCO), 174.2 (C=O). **IR** (ν, cm^{-1}): 3412, 3351, 2980, 2928, 1718, 1679, 1518, 1456, 1402, 1392, 1363, 1322, 1283, 1239, 1216, 1195, 1178, 1162, 1109, 1080, 1063, 1047, 1021. **HRMS** (ESI, MeOH) calculated for $C_{18}H_{25}NO_6$: 351.1682, found M+Na: 374.1575.
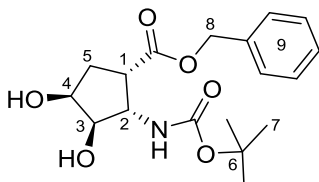
Benzyl (1*S*,2*S*,3*R*,4*S*)-2-((*tert*-butoxycarbonyl)amino)-3,4.dihydroxycyclopentane-1-carboxylate (10b). **Yield** 90%. **mp** 181-189°C. **^{1}H NMR** (400 MHz, CDCl$_3$): δ 1.42 (s, 9H, H$_7$), 1.68 (br.s, 2H, OH), 2.10 (dd, J = 14.0 Hz, J = 9.6 Hz, 1H, H$_5$), 2.22 (dt, J = 14.4 Hz, J = 5.6 Hz 1H, H$_5$), 3.35 (td, J = 8.8 Hz, J = 6.4 Hz, 1H, H$_1$), 4.00 (dd, J = 8.8 Hz, J = 4.8 Hz m, 1H, H$_4$), 4.08-4.25 (m, 2H, H$_3$ and H$_2$), 5.14 (s, 2H, H$_8$), 5.50 (br.s, 1H, NH), 7.29-7.43 (m, 5H, H$_9$). **^{13}C NMR** (100 MHz, CDCl$_3$): 28.4 (C$_7$), 33.9 (C$_5$), 42.0 (C$_1$), 56.9 (C$_4$), 67.1 (C$_8$), 70.2 (C$_3$), 79.0 (C$_2$), 80.6 (C$_6$), 128.2 (C$_9$), 128.4 (C$_9$), 128.7 (C$_9$), 128.8 (C$_9$), 153.2 (C=O, NHCO), 174.2 (C=O). **IR** (ν, cm^{-1}): 3408, 3350, 2980, 2929, 1719, 1681, 1515, 1455, 1391, 1364, 1319, 1283, 1239, 1216, 1195, 1161, 1112, 1089, 1045, 1021. **HRMS** (ESI, MeOH) calculated for $C_{18}H_{25}NO_6$: 351.1682, found M+Na: 374.1564.
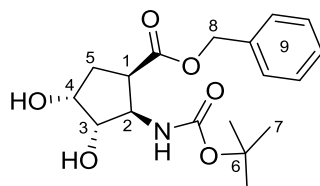
Benzyl (1R,2R,3S,4R)-2-((tert-butoxycarbonyl)amino)-3,4-dihydroxycyclopentane-1-carboxylate (10c). Yield 90%. **mp** 183-190ºC. **¹H NMR** (400 MHz, CDCl₃): δ 1.43 (s, 9H, H₇), 2.0 (dd, J = 14.8 Hz, J = 9.2 Hz, 1H, H₅), 2.24 (dt, J = 14.8 Hz, J = 6.0 Hz, 1H, H₅), 2.73 (br.s, 1H, OH), 3.35 (td, J = 9.2 Hz, J = 6.4 Hz, 1H, H₁), 4.00 (dd, J = 8.4 Hz, J = 4.8 Hz, 1H, H₄), 4.15-4.21 (m, 3H, H₃, H₂ and OH), 5.14 (s, 2H, H₈), 5.52 (br.s, 1H, NH), 7.33-7.38 (m, 5H, H₉). **¹³C NMR** (100 MHz, CDCl₃): 28.4 (C₇), 33.5 (C₅), 41.8 (C₁), 56.7 (C₄), 66.9 (C₈), 70.1 (C₃), 78.9 (C₂), 128.4 (C₉), 173.8 (C=O). **IR** (ν, cm⁻¹): 3349, 2980, 2928, 1719, 1681, 1517, 1457, 1391, 1363, 1319, 1284, 1239, 1216, 1197, 1175, 1162, 1113, 1089, 1062, 1045, 1021. **HRMS** (ESI, MeOH) calculated for $C_{18}H_{25}NO_6$: 351.1682, found M+Na: 374.1564.

3.2.9 MONOMERS CHARACTERISATION
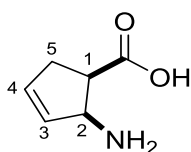
2-aminocyclopent-3-ene-1-carboxylic acid (MMU). Yield 91%. **mp** 160-165ºC. **¹H NMR** (400 MHz, D₂O): δ 2.59 (ddd, J = 17.2 Hz, J = 8.4 Hz, J = 2.0 Hz, 1H, H₅), 2.73 (ddt, J = 17.2 Hz, J = 8.8 Hz, J = 2.0 Hz, 1H, H₅), 3.29 (q, J = 8.4 Hz, 1H, H₁), 4.25-4.36 (m, 1H, H₂), 5.75-5.89 (m, 1H, H₄), 6.16-6.34 (m, 1H, H₃). **¹³C NMR** (100 MHz,

D_2O): 34.9 (C_5), 45.6 (C_1), 56.0 (C_2), 126.4 (C_4), 139.3 (C_3), 179.4 (C=O). **IR** (ν, cm^{-1}):

2850, 2686, 2589, 2164, 1615, 1591, 1562, 1458, 1370, 1335, 1274, 1251, 1177, 1150,

1088, 1097, 1022. **HRMS** (ESI, H_2O) calculated for $C_6H_9NO_2$: 127.0633, found M+Na:

150.0524.
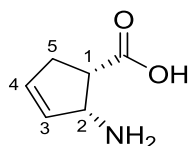
(1*S*,2*R*)-aminocyclopent-3-ene-1-carboxylic acid (MCDU). Yield 85%. **mp** 173-

175ºC. **^{1}H NMR** (400 MHz, D_2O): δ 2.59 (ddd, *J* = 17.2 Hz, *J* = 8.0 Hz, *J* = 2.0 Hz, 1H,

H_5), 2.72 (ddt, *J* = 17.2 Hz, *J* = 9.2 Hz, *J* = 2.0 Hz, 1H, H_5), 3.29 (q, *J* = 8.4 Hz, 1H,

H_1), 4.30 (d, *J* = 7.6 Hz, 1H, H_2), 5.82 (dd, *J* = 6.0 Hz, *J* = 2.4 Hz, 1H, H_4), 6.26 (t, *J* =

2.8 Hz, 1H, H_3). **^{13}C NMR** (100 MHz, D_2O): 35.0 (C_5), 45.5 (C_1), 56.3 (C_2), 126.3 (C_4),

139.3 (C_3), 179.4 (C=O). $[\alpha]_D^{20}$ - 77.3, *c* = 0.01 g.mL^{-1}in H_2O. **IR** (ν, cm^{-1}): 3144,

2851, 2112, 1975, 1610, 1557, 1442, 1385, 1340, 1294, 1268, 1183, 1135, 1071, 1022,

1007. **HRMS** (ESI, H_2O) calculated for $C_6H_9NO_2$: 127.0633, found M+H: 128.0706.
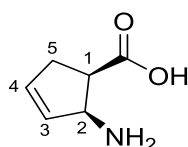
(1*R*,2*S*)-2-aminocyclopent-3-ene-1-carboxylic acid (MCUU). Yield 98%. **mp** 207-

210ºC, (lit.[85] > 240ºC). **^{1}H NMR** (400 MHz, D_2O): δ 2.59 (ddd, *J* = 17.2 Hz, *J* = 8.0 Hz,

J = 2.0 Hz, 1H, H_5), 2.73 (ddt, *J* = 17.2 Hz, *J* = 9.2 Hz, *J* = 2.4 Hz, 1H, H_5), 3.29 (q, *J* =

8.4 Hz, 1H, H_1), 4.30 (d, *J* = 7.6 Hz, 1H, H_2), 5.82 (dd, *J* = 6.0 Hz, *J* = 2.0 Hz, 1H, H_4),

6.26 (t, *J* = 2.8 Hz, 1H, H_3). **^{13}C NMR** (100 MHz, D_2O): 34.9 (C_5), 45.7 (C_1), 56.1 (C_2),

126.4 (C$_4$), 139.2 (C$_3$), 179.5 (C=O). $[\alpha]_D^{20}$ + 95.0, c = 0.01 g.mL^{-1} in H$_2$O (lit.[85] $[\alpha]_D^{25}$ + 96.7, c = 0.30 in H$_2$O). **IR** (ν, cm^{-1}): 2594, 2160, 1593, 1562, 1459, 1370, 1335, 1275, 1178, 1150, 1087, 1022. **HRMS** (ESI, H$_2$O) calculated for C$_6$H$_9$NO$_2$: 127.0633, found M+H: 128.0703.
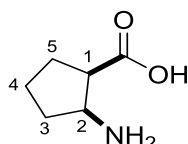
2-aminocyclopentane-1-carboxylic acid (MMS). Yield 70%. **mp** 204-210ºC. **^{1}H NMR** (400 MHz, D$_2$O): δ 1.55-189 (m, 4H, H$_5$ and H$_4$), 1.90-2.17 (m, 2H, H$_3$), 2.80 (q, J = 6.8 Hz, 1H, H$_1$), 3.56-3.81 (m, 1H, H$_2$). **^{13}C NMR** (100 MHz, D$_2$O): 21.2 (C$_4$), 27.9 (C$_3$), 29.4 (C$_5$), 47.6 (C$_1$), 52.9 (C$_2$), 180.9 (C=O). **IR** (ν, cm^{-1}): 2914, 2657, 2160, 1621, 1573, 1504, 1459, 1436, 1409, 1385, 1336, 1310, 1197, 1180, 1122, 1073. **HRMS** (ESI, H$_2$O) calculated for C$_6$H$_{11}$NO$_2$: 129.0790, found M+H: 130.0860.
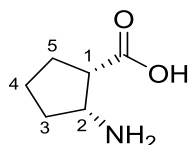
(1S,2R)-2-aminocyclopentane-1-carboxylic acid (MCDS). Yield 95%, over three steps. **mp** 209-213ºC. **^{1}H NMR** (400 MHz, D$_2$O): δ 1.62-1.89 (m, 4H, H$_3$ H$_5$ and 2xH$_4$), 1.96-2.15 (m, 2H, H$_3$ and H$_5$), 2.84 (ddd, J = 16.8 Hz, J = 8.4 Hz, J = 6.4 Hz, 1H, H$_1$), 3.70 (ddd, J = 13.6 Hz, J = 6.8 Hz, J = 4.8 Hz, 1H, H$_2$). **^{13}C NMR** (100 MHz, D$_2$O): 21.2 (C$_4$), 27.9 (C$_3$), 29.4 (C$_5$), 47.5 (C$_1$), 52.9 (C$_2$), 180.9 (C=O). **IR** (ν, cm^{-1}): 2934, 2195, 1644, 1520, 1463, 1438, 1407, 1377, 1333, 1319, 1305, 1287, 1208, 1165, 1114,

1071, 1025, 1006. **HRMS** (ESI, H_2O) calculated for $C_6H_9NO_2$: 129.0790, found M+H: 130.0860.
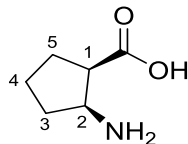
(1R,2S)-2-aminocyclopentane-1-carboxylic acid (MCUS). Yield 99%. **mp** 203-206ºC. **^{1}H NMR** (400 MHz, D_2O): δ 1.57-1.90 (m, 4H, H_3, H_5 and 2xH_4), 1.96-2.14 (m, 2H, H_3 and H_5), 2.84 (q, J = 6.8 Hz, 1H, H_1), 3.70 (q, J = 6.4 Hz, 1H, H_2). **^{13}C NMR** (100 MHz, D_2O): 21.2 (C_4),27.9 (C_3), 29.4 (C_5), 47.6 (C_1), 52.9 (C_2), 180.9 (C=O). **IR** (ν, cm^{-1}): 2936, 2361, 2182, 2169, 2142, 2047, 2027, 2019, 2001, 1968, 1957, 1942, 1540, 1463, 1438, 1410, 1377, 1333, 1319, 1305, 1287, 1165, 1114, 1071. **HRMS** (ESI, H_2O) calculated for $C_6H_{11}NO_2$: 129.0790, found M+H: 130.0860.
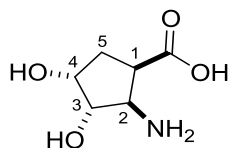
2-amino-3,4-dihydroxycyclopentane-1-carboxylic acid (MMH). Yield 62%, over 3 steps. **mp** 203-207ºC. (lit.[87] 230-232ºC). **^{1}H NMR** (400 MHz, D_2O): δ 2.12 (ddd, J = 14.8 Hz, J = 9.6 Hz, J = 2.0 Hz, 1H, H_5), 2.20 (dt, J = 14.8 Hz, J = 6.0 Hz, 1H, H_5), 3.09 (dt, J = 15.6 Hz, J = 6.4 Hz, 1H, H_1), 3.57 (t, J = 9.2 Hz, 1H, H_2), 4.15 (td, J = 5.2 Hz, J = 2.4 Hz, 1H, H_4), 4.19 (dd, J = 8.8 Hz, J = 4.8 Hz, 1H, H_3). **^{13}C NMR** (100 MHz, $CDCl_3$): 34.7 (C_5), 40.5 (C_1), 55.0 (C_2), 69.5 (C_4), 75.0 (C_3), 180.2 (C=O). **IR** (ν, cm^{-1}):3302, 3209, 3074, 2862, 1644, 1570, 1484, 1391, 1374, 1355, 1324, 1302, 1248,

1226, 1158, 1141, 1114, 1079, 1026. **HRMS** (ESI, H_2O) calculated for $C_6H_{11}NO_4$: 161.0688, found M+H: 162.0759.
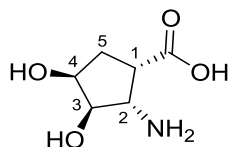
(1S,2S,3R,4S)-2-amino-3,4-dihydroxycyclopentane-1-carboxylic acid (MCDH).

Yield 95%, over 3 steps. **mp** 192-196ºC. **^{1}H NMR** (400 MHz, D_2O): δ 2.14 (ddd, J = 12.0 Hz, J = 9.6 Hz, J = 2.4 Hz, 1H, H_5), 2.22 (dt, J = 11.6 Hz, J = 6.0 Hz, 1H, H_5), 3.11 (dt, J = 9.2 Hz, J = 6.4 Hz, 1H, H_1), 3.60 (t, J = 8.8 Hz, 1H, H_2), 4.17 (td, J = 5.6 Hz, J = 2.4 Hz, 1H, H_4), 4.21 (dd, J = 9.2 Hz, J = 5.2 Hz, 1H, H_3). **^{13}C NMR** (100 MHz, $CDCl_3$): 35.0 (C_5), 40.3 (C_1), 55.1 (C_2), 69.7 (C_4), 75.1 (C_3), 180.4 (C=O). $[\alpha]_D^{20}$ + 87.6, c = 0.01 g.mL^{-1} in H_2O. **IR** (ν, cm^{-1}): 2188, 2160, 2031, 1972, 1605, 1505, 1397, 1354, 1311, 1178, 1104. **HRMS** (ESI, H_2O) calculated for $C_6H_{11}NO_4$: 161.0688, found M+H: 162.0759.
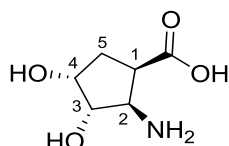
(1R,2R,3S,4R)-2-amino-3,4-dihydroxycyclopentane-1-carboxylic acid (MCUH).

Yield 91%, over 3 steps. **mp** 197-200ºC. **^{1}H NMR** (400 MHz, D_2O): δ 2.14 (ddd, J = 14.8 Hz, J = 9.6 Hz, J = 2.4 Hz, 1H, H_5), 2.22 (dt, J = 15.2 Hz, J = 6.0 Hz, 1H, H_5), 3.11 (dt, J = 15.6 Hz, J = 6.4 Hz, 1H, H_1), 3.57 (t, J = 8.8 Hz, 1H, H_2), 4.17 (td, J = 5.2 Hz, J = 2.4 Hz, 1H, H_4), 4.21 (dd, J = 9.2 Hz, J = 4.8 Hz, 1H, H_3). **^{13}C NMR** (100 MHz, $CDCl_3$): 34.8 (C_5), 40.5 (C_1), 55.0 (C_2), 69.5 (C_4), 75.0 (C_3), 180.2 (C=O). $[\alpha]_D^{20}$ - 104,

$c = 0.01$ g.mL^{-1} in H$_2$O. **IR** (ν, cm^{-1}): 2189, 2150, 2136, 2066, 2036, 1607, 1506, 1396, 1355, 1311, 1178, 1125. **HRMS** (ESI, H$_2$O) calculated for C$_6$H$_{11}$NO$_4$: 161.0688, found M+H: 162.0759.
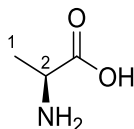
_L_-alanine (L-Ala): L-Alanine was synthesised _via_ hydrogenation from commercially available L-Alanine _O_Bn. Yield 90%. **mp** 220-223ºC. **^{1}H NMR** (400 MHz, D$_2$O): δ 1.44 (d, _J_ = 7.2 Hz, 3H, H$_1$), 3.75 (q, _J_ = 7.2 Hz, 1H, H$_2$). **^{13}C NMR** (100 MHz, D$_2$O): 16.2 (C$_1$), 50.5 (C$_2$), 175.8 (C=O). **IR** (ν, cm^{-1}): 3037, 2807, 2600, 1759, 1615, 1588, 1519, 1453, 1408, 1360, 1305, 1236, 1151, 1113, 1013. **HRMS** (ESI, H$_2$O) calculated for C$_3$H$_7$NO$_2$: 89.0940, found M+H: 90.0545.

3.3 RESULTS AND DISCUSSION

3.3.1 SYNTHESIS OF THE UNSATURATED, SATURATED AND HYDROXYLATED MONOMERS AS A MIXTURE OF TWO ENANTIOMERS.

The unnatural β amino acids were synthesised according to the synthetic route described in this section. The key amino acid **8a** (Scheme 3.3) was obtained _via_ a cycloaddition followed by acid hydrolysis of lactam **2a**.
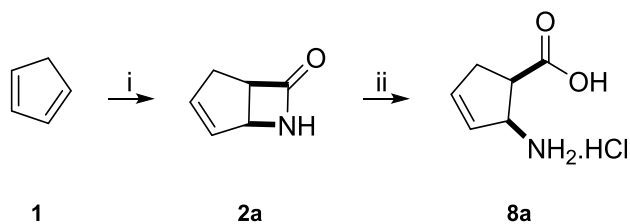
Scheme 3.3 Synthetic route to obtain precursor 8a. i) CSI, Et$_2$O, -20ºC; ii) 10% HCl, r.t.

Compound **2a** was synthesised adding CPD to an isocyanate. It has been reported that this reaction's yield is solvent dependent and the product is reaction time and temperature dependent.[88,89] At room temperature its product is the well-known compound "Vince lactam" used in the synthesis of antiviral drugs.[90,91] The thermodynamic control of this reaction, at -20ºC, leads to a [2+2] cycloaddition resulting from the formation of two new σ bonds from a pair of electrons of a π bond from the diene (CPD) and another pair from a π bond from the dienophile (CSI) according to the mechanism illustrated in Figure 3.2.
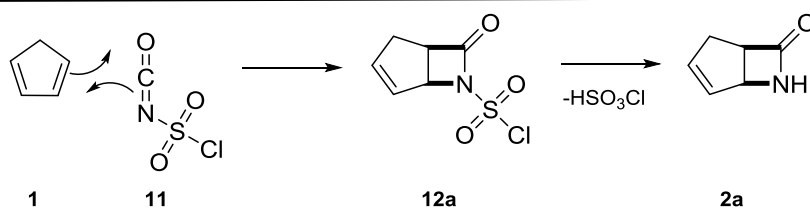
Figure 3.2 Proposed mechanism for the formation of compound 2a.

Two pairs of enantiomers, with *cis* conformation are formed, compound **2a** and 2% (calculated by ^{1}H NMR) of the constitutional isomer **2a'** (Figure 3.3), when the best reaction conditions are achieved. The retention factor of both compounds is very

similar, and the last fractions of the purification procedure are a mixture of both compounds. Figure 3.4 shows the ^{1}H NMR spectrum of the unseparated mixture. The highlighted peaks indicate the NMR shifts for the minority compound. The double bond lower field shifts (6.6 and 6.7 ppm) for compound **2a'** can be explained by its proximity to a more electronegative atom than in the majority compound (**2a**).

Figure 3.3 Structure of the cycloaddition reaction products.

Theoretically, there is a 50% chance for both products to form but, in fact, this does not happen. This could be explained by the higher stability of the major product in detriment to the stability of **2a'**.

This reaction is described in the literature with a 40-60% yield but, when the reaction conditions were optimized, the yield improved to 95%. Fresh doubly-distilled CPD, controlled temperature (-20ºC, MeOH bath cooled with a cryocooler), an amber round bottom flask and dropwise addition of CSI were the best reaction conditions found, as well as a slight change in the workup to maximize the yield. Durst and O'Sullivan[92] investigated the reduction of *N*-Chlorosulfonyl β-lactams with sodium sulfite and Benedek *et al.*[87] report the workup as treating the reaction mixture with an aqueous solution of Na_2SO_3 and pH adjustment to 8-9 with 15% KOH solution in water.
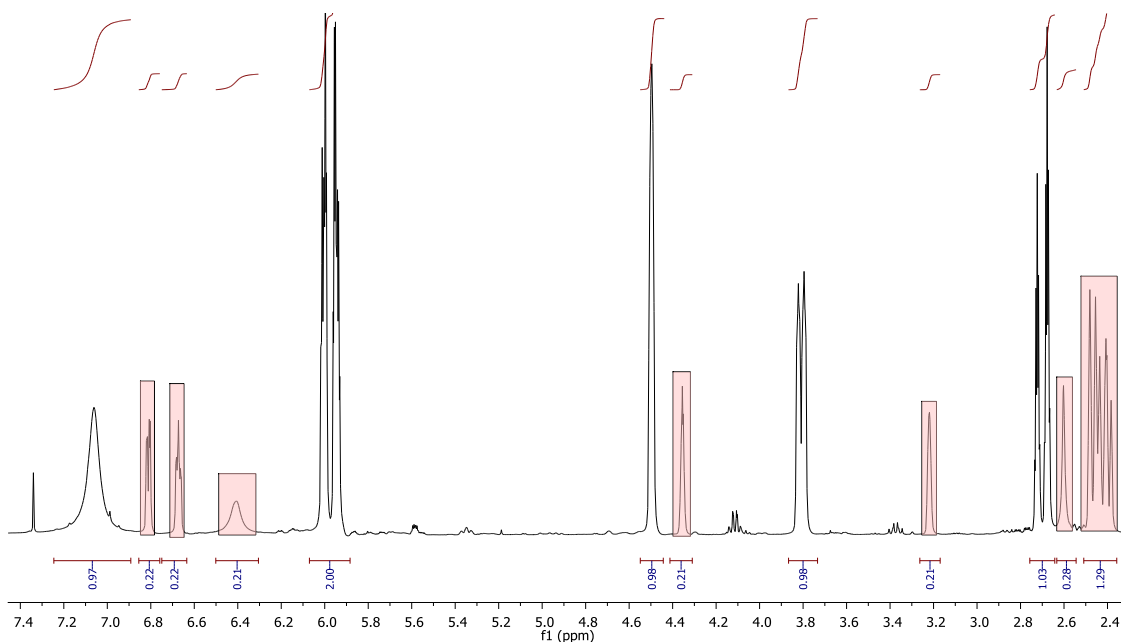
Figure 3.4 ^{1}H NMR spectrum of the unseparated mixture of the products from the cycloaddition reaction.

The expected results were not obtained. It was theorised that the neutralization of the chlorosulfuric acid ($pK_a(HSO_3Cl)\cong$-6.0) from the leaving group wasn't very successful and the corresponding amino acid was formed and lost to the aqueous layer during workup. This observation led to a change in the workup. Based on a theoretical study,[93] the ring opening of a lactam is less favoured in alkaline conditions and so, treating the reactional mixture simultaneously with both aqueous solutions (increasing the alkaline power of the aqueous layer), led to a shorter and more efficient workup. A yield of 95 % was achieved when scaling up the reaction.

Compound **8a** was generated by acidic hydrolysis of **2a** (Scheme 3.3), according to the mechanism shown in Figure 3.5, and isolated by precipitation with Et$_2$O from EtOH. In

the literature,[87] concentrated HCl is used and a 74% yield is achieved, the reproduction of this procedure gave a brownish solid with variable yield (50-80%). A 10% HCl solution gave higher yields (80-95%) and a cleaner product.
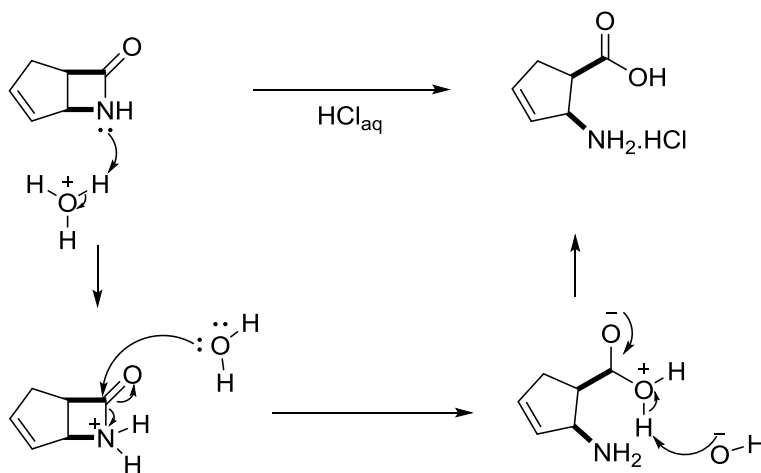
Figure 3.5 Proposed mechanism for the acidic lactam ring opening.

Hydrochloride **8a** was converted into the free β amino acid **MMU** with an ion exchange resin, scheme 3.4. The hydrochloride was loaded into a column packed with Dowex® hydrogen form and neutralised to the corresponding salt with 2M NH_4OH aqueous solution. The column was then rinsed with water to recover the free amino acid.
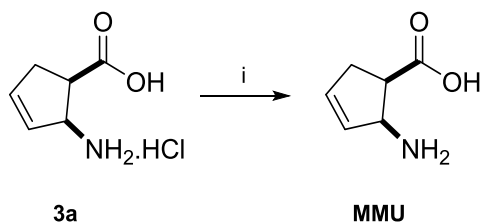
Scheme 3.4 Hydrochloride neutralisation followed by ion exchange. i) Dowex®, 2M NH_4OH, H_2O.

Compound **MMU** gave the starting material to obtain the saturated compound **MMS** *via* hydrogenation at atmospheric pressure with Pd/C catalyst as depicted in Scheme 3.5 following the mechanism illustrated in Figure 3.6.
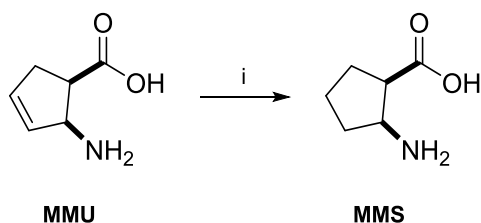
Scheme 3.5 Hydrogenation reaction. i) H_2, Pd/C, MeOH.

Hydrogen and the alkene attach to the catalyst surface and two hydrogen atoms are added to the same face of the double bond (*syn* addition) and the saturated alkane is released from the catalyst surface.
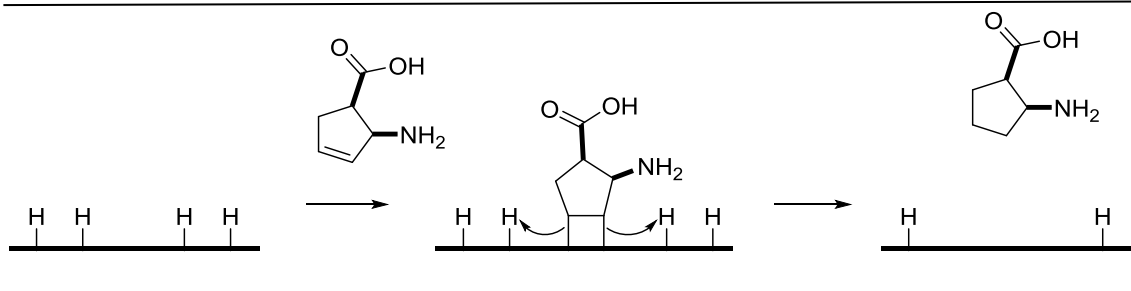
Figure 3.6 Postulated mechanism for the olefin hydrogenation.

Scheme 3.6 illustrates the steps followed to obtain the hydroxylated derivative **MMH**.
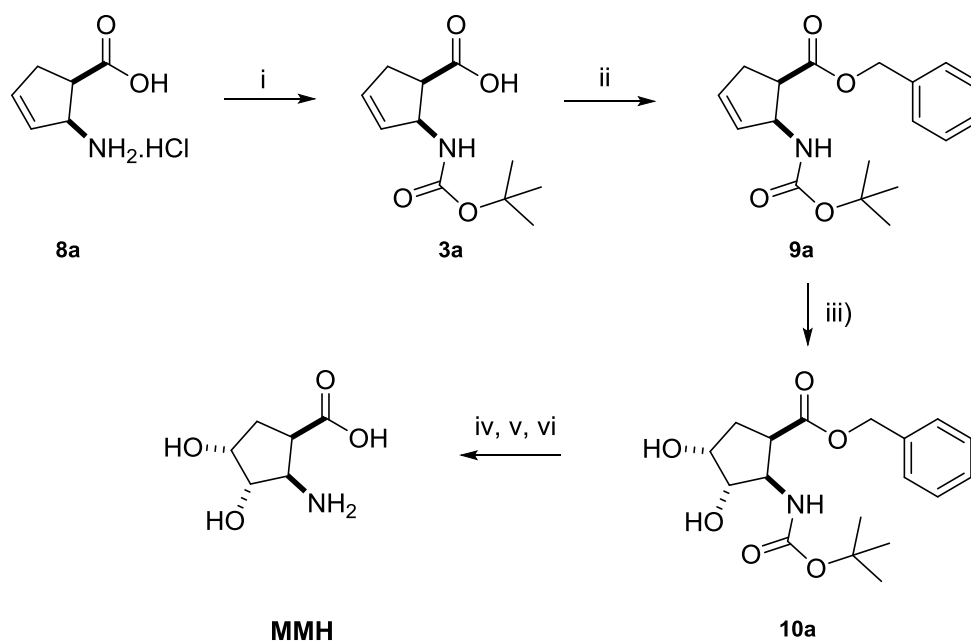
Scheme 3.6 Synthetic route to obtain compound MMH. i) Boc$_2$O, 1M NaOH, Dioxane:H$_2$O; ii) BnOH, Pybop, DIPEA, DCM; iii) OsO$_4$, NMO, Acetone; iv) H$_2$, Pd/C, MeOH; v) TFA, DCM, vi) Dowex®, 2M NH$_4$OH, H$_2$O.

N-Boc protection of amino groups and *O*-Bn protection of carboxylic acid groups is a common strategy in solution phase peptide synthesis because they are orthogonal protecting groups and easily allow access to free acid or amino groups for further coupling. Treating **8a** with NaOH and Boc$_2$O led to compound **3a** according to the mechanism shown in Figure 3.7.
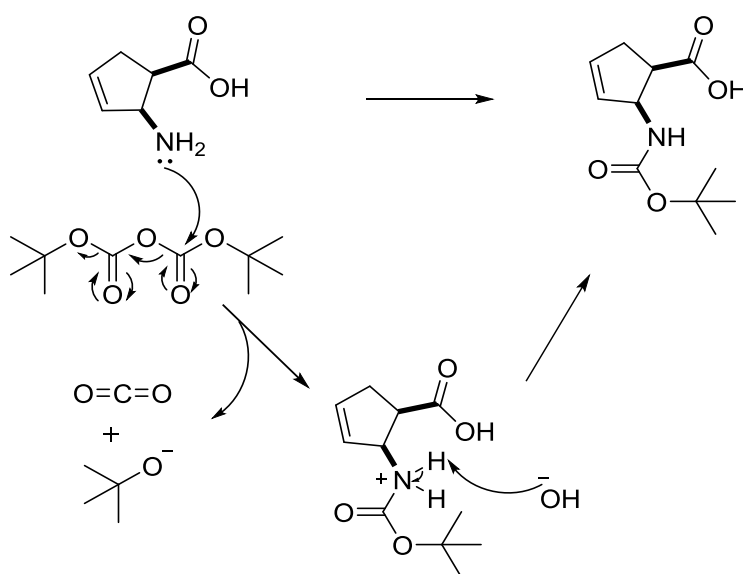
Figure 3.7 Proposed mechanism for the amino group protection.

The lone pair in the nitrogen attacks one of the carbonyl groups of Boc$_2$O adding the Boc group. The protonated amine is deprotonated in alkaline conditions and the final product is formed.

The first attempt to couple **3a** and BnOH was made *via* a Steglich esterification using dicyclohexylcarbodiimide (DCC) and 4-(dimethylamino)pyridine (DMAP). The synthesis was successful but with a low yield (20%). Furthermore, DCC has a side

product that is difficult to remove (dicyclohexylurea - DCU). Compound **9a** was synthesised using a coupling agent (benzotriazol-1-yloxy)tripyrrolidinophosphonium hexafluorophosphate – PyBop) according to the mechanism illustrated in Figure 3.8. PyBop has long been used in peptide synthesis and it was first reported as a substituent for Bop coupling agents due to its lower reaction times, lower toxicity and low racemization effects.[94] The carboxylic acid is activated to a better leaving group with PyBop and the esterification occurs in higher yields (64%) than with DCC coupling agent.
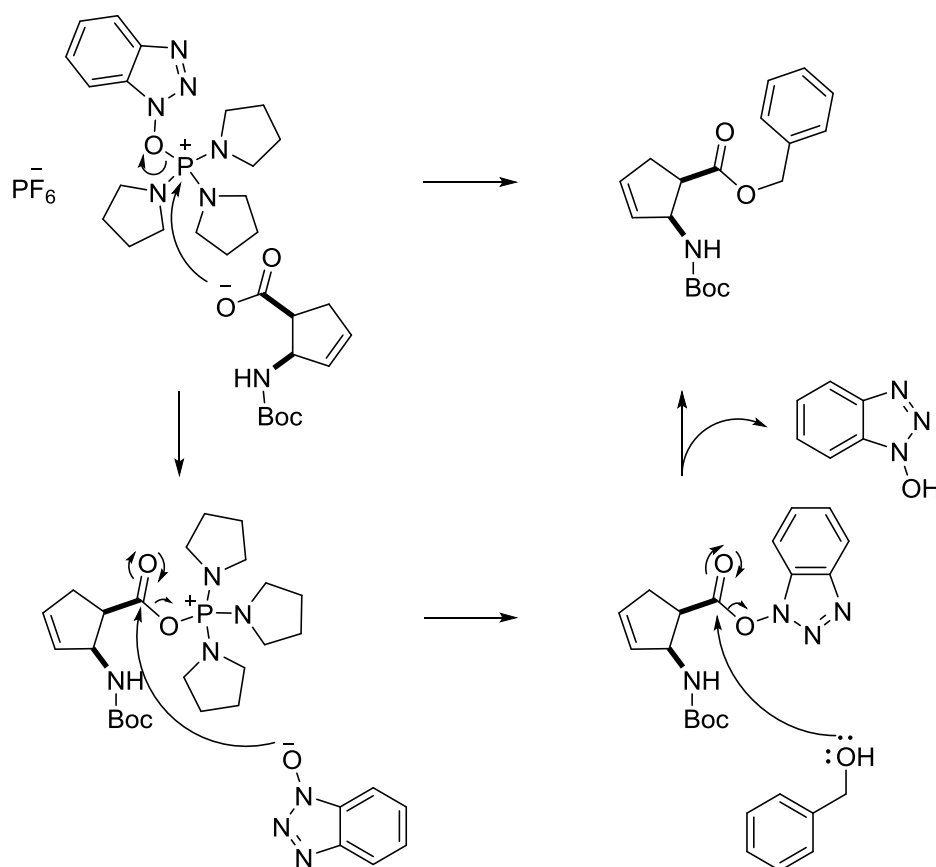
Figure 3.8 Proposed mechanism for the acid group protection.

Finally, an Upjohn dihydroxylation was performed to access the hydroxylated derivative (**MMH**). Compound **10a** was oxidised with OsO_4 (catalytic amount) as oxidant and NMO as co-oxidant[95] (Figure 3.9). This reaction gives access to a *cis* diol preserving the desired "enantiopure character" of these compounds as the bulk of the osmium complex results in dihydroxylation from the least hindered face.
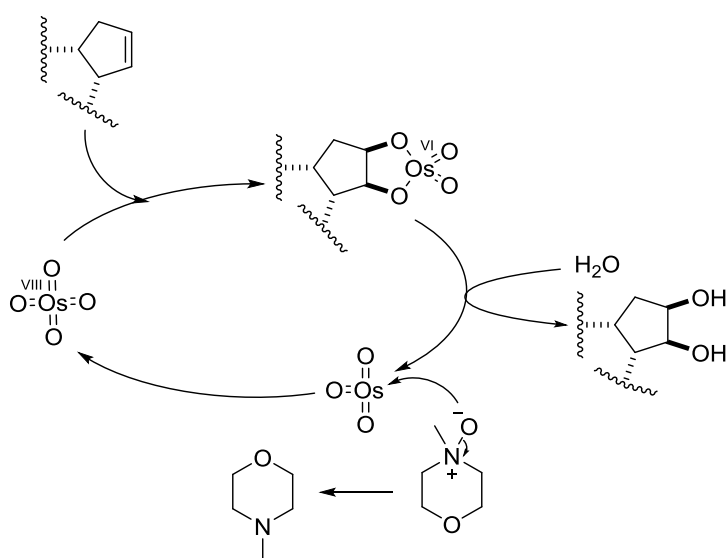
Figure 3.9 Catalytic cycle for the Upjohn dihydroxylation.

To obtain the final compound, **10a** was orthogonally deprotected in two steps. The benzyl group was eliminated via catalytic hydrogenation (Figure 3.10) and the Boc group was cleaved (Figure 3.11) resulting in a TFA salt derivative. The *tert*-butyl carbamate is protonated and the loss of *tert*-butyl cation results in carbamic acid that decarboxylates resulting in the free amine. Under acidic conditions the amine protonates to give the final product as a TFA salt. ^{1}H NMR analysis was run to confirm the

removal of the benzyl peaks in the aromatic region (7.20-7.50 ppm) as well as the

singlet at 5.14 ppm for the -CH$_2$-, and the singlet (1.42 ppm) corresponding to the *tert*-

butyl group.

As described before, the final product was isolated running a column packed with

Dowex® and eluting with 2M NH$_4$OH solution and water.
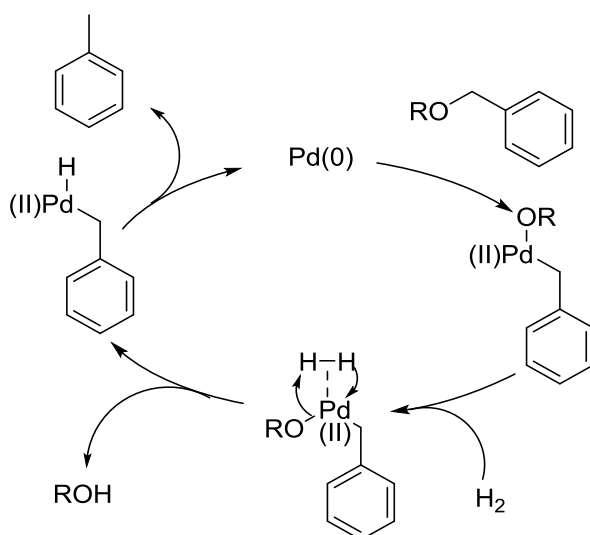
Figure 3.10 Catalytic cycle for the benzyl hydrogenation.

The orthogonal deprotection of **9a-c** also led to **MMS**, **MCDS** and **MCUS** as illustrated

in Scheme 3.2. This route was only used when the compound was needed and **MMU**,

MCDU and **MCUU** were not available.
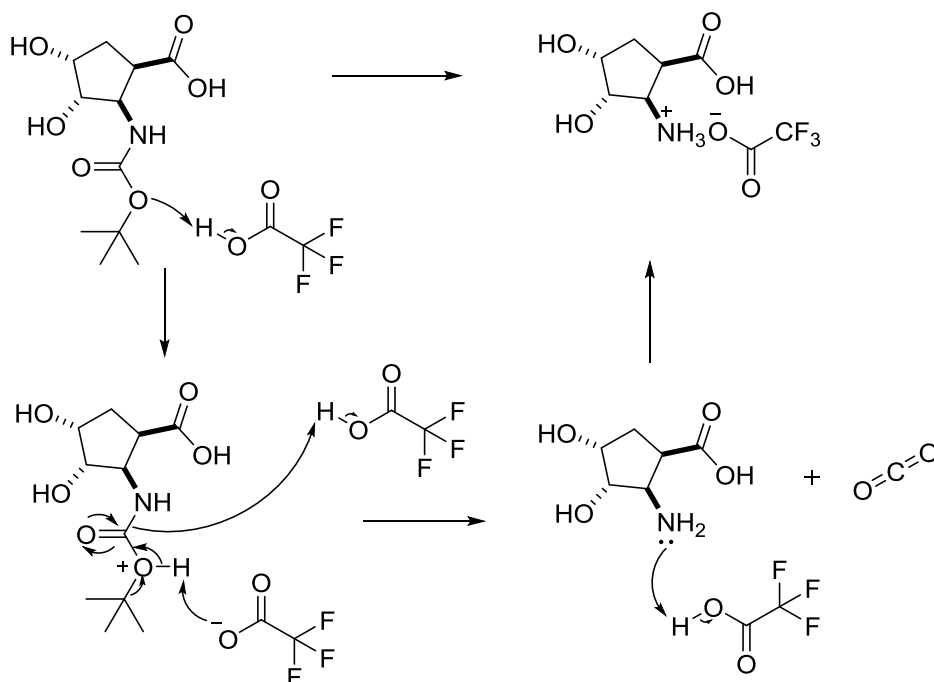
Figure 3.11 Proposed mechanism for the cleavage of the amine protecting group.

3.3.2. SYNTHESIS OF ENANTIOMERICALLY PURE UNSATURATED, SATURATED AND HYDROXYLATED MONOMERS

Nature is a perfect synthetic chemist and essentially makes all types of molecules by enzymes. As a result of the commercial availability of a large library of different enzymes, their application in synthesis has become more and more useful.[96] The drawback of the use of enzymes is that they, often, are specific to one chemical transformation. Lipases are versatile enzymes and have been reported to perform a wide variety of transformations[97,98] and, very often, with enviable enantiomeric excesses (*ee*). An enzymatic resolution was performed to assess the compounds previously synthesised in their enantiomerically pure forms (*cis* conformation). A Lipase from

Candida antarctica was used to "digest" one of the enantiomers of lactam **2a** as reported by Forró *et al.*[99,85] (Scheme 3.7). The authors used diisopropyl ether (^{i}Pr$_2$O) as solvent; for safety reasons, here the solvent was substituted by MTBE.
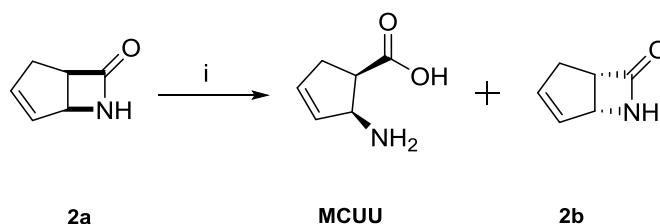
Scheme 3.7 Enzymatic resolution of lactam 2a. i) Lipase, MTBE, H$_2$O.

A catalytic triad of amino acid residues is responsible for the activity of *Candida antarctica*. The triad consists of Aspartate (Asp), Histidine (His) and Serine (Ser),[100] and the mechanism of action is outlined in Figure 3.12.
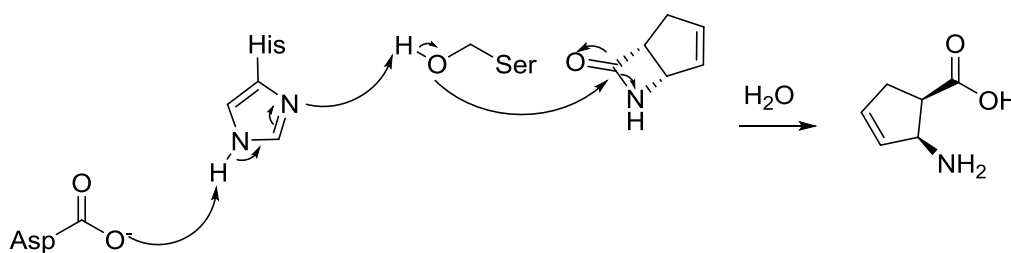
Figure 3.12 Proposed mechanism for the enzymatic resolution.

The enzyme preferentially digests the enantiomer **MCUU** leaving lactam **2b** enantiomerically pure in solution. Filtering the reaction mixture and eliminating MTBE under reduced pressure allowed isolation of **2b**. Washing the filtered solid with water

and filtering the solution gave access to enantiomerically pure **MCUU**. The isolated enzyme was stored at 4ºC and reused. The reaction was monitored by HPLC, monitoring the progressive decrease of lactam **2c**. Figure 3.13 shows the chromatogram of racemic **2a** and enantiomerically pure **2b**, after 48 h. To evaluate the activity of the enzyme in different solvents and its behaviour when recovered, an incipient experiment was run (Table 3.1). The enzyme lost some activity when reused; it took 3 more days to resolve less than half of the amount of substrate. The replacement of ^{i}Pr$_2$O by MTBE resulted in half the reaction time even with approximately 2.5-fold the amount of substrate. A single crystal X-ray analysis (Figure 3.14) confirmed that the Rt of 14 minutes corresponded to lactam **2b**.

Table 3.1 Solvent and recovered/fresh enzyme reaction times dependence.

	Solvent	Lipase (g)	Substrate (g)	Time (days)	*ee* (%)
Recovered	MTBE	2.96	1.88	5	>99
Fresh	^{i}Pr$_2$O	2.99	1.82	4	>99
Fresh	MTBE	7.95	4.81	2	>99
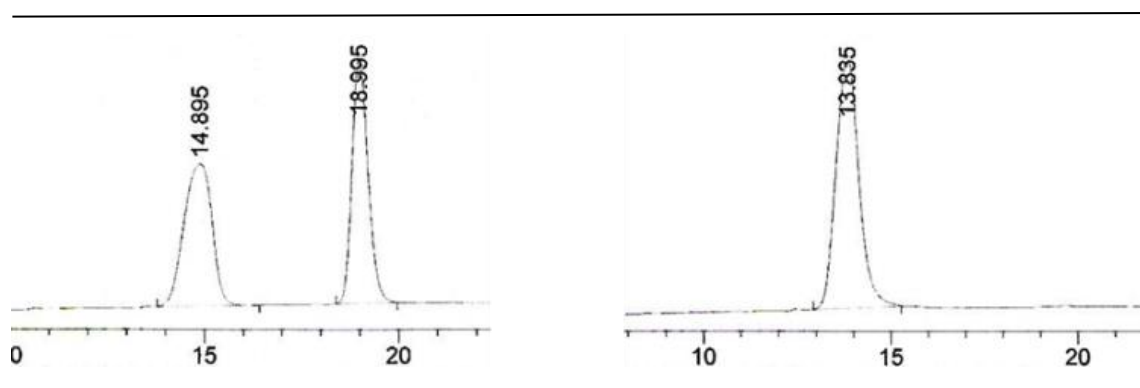
Figure 3.13 HPLC trace for compounds 2a (left) and 2b (right).
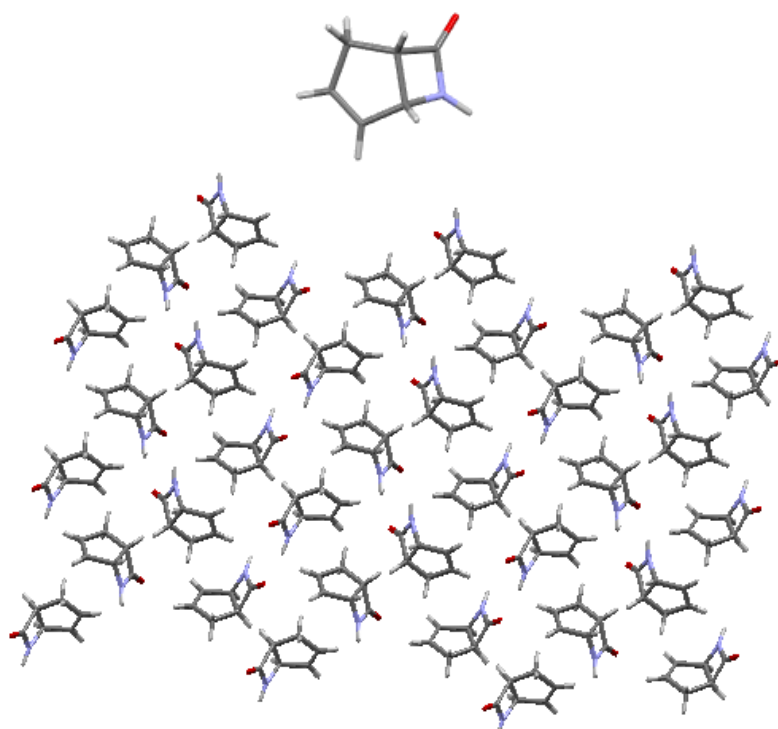
Figure 3.14 a) Structure determined from a single crystal X-Ray of compound 2b. b) Packing pattern of crystal structure.

Compounds **2b** and **MCUU** provided the starting materials to synthesise the enantiomerically pure versions of racemic **MMU**, **MMS** and **MMH**; following the same synthetic steps previously described.

3.3.3. WATER UPTAKE DETERMINATION

The water uptake of each synthesised compound was determined by thermogravimetric analysis. TGA is a technique in which one (or more) property of a sample is studied

while subjected to a controlled temperature program. Particularly, the mass loss (of water) from hydrated samples was evaluated while heating at 5°C/min. As a positive control, α-lactose monohydrate was used. Thermograms for each compound can be found in Appendix A5.

By way of example, urea is a highly hydrophilic[101] molecule widely used in cosmetic and pharmaceutical formulations and it has a Donor/Acceptor (D/A) hydrogen bond count of 2/3 and a D/A binding sites of 4/4. Potentially, it could bind to a total of 8 molecules of water but it binds to 5 as demonstrated by Rezus *et al.*[102] (Figure 3.15). An analogous analysis was done to determine the D/A ratio for the monomeric structures in study, with the majority having the same D/A relationship (Table 3.2).

D/A count: 2/3

D/A sites: 4/4
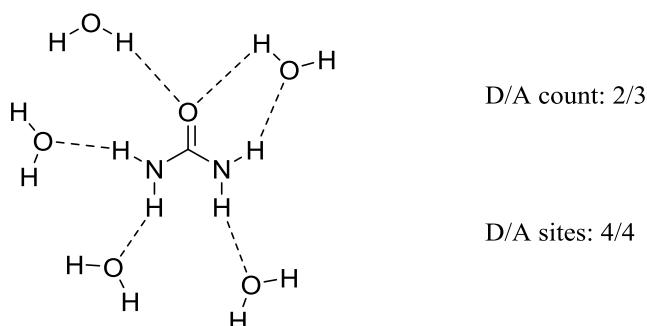
Figure 3.15 Urea solvated in five molecules of water. Adapted from[102]

Figure 3.16 shows the loss of 5% of α-lactose monohydrate's (360.31 Da) weight up to approximately 160°C corresponding to the loss of one molecule of water per molecule of lactose. The region of the thermogravimetric profiles (Figure 3.17) of particular interest for this study is the up to ~145°C. The weight loss up to ~115°C is due to

adsorbed water evaporation from the material surface (water that is not "bound"). The second weight loss observed is due to "bound" or "structural" water that is typically hydrogen bonded to the material. For the example in Figure 3.19, bound water is measured between 123 and 144 ºC with a loss of 2.539 mg, corresponding to 3 molecules of water per molecule of **MCUU**. All samples were run in triplicate and the reproducibility of the results is exemplified in Figure 3.18, for **MCUU**. Figure 3.20 illustrates the results for all the monomers and Table 3.2 lists the temperature interval at which the weight loss was measured and the number of water molecules (N_w) bound per monomer molecule.

The first approach to calculate N_w was done by means of use of the first derivative of the weight loss (Table 3.3). Comparing both results it can be observed that the first and second derivative give approximately the same results but the second derivative was chosen because the differences in mass loss were larger and it gave lower standard deviation values; besides, the weight loss step was often difficult to visualise using the first derivative.

As mentioned before, the wight loss profile up to ~100ºC is due to surface water and all samples present the same profile except for compound **MCUH**. This monomer presents a weight loss step at ~40ºC that could be due to structural changes in the molecule caused by the raising temperature. This behaviour was also observed in larger molecules (see Chapter 4 and 5) and it would be of interest to run further studies to better understand what was happening with this specific molecules; due to lack of time and no interest in this temperature intervals no further studies were conducted.
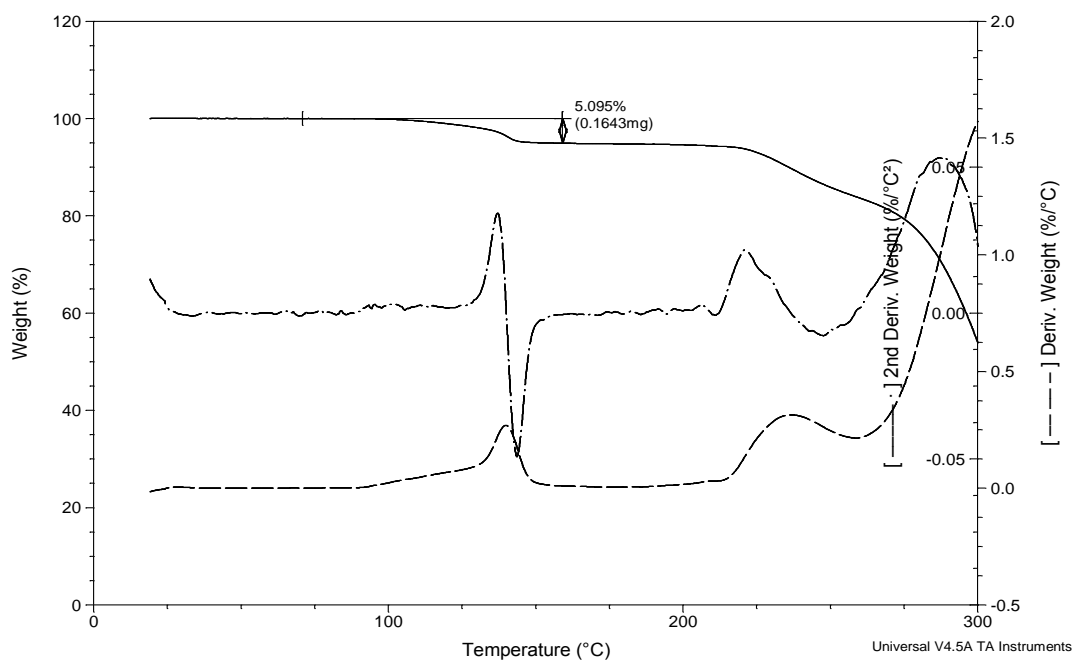
Figure 3.16 Thermogravimetric profile of α-lactose monohydrate showing the loss of 5% of its weight.
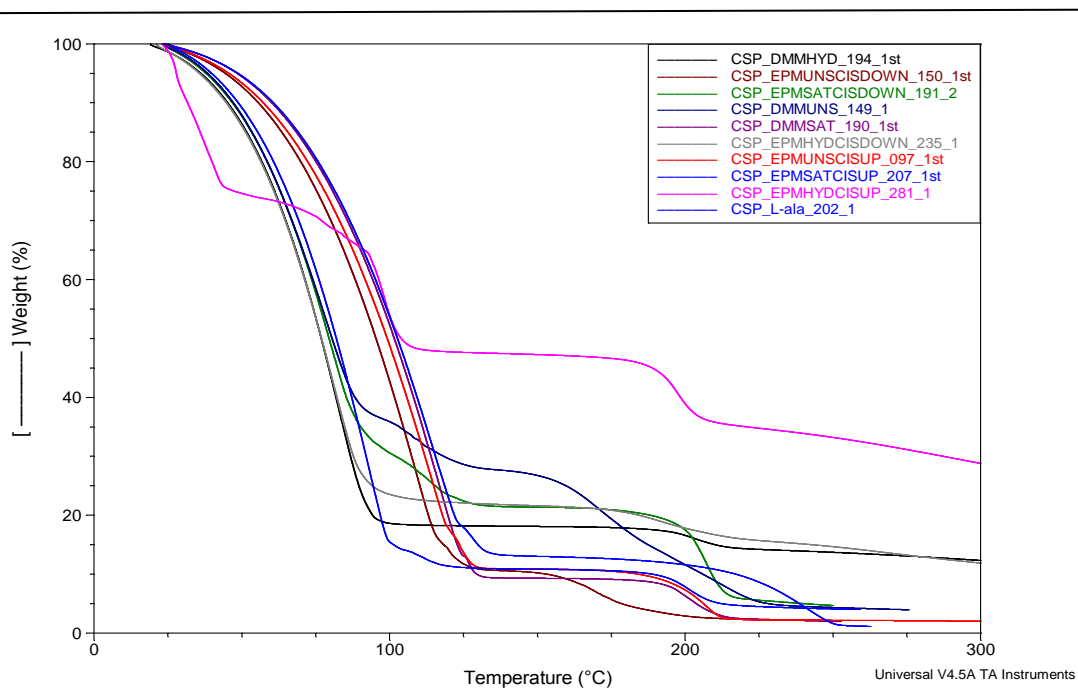
Figure 3.17 Thermogravimetric profiles of the monomeric structures.
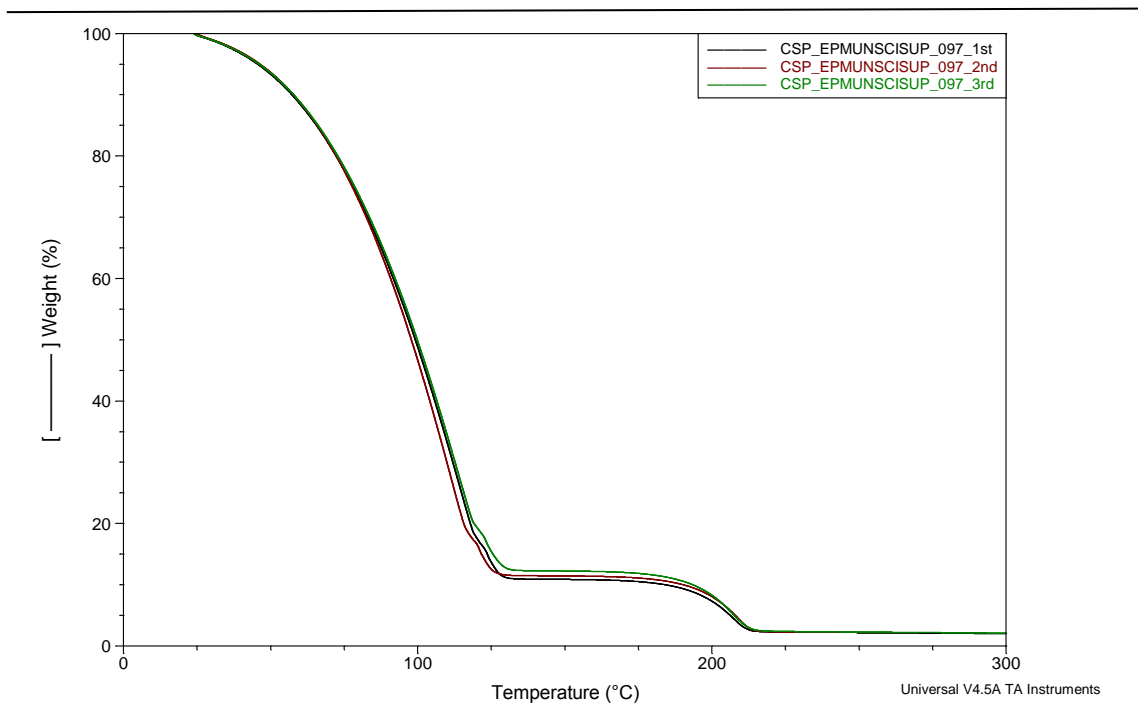
Figure 3.18 Experimental reproducibility of the thermogravimetric profile for compound MCUU.
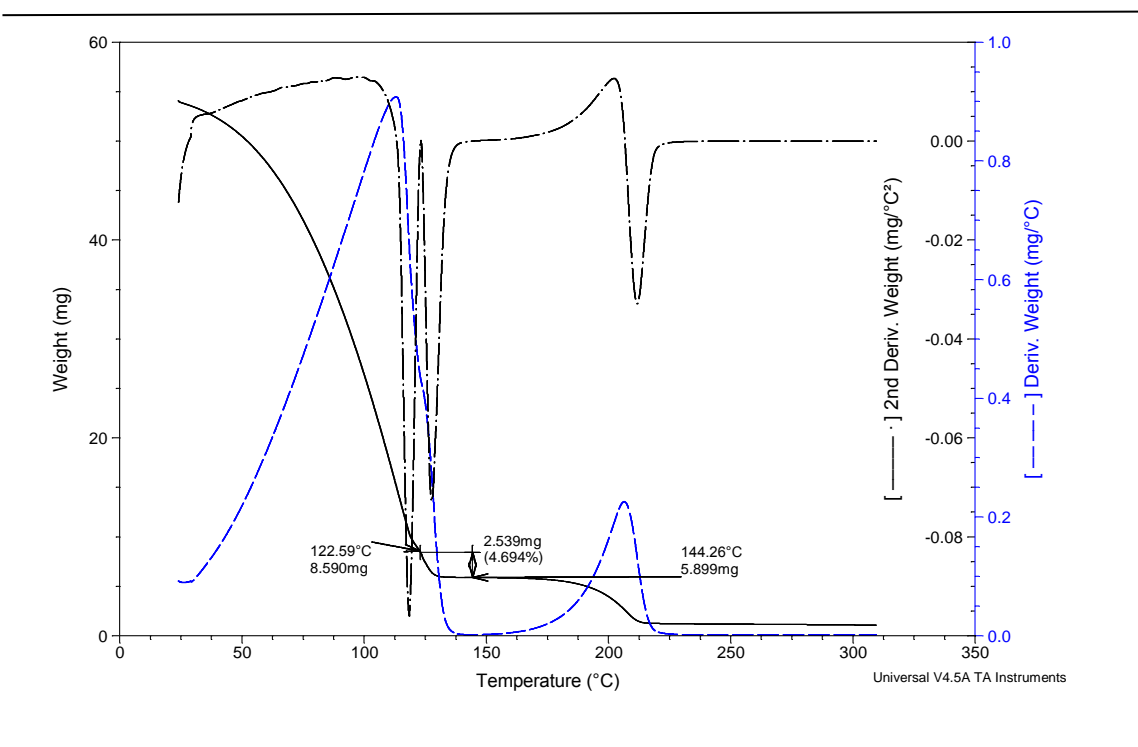
Figure 3.19 Analysis of the thermogravimetric profile for compound MCUU.
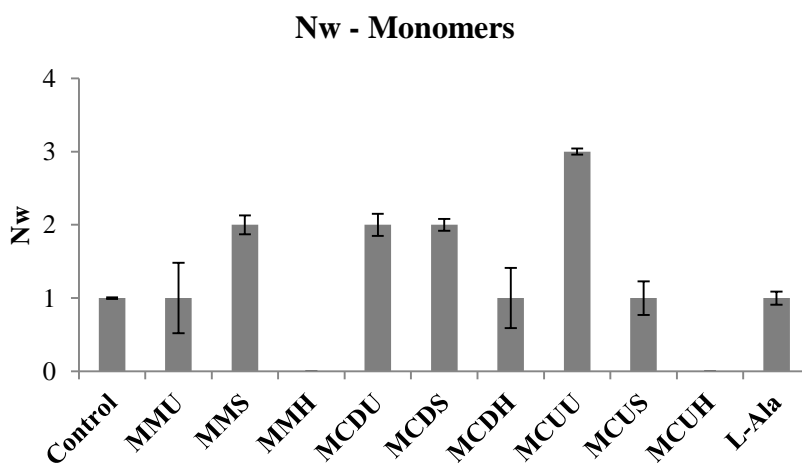
Figure 3.20 Water uptake of the monomeric structures. Data are mean ± SD from n=3.

Thermogravimetric analysis profile screening revealed that the N_w bound to each compound is different from theoretically expected when analysing the D/A possibilities. In fact, the hydroxylated series contradicts expectations, since it was predicted to have the highest water holding capacity (**MCDH** presents one water molecule bound, but the number was rounded from 0.54 to the nearest unit with a SD of ±0.41). The monomers from the unsaturated series (**MMU, MCDU** and **MCUU**) have a significantly different N_w between enantiomerically pure and mixture of two enantiomers. **MCUU** has 1.5 and 3-fold higher water holding capacity than its mirror image and the mixture, respectively. The saturated series also presents marked differences between mixture and enantiomerically pure compounds. Whilst N_w in **MMS** and **MCDS** is the same, **MCUS** binds to half the amount of water molecules.

The monomers discussed in this chapter are hydrophilic molecules and six of them have a D/A count of 2/3 and D/A sites of 3/5; the other three have a D/A count of 4/5, and

D/A sites of 5/9. This would imply that these molecules might hydrogen bond in higher rates than the ones observed. It can be assumed that the coordination level between water and monomers is not linear and this could be due to two possible events: more than one binding site, within the same molecule, coordinates with one water molecule or/and the intermolecular bonds between the monomeric structures prevent them from being available to bind to water.

Table 3.2 Physico chemical properties of the monomers.
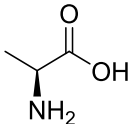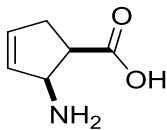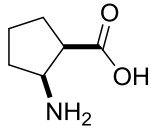
Structure	Mw	T/ºC	mp/ºC	D/A	D/A sites	N_w
Control						
	360.31	100-160	219	8/11	8/22	1±0.01
α-lactose monohydrate						
	89.09	128-148	220-223	2/3	3/5	1±0.09
L-Ala						
	127.14	105-130	160-165	2/3	3/5	1±0.48
MMU						
	129.16	110-135	204-210	2/3	3/5	2±0.13
MMS						

Table 3.2 (Continued)
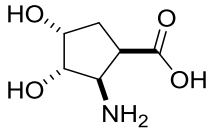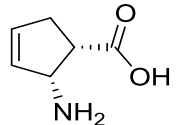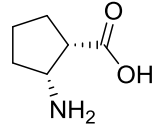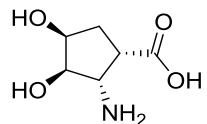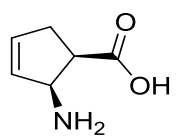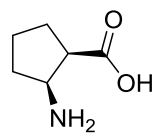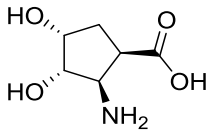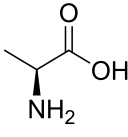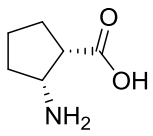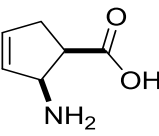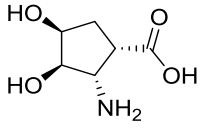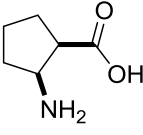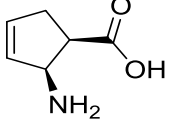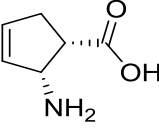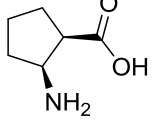
Structure	Mw	T/ºC	mp/ºC	D/A	D/A sites	N_w
MMH	161.16	100-150	203-207	4/5	5/9	0
MCDU	127.14	115-135	173-175	2/3	3/5	2±0.15
MCDS	129.16	108-140	209-213	2/3	3/5	2±0.08
MCDH	161.16	110-145	192-196	4/5	5/9	1±0.41
MCUU	127.14	122-143	207-210	2/3	3/5	3±0.04
MCUS	129.16	115-135	203-206	2/3	3/5	1±0.23
MCUH	161.16	100-150	197-200	4/5	5/9	0

Table 3.3 Number of waters determined using the first weight loss derivative

Structure	N_w	Structure	N_w
L-Ala	2±0.41	MCDS	2±0.78
MMU	1±0.66	MCDH	1±0.35
MMS	3±0.56	MCUU	4±0.33
MCDU	2±0.26	MCUS	3±1.23

3.4 CONCLUSIONS

Three series of amino acids (unsaturated, saturated and hydroxylated) have been synthesised in good yields. All synthesised structures were successfully characterised by NMR, IR and MS. The enantiomerically pure compounds were obtained *via* enzymatic resolution of lactam **2a** with an excellent *ee* value (> 99%) and the structure of lactam **2b** was confirmed by X-Ray analysis.

91

The thermogravimetric profile of the monomeric structures shows that chirality is an important feature to account for when it comes to hydrogen bonding to water. **MCUU** binds to 3-fold the N_w when compared to the racemic and 1.5-fold when compared to its mirror image. The saturated series presents no difference between **MMS** and **MCDS** but **MCUS** binds to half the N_w. The hydroxylated series does not bind to water.

Chapter 4 describes a series of peptides (dimers) derived from the monomers herein discussed and evaluates the effects of increasing D/A ratio as well as the increase of the molecular weight.

CHAPTER 4

4. SYNTHESIS AND WATER UPTAKE OF PEPTIDES (DIMERS)

4.1 INTRODUCTION

This chapter is divided, as Chapter 3, into four sections. The current section gives an overview of the compounds synthesised and the synthetic strategy followed. Section 4.2 describes the synthetic procedures involved in obtaining the dimers (Figure 4.1) and their characterisation. Section 4.3 discusses the synthetic approaches and the results obtained when assessing the water uptake ability of the referred dimers and finally, section 4.4 provides the chapter's conclusions. The rational followed in Chapter 3 to code dimers (**D** here as opposed to **M** in Chapter 3 for monomers) and identify compounds **a**, **b** and **c** was applied.
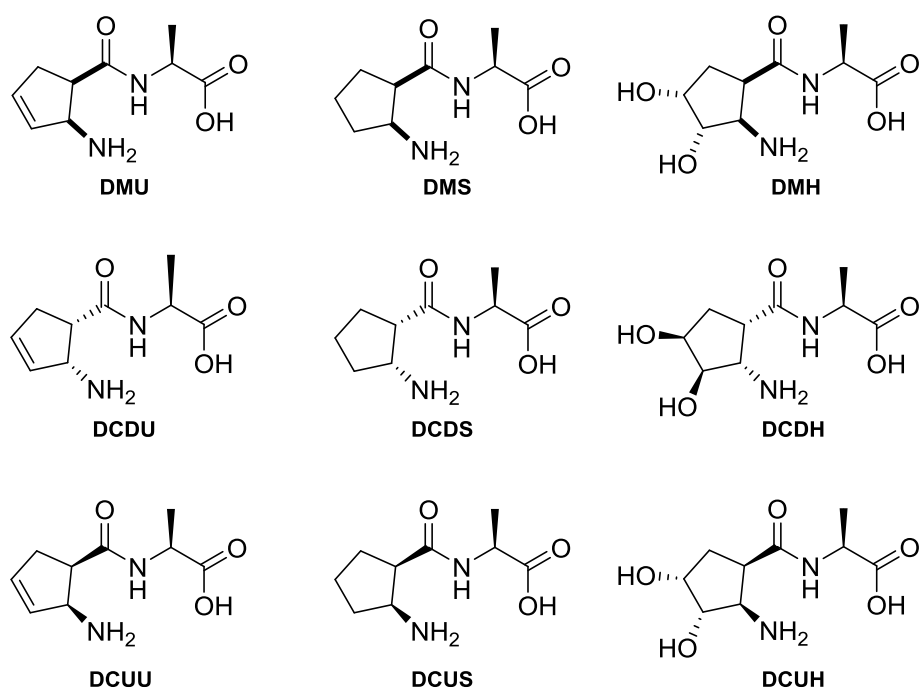
Figure 4.1 Summary of the synthesised dimeric structures.

The synthetic strategy is outlined in Schemes 4.1 and 4.2. Spectral data for the described compounds can be found in Appendix A6.
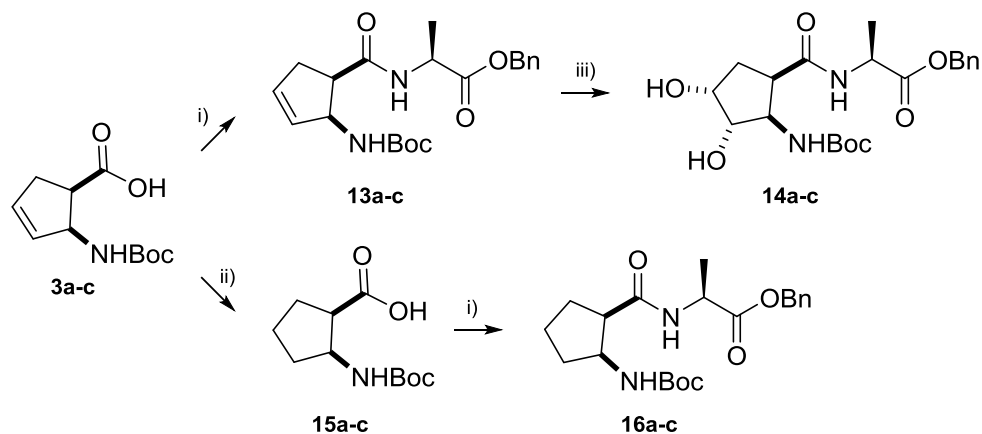
Scheme 4.1 Synthetic route to obtain the dimeric precursors. i) Coupling: L-Ala, DIPEA, PyBop, DCM; ii) Hydrogenation: H_2, Pd/C, MeOH; iii) Hydroxylation: OsO_4, NMO, Acetone.
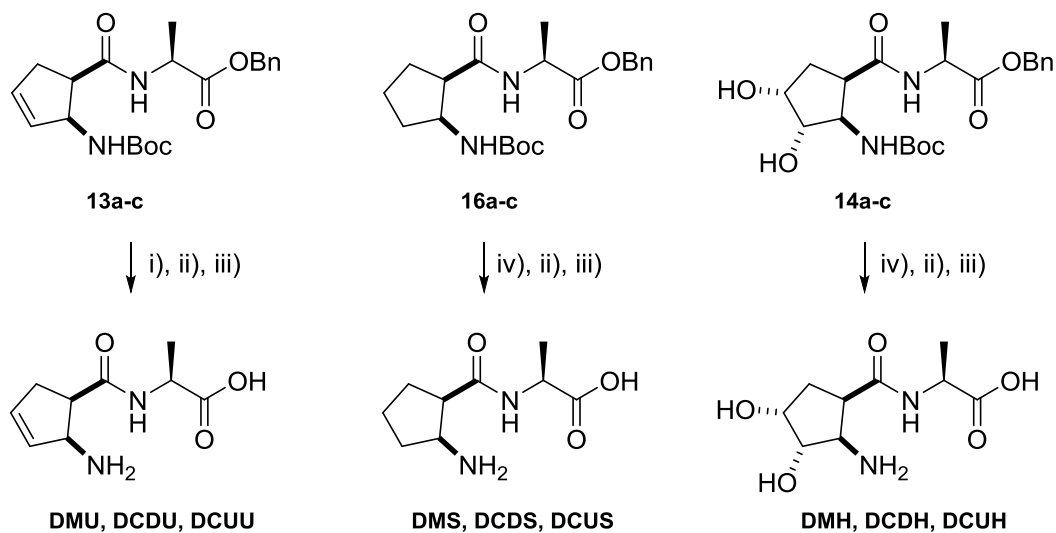
Scheme 4.2 Synthetic route to obtain the dimers. i) LiOH, MeOH, r.t; ii) TFA, DCM; iii) Dowex®, 2M NH_4OH, H_2O; iv) H_2, Pd/C, MeOH.

95

4.2 EXPERIMENTAL

4.2.1 COUPLING

Procedure to synthesise compounds **13a-c** and **16a-c**. DIPEA (1.72 mL, 9.86 mmol) followed by PyBop (2.05 g, 3.94 mmol) was added to a solution of **3a** (0.75 g, 3.29 mmol) in DCM and left stirring for 15 minutes at room temperature. *L*-alanine-*O*Bn was added (0.71 g, 3.29 mmol) and the mixture left stirring for 24 hours. Water was added and the layers separated. The organic layer was washed with sat. $NaHCO_3$, H_2O, HCl 1M in repetitive cycles until almost complete elimination of HOBt (by-product of PyBOP). The organic layer was then dried over anhydrous Na_2SO_4, filtered and concentrated under reduced pressure. The crude was purified by column chromatography (CC) and eluted with Hexane:EtOAc (1:1) to afford 1.18 g (92%, Rf=0.70) of the desired product.

4.2.2 HYDROXYLATION

Procedure to synthesise compounds **14a-c**. As described in Chapter 3, section 3.2.5.

4.2.3 ORTHOGONAL DEPROTECTION OF THE AMINO AND ACID GROUPS

4.2.3.1 Acid group deprotection

Via alkaline hydrolysis (Saponification)

Compound **13a** (0.51 g, 1.32 mmol) was dissolved in MeOH (5.00 mL) and lithium hydroxide (LiOH) (0.33 g, 7.89 mmol) was added. The mixture was left stirring at room temperature and controlled by TLC for 24 hours. The reaction mixture was concentrated

under reduced pressure and the crude taken in H_2O (5.00 mL) and cooled to 0ºC. 1M H_2SO_4 was added dropwise until pH 4. The water was eliminated under reduced pressure and the crude dissolved in $CHCl_3$. The precipitate (Li_2SO_4) was filtered and the filtrate concentrated under reduced pressure to afford the free carboxylic acid (0.33 g, 84%). ^1H NMR was run to confirm the absence of the benzyl group and the product taken into the next step without further purification.

Via Hydrogenation

As described in Chapter 3, section 3.2.6.1.

4.2.3.2 Amino group deprotection

As described in Chapter 3, *via* TFA cleavage, section 3.2.6.2.

4.2.4 ION EXCHANGE

Procedure to synthesise compounds **DMU**, **DMS**, **DMH**, **DCDU**, **DCDS**, **DCDH**, **DCUU**, **DCUS** and **DCUH**. As described in Chapter 3, section 3.2.7.

4.2.5 PRECURSORS CHARACTERISATION
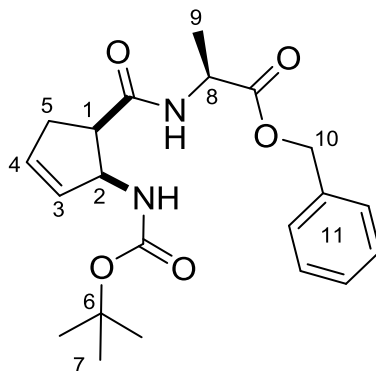
Benzyl (2-((*tert*-butylcarbonyl)amino)cyclopent-3-ene-1-carbonyl)-*L*-alaninate (13a). **Yield** 92%. **mp** 117-121ºC. **^{1}H NMR** (400 MHz, CDCl$_3$): diastereomers δ 1.37-1.43 (m, 12H, H$_7$ and H$_9$), 2.43-2.52 (m, 1H, H$_5$), 2.81-2.90 (m, 1H, H$_5$), 3.15-3.23 (m, 1H, H$_1$), 4.46-4.63 (m, 1H, H$_8$), 4.86 (m, 1H, CONH), 4.98-5.05 (m, 1H, H$_2$), 5.09-5.23 (m, 1H, H$_{10}$), 5.56-5.61 (m, 1H, H$_4$), 5.88-5.92 (m, 1H, H$_3$), 6.29 (d, *J* = 6.8 Hz, 1H, N$\underline{H}$COOCCH$_3$), 6.53 (d, *J* = 5.2 Hz, 1H, N$\underline{H}$COOCCH$_3$), 7.31-7.39 (m, 5H, H$_{11}$). **^{13}C NMR** (100 MHz, CDCl$_3$): 18.0, (C$_9$), 28.4 (C$_7$), 34.5 (C$_5$), 46.9 (C$_1$), 48.6 (C$_8$), 57.4 (C$_2$), 66.9 (C$_{10}$), 79.6 (C$_6$), 128.3 (C$_{11}$), 128.4 (C$_{11}$), 128.6 (C$_{11}$), 128.7 (C$_{11}$), 129.8 (C$_4$), 135.7 (C$_3$), 155.7 (C=O, NH$\underline{C}$OOC(CH$_3$)$_3$), 171.6 (C=O, COOBn), 173.3 (C=O, CONH). **IR** (ν, cm^{-1}): 3325, 2982, 2936, 1753, 1725, 1675, 1646, 1623, 1514, 1445, 1365, 1353, 1335, 1296, 1280, 1245, 1204, 1161, 1108, 1072, 1045, 1027, 1008. **HRMS** (ESI, MeOH) calculated for C$_{21}$H$_{28}$N$_2$O$_5$: 388.4640, found M+Na: 411.1882.
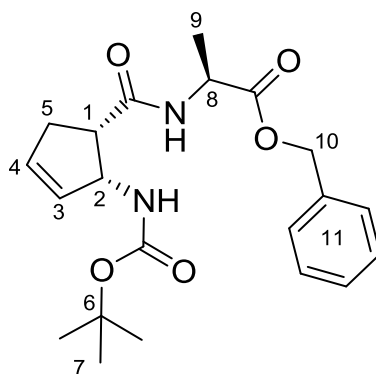
Benzyl ((1*S*,2*R*)-2-((*tert*-butoxycarbonyl)amino) cyclopent-3-ene-1-carbonyl)-*L*-alaninate (13b). **Yield** 54%. **mp** 134-139ºC. **¹H NMR** (400 MHz, CDCl₃): δ 1.37 (s, 9H, H_7), 1.42 (d, *J* = 7.2 Hz, 3H, H_9), 2.44-2.53 (m, 1H, H_5), 2.78-2.89 (m, 1H, H_5), 3.13-3.21 (m, 1H, H_1), 4.44-4.57 (m, 1H, H_8), 4.86 (d, *J* = 9.6 Hz, 1H, N$\underline{H}$COOC(CH₃)₃), 4.98-5.04 (m, 1H, H_2), 5.07-5.25 (m, 2H, H_{10}), 5.57-5.62 (m, 1H, H_4), 5.88-5.94 (m, 1H, H_3), 6.55 (d, *J* = 5.2 Hz, 1H, CONH), 7.29-7.39 (m, 5H, H_{11}).

¹³C NMR (100 MHz, CDCl₃): 19.0 (C_9), 28.4 (C_7), 34.7 (C_5), 47.1 (C_1), 48.8 (C_8), 57.5 (C_2), 67.1 (C_{10}), 79.6 (C_6), 128.2 (C_{11}), 128.3 (C_{11}), 128.5 (C_{11}), 128.7 (C_{11}) 130.1 (C_4), 133.5 (C_3), 155.9 (C=O, NH$\underline{C}$OOC(CH₃)₃), 171.9, (C=O, COOBn), 172.6 (C=O, CONH). $[\boldsymbol{\alpha}]_D^{20}$ - 36.8, *c* = 0.01 g.mL⁻¹ in CHCl₃. **IR** (ν, cm⁻¹): 3321, 3050, 2036, 1751, 1726, 1676, 1647, 1631, 1595, 1565, 1543, 1517, 1459, 1417, 1336, 1250, 1212, 1162, 1110, 1065, 1045, 1028. **HRMS** (ESI, MeOH) calculated for C₂₁H₂₈N₂O₅: 388.4640, found M+Na: 411.1882.
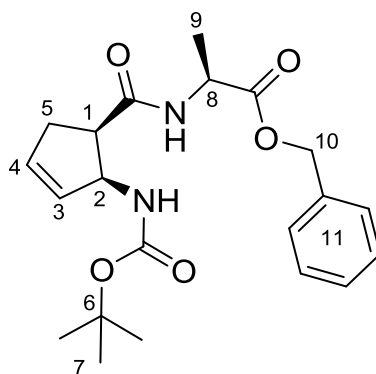
Benzyl ((1*R*,2*S*)-2-((*tert*-butoxycarbonyl)amino)cyclopent-3-ene-1-carbonyl)-*L*-alaninate (13c). **Yield** 86%. **mp** 135-139ºC. **^{1}H NMR** (400 MHz, CDCl$_3$): δ 1.31-1.48 (m, 12H, H$_7$ and H$_9$), 2.37-2.54 (m, 1H, H$_5$), 2.77-2.93 (m, 1H, H$_5$), 3.15-3.26 (m, 1H, H$_1$), 4.59 (q, *J* = 7.2 Hz, 1H, H$_8$), 4.83 (d, *J* = 9.6 Hz, 1H, N<u>H</u>COOC(CH$_3$)$_3$), 5.03 (t, *J* = 9.2 Hz, 1H, H$_2$), 5.17 (dd, *J* = 18.0 Hz, *J* = 6.4 Hz, 2H, H$_{10}$), 5.54-5.60 (m, 1H, H$_4$), 5.88-5.94 (m, 1H, H$_3$), 6.28 (d, *J*=6.8, 1H, CONH), 7.29-7.41 (m, 5H, H$_{11}$). **^{13}C NMR** (100 MHz, CDCl$_3$): 18.3 (C$_9$), 28.5 (C$_7$), 34.6 (C$_5$), 47.1 (C$_1$), 48.3 (C$_8$), 57.8 (C$_2$), 67.3 (C$_{10}$), 79.6 (C$_6$), 128.3 (C$_{11}$), 128.66 (C$_{11}$), 128.7 (C$_{11}$), 129.9 (C$_{11}$) 133.8 (C$_4$), 135.6 (C$_3$), 155.7 (C=O, NH<u>C</u>OOC(CH$_3$)$_3$), 171.6, (C=O, COOBn), 173.0 (C=O, CONH). $[\boldsymbol{\alpha}]_D^{20}$ + 17.4, *c* = 0.01 g.mL^{-1} in CHCl$_3$. **IR** (ν, cm^{-1}): 3346, 3322, 2958, 2171, 1753, 1731, 1682, 1647, 1624, 1526, 1446, 1388, 1364, 1353, 1337, 1314, 1280, 1245, 1219, 1196, 1161, 1069, 1048, 1031. **HRMS** (ESI, MeOH) calculated for C$_{21}$H$_{28}$N$_2$O$_5$: 388.4640, found M+Na: 411.1884.
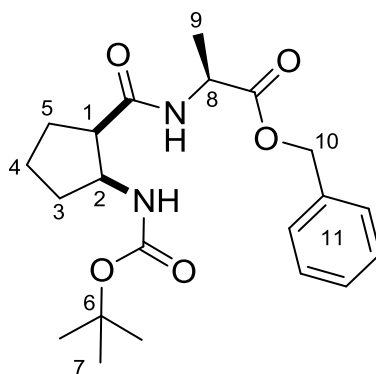
Benzyl (2-((*tert*-butoxycarbonyl)amino)cyclopentane-1-carbonyl)-*L*-alaninate (16a). Yield 77%. **mp** 114-117°C. ^{1}**H NMR** (400 MHz, CDCl$_3$): δ 1.37-1.43 (m, 12H, H$_7$ and H$_9$), 1.61-1.75 (m, 2H, H$_3$ and H$_4$), 1.77-2.07 (m, 4H, H$_3$, H$_4$ and H$_5$), 2.80-2.88 (m, 1H, H$_1$), 4.08-4.13 (m, 1H, H$_2$), 4.50-4.63 (m, 1H, H$_8$), 4.99 (d, *J* = 8.0 Hz, 1H, N$\underline{H}$COOC(CH$_3$)$_3$), 5.11-5.24 (m, 2H, H$_{10}$), 6.18 (br.s, 1H, CONH), 7.31-7.39 (m, 5H, H$_{11}$). ^{13}**C NMR** (100 MHz, CDCl$_3$): 18.6, (C$_9$), 22.2 (C$_4$), 27.8 (C$_5$), 28.4 (C$_7$), 32.9 (C$_3$), 47.8 (C$_1$), 48.3 (C$_8$), 54.0 (C$_2$), 66.9 (C$_{10}$), 79.4 (C$_6$), 128.3 (C$_{11}$), 128.4 (C$_{11}$), 128.6 (C$_{11}$), 128.7 (C$_{11}$), 155.8 (C=O, NH$\underline{C}$OOC(CH$_3$)$_3$), 172.9 (CONH and COOBn). **IR** (ν, cm^{-1}): 3344, 2981, 1732, 1687, 1645, 1532, 1519, 1455, 1365, 1355, 1329, 1312, 1286, 1246, 1213, 1171, 1108, 1050, 1015. **HRMS** (ESI, MeOH) calculated for C$_{21}$H$_{30}$N$_2$O$_5$: 390.4800, found M+Na: 413.2047.
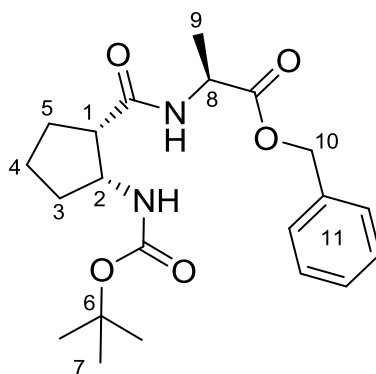
Benzyl **((1*S*,2*R*)-2-((*tert*-butoxycarbonyl)amino)** **cyclopentane-1-carbonyl)-*L*-alaninate (16b)**. **Yield** 72%. **mp** 130-133ºC . **^{1}H NMR** (400 MHz, CDCl$_3$): δ 1.37-1.42 (m, 12H, H$_7$ and H$_9$), 1.61-1.75 (m, 2H, H$_3$ and H$_4$), 1.76-2.06 (m, 4H, H$_3$, H$_4$ and H$_5$), 2.74-2.87 (m, 1H, H$_1$), 4.03-4.18 (m, 1H, H$_2$), 4.46-4.60 (m, 1H, H$_8$), 5.05-5.29 (m, 3H, NHCOOC(CH$_3$)$_3$ and H$_{10}$), 6.19 (d, *J* = 6.0 Hz, 1H, CONH), 7.28-7.42 (m, 5H, H$_{11}$). **^{13}C NMR** (100 MHz, CDCl$_3$): 18.1, (C$_9$), 22.2 (C$_4$), 27.8 (C$_5$), 28.5 (C$_7$), 32.2 (C$_3$), 47.5 (C$_1$), 48.5 (C$_8$), 54.4 (C$_2$), 67.2 (C$_{10}$), 79.3 (C$_6$), 128.4 (C$_{11}$), 128.6 (C$_{11}$), 128.8 (C$_{11}$), 135.5 (C$_{11}$), 156.1 (C=O, NHCOOC(CH$_3$)$_3$), 172.8 (C=O, COOBn), 173.7 (NHCO). $[\alpha]_D^{20}$ + 36.7, *c* = 0.01 g.mL^{-1} in CHCl$_3$. **IR** (ν, cm^{-1}): 3343, 2937, 2868, 2359, 1726, 1682, 1645, 1518, 1455, 1389, 1365, 1353, 1328, 1312, 1286, 1244, 1204, 1167, 1108, 1049, 1015. **HRMS** (ESI, MeOH) calculated for C$_{21}$H$_{30}$N$_2$O$_5$: 390.4800, found M+Na: 413.2059.
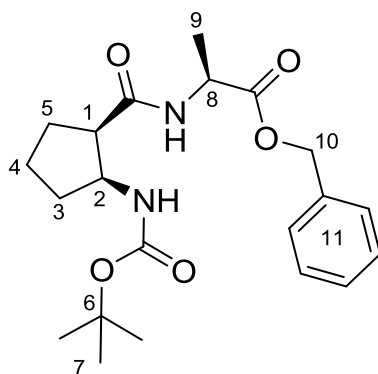
Benzyl ((1R,2S)-2-((tert-butoxycarbonyl)amino) cyclopentane-1-carbonyl)-L-alaninate (16c). Yield 77%. **mp 131-134ºC** . ^{1}**H NMR** (400 MHz, CDCl$_3$): δ 1.32-1.47 (m, 12H, H$_7$ and H$_9$), 1.48-1.51 (m, 1H, H$_4$), 1.62-1.73 (m, 1H, H$_3$), 1.77-2.06 (m, 4H, H$_3$, H$_4$ and H$_5$), 2.80-2.89 (m, 1H, H$_1$), 4.08-4.19 (m, 1H, H$_2$), 4.60 (q, J = 7.2 Hz, 1H, H$_8$), 4.99 (d, J = 8.0 Hz, 1H, N<u>H</u>COOC(CH$_3$)$_3$), 5.17 (dd, J = 21.2 Hz, J = 8.8 Hz, 2H, H$_{10}$), 6.16 (d, J = 6.8 Hz, 1H, CONH), 7.29-7.40 (m, 5H, H$_{11}$). ^{13}**C NMR** (100 MHz, CDCl$_3$): 18.7, (C$_9$), 22.7 (C$_4$), 28.1 (C$_5$), 28.6 (C$_7$), 32.9 (C$_3$), 47.9 (C$_1$), 48.4 (C$_8$), 54.3 (C$_2$), 67.3 (C$_{10}$), 79.4 (C$_6$), 128.3 (C$_{11}$), 128.6 (C$_{11}$), 128.8 (C$_{11}$), 154.9 (C=O, NH<u>C</u>OOC(CH$_3$)$_3$), 172.9 (C=O, COOBn) 173.5 (C=O, NHCO). $[\alpha]_D^{20}$ - 67.9, c = 0.01 g.mL^{-1} in CHCl$_3$. **IR** (ν, cm^{-1}): 3344, 2979, 2936, 2161, 2029, 1731, 1686, 1644, 1530, 1516, 1448, 1386, 1364, 1352, 1312, 1286, 1244, 1212, 1169, 1101, 1059, 1039, 1009. **HRMS** (ESI, MeOH) calculated for C$_{21}$H$_{30}$N$_2$O$_5$: 390.4800, found M+Na: 413.2047.
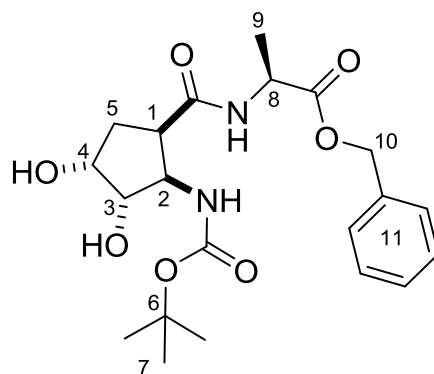
Benzyl (2-((*tert*-butylcaboxyl)amino)-3,4-dihydroxycyclopentane-1-carbonyl)-*L*-alaninate (14a). **Yield** 85%. **mp** 190-195ºC. **^{1}H NMR** (400 MHz, CDCl$_3$): δ 1.33-1.50 (m, 12H, H$_7$ and H$_9$), 1.91-2.09 (m, 1H, H$_5$), 2.10-2.27 (m, 1H, H$_5$), 3.12-3.34 (m, 2H, H$_1$ and OH), 3.80 (br.s, 1H, OH), 4.05 (br.s, 1H, H$_2$), 4.16 (br.s, 2H, H$_3$ and H$_4$), 4.46-4.62 (m, 1H, H$_8$), 5.07-5.25 (m, 2H, H$_{10}$), 5.51 (d, *J* = 7.6 Hz, 1H, NHCOdiastereomers), 5.75 (d, *J* = 6.6 Hz, 1H, NHCOdiastereomers), 6.54 (br.s, 1H, CONH), 6.66 (d, *J* = 5.3 Hz, 1H, COOBn), 7.28-7.43 (m, 5H, H$_{11}$). **^{13}C NMR** (100 MHz, CDCl$_3$): 18.4 (C$_9$), 28.5 (C$_7$), 33.6 (C$_5$), 43.4 (C$_1$), 48.4 (C$_8$), 57.1 (C$_4$), 67.3 (C$_{10}$), 70.8 (C$_3$), 78.6 (C$_2$), 80.2 (C$_6$), 128.3 (C$_{11}$), 128.6 (C$_{11}$), 128.8 (C$_{11}$), 155.0 (NH$\underline{C}$OOC(CH$_3$)$_3$), 172.7 (C=O, COOBn), 173.4 (C=O, CONH). **IR** (ν, cm^{-1}): 3331, 2977, 2935, 1729, 1689, 1645, 1532, 1455, 1390, 1364, 1335, 1288, 1245, 1163, 1112, 1061, 1028. **HRMS** (ESI, MeOH) calculated for C$_{21}$H$_{30}$N$_2$O$_7$: 422.4780, found M+Na: 445.1945.
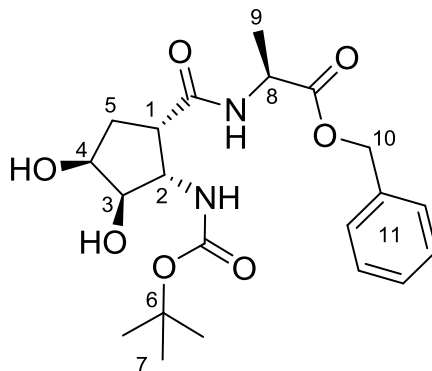
Benzyl ((1S,2S,3R,4S)-2-((*tert*-butoxycarbonyl) amino)-3,4-dihydroxycyclopentane-1-carbonyl)-L-alaninate (14b). **Yield** 68%. **mp** 168-172ºC. ^{1}**H NMR** (400 MHz, CDCl$_3$): δ rotamers 1.38 (d, J = 7.2 Hz, 3H, H$_9$), 1.43 (s, 9H, H$_7$), 1.63 (br.s, 2H, OH), 1.97-2.06 (m, 1H, H$_5$), 2.16-2.26 (m, 1H, H$_5$), 3.11-3.21 (m, 1H, H$_1$), 4.01-4.09 (m, 1H, H$_2$) 4.12-4.22 (m, 2H, H$_3$ and H$_4$), 4.46-4.52 (m, 1H, H$_8$), 5.03 (d, J = 7.6 Hz, 1H, NHCOOC(CH$_3$)$_3$), 5.10-5.26 (m, 2H, H$_{10}$), 6.22 (d, J = 6.8 Hz, 1H, CONH), 7.29-7.42 (m, 5H, H$_{11}$). ^{13}**C NMR** (100 MHz, CDCl$_3$): 19.1 (C$_9$), 28.5 (C$_7$), 33.3 (C$_5$), 43.5 (C$_1$), 48.6 (C$_8$), 57.5 (C$_4$), 67.2 (C$_{10}$), 70.6 (C$_3$), 79.5 (C$_2$), 80.3 (C$_6$), 128.2 (C$_{11}$), 128.4 (C$_{11}$), 128.7 (C$_{11}$), 128.8 (C$_{11}$), 156.3 (NHCOOC(CH$_3$)$_3$), 172.7 (C=O, COOBn), 173.2 (C=O, CONH). **IR** (ν, cm^{-1}): 3326, 2934, 2361, 2342, 1750, 1730, 1684, 1661, 1645, 1632, 1540, 1455, 1388, 1366, 1336, 1285, 1249, 1199, 1172, 1111, 1061, 1021. **HRMS** (ESI, MeOH) calculated for C$_{21}$H$_{30}$N$_2$O$_7$: 422.4780, found M+Na: 445.1945.
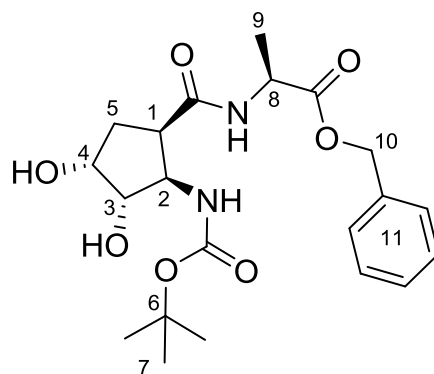
Benzyl ((1*R*,2*R*,3*S*,4*R*)-2-((*tert*-butoxycarbonyl)amino)-3,4-dihydroxycyclopentane-1-carbonyl)-*L*-alaninate (14c). **Yield** 83%. **mp** 180-185°C. **^{1}H NMR** (400 MHz, CDCl$_3$): δ 1.34-1.47 (m, 12H, H$_7$ and H$_9$), 1.86 (br.s, 1H, OH), 1.94-2.06 (m, 1H, H$_5$), 2.11-2.25 (m, 1H, H$_5$), 3.15 (br.s, 1H, OH), 3.17-3.29 (m, 1H, H$_1$), 3.99-4.07 (m, 1H, H$_2$) 4.11-4.22 (m, 2H, H$_3$ and H$_4$), 4.57 (q, *J* = 7.2 Hz, 1H, H$_8$), 5.15 (dd, *J* = 23.3 Hz, *J* = 10.8 Hz, 2H, H10), 5.52 (d, *J* = 7.6 Hz, 1H, N<u>H</u>COOC(CH$_3$)$_3$), 6.55 (d, *J* = 7.2 Hz, 1H, CONH), 7.29-7.40 (m, 5H, H$_{11}$). **^{13}C NMR** (100 MHz, CDCl$_3$): 18.4 (C$_9$), 28.5 (C$_7$), 33.7 (C$_5$), 43.4 (C$_1$), 48.4 (C$_8$), 57.1 (C$_4$), 67.4 (C$_{10}$), 70.8 (C$_3$), 78.8 (C$_2$), 80.2 (C$_6$), 128.4 (C$_{11}$), 128.7 (C$_{11}$), 128.8 (C$_{11}$), 157.3 (NH<u>C</u>OC(CH$_3$)$_3$), 172.7 (C=O, COOBn), 173.2 (C=O, CONH). $[\alpha]_D^{20}$ - 117, *c* = 0.01 g.mL^{-1} in MeOH. **IR** (ν, cm^{-1}): 3334, 2985, 1733, 1682, 1644, 1538, 1526, 1449, 1428, 1389, 1364, 1314, 1284, 1251, 1215, 1166, 1104, 1064, 1048, 1020. **HRMS** (ESI) calculated for C$_{21}$H$_{30}$N$_2$O$_7$: 422.4780, found M+Na: 445.1946.

4.2.6 DIMERS CHARACTERISATION
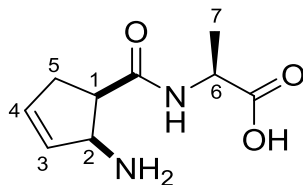
(2-aminocyclopent-3-ene-1-carbonyl)-*L*-alanine (DMU). Yield 54%. **mp** 103-106ºC.

¹H NMR (400 MHz, D₂O): diastereomers δ 1.33 (d, J = 7.2 Hz, 3H, H₇), 1.34 (d, *J* =

7.6 Hz, 3H, H₇), 2.63 (ddt, *J* = 17.2 Hz, *J* = 8.8 Hz, *J* = 2 Hz, 1H, H₅), 2.71-2.83 (m,

1H, H₅), 3.78 (q, *J* = 8.0 Hz, 1H, H₁), 3.46 (q, *J* = 8.0 Hz, H₁), 4.12 (q, *J* = 7.2 Hz, 1H,

H₆), 4.12 (q, *J* = 7.6 Hz, 1H, H₆), 4.42 (d, *J* = 8.0 Hz, 1H, H₂), 4.50 (d, *J* = 8.0,1H, H₂),

5.76 (ddd, *J* = 8.0 Hz, *J* = 4.4 Hz, *J* = 2.4 Hz, 1H, H₄), 6.26 (t, *J* = 4.8 Hz, 1H, H₃). **¹³C**

NMR (100 MHz, D2O): 16.7 (C₇), 17.0 (C₇), 33.8 (C₅), 34.8 (C₅), 44.2 (C₁), 44.1 (C₁)

51.0 (C₆), 51.2 (C₆), 57.1 (C₂), 58.1 (C₂), 125.3 (C₃), 125.8 (C₃), 138.8 (C₄), 139.1 (C₄),

172.5 (C=O, CONH), 172.6 (C=O, CONH), 180.2 (C=O, COOH), 180.5 (C=O,

COOH). **IR** (ν, cm⁻¹): 2924, 1548, 1451, 1393, 1359, 1307, 1269, 1237, 1136, 1051,

1020. **HRMS** (ESI, H₂O) calculated for C₉H₁₄N₂O₃: 198.1004, found M+H: 199.1077.
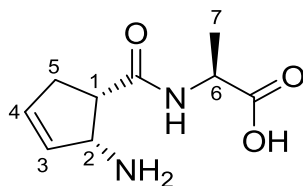
((1*S*,2*R*)-2-aminocyclopent-3-ene-1-carbonyl-*L*-alanine (DCDU). Yield 64%. **mp**

210-213ºC. **¹H NMR** (400 MHz, D₂O): δ 1.35 (d, *J* = 7.2 Hz, 3H, H₇), 2.60 (ddt, *J* =

17.6 Hz, *J* = 8.8 Hz, *J* = 2.4 Hz, 1H, H₅), 2.76 (ddd, *J* = 17.6 Hz, *J* = 8.0 Hz, *J* = 2.4 Hz,

1H, H₅), 3.45 (q, *J* = 8.4 Hz, 1H, H₁), 4.15 (q, *J* = 7.2 Hz, 1H, H₆), 4.48-4.54 (m, 1H,

H$_2$), 5.74-5.82 (m, 1H, H$_4$), 6.25-6.29 (m, 1H, H$_3$). ^{13}**C NMR** (100 MHz, D$_2$O): 16.6 (C$_7$), 33.8 (C$_5$), 44.3 (C$_1$), 50.9 (C$_6$), 58.1 (C$_2$), 125.2 (C$_4$), 139.1 (C$_3$), 172.4 (C=O, CONH), 180.5 (C=O, COOH). $[\alpha]_D^{20}$ - 52.1, c = 0.01 g.mL^{-1}in H$_2$O. **IR** (ν, cm^{-1}): 3451, 3292, 2002, 2156, 1620, 1590, 1573, 1455, 1398, 1368, 1334, 1317, 1266, 1244, 1143, 1065, 1031, 1001. **HRMS** (ESI, H$_2$O) calculated for C$_9$H$_{14}$N$_2$O$_3$ 198.1004, found M+H: 199.1077
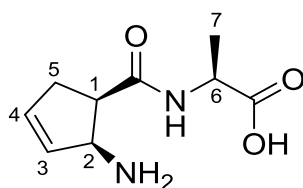
((1R,2S)-2-aminocyclopent-3-ene-1-carbonyl)-L-alanine (DCUU). Yield 74%. **mp** 176-180ºC. ^{1}**H NMR** (400 MHz, D$_2$O): δ 1.35 (d, J = 7.2 Hz, 3H, H$_7$), 2.72-2.81 (m, 2H, H$_5$), 3.39 (q, J = 8.4 Hz, 1H, H$_1$), 4.13 (q, J = 7.2 Hz, 1H, H$_6$), 4.45 (d, J = 7.6 Hz, 1H, H$_2$), 5.77-5.84 (m, 1H, H$_4$), 6.25-6.32 (m, 1H, H$_3$). ^{13}**C NMR** (100 MHz, D$_2$O): 16.9 (C$_7$), 34.5 (C$_5$), 44.1 (C$_1$), 51.0 (C$_6$), 57.1 (C$_2$), 125.8 (C$_4$), 139.0 (C$_3$), 171.0 (C=O, CONH), 180.6 (C=O, COOH). $[\alpha]_D^{20}$ + 31.3, c = 0.01 g.mL^{-1}in H$_2$O. **IR** (ν, cm^{-1}): 3306, 2988, 2063, 1646, 1615, 1556, 1459, 1442, 1395, 1374, 1364, 1340, 1287, 1258, 1240, 1173, 1127, 1117, 1081, 1022. **HRMS** (ESI, H$_2$O) calculated for C$_9$H$_{14}$N$_2$O$_3$ 198.1004, found M+H: 199.1077
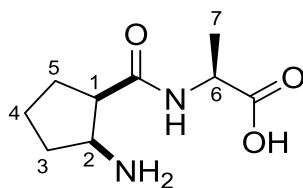
(2-aminocyclopentane-1-carbonyl)-*L*-alanine (DMS). **Yield** 62%. **mp** 205-208ºC. [1]**H**

NMR (400 MHz, CDCl$_3$): diastereomers δ 1.36 (d, J = 7.2 Hz, 3H, H$_7$), 1.62-1.93 (m,

4H, H$_3$, 2xH$_4$ and H$_5$), 1.97- 2.13 (m, 2H, H$_3$ and H$_5$), 2.90-3.03 (m, 1H, H$_1$), 3.72-3.87

(m, 1H, H$_2$), 4.21-4.37 (m, 1H, H$_6$). [13]**C NMR** (100 MHz, CDCl$_3$): 16.8 (C$_7$), 17.0 (C$_7$),

21.5 (C$_4$), 21.9 (C$_4$), 27.4 (C$_5$), 27.5 (C$_5$), 30.3 (C$_3$), 30.4 (C$_3$), 51.0 (C$_1$), 51.1 (C$_1$), 53.7

(C$_2$), 54.1 (C$_2$), 173.6 (C=O, CONH), 173.8 (C=O, CONH), 180.2 (C=O, COOH),

180.5 (C=O, COOH). **IR** (ν, cm^{-1}): 3288, 2972, 2872, 2355, 2164, 1681, 1632, 1606,

1537, 1493, 1455, 1403, 1361, 1303, 1277, 1253, 1166, 1069, 1000. **HRMS** (ESI, H$_2$O)

calculated for C$_9$H$_{16}$N$_2$O$_3$ 200.2380, found M+H: 201.1234.
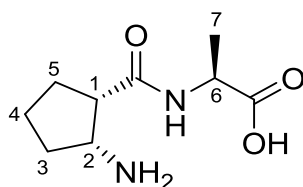
((1*S*,2*R*)-2-aminocyclopentane-1-carbonyl)-*L*-alanine (DCDS). **Yield** 63%. **mp** 188-

191ºC. [1]**H NMR** (400 MHz, D$_2$O): δ 1.32 (d, J = 7.2 Hz, 3H, H$_7$), 1.64-1.96 (m, 4H, H$_3$,

2xH$_4$ and H$_5$), 1.97- 2.08 (m, 1H, H$_3$), 2.09-2.20 (m, 1H, H$_5$), 3.04 (td, J = 7.2 Hz, J =

6.8 Hz, 1H, H$_1$), 3.86 (td, J = 6.8 Hz, J = 4.8 Hz, 1H, H$_2$), 4.11 (q, J = 7.2 Hz, 1H, H$_6$).

[13]**C NMR** (100 MHz, D$_2$O): 16.7 (C$_7$), 21.3 (C$_4$), 27.3 (C$_3$), 30.4 (C$_5$), 46.1 (C$_1$), 50.9

(C$_6$), 54.1 (C$_2$), 173.8 (C=O, CONH), 180.5 (C=O, COOH). $[\alpha]_D^{20}$ - 30.5, c = 0.01

g.mL^{-1}in H$_2$O. **IR** (ν, cm^{-1}): 3359, 3212, 3039, 2926, 2179, 1648, 1630, 1568, 1547,

1503, 1462, 1393, 1365, 1313, 1276, 1256, 1220, 1185, 1163, 1129, 1056, 1046.

HRMS (ESI, H_2O) calculated for $C_9H_{16}N_2O_3$ 200.2380, found M+H: 201.1234.
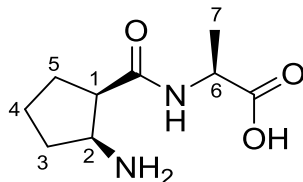
((1*R*,2*S*)-2-aminocyclopentane-1-carbonyl)-*L*-alanine (DCUS). **Yield** 63%. **mp** 172-178°C. **¹H NMR** (400 MHz, D_2O): δ 1.32 (d, *J* = 7.2 Hz, 3H, H_7), 1.68-1.97 (m, 4H, H_3, $2xH_4$ and H_5), 2.05-2.18 (m, 2H, H_3 and H_5), 2.98 (td, *J* = 8.4 Hz, *J* = 6.0 Hz, 1H, H_1), 3.83 (td, *J* = 6.4 Hz, *J* = 4.0 Hz, 1H, H_2), 4.09 (q, *J* = 7.2 Hz, 1H, H_6). **¹³C NMR** (100 MHz, D_2O): 7.0 (C_7), 21.5 (C_4), 27.5 (C_3), 30.3 (C_5), 46.0 (C_1), 51.1 (C_6), 53.7 (C_2), 173.7 (C=O, CONH), 180.2 (C=O, COOH). $[\alpha]_D^{20}$ - 19.2, *c* = 0.01 g.mL⁻¹in H_2O. **IR** (ν, cm⁻¹): 3286, 2972, 2872, 1681, 1632, 1607, 1537, 1493, 1455, 1404, 1361, 1303, 1277, 1253, 1253, 1166, 1069, 1000. **HRMS** (ESI, H_2O) calculated for $C_9H_{16}N_2O_3$ 200.2380, found M+H: 201.1234.
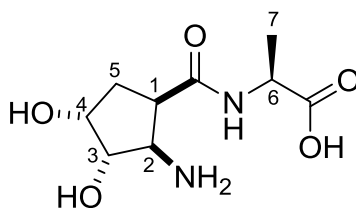
(2-amino-3,4-dihydroxycyclopentane-1-carbonyl)-*L*-alanine (DMH). **Yield** 54%. **mp** 228-233°C. **¹H NMR** (400 MHz, D_2O): diastereomers δ 1.31 (d, *J* = 7.2 Hz, 3H, H_7), 2.00-2.25 (m, 2H, H_5), 3.26-3.42 (m, 1H, H_1), 3.63-3.77 (m, 1H, H_2), 4.02-4.13 (m, 1H, H_6), 4.15-4.30 (m, 2H, H_3 and H_4). **¹³C NMR** (100 MHz, D_2O): 16.9 (C_7), 33.8

(C$_5$), 40.3 (C$_1$), 50.9 (C$_6$), 55.8 (C$_2$), 69.9 (C$_4$), 75.5 (C$_3$), 173.2 (C=O, CONH), 180.5 (C=O, COOH). **IR** (ν, cm^{-1}): 3452, 3300, 2882, 1661, 1651, 1615, 1562, 1556, 1552, 1538, 1524, 15199, 1455, 1431, 1408, 1368, 1348, 1304, 1287, 1247, 1232, 1185, 1110, 1049, 1039. **HRMS** (ESI, H$_2$O) calculated for C$_9$H$_{16}$N$_2$O$_5$ 232.2360, found M+H: 233.1133.
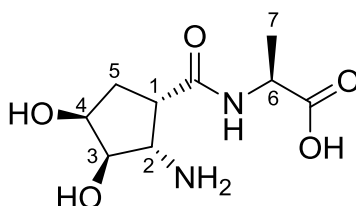
((1S,2S,3R,4S)-2-amino-3,4-dihydroxycyclopentane-1-carbonyl)-$_L$-alanine (DCDH).

Yield 85%. **mp** 225-229°C. **^{1}H NMR** (400 MHz, D$_2$O): δ 1.35 (d, J = 7.2 Hz, 3H, H$_7$), 2.08-2.14 (m, 1H, H$_5$), 2.18-2.25 (m, 1H, H$_5$), 3.40 (q, J = 8.8 Hz, 1H, H$_1$), 3.76 (t, J = 9.2 Hz, 1H, H$_2$), 4.13 (q, J = 7.2 Hz, 1H, H$_6$), 4.23 (t, J = 4 Hz, 1H, H$_4$), 4.28 (dd, J = 9.2 Hz, J = 4.8 Hz, 1H, H$_3$). **^{13}C NMR** (100 MHz, D$_2$O): 16.9 (C$_7$), 33.8 (C$_5$), 40.3 (C$_1$), 51.2 (C$_6$), 55.7 (C$_2$), 70.0 (C$_4$), 75.7 (C$_3$), 173.2 (C=O, CONH), 180.3 (C=O, COOH). $[\alpha]_D^{20}$ + 26.5, c = 0.01 g.mL^{-1}in H$_2$O. **IR** (ν, cm^{-1}): 3284, 2872, 2650, 1659, 1550, 1457, 1404, 1372, 1304, 1288, 1242, 1209, 1166, 1115, 1099, 1057. **HRMS** (ESI, H$_2$O) calculated for C$_9$H$_{16}$N$_2$O$_5$ 232.2360, found M+H: 233.1132.
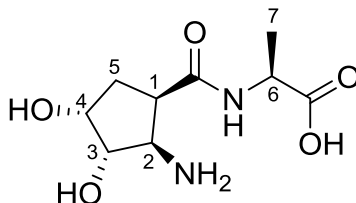
((1R,2R,3S,4R)-2-amino-3,4-dihydroxycyclopentane-1-carbonyl)-L-alanine

(DCUH). Yield 78%. **mp** 216-220ºC. ¹**H NMR** (400 MHz, D$_2$O): δ 1.31 (d, J = 7.2 Hz, 3H, H$_7$), 2.11-2.23 (m, 2H, H$_5$), 3.32 (q, J = 8.8 Hz, 1H, H$_1$), 3.69 (t, J = 9.2 Hz, 1H, H$_2$), 4.06 (q, J = 7.2 Hz, 1H, H$_6$), 4.19 (dt, J = 4.8 Hz, J = 2.4 Hz, 1H, H$_4$), 4.27 (dd, J = 9.2 Hz, J = 4.8 Hz, 1H, H$_3$). ¹³**C NMR** (100 MHz, D$_2$O): 17.0 (C$_7$), 34.3 (C$_5$), 39.8 (C$_1$), 51.2 (C$_6$), 55.4 (C$_2$), 70.0 (C$_4$), 75.7 (C$_3$), 173.1 (C=O, CONH), 180.0 (C=O, COOH). $[\alpha]_D^{20}$ - 86.7, c = 0.01 g.mL^{-1}in H$_2$O. **IR** (ν, cm^{-1}): 3447, 3301, 2876, 1654, 1611, 1551, 1523, 1455, 1430, 1408, 1393, 1367, 1347, 1332, 1286, 1248, 1230, 1184, 1127, 1109, 1048, 1030. **HRMS** (ESI, H$_2$O) calculated for C$_9$H$_{16}$N$_2$O$_5$ 232.2360, found M+H: 233.1133.

4.3 RESULTS AND DISCUSSION

4.3.1 SYNTHESIS OF THE UNSATURATED, SATURATED AND HYDROXYLATED DIMERS.

The first attempt to synthesise compound **13a** was made following the synthetic route in Scheme 4.3.
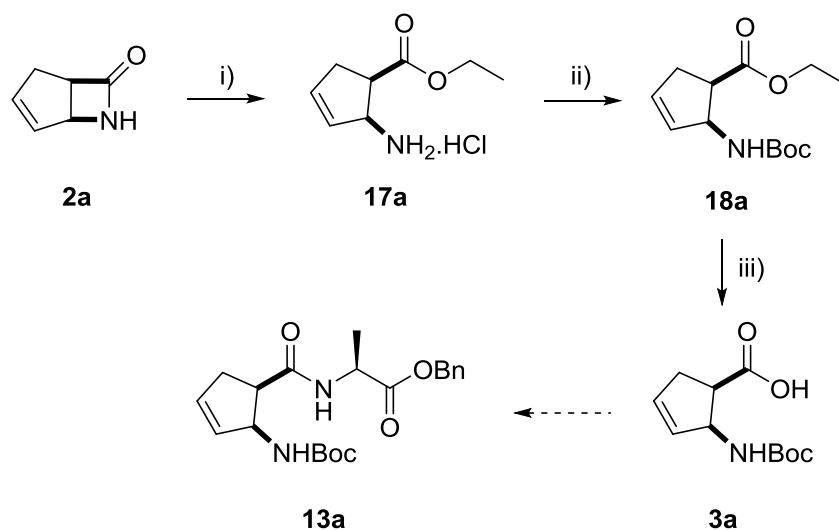
Scheme 4.3 Synthetic route to obtain dipeptide 13a. i) 22% HCl/EtOH, r.t.; ii) Et$_3$N, Boc$_2$O, Dioxane:H$_2$O, r.t.; iii) 0.1 M NaOH, EtOH, then 1 M HCl (workup).

Compound **17a** and **18a** were successfully synthesised, but in lower yields than expected, 47% and 59% respectively (64% and 69%).[87] The ester hydrolysis to obtain compound **3a** was also successfully carried out *via* saponification with NaOH forming a sodium carboxylate salt followed by acid hydrolysis during workup. The ^{1}H NMR analysis (Figure 4.2) of the product revealed a duplication of the peaks and it was theorised that there was epimerization at the α carbon compromising the subsequent enantiomerically pure desired compounds; for this reason, the synthetic route was abandoned. Compound **13a** was synthesised through the steps indicated in Scheme 4.1.
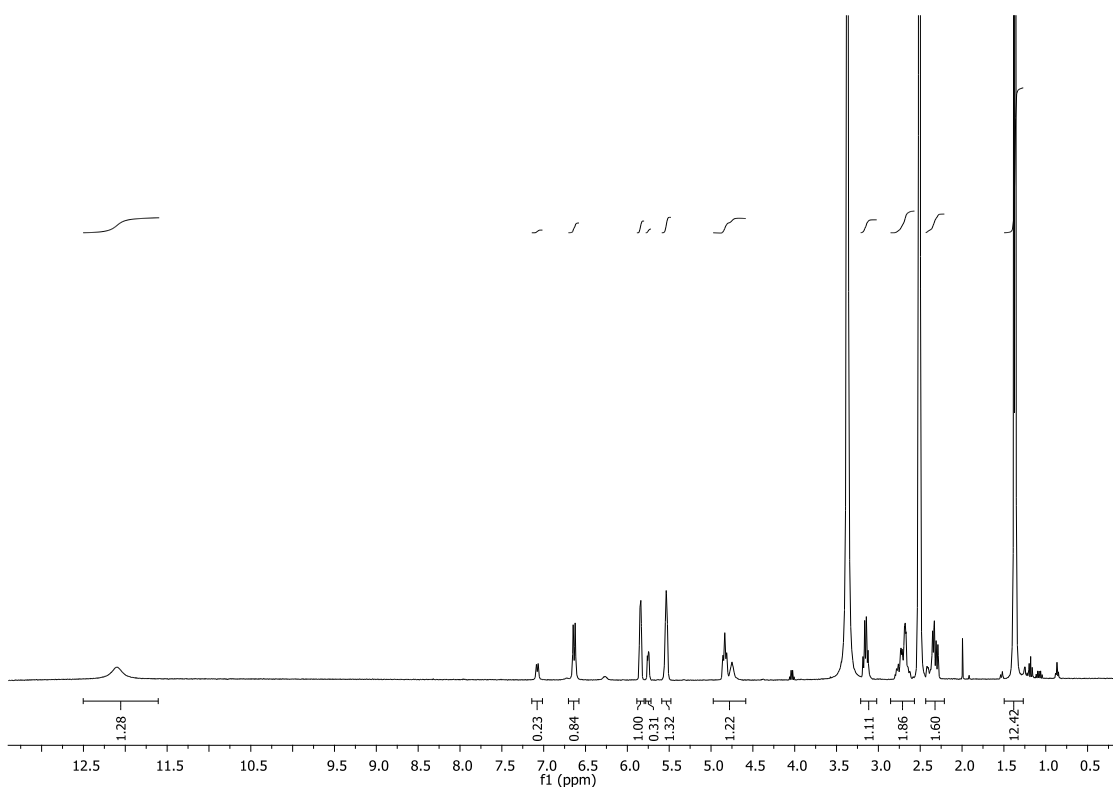
Figure 4.2 ^{1}H NMR spectrum showing possible epimerization of compound 3a.

Compound **14a** was synthesised as a derivative of **13a** allowing access to the hydroxylated precursor, using the same strategy as for the hydroxylated series of the monomers described in Chapter 3. The saturated series was obtained via the synthetic steps illustrated in Scheme 4.4.
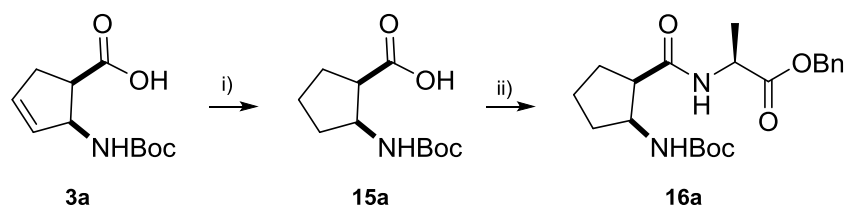
Scheme 4.4 Synthetic route to obtain the dimeric saturated precursor, 16a. i) H_2, Pd/C, MeOH; ii) L-Ala-*O*Bn.HCl, DIPEA, PyBop, DCM.

The orthogonal deprotection of compounds **14a** and **16a**, performed as described in Chapter 3, gave access to the final dimeric structures **DMS** and **DMH**, respectively. The unsaturated dimer could not be deprotected as previously described because the catalytic hydrogenation of **13a** reduced the double bond in the five membered ring (Scheme 4.5) giving **20a** as the product and a different approach had to be used.
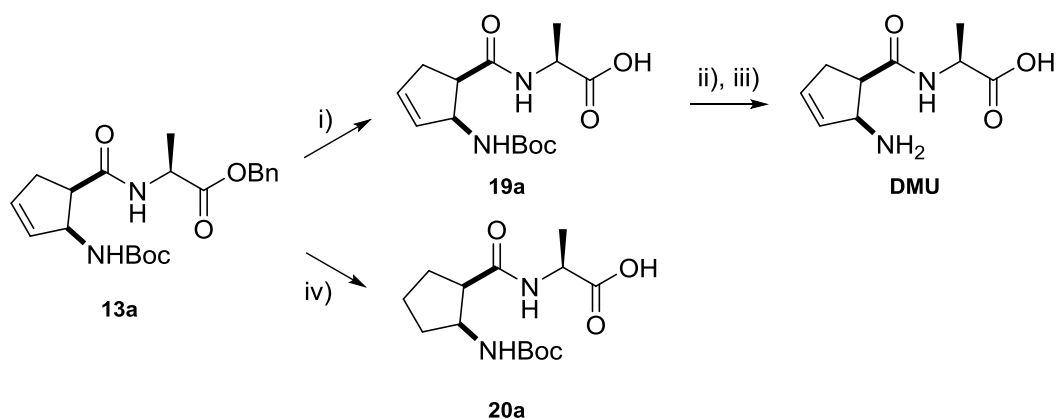
Scheme 4.5 Synthetic steps to obtain DMU. i) LiOH, MeOH, r.t.; ii) TFA, DCM, r.t.; iii) Dowex®, 2M NH_4OH, H_2O; iv) H_2, Pd/C, MeOH.

The second attempt to deprotect compound **13a** was carried out following the work of Giulliano *et al.*[103] with 4M HCl (Scheme 4.6) for 3 hours to cleave the Boc group. Reproduction of this procedure did not give the expected result (compound **21a**). After 3 hours there was still evidence of the starting material (TLC analysis) and after 5 hours a sample was analysed by NMR (Figure 4.3). It was evident that the acid labile group (Boc) was successfully removed (no peak at 1.29 ppm integrating for a total of 12 H) but the benzyl group was also removed (integration between 7.2 and 7.4 ppm is not proportional to the remaining peaks, 5 H were expected). A different method, by Kaul *et al.*,[104] described the removal of both protective groups with $ZnBr_2$ in DCM. Unfortunately, again the expected result was not achieved, and the product was compound **23a** (Scheme 4.6; NMR in Figure 4.4). Though it was also of interest to have a method that would give access to the final compound in one step, the orthogonal deprotection was needed for further coupling.
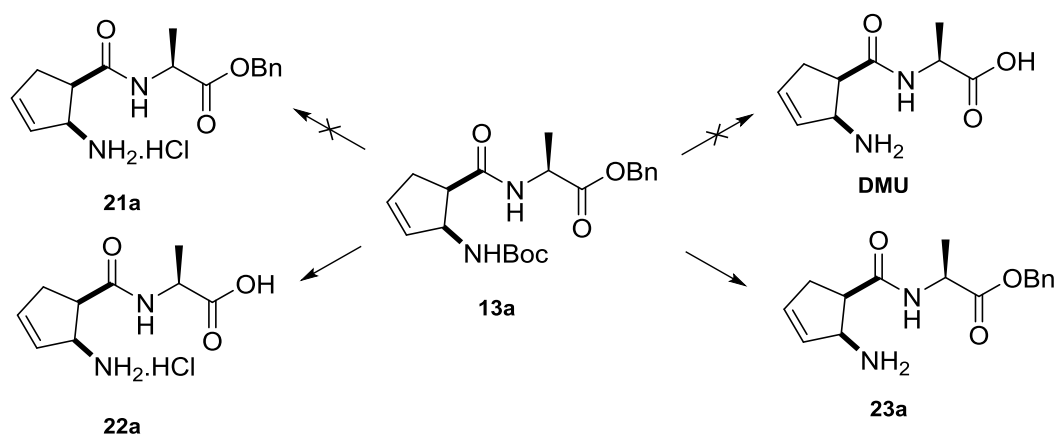
Scheme 4.6 Synthetic approaches to deprotect 13a.
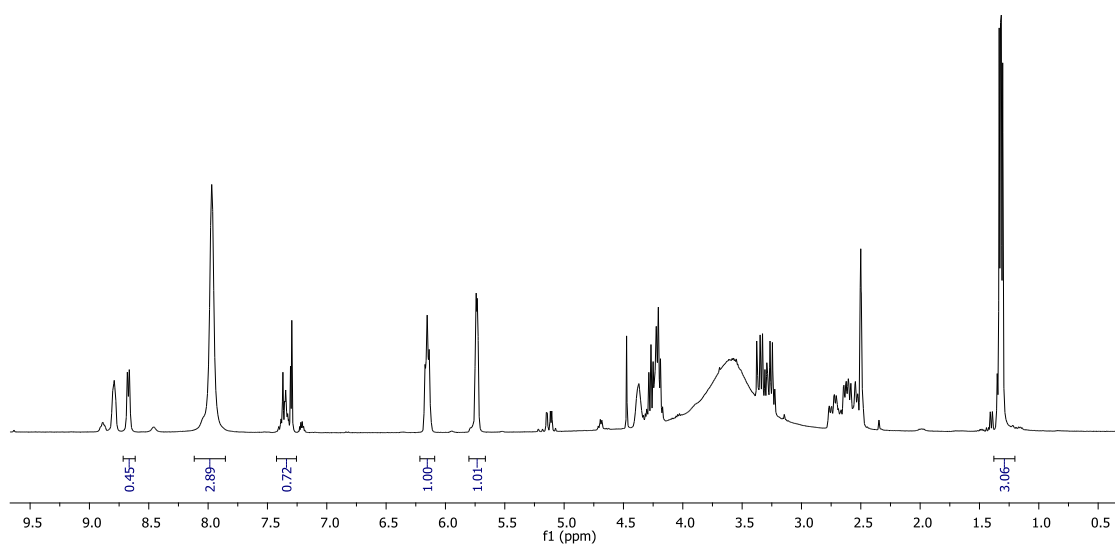
Figure 4.3 ^{1}H NMR of compound 21a.
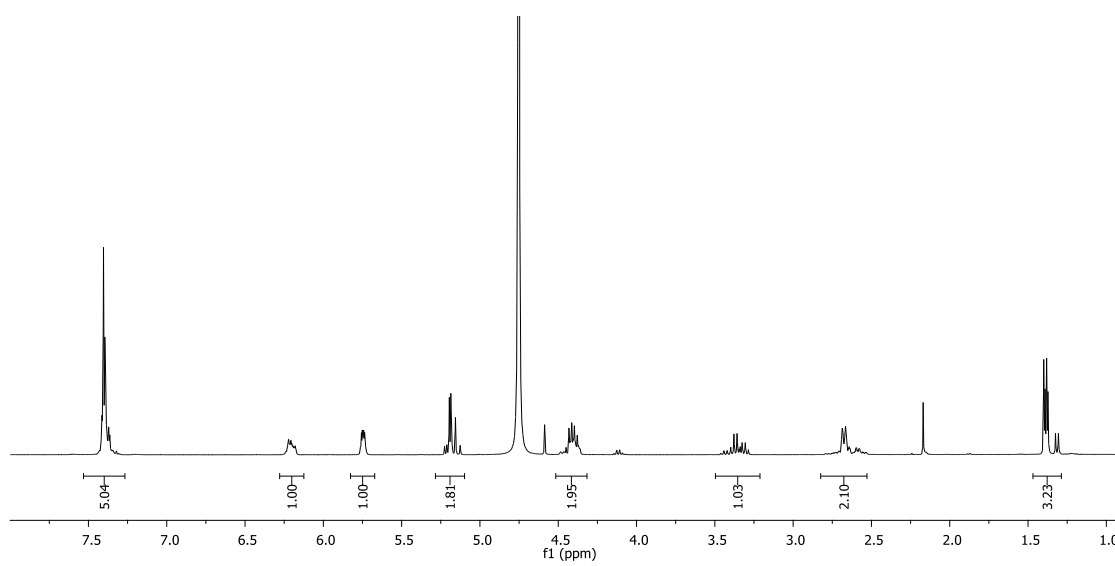
Figure 4.4 ^{1}H NMR of compound 23a.

Compound **19a** was obtained via alkaline hydrolysis (saponification) of **13a** as suggested in Figure 4.5. LiOH was used as base to avoid possible epimerization, as previously observed with a stronger nucleophile (NaOH).
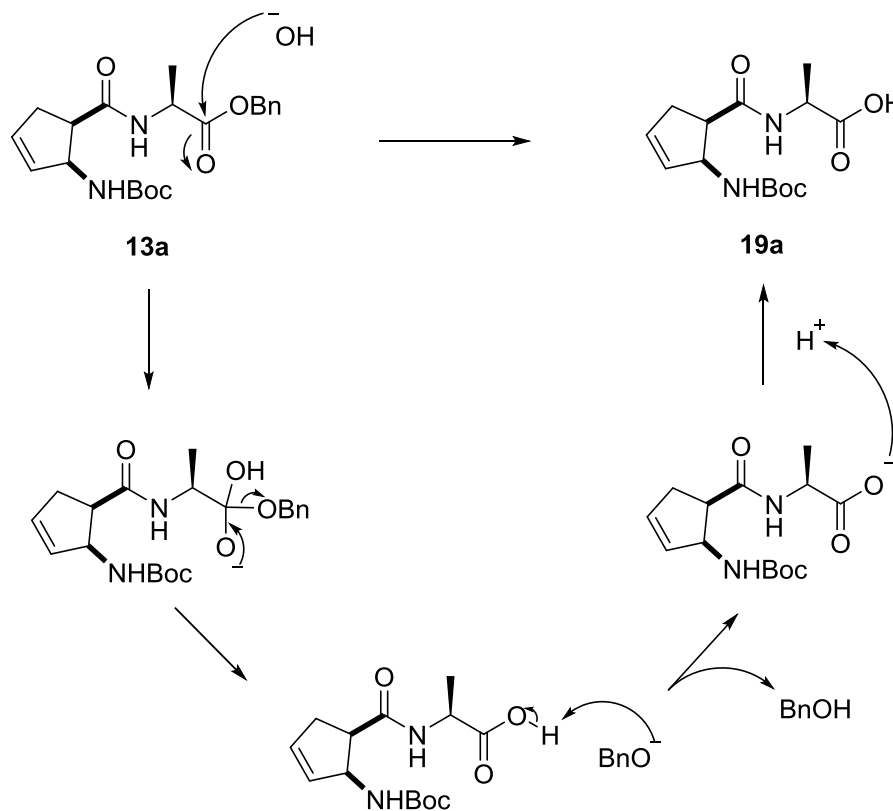
Figure 4.5 Proposed mechanism for the alkaline hydrolysis of 13a.

4.3.2 SYNTHESIS OF ENANTIOMERICALLY PURE UNSATURATED, SATURATED AND HYDROXYLATED DIMERS.

The synthetic steps to obtain the enantiomerically pure dimers were a repeat of the previous section; the difference resided in the starting materials being, of course, the enantiomerically pure precursors synthesised in Chapter 3. There were no special events in the synthetic strategy and the yields were essentially the same. The exception was the

occurrence of, what was theorised to be, rotamers (Figure 4.6) when synthesising compound **3b**.
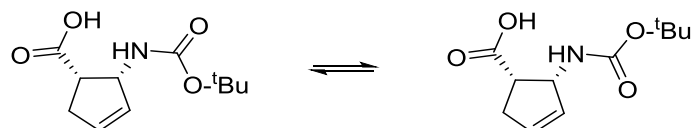
Figure 4.6 Representation of the rotation of the carbamate group for compound 3b.

It is not uncommon to observe the presence of rotamers when a Boc carbamate is present in a molecule. The reported compounds are no exception and it was most notorious in compound **3b**. Figure 4.7 shows the variable temperature proton NMR experiment (VT-^{1}H NMR) that was run to confirm the observation of rotamers. The selected region of the spectrum shows that the peaks corresponding to the NH (6.60 and 7.00 ppm) proton, as well as the peaks from the double bond (5.55 and 5.85 ppm) and the chiral proton at 4.80 ppm, coalesce as temperature rises.
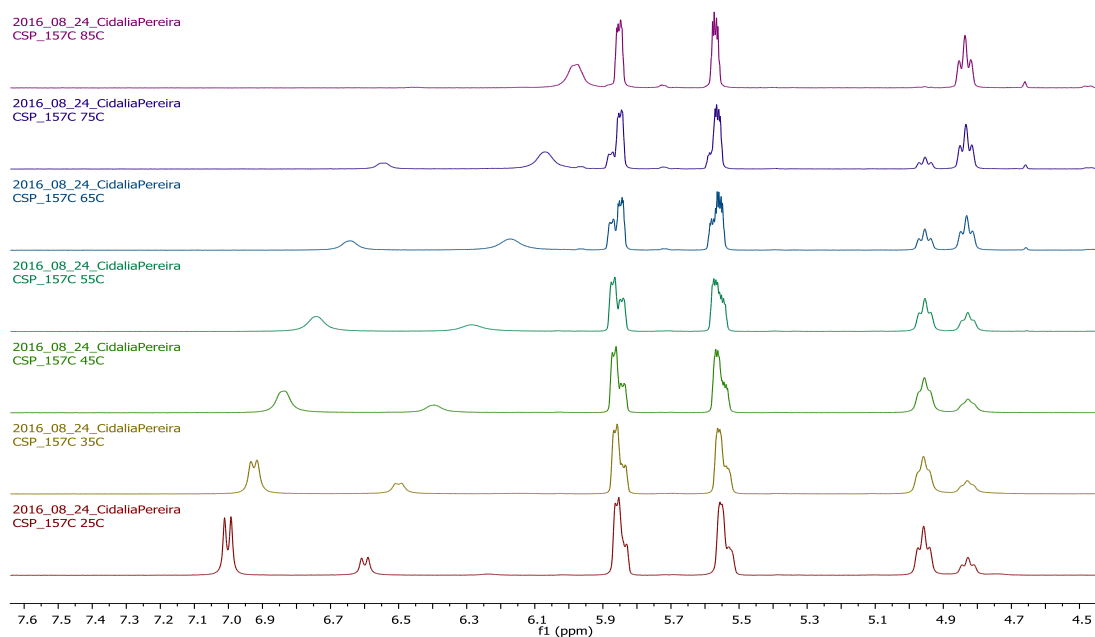
Figure 4.7 VT-^{1}H NMR experiment for compound 3b, from 25 to 85ºC.

Given this strong evidence that 3b is a rotamer, the previous assumption of epimerization of compound **3a** (section 4.3.1) is questionable as the result could also be explained by the presence of rotamers. Further scrutiny of both NMR spectra seems to support this conclusion for both compounds. However, as the synthetic route to compound **3a** was abandoned, no further studies were performed, though could be pursued as future studies. IR analysis can also provide evidence of rotamers as it is possible to observe multiple stretching bands for the C=O groups.

4.3.3 WATER UPTAKE DETERMINATION

The weight loss profile of the dimers was analysed as previously for the monomeric structures. Figure 4.8 shows their behaviour as temperature rises and Figure 4.9 illustrates the N_w per molecule of dimer. When analysing the weight loss profile, it is notable that some compounds show no weight change. These compounds (**DCUH** and **DMH**, 204 and 154, respectively in Figure 4.8) were "dry" after one week exposure to 100% RH. In contrast, **DCDU**, **DCDH** and **DMS** (186, 228 and 169, respectively in Figure 4.8) were in solution but all the water is lost up to ~100ºC and the compounds then maintain their weight until they reach their decomposition temperatures.
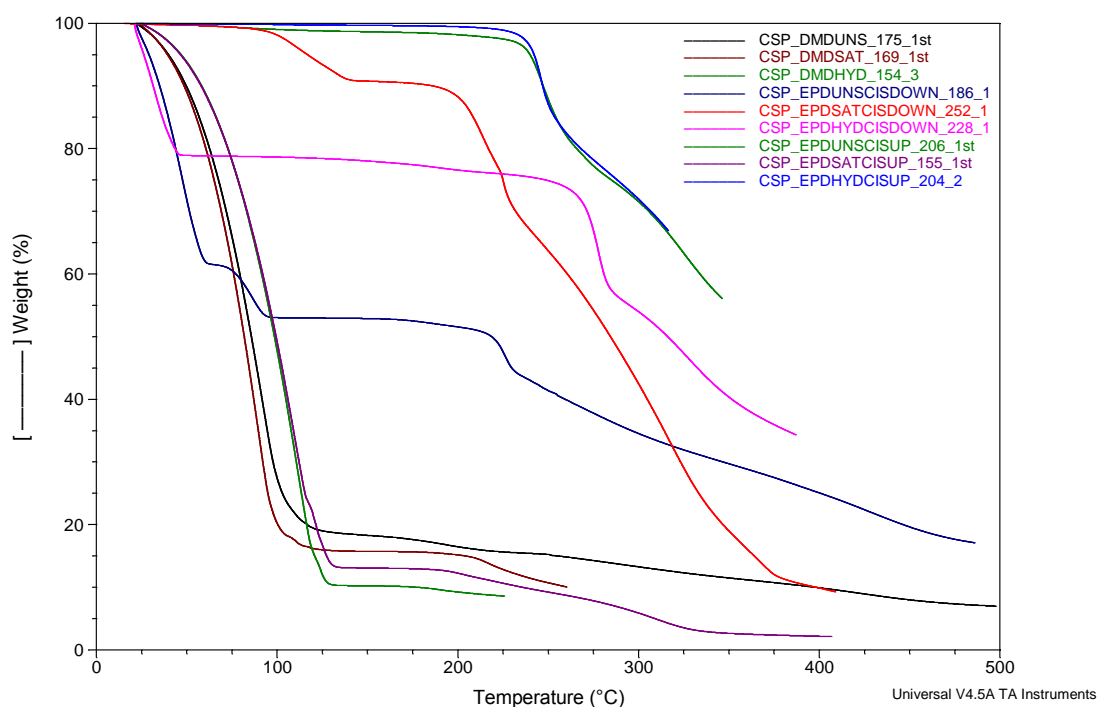
Figure 4.8 Thermogravimetric profiles for the dimeric structures. Sample codes, top to bottom: 175 – DMU, 169 – DMS, 154 – DMH, 186 – DCDU, 252 – DCDS, 228 – DCDH, 206 – DCUU, 155 – DCUS, 204 – DCUH.

As observed in the monomeric structures, the hydroxylated series has no water holding capacity suggesting that either intra or intermolecular hydrogen bonds occur and the hydrogen bond donor/acceptor (D/A) sites are not available to bind to water. The most remarkable observation comes from the saturated series. Having the same D/A relationship (Table 4.1), **DMS** holds one molecule of water whilst **DCUS** and **DCDS** bind to 7 and 1 molecule of water, respectively. Thermograms for each compound can be found in Appendix A7.
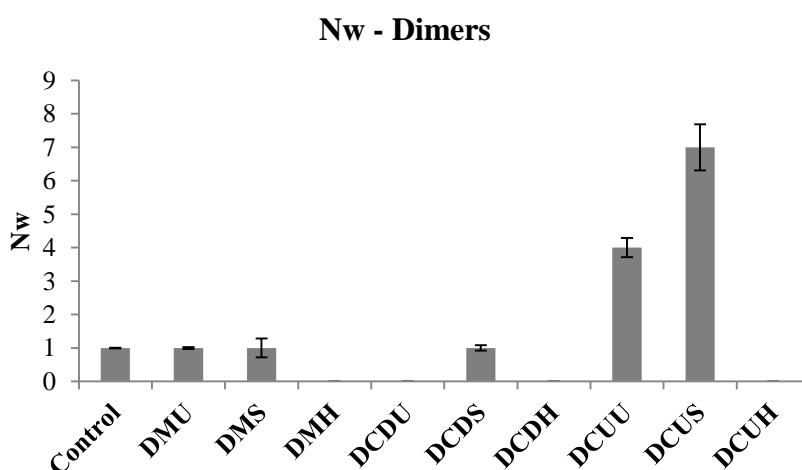
Figure 4.9 Water uptake of the dimeric structures, given as the number of water molecules per dimer molecule. Data are mean $\pm$ SD from n=3.

Table 4.1 Physico chemical properties of the dimers.
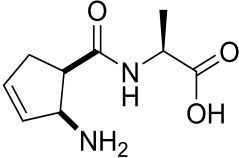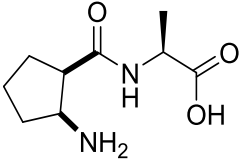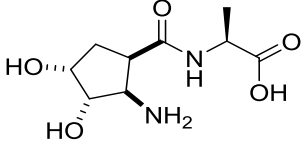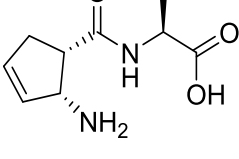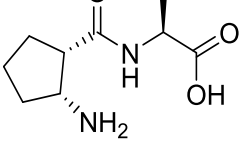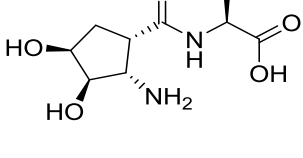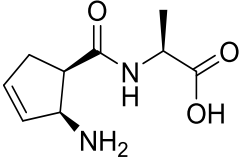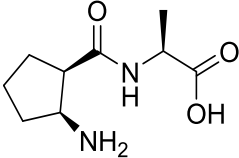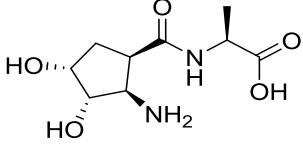
Structure	Mw	T/ºC	mp/ºC	D/A	D/A sites	N_w
DMU	198.22	112-140	103-106	3/5	4/8	1±0.03
DMS	200.12	112-135	205-208	3/5	4/8	1±0.28
DMH	232.24	100-150	228-233	5/7	6/12	0
DCDU	198.22	100-150	210-213	3/5	4/8	0
DCDS	200.12	118-153	188-191	3/5	4/8	1±0.08
DCDH	232.24	100-150	225-229	5/7	6/12	0

Table 4.1 (Continued)

Structure	Mw	T/ºC	mp/ºC	D/A	D/A sites	N_w
DCUU	198.22	125-150	176-180	3/5	4/8	4±0.29
DCUS	200.12	116-145	172-175	3/5	4/8	7±0.69
DCUH	232.24	100-150	216-220	5/7	6/12	0

In an attempt to explain these data, at a structural level, NOESY (Nuclear Overhauser Effect Spectroscopy) NMR experiments were run on compounds **DCUU**, **DCUS**, **DCDU**, **DCDS**, **DCUH** and **DCDH** (Appendix A8).

The results provide insight into the spatial arrangement of atoms in these molecules, and the results are summarised in Figure 4.10. The NOESY experiment can be used to measure interatomic distances; in this way, a strong NOE (red) means that the atoms are of 1.8-2.7 Å apart, a medium NOE (green) up to ~3.3 Å and a weak NOE (blue) for

atoms up to 5.0 Å. In this study data was used qualitatively to understand proximity between atoms.
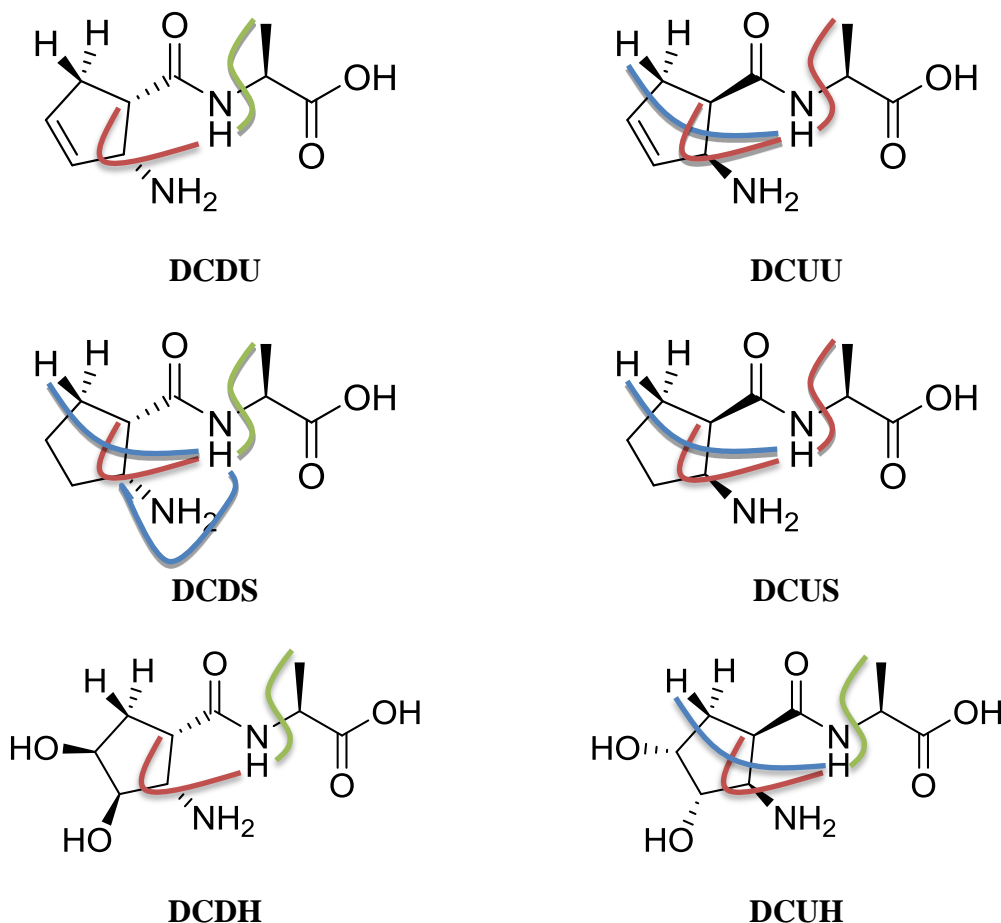
Figure 4.10 NOEs of the enantiomerically pure dimers. Samples were prepared at ~20 mg/mL in H_2O:D_2O (9:1, v:v).

With regard to the water holding capacity studies, some observations about geometry can be inferred. The unsaturated compounds (**DCDU** and **DCUU**) only share a strong NOE to the α hydrogen, implying that their geometry is significantly different, and this might be the reason of such different behaviour towards water holding capacity. The saturated compounds (**DCDS** and **DCUS**) differ in the proximity of the amide hydrogen

125

to the hydrogens in the methyl group of the alanine residue, conferring a different volume to the molecules and hence, a different availability of D/A sites. Finally, the hydroxylated compounds (**DCDH** and **DCUH**) have similar NOEs.

An attempt was made to further understand how water was binding to each structure; ChemDraw's Chem3D package was used to generate theoretical spatial arrangements of the dimers. Water molecules were added to the minimised energy structure of each compound and molecular dynamics calculations were performed. Three of the structures failed to reach an equilibrium state and so would require more detailed modelling studies. Figure 4.11 shows the results obtained where modelling was realistic. It is clear that all successfully modelled structures can "theoretically" bind to water, contradicting experimental data. In order to test the reliability of the modelling, measurements for expected NOEs were taken (Figure 4.11, right side) and the results are illustrated in Figure 4.12, comparing the experimentally derived NOE interactions against those from the theoretical modelling, using the same simplified scheme for interatomic distances.

The results in Figure 4.11 and 4.12 show that the generated theoretical structures are close to the experimental ones. **DCUS** and **DCUU** have an experimental/theoretical N_w of 7/7 and 4/5 respectively, and it can be assumed that the atomic spatial arrangement is fairly well represented by the theoretically modelled structures. The same conclusion cannot be drawn for compound **DCDU** (N_w, 0/7); experimental data showed no water holding capacity contradicting expectations. It was theorised that the structures could dimerise, and two molecules of each compound were modelled to understand how they could interact. As previously, the modelling was not successful for all compounds and the generated structures can be found in Appendix A9.
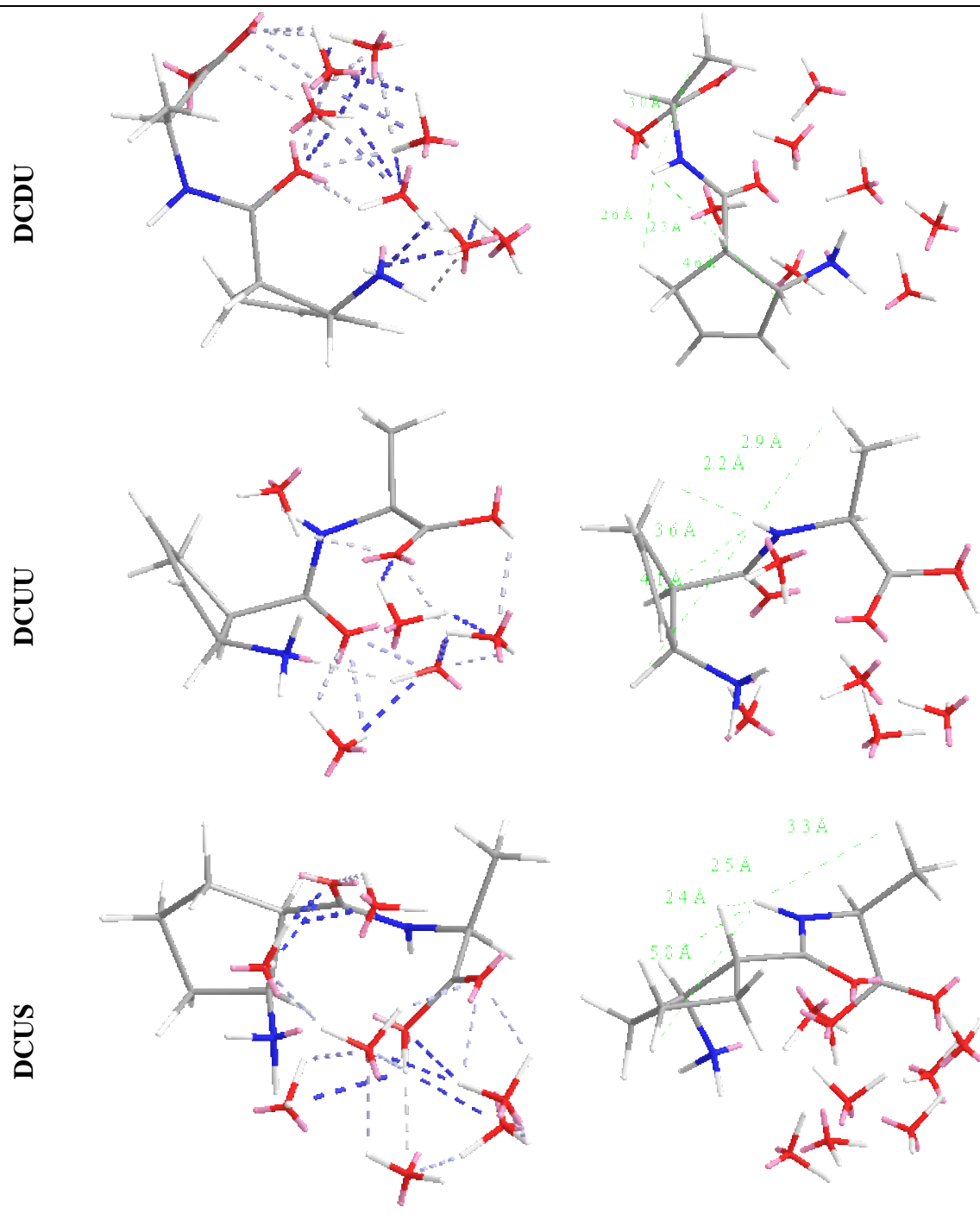
Figure 4.11 Theoretically bound water (left) and atomic distances (right) for DCDU, DCUU and DCUS.
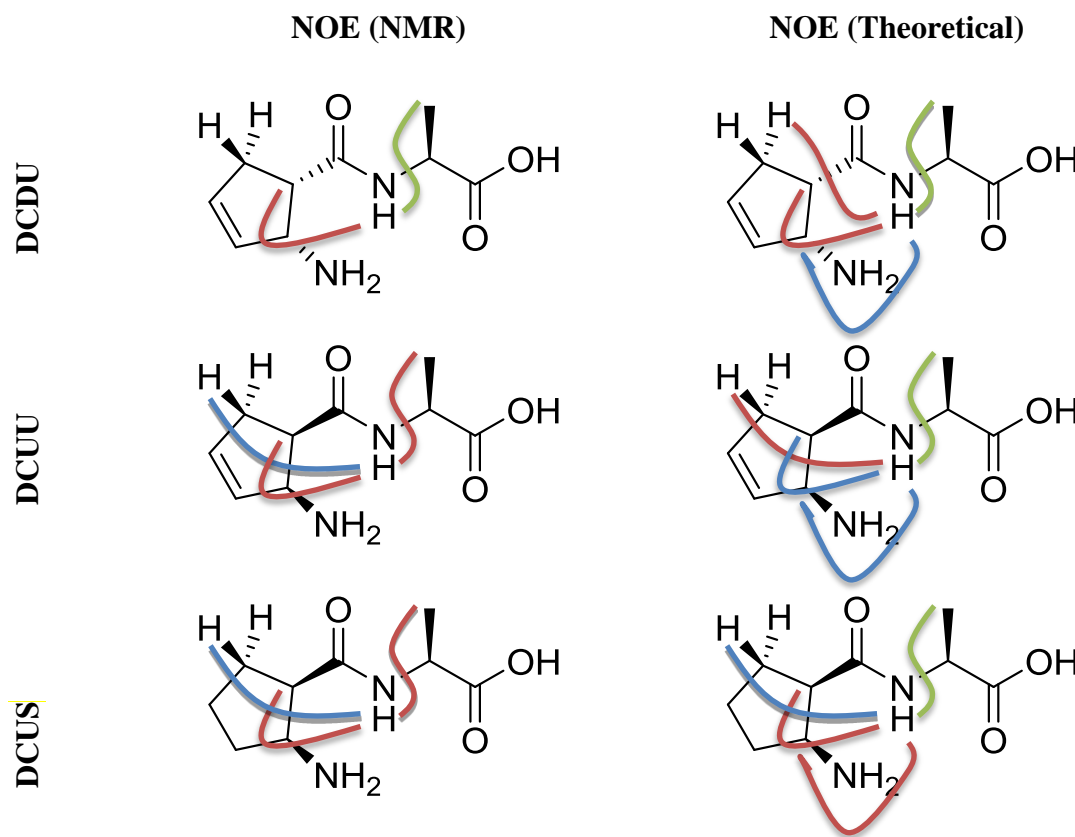
Figure 4.12 Comparison of proximity inferences between experimental and theoretical atomic distances.

4.4 CONCLUSIONS

Three series of dimers (unsaturated, saturated and hydroxylated) were synthesised in good yields providing a total of 9 compounds. The coupling agent gave higher yields for the amide condensation than those obtained for the ester (Chapter 3).

The increase of the molecule size had a significant impact on water uptake. Increasing the D/A relationship had no pronounced effect except for compounds **DCUS** and **DCDU**. There is no marked difference between racemic and enantiomerically pure

compounds except for **DCUU** and **DCUS**. Both compounds are derived from the same *cis* conformation (*cis* up). The compounds with the opposite conformation (*cis* down) do not bind to water. The hydroxylated series has the same behaviour as in the monomeric structures with no water holding capacity. Theoretically generated structures agree with experimental data for compound **DCUU** and **DCUS**, with experimental/theoretical N_w of 4/5 and 7/7, respectively.

Chapter 5 further investigates these results by generating potentially foldameric structures with additional rotational degree of freedom and analysing the possible inter/intramolecular interactions.

CHAPTER 5

5. Synthesis and Water Uptake of Higher Molecular Weight Molecules

5.1. Introduction

This chapter follows the same organisational logic of the previous two. An overview of the synthesised compounds (Figure 5.1) and the synthetic route followed is given in the current section. Synthetic procedures and the characterisation of the synthesised compounds are given in section 5.2. Section 5.3 discusses the synthetic approaches and the results obtained for water holding capacity and finally, section 5.4 provides the chapter's conclusions. The rational followed in previous chapters to code the structures herein synthesised was applied (**T** for tetramer, **H** for hexamer and **O** for octamer substitutes **D** for dimer from Chapter 4 and **M** for monomer from Chapter 3).
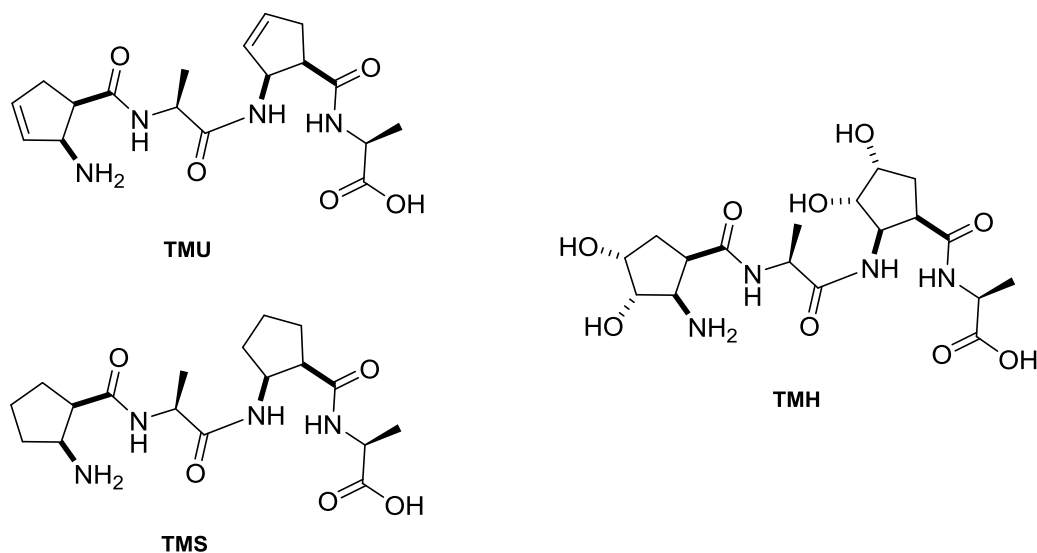
Figure 5.1 Summary of the synthesised structures.

TCDU

TCDH

TCDS

TCUU

TCUH

TCUS

Figure 5.1 (Continued).

HCUS

HCDH

HCUH

OCUS
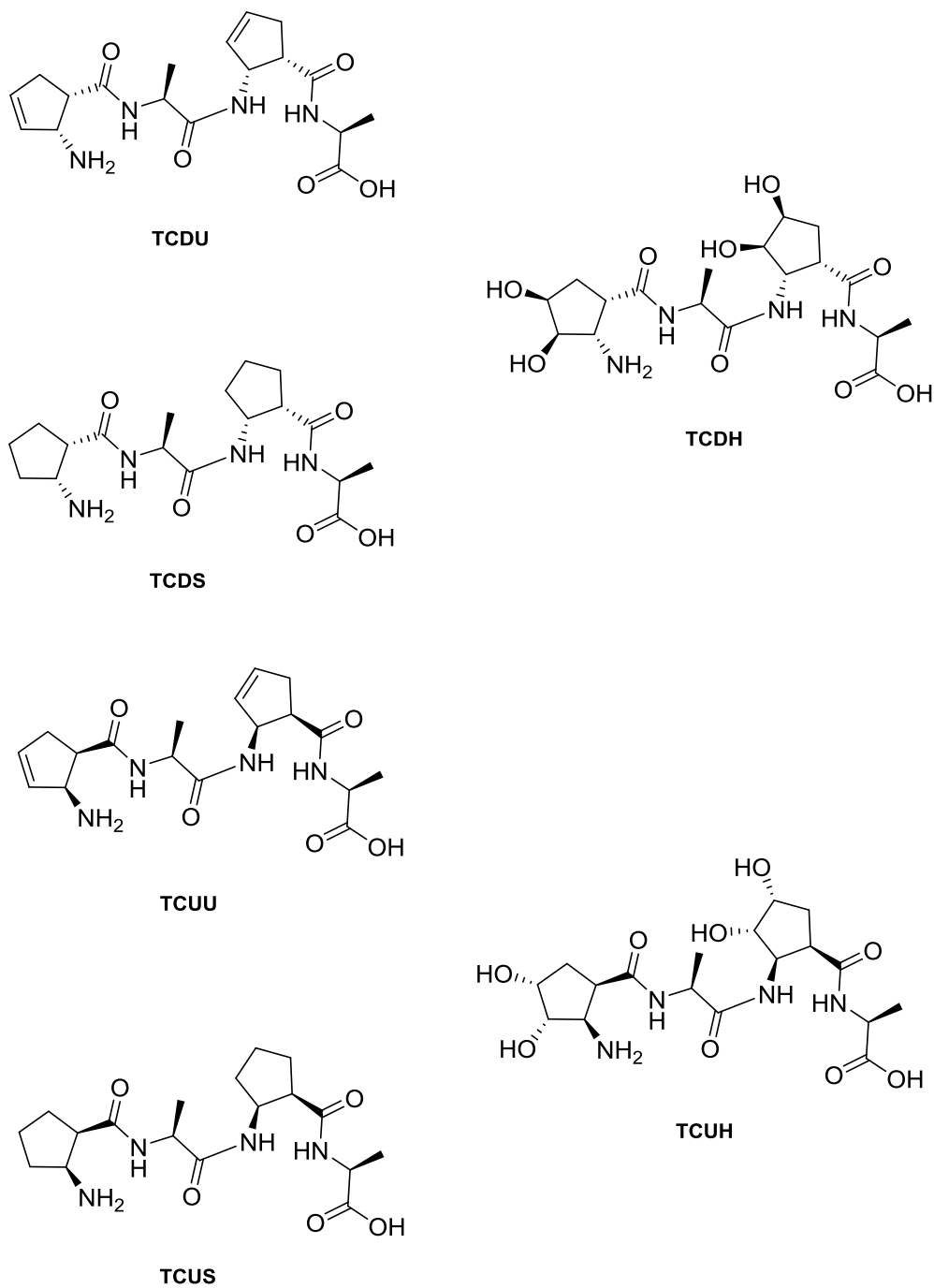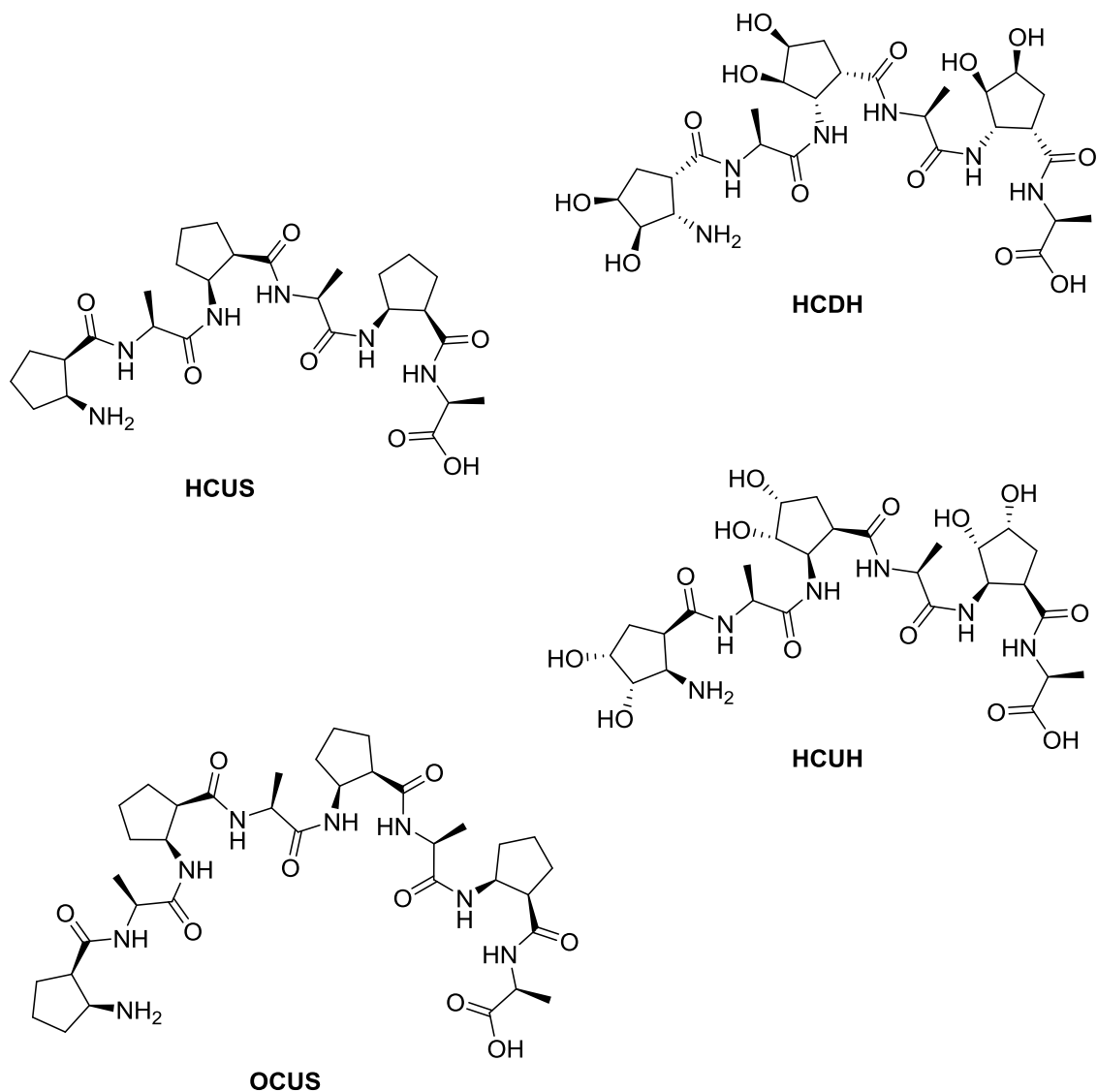
Figure 5.1 (continued)

The synthetic route (Schemes 5.1 and 5.2) follows the same strategy as previously described in Chapter 4. It involves the orthogonal deprotection of the amine and the acid groups followed by condensation into an amide bond.
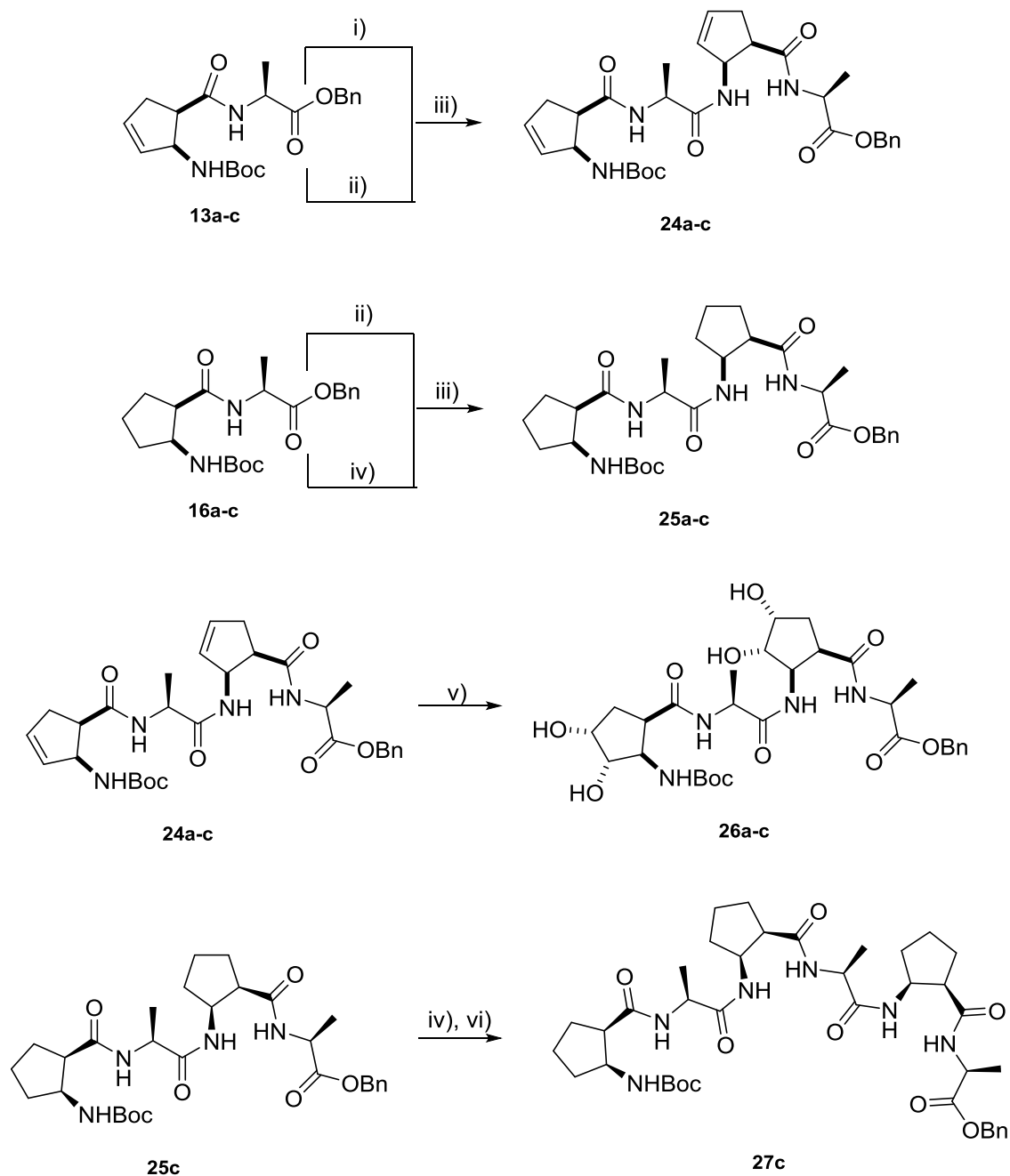
Scheme 5.1 Synthetic route to obtain the foldameric precursors. i) LiOH, MeOH, r.t. ii) TFA, DCM, 0°C iii) Pybop, DIPEA, DMSO iv) H$_2$, Pd/C, MeOH v) OsO4, NMO, Acetone. vi) 20c, Pybop, DIPEA, DMSO.

24b-c

ii), vii)

28b-c

v)

29b-c

i)

25c

iii)

ii)

30c
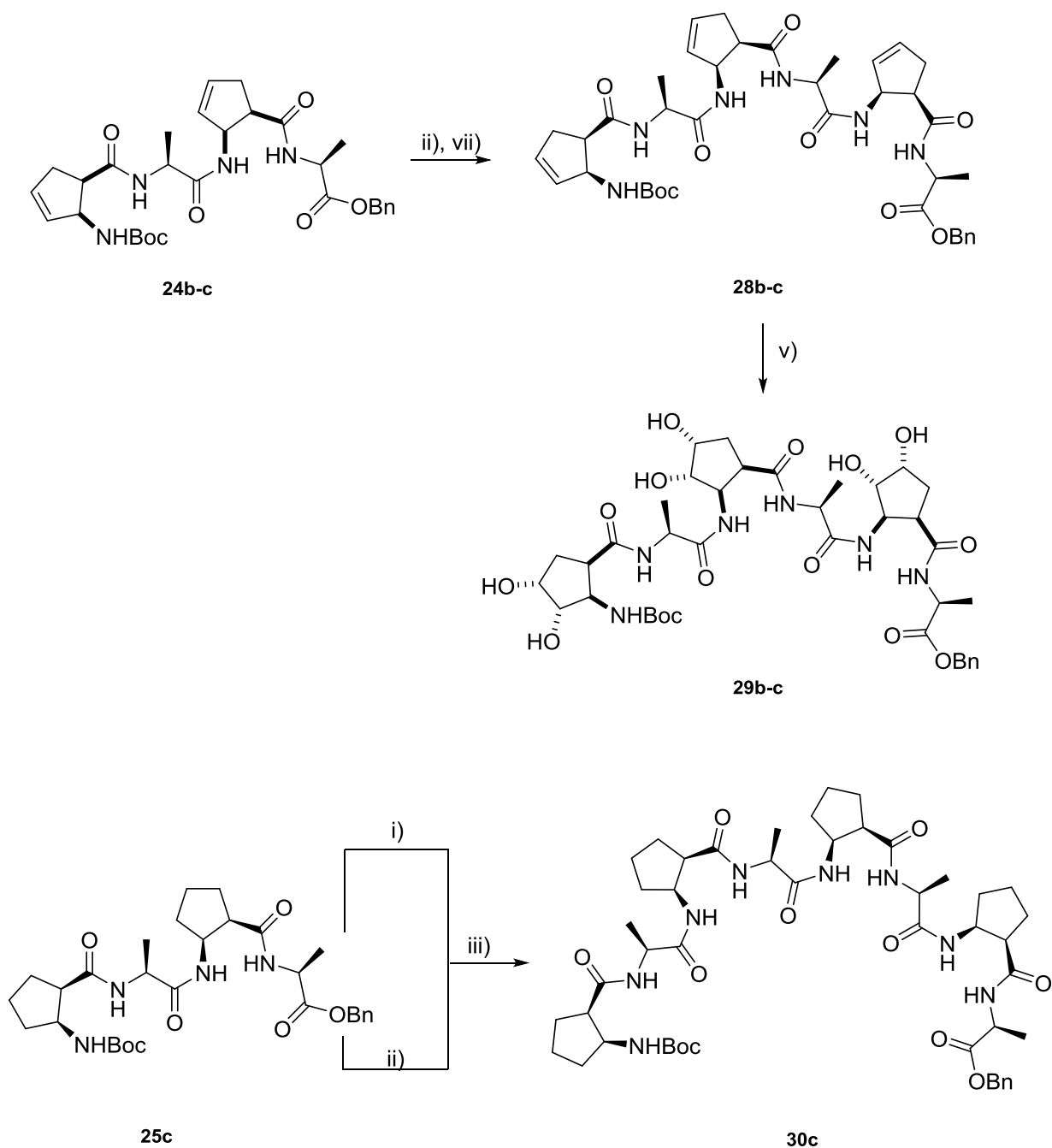
Scheme 5.1 (continued). vii) 19b or 19c, PyBop, DIPEA, DMSO.

The final compounds were obtained, as before, by deprotecting the acid and the amino group followed by ion exchange to assess the free foldameric structures illustrated in Figure 5.1. Spectral data for the described compounds can be found in Appendix A10.

5.2 EXPERIMENTAL

5.2.1 ORTHOGONAL DEPROTECTION OF THE AMINO AND ACID GROUPS

5.2.1.1 Acid group deprotection

As described in Chapter 4, *via* saponification, section 4.3.3.1.

Via hydrogenation

As described in Chapter 3, *via* hydrogenation, section 3.2.6.1.

5.2.1.2 Amino group deprotection

As described in Chapter 3, *via* TFA cleavage, section 3.2.6.2.

5.2.2 COUPLING

Procedure to synthesise compounds **24a-c**, **25a-c**, **27c**, **28b-c** and **30c**. DIPEA (6.03 mL, 4.47 mmol) followed by PyBop (0.93 g, 1.79 mmol) was added to a solution of the suitable *O*Bn deprotected dimer (0.45 g, 1.49 mmol) in DMSO and left stirring for 15 minutes at room temperature. The corresponding Boc deprotected dimer (0.60 mL, 1.49 mmol) and the mixture was left stirring for 48 hours. Water was added, and the mixture poured into a separating funnel. EtOAc (3x) was added and the layers separated. The

combined organic layers were dried over anhydrous Na_2SO_4, filtered and concentrated under reduced pressure. EtOAc was added (minimum amount) followed by hexane to precipitate the product. The solid (white/creamy powder) was then filtered and dried under suction.

5.2.3 HYDROXYLATION

Procedure to synthesise compounds **26a-c** and **29b-c**. As described in Chapter 3, section 3.2.5.

5.2.4 ION EXCHANGE

Procedure to synthesise compounds **TMU**, **TMS**, **TMH**, **TCDU**, **TCDS**, **TCDH**, **TCUU**, **TCUS**, **TCUH**, **HCUS**, **HCDH**, **HCUH**, and **OCUS**. As described in Chapter 3, section 3.2.7.

5.2.5 PRECURSORS CHARACTERISATION
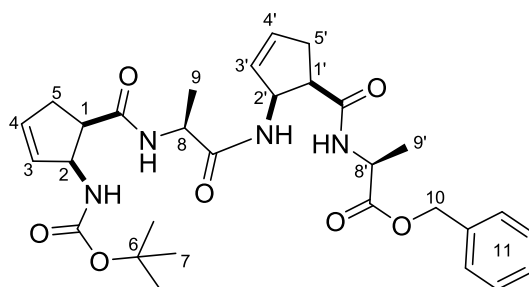
Benzyl (2-((2*S*)-2-(2-((*tert*-butoxycarbonyl)amino)cyclopent-3-ene-1-carboxamino) propanamido)cyclopent-3-ene-1-carbonyl)-*L*-alaninate (24a). **Yield** 96%. **^{1}H NMR** (400 MHz, DMSO): diastereomers δ 1.06-1.13 (m, 3H, H$_9$), 1.28 (m,3H, H$_{9'}$), 1.29-1.43 (m, 9H, H$_7$), 2.18-2.43 (m, 2H, H$_5$ and H$_{5'}$), 2.55-2.78 (m, 2H, H$_5$ and H$_{5'}$), 3.10-3.28

137

(m, 2H, H_1 and $H_{1'}$), 4.10-4.32 (m, 2H, H_8 and $H_{8'}$), 4.64-4.84 (m, 1H, H_2), 5.00-5.18

(m, 3H, $H_{2'}$ and H_{10}), 5.42-5.58 (m, 2H, H_4 and $H_{4'}$), 5.72-5.97 (m, 2H, H_3 and $H_{3'}$),

6.07-6.50 (m, 1H, N<u>H</u>COOCCH_3), 7.29-7.41 (m, 5H, H_{11}), 7.46-7.93 (m, 2H, CONH_{H1}

and CONH_{H2'}), 8.15-8.40 (m, 1H, CONH_{H1'}). ^{13}**C NMR** (100 MHz, DMSO): 16.6 ($C_{9'}$),

17.8 (C_9), 28.2 (C_7), 32.9 (C_5 and $C_{5'}$), 45.3 (C_1 and $C_{1'}$), 48.3 ($C_{8'}$), 49.8 (C_8), 55.0

($C_{2'}$), 57.0 (C_2), 65.7 (C_{10}), 82.7 (C_6), 127.6 (C_{11}), 127.7 (C_{11}), 128.0 (C_{11}), 128.4 (C_{11}),

130.1 (C_4 and $C_{4'}$), 132.3 (C_3 and $C_{3'}$), 136.1 (C_{11}), 156.7 (C=O, NH<u>C</u>OOCCH_3), 171.4

(C=O, CONH_{H1} and CONH_{H1'}), 172.3 (C=O, CONH_{H2'}), 173.4 (C=O, COOBn).

HRMS (ESI, MeOH) calculated for $C_{30}H_{40}N_4O_7$: 568.6710, found M+Na: 591.2777.
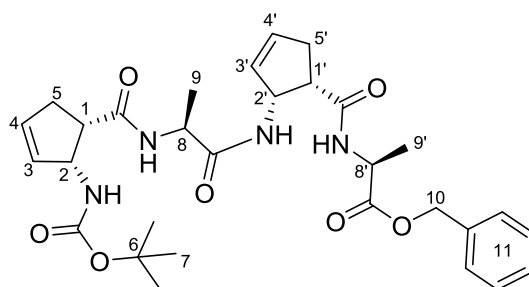
Benzyl ((1S,2R)-2-((S)-2((1S,2R)-2((tert-butoxycarbonyl)amino)cyclopent-3-ene-1-carboxamido)propanamido)cyclopent-3-ene-1-carbonyl)-L-alaninate (24b). **Yield**

55%. ^{1}**H NMR** (400 MHz, DMSO): δ rotamers, 1.09 (d, J = 7.2 Hz, 3H, H_9), 1.26 (d, J

= 7.2 Hz, 3H, $H_{9'}$), 1.32 (s, 9H, H_7), 2.23-2.39 (m, 2H, H_5 and $H_{5'}$), 2.55-2.74 (m, 1H,

H_5 and $H_{5'}$), 3.13-3.26 (m, 2H, H_1 and $H_{1'}$), 4.15-4.24 (m, 1H, H_8), 4.26-4.33 (m, 1H,

$H_{8'}$), 4.73-4.85 (m, 1H, H_2), 4.96-5.06 (m, 1H, $H_{2'}$), 5.07-5.15 (m, 2H, H_{10}), 5.45-5.61

(m, 2H, H_4 and $H_{4'}$), 5.76-5.93 (m, 2H, H_3 and $H_{3'}$), 6.07 (d, J = 9.2 Hz, 1H,

N<u>H</u>COOCCH_3), 7.29-7.41 (m, 5H, H_{11}), 7.55 (d, J = 8.8 Hz, 1H, CONH_{H2'}), 7.89 (d, J

= 7.2 Hz, 1H, CONH_{H1}), 8.37 (d, J = 7.2 Hz, 1H, CONH_{H1'}). ^{13}**C NMR** (100 MHz,

DMSO): 17.4 ($C_{9'}$), 17.9 (C_9), 28.2 (C_7), 33.7 ($C_{5'}$), 34.8 (C_5), 45.0 (C_1), 45.7 ($C_{1'}$), 47.8

(C$_{8'}$), 48.3 (C$_8$), 55.0 (C$_{2'}$), 57.0 (C$_2$), 66.8 (C$_{10}$), 77.6 (C$_6$), 127.7 (C$_{11}$), 128.3 (C$_{11}$), 128.4 (C$_{11}$), 129.8 (C$_{11}$), 130.3 (C$_4$ and C$_{4'}$), 132.8 (C$_3$ and C$_{3'}$), 136.0 (C$_{11}$), 154.6 (C=O, NH$\underline{C}$OOCCH$_3$), 171.2 (C=O, CONH$_{H1}$), 171.3 (C=O, CONH$_{H1'}$), 172.2 (C=O, CONH$_{H2'}$), 173.4 (C=O, COOBn). **IR** (ν, cm^{-1}): 3293, 2929, 1750, 1714, 1687, 1634, 1537, 1452, 1386, 1357, 1333, 1247, 1213, 1197, 1172, 1147, 1051, 1026. **HRMS** (ESI, MeOH) calculated for C$_{30}$H$_{40}$N$_4$O$_7$: 568.6710, found M+Na: 591.2785.
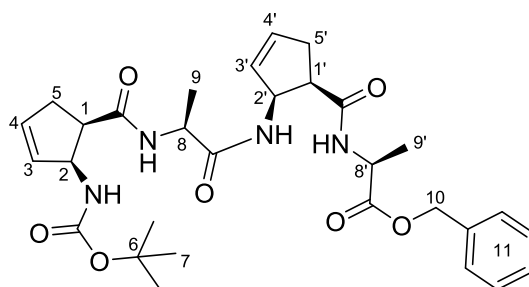
Benzyl ((1R,2S)-2-(((S)-2((1R,2S)-2-(($tert$-butoxycarbonyl)amino)cyclopent-3-ene-1-carboxamido)propanamido)cyclopent-3-ene-1-carbonyl)-L-alaninate (24c). Yield 91%. ^{1}**H NMR** (400 MHz, DMSO): δ rotamers, 1.10 (d, J = 7.2 Hz, 3H, H$_9$), 1.19-1.27 (m, J = 7.2 Hz, 3H, H$_{9'}$), 1.33 (s, 9H, H$_7$), 2.18-2.40 (m, 2H, H$_5$ and H$_{5'}$), 2.56-2.78 (m, 1H, H$_5$ and H$_{5'}$), 2.98-3.28 (m, 2H, H$_1$ and H$_{1'}$), 4.09-4.38 (m, 1H, H$_8$ and H$_{8'}$), 4.54-4.87 (m, 1H, H$_2$), 5.01-5.19 (m, 3H, H$_{2'}$ and H$_{10}$), 5.40-5.74 (m, 2H, H$_4$ and H$_{4'}$), 5.75-5.97 (m, 2H, H$_3$ and H$_{3'}$), 6.26 (dd, J = 9.2 Hz, J=8.8 Hz, 1H, N$\underline{H}$COOCCH$_3$), 7.28-7.41 (m, 5H, H$_{11}$), 7.54 (dd, J=8.8 Hz, J = 9.6 Hz, 1H, CONH$_{H2'}$), 7.85 (dd, J = 7.6 Hz, J = 7.6 Hz, 1H, CONH$_{H1'}$), 8.37 (dd, J = 6.8 Hz, J = 6.8 Hz, 1H, CONH$_{H1}$). ^{13}**C NMR** (100 MHz, DMSO): 16.6 (C$_{9'}$), 18.4 (C$_9$), 28.2 (C$_7$), 34.7 (C$_{5'}$), 35.4 (C$_5$), 45.9 (C$_1$ and C$_{1'}$), 48.5 (C$_8$ and C$_{8'}$), 55.6 (C$_{2'}$), 57.3 (C$_2$), 65.7 (C$_{10}$), 77.8 (C$_6$), 127.7 (C$_{11}$), 128.0 (C$_{11}$), 128.4 (C$_{11}$), 129.3 (C$_{3'}$), 19.4 (C$_4$ and C$_{4'}$), 129.6 (C$_3$), 136.1 (C$_{11}$), 154.7 (C=O,

NH$\underline{C}$OOCCH$_3$), 170.6 (C=O, CONH$_{H1}$), 171.5 (C=O, CONH$_{H1'}$), 172.4 (C=O, CONH$_{H2'}$), 174.9 (C=O, COOBn). **IR** (ν, cm^{-1}): 3293, 2930, 2360, 2341, 1738, 1686, 1637, 1532, 1452, 1389, 1364, 1355, 1281, 1244, 1218, 1152, 1051. **HRMS** (ESI, MeOH) calculated for C$_{30}$H$_{40}$N$_4$O$_7$: 568.6710, found M+Na: 591.2786.
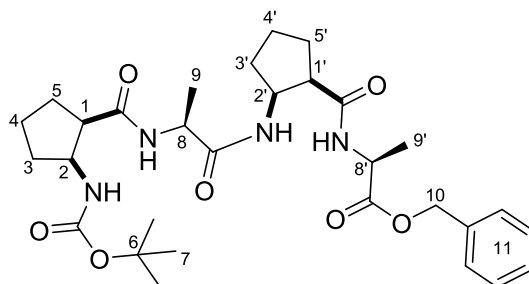
Benzyl **(2-((2*S*)-2-(2-((*tert*-butoxycarbonyl)amino)cyclopentane-1-carboxamido)propanamido)cyclopentane-1-carbonyl)-*L*-alaninate** **(25a)**. **Yield** 27%. **^{1}H NMR** (400 MHz, DMSO): δ diastereomers, 1.07-1.18 (m, 3H, H$_9$), 1.20-1.30 (m, 3H, H$_{9'}$), 1.34 (s, 9H, H$_7$), 1.39-1.91 (m, 12H, H$_3$, H$_{3'}$, H$_4$, H$_{4'}$, H$_5$ and H$_{5'}$), 2.65-2.89 (m, 2H, H$_1$ and H$_{1'}$), 3.85-4.06 (m, 1H, H$_2$), 4.08-4.34 (m, 3H, H$_{2'}$, H$_8$ and H$_{8'}$), 5.02-5.17 (m, 2H, H$_{10}$), 6.19-6.46 (m, 1H, N$\underline{H}$COOCCH$_3$), 7.27-7.41 (m, 5H, H$_{11}$), 7.54 (dddd, *J* = 8.4 Hz, *J* = 8.4 Hz, *J* = 7.6 Hz, *J* = 7.2 Hz, 1H, CONH$_{H2'}$), 7.85 (ddd, *J* = 7.6 Hz, *J* = 6.8 Hz, *J* = 6.8 Hz, 1H, CONH$_{H1'}$), 8.37 (ddd, *J* = 8.0 Hz, *J* = 6.4 Hz, *J* = 3.2 Hz, 1H, CONH$_{H1}$). **^{13}C NMR** (101 MHz, DMSO): 17.1 (C$_{9'}$), 18.6 (C$_9$), 22.2 (C$_4$ and C$_{4'}$), 27.6 (C5 and C$_{5'}$), 28.5 (C$_7$), 32.2 (C$_3$ and C$_{3'}$), 46.8 (C$_1$ and C$_{1'}$), 48.2 (C$_8$), 48.8 (C$_{8'}$), 52.4 (C$_{2'}$), 54.0 (C$_2$), 66.4 (C$_{10}$), 128.4 (C$_{11}$), 173.0 (4xC=O, CONH). **HRMS** (ESI, MeOH) calculated for C$_{30}$H$_{44}$N$_4$O$_7$: 572.7030, found M+Na: 595.3096.
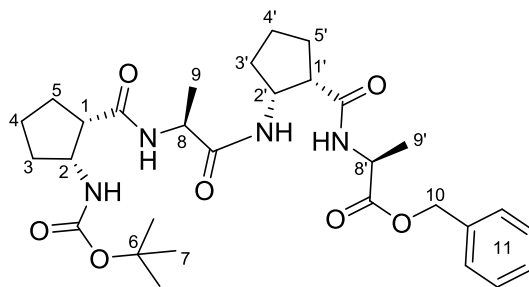
Benzyl **((1S,2R)-2-((S)-2((1S,2R)-2((*tert*-butoxycarbonyl)amino)cyclopentane-1-carboxamido)propanamido)cyclopentane-1-carbonyl)-*L*-alaninate** **(25b)**. **Yield** 59%. **¹H NMR** (400 MHz, DMSO): δ rotamers, 1.10 (d, *J* = 6.8 Hz, 3H, H₉), 1.26 (d, *J* = 7.2 Hz, 3H, H₉'), 1.33 (s, 9H, H₇), 1.46-1.93 (m, 12H, H₃, H₃', H₄, H₄' H₅, and H₅'), 2.79 (dd, *J* = 7.2 Hz, *J* = 7.6 Hz, H₁ and H₁'), 3.92-4.07 (m, 1H, H₂), 4.10-4.23 (m, 2H, H₂' and H₈), 4.23-4.34 (m, 1H, H₈'), 5.10 (s, 2H, H₁₀), 6.25 (d, *J* = 7.2 Hz, N<u>H</u>COOCCH₃), 7.26-7.42 (m, 5H, H₁₁), 7.46 (d, *J* = 8.0 Hz, 1H, CONH_{H1}), 7.81 (d, *J* = 7.2 Hz, 1H, CONH_{H2'}), 8.34 (d, *J* = 6.8 Hz, J=6.8 Hz1H, CONH_{H1'}). **¹³C NMR** (101 MHz, DMSO): 17.1 (C₉'), 17.6 (C₉), 21.9 (C4 and C₄'), 27.5 (C5 and C₅'), 28.2 (C₇), 32.1 (C₃ and C₃'), 45.9 (C₁ and C₁'), 47.6 (C₈), 48.1 (C₈'), 53.1 (C₂'), 53.6 (C₂), 65.9 (C₁₀), 77.7 (C₆), 127.9 (C₁₁), 128.1 (C₁₁), 128.5 (C₁₁), 135.9 (C₁₁), 154.8 (C=O, NH<u>C</u>OOCCH₃), 171.5 (C=O, CONH_{H1}), 172.2 (C=O, CONH_{H1'}), 172.4 (C=O, CONH_{H2'}), 172.8 (C=O, COOBn). **IR** (ν, cm⁻¹): 3325, 2966, 2359, 1740, 1684, 1646, 1637, 1536, 1449, 1389, 1366, 1315, 1288, 1247, 1215, 1195, 1173, 1138, 1058, 1042, 1018. **HRMS** (ESI, MeOH) calculated for $C_{30}H_{44}N_4O_7$: 572.7030, found M+Na: 595.3095.
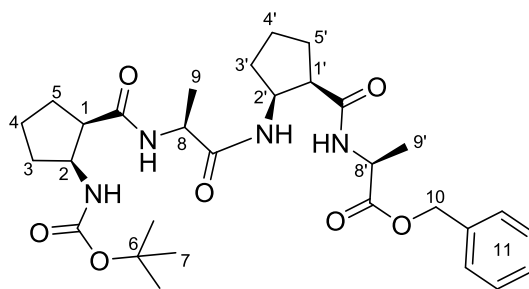
Benzyl **((1*R*,2*S*)-2-((*S*)-2((1*R*,2*S*)-2((*tert*-butoxycarbonyl)amino)cyclopentane-1-carboxamido)propanamido)cyclopentane-1-carbonyl)-*L*-alaninate** **(25c).** **Yield** 93%. **^{1}H NMR** (400 MHz, DMSO): δ, 1.11 (d, *J* = 7.2 Hz, 3H, H$_9$), 1.23 (d, *J* = 7.6 Hz, 3H, H$_{9'}$), 1.34 (s, 9H, H$_7$), 1.42-1.92 (m, 12H, H$_3$, H$_{3'}$, H$_4$, H$_{4'}$ H$_5$, and H$_{5'}$), 2.73-2.87 (m, 2H, H$_1$ and H$_{1'}$), 3.92-4.07 (m, 1H, H$_2$), 4.09-4.34 (m, 3H, H$_{2'}$, H$_8$ and H$_{8'}$), 5.09 (dd, *J* = 20.0 Hz, *J* = 12.8 Hz, 2H, H$_{10}$), 6.31 (d, *J* = 8.0 Hz, N<u>H</u>COOCCH$_3$), 7.24-7.42 (m, 5H, H$_{11}$), 7.53 (d, *J* = 8.4 Hz, 1H, CONH$_{H1}$), 7.78 (d, *J* = 7.2 Hz, 1H, CONH$_{H2'}$), 8.29 (d, *J* = 6.4 Hz, 1H, CONH$_{H1'}$). **^{13}C NMR** (101 MHz, DMSO): 16.1 (C$_{9'}$), 18.3 (C$_9$), 22.4 (C4 and C$_{4'}$), 28.1 (C5 and C$_{5'}$), 28.2 (C$_7$), 32.2 (C$_3$ and C$_{3'}$), 46.4 (C$_1$ and C$_{1'}$), 47.7 (C$_8$ and C$_{8'}$), 51.6 (C$_2$ and C$_{2'}$), 65.7 (C$_{10}$), 77.5 (C$_6$), 128.0 (C$_{11}$), 171.6 (C=O, CONH$_{H1}$ and C=O, CONH$_{H1'}$), 172.6 (C=O, CONH$_{H2'}$ and C=O, COOBn). **IR** (ν, cm$^-$^{1}): 3323, 2961, 2358, 2342, 2177, 1759, 1685, 1638, 1529, 1447, 1364, 1311, 1286, 1167, 1055, 1011. **HRMS** (ESI, MeOH) calculated for C$_{30}$H$_{44}$N$_4$O$_7$: 572.7030, found M+Na: 595.3091.
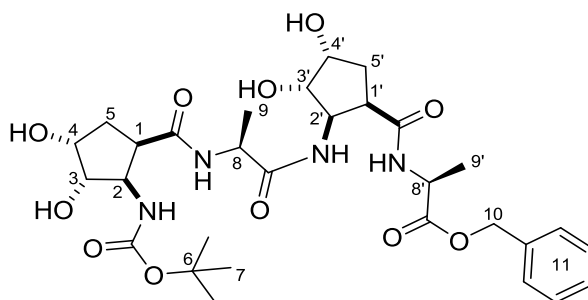
Benzyl (2-((2S)-2-(2-((*tert*-butoxycarbonyl)amino)-3,4-dihydroxycyclopentane-1-carboxamido)propanamido)-3,4-dihydroxycyclopentane-1-carbonyl)-*L*-alaninate (26a). Yield 53%. **^{1}H NMR** (400 MHz, DMSO): δ diastereomers, 1.10 (dd, *J* = 6.8 Hz, *J* = 6.8 Hz, 3H, H$_9$), 1.22 (d, *J* = 7.2 Hz, 3H, H$_{9'}$), 1.35 (s, 9H, H$_7$), 1.53-1.69 (m, 2H, H$_5$ and H$_{5'}$), 1.86-2.05 (m, 2H, H$_5$ and H$_{5'}$), 2.97-3.13 (m, 2H, H$_1$ and H$_{1'}$), 3.70-3.96 (m, 5H, H$_2$, H$_{2'}$, H$_3$, H$_4$ and H$_{4'}$), 4.09-4.38 (m, 3H, H$_{3'}$, H$_8$ and H$_{8'}$), 4.67 (s.br, 4H, OH), 5.01-5.19 (m, 2H, H$_{10}$), 6.16 (dddd, *J* = 8.4 Hz, *J* = 8.4 Hz, *J* = 8.4 Hz, *J* = 4.8 Hz, 1H, N<u>H</u>COOCCH$_3$), 7.26-7.41 (m, 5H, H$_{11}$), 7.48 (d, *J* = 9.2 Hz, 1H, CONH$_{H2'}$), 7.81 (dd, *J* = 8.0 Hz, *J* = 6.0 Hz, 1H, CONH$_{H1'}$), 8.33 (ddd, *J* = 8.0 Hz, *J* = 6.8 Hz, *J* = 6.4 Hz, 1H, CONH$_{H1}$). **^{13}C NMR** (101 MHz, DMSO): 16.8 (C$_{9'}$), 18.6 (C$_9$), 28.5 (C$_7$), 34.4 (C$_{5'}$), 34.2 (C$_5$), 42.6 (C$_1$ and C$_{1'}$), 48.4 (C$_8$ and C$_{8'}$), 55.2 (C$_{2'}$), 56.8 (C$_4$), 66.1 (C$_{10}$), 70.0 (C3), 77.8 (C$_6$), 127.6 (C$_{11}$), 128.0 (C$_{11}$), 128.4 (C$_{11}$), 136.1 (C$_{11}$), 172.5 (C=O, CONH$_{H1}$), 173.2 (C=O, CONH$_{H1'}$), 173.4 (C=O, CONH$_{H2'}$), 173.8 (C=O, COOBn).

Benzyl   ((1*S*,**2***S*,**3***R*,**4***S*)-2((***S***)-2-((1S,2S,3R,4S)-2-((***tert***-butoxycarbonyl)amino)-3,4-dihydroxycyclopentane-1-carboxamido)propanamido)-3,4-dihydroxycyclopentane-1-carbonyl)-***L***-alaninate (26b). Yield:** 56%. **^{1}H NMR** (400 MHz, DMSO) δ 1.09 (d, J = 6.8 Hz, 3H, H_9), 1.23 (d, J = 7.2 Hz, 3H, $H_{9'}$), 1.33 (s, 9H, H_7), 1.55-1.69 (m, 2H, H_5 and $H_{5'}$), 1.90-2.05 (m, 2H, H_5 and $H_{5'}$), 2.98-3.14 (m, 2H, H_1 and $H_{1'}$), 3.69-3.99 (m, 5H, H_2, $H_{2'}$, H_3, H_4 and $H_{4'}$), 4.11-4.32 (m, 3H, $H_{3'}$, H_8 and $H_{8'}$), 4.56 (s.br, 4H, OH), 5.08 (s.br, 2H, H_{10}), 6.04 (d, J = 8.4 Hz, 1H, N$\underline{H}$COOCCH$_3$), 7.26-7.46 (m, 6H, H_{11} and CONH$_{H2'}$), 7.83 (d, J = 7.6 Hz, 1H, CONH$_{H1'}$), 8.36 (d, J = 6.8 Hz, 1H, CONH$_{H1}$). **^{13}C NMR** (101 MHz, DMSO) 17.3 ($C_{9'}$), 18.3 (C_9), 28.3 (C_7), 33.0 ($C_{5'}$), 33.7 (C_5), 42.0 (C_1) 42.7 ($C_{1'}$), 47.7 (C_8 and $C_{8'}$), 55.1 (C_2 and $C_{2'}$), 56.5 (C_4 and $C_{4'}$), 66.1 (C_{10}), 69.1 (C_3 and $C_{3'}$), 76.2 (C_6), 127.9 (C_{11}), 128.5 (C_{11}), 136.0 (C_{11}), 171.7 (C=O, CONH$_{H1}$), 173.0 (C=O, CONH$_{H1'}$; C=O, CONH$_{H2'}$ and C=O, COOBn). **IR** (ν, cm^{-1}): 3304, 2973, 1739, 1632, 1537, 1451, 1391, 1365, 1318, 1198, 1167, 1113, 1060.

Benzyl ((1*R*,2*R*,3*S*,4*R*)-2-((*S*)-2-((1R,2R,3S,4R)-2-((*tert*-butoxycarbonyl)amino)-3,4-dihydroxycyclopentane-1-carboxamido)propanamido)-3,4-dihydroxycyclopentane-1-carbonyl)-*L*-alaninate (26c). Yield 62%. **^{1}H NMR** (400 MHz, DMSO) δ 1.11 (d, *J* = 6.4 Hz, 3H, H$_9$), 1.20 (d, *J* = 7.2 Hz, 3H, H$_{9'}$), 1.35 (s, 9H, H$_7$), 1.55-1.69 (m, 2H, H$_5$ and H$_{5'}$), 1.90-2.05 (m, 2H, H$_5$ and H$_{5'}$), 3.01-3.14 (m, 2H, H$_1$ and H$_{1'}$), 3.50-3.97 (m, 5H, H$_2$, H$_{2'}$, H$_3$, H$_4$ and H$_{4'}$), 4.09-4.26 (m, 3H, H$_{3'}$, H$_8$ and H$_{8'}$), 4.58 (s.br, 4H, OH), 5.08 (dd, *J* = 29.6 Hz, *J* = 12.8 Hz, 2H, H$_{10}$), 6.12 (d, *J* = 8.8 Hz, 1H, N$\underline{H}$COOCCH$_3$), 7.26-7.41 (m, 5H, H$_{11}$), 7.47 (d, *J* = 8.4 Hz, 1H, CONH$_{H2'}$), 7.77 (d, *J* = 7.6 Hz, 1H, CONH$_{H1'}$), 8.27 (d, *J* = 6.0 Hz, 1H, CONH$_{H1}$). **^{13}C NMR** (101 MHz, DMSO) 16.9 (C$_{9'}$), 19.1 (C$_9$), 28.5 (C$_7$), 33.0 (C$_{5'}$), 33.3 (C$_5$ and C$_{5'}$), 42.8 (C$_1$) 42.7 (C$_{1'}$), 47.7 (C$_8$ and C$_{8'}$), 55.1 (C$_2$ and C$_{2'}$), 56.5 (C$_4$ and C$_{4'}$), 65.9 (C$_{10}$), 70.2 (C$_3$ and C$_{3'}$), 76.7 (C$_6$), 128.3 (C$_{11}$), 173.8 (C=O, CONH$_{H1}$; C=O, CONH$_{H1'}$; C=O, CONH$_{H2'}$ and C=O, COOBn). **HRMS** (ESI, MeOH) calculated for C$_{30}$H$_{44}$N$_4$O$_{11}$: 636.6990, found M+Na: 659.2900.

Benzyl ((1*S*,2*R*)-2-((*S*)-2-((1*S*,2*R*)-2-((*S*)-2-((1*S*,2*R*)-2-((tert-butoxycarbonyl)amino)

cyclopent-3-ene-1-carboxamido)propanamido)cyclopent-3-ene-1-carboxamido)

propanamido)cyclopent-3-ene-1-carbonyl)-*L*-alaninate (28b). Yield 51%. **^{1}H NMR**

(400 MHz, DMSO) δ 1.08 (d, *J* = 7.2 Hz, 3H, H$_9$), 1.14 (d, *J* = 6.8 Hz, 3H, H$_{9'}$), 1.29 (d,

J = 7.2 Hz, 3H, H$_{9''}$), 1.33 (s, 9H, H$_7$), 2.24-2.46 (m, 3H, H$_5$, H$_{5'}$ and H$_{5''}$), 2.57-2.84

(m, 3H, H$_5$, H$_{5'}$ and H$_{5''}$), 2.98-3.28 (m, 3H, H$_1$, H$_{1'}$ and H$_{1''}$), 3.91-4.12 (m, 3H, H$_8$, H$_{8'}$

and H$_{8''}$), 4.59-4.87 (m, 1H, H$_2$), 4.90-5.20 (m, 4H, H$_{2'}$, H$_{2''}$ and H$_{10}$), 5.38-5.65 (m, 3H,

H$_4$, H$_{4'}$ and H$_{4''}$), 5.76-5.97 (m, 3H, H$_3$, H$_{3'}$ and H$_{3''}$), 6.26 (dd, *J* = 9.2 Hz, *J* = 8.0 Hz,

1H, N*H*COOCCH$_3$), 7.28-7.41 (m, 5H, H$_{11}$), 7.42-7.65 (m, 2H, CONH$_{H1}$ and

CONH$_{H2'}$), 7.72-8.25 (m, 2H, CONH$_{H1'}$ and CONH$_{H2''}$), 8.40 (d, *J* = 7.2 Hz, 1H,

CONH$_{H1''}$). **^{13}C NMR** (101 MHz, DMSO): 18.5 (C$_9$, C$_{9'}$ and C$_{9''}$), 28.5 (C$_7$), 35.1 (C$_5$,

C$_{5'}$ and C$_{5''}$), 45.6 (C$_1$, C$_{1'}$ and C$_{1''}$), 48.2 (C$_8$, C$_{8'}$ and C$_{8''}$), 55.3 (C$_2$, C$_{2'}$ and C$_{2''}$), 66.2

(C$_{10}$), 128.5 (C$_{11}$), 130.4 (C$_4$, C$_{4'}$ and C$_{4''}$), 133.6 (C$_3$, C$_{3'}$ and C$_{3''}$), 173.2 (6xC=O).

HRMS (ESI, MeOH) calculated for C$_{39}$H$_{52}$N$_6$O$_9$: 748.8280, found M+Na: 771.3696.
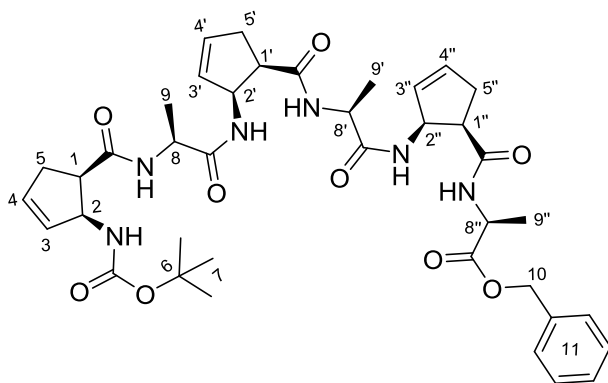
Benzyl ((1*R*,2*S*)-2-((*S*)-2-((1*R*,2*S*)-2-((*S*)-2-((1*R*,2*S*)-2-((tert-butoxycarbonyl)amino) cyclopent-3-ene-1-carboxamido)propanamido)cyclopent-3-ene-1-carboxamido) propanamido)cyclopent-3-ene-1-carbonyl)-*L*-alaninate (28c). **Yield** 98%. **^{1}H NMR** (400 MHz, DMSO) δ rotamers 1.07 (d, *J* = 7.2 Hz, 3H, H$_9$), 1.08 (d, *J* = 6.8 Hz, 3H, H$_9$'), 1.24 (d, *J* = 6.8 Hz, 3H, H$_9$''), 1.33 (s, 9H, H$_7$), 2.18-2.41 (m, 3H, H$_5$, H$_5$' and H$_5$''), 2.56-2.84 (m, 3H, H$_5$, H$_5$' and H$_5$''), 2.96-3.28 (m, 3H, H$_1$, H$_1$' and H$_1$''), 4.02-4.38 (m, 3H, H$_8$, H$_8$' and H$_8$''), 4.58-4.98 (m, 1H, H$_2$), 5.00-5.20 (m, 4H, H$_2$', H$_2$'' and H$_{10}$), 5.41-5.63 (m, 3H, H$_4$, H$_4$' and H$_4$''), 5.75-5.97 (m, 3H, H$_3$, H$_3$' and H$_3$''), 6.25 (dd, *J* = 9.2 Hz, *J* = 8.4 Hz, 1H, N*H*COOCCH$_3$), 7.30-7.40 (m, 5H, H$_{11}$), 7.51 (ddd, *J* = 9.6 Hz, *J* = 9.2 Hz, *J* = 8.4 Hz, 2H, CONH$_{H1}$ and CONH$_{H2'}$), 7.85 (dd, *J* = 11.6 Hz, *J* = 6.8 Hz, 2H, CONH$_{H1'}$ and CONH$_{H2''}$), 8.20 (dd, *J* = 6.4 Hz, *J* = 5.6 Hz, 1H, CONH$_{H1''}$). **^{13}C NMR** (101 MHz, DMSO) 18.6 (C$_9$, C$_9$' and C$_9$''), 28.5 (C$_7$), 34.5 (C$_5$, C$_5$' and C$_5$''), 46.1 (C$_1$, C$_1$' and C$_1$''), 48.8 (C$_8$, C$_8$' and C$_8$''), 55.3 (C$_2$, C$_2$' and C$_2$''), 66.0 (C$_{10}$), 128.4 (C$_{11}$), 130.0 (C$_4$, C$_4$' and C$_4$''), 133.7 (C$_3$, C$_3$' and C$_3$''), 173.1 (6xC=O). **HRMS** (ESI, MeOH) calculated for C$_{39}$H$_{52}$N$_6$O$_9$: 748.8280, found M+Na: 771.3685.
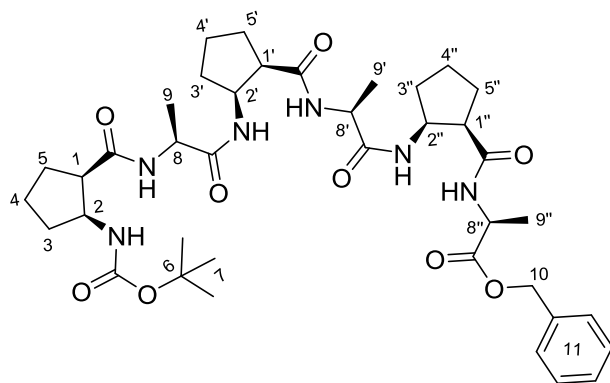
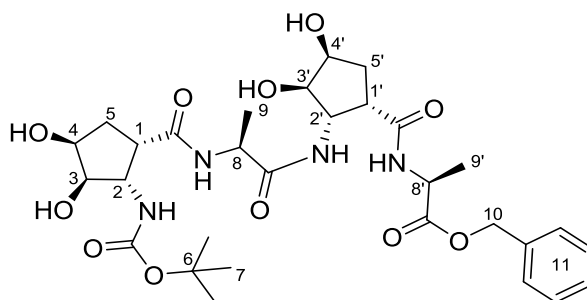**Benzyl** **((1*R*,2*S*)-2-((*S*)-2((1*R*,2*S*)-2-((*S*)-(1*R*,2*S*)-2-((tert-butoxycarbonyl)amino) cyclopentane-1-carboxamido)propanamido)cyclopentane-1-carboxamido) propanamido)cyclopentane-1-carbonyl)-*L*-alaninate (27c)**. **Yield** 90%. **^{1}H NMR** (400 MHz, DMSO) δ rotamers 1.03-1.20 (m, 6H, H_9 and $H_{9'}$), 1.25 (d, *J* = 7.2 Hz, 3H, $H_{9''}$), 1.33 (s, 9H, H_7), 1.38-2.02 (m, 18H, H_3, $H_{3'}$, $H_{3''}$, H_4, $H_{4'}$, $H_{4''}$, H_5, $H_{5'}$ and $H_{5''}$), 2.64-2.90 (m, 3H, H_1, $H_{1'}$ and $H_{1''}$), 3.90-4.39 (m, 6H, H_2, $H_{2'}$, $H_{2''}$, H_8, $H_{8'}$ and $H_{8''}$), 4.96-5.21 (m, 2H, H_{10}), 6.29 (ddd, *J* = 8.4 Hz, *J* = 7.2 Hz, *J* = 6.8 Hz, 1H, N<u>H</u>COOCCH$_3$), 7.25-7.42 (m, 5H, H_{11}), 7.42-8.02 (m, 4H, $CONH_{H1}$, $CONH_{H2'}$, $CONH_{H1'}$ and $CONH_{H2''}$), 8.22 (dd, *J* = 6.4 Hz, *J* = 6.0 Hz, 1H, $CONH_{H1''}$). **^{13}C NMR** (101 MHz, DMSO): 16.9 (C_9 and $C_{9'}$), 18.6 ($C_{9''}$), 22.5 (C_4, $C_{4'}$ and $C_{4''}$), 27.2 (C_5, $C_{5'}$ and $C_{5''}$), 28.5 (C_3, $C_{3'}$ and $C_{3''}$), 47.2 (C_1, $C_{1'}$ and $C_{1''}$), 52.0 (C_8, $C_{8'}$ and $C_{8''}$), 54.1 (C_2, $C_{2'}$ and $C_{2''}$), 66.0 (C_{10}), 128.3 (C_{11}), 173.2 (6xC=O). **HRMS** (ESI, MeOH) calculated for $C_{39}H_{58}N_6O_9$: 754.9260, found M+Na: 777.4142.
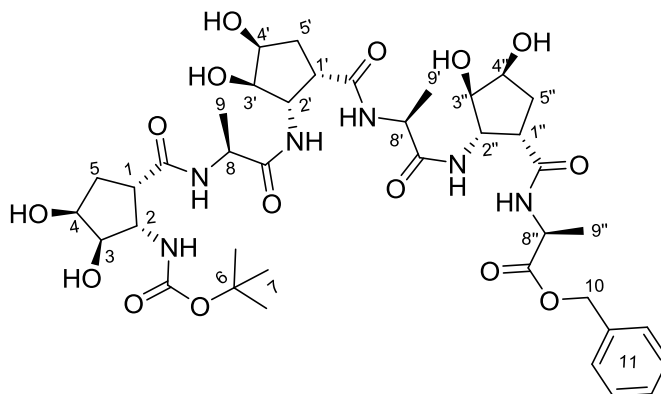
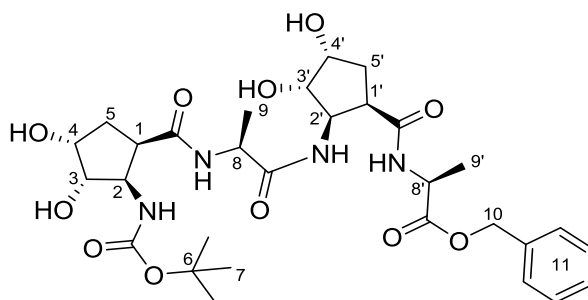**Benzyl** **((1*S*,2*S*,3*R*,4*S*)-2-((*S*)-2-((1*S*,2*S*,3*R*,4*S*)-2-((*S*)-2-((1*S*,2*S*,3*R*,4*S*)-2-((tert-butoxycarbonyl)amino)-3,4-dihydroxycyclopentane-1-carboxamido)propanamido)-3,4-dihydroxycyclopentane-1-carboxamido)propanamido)-3,4-dihy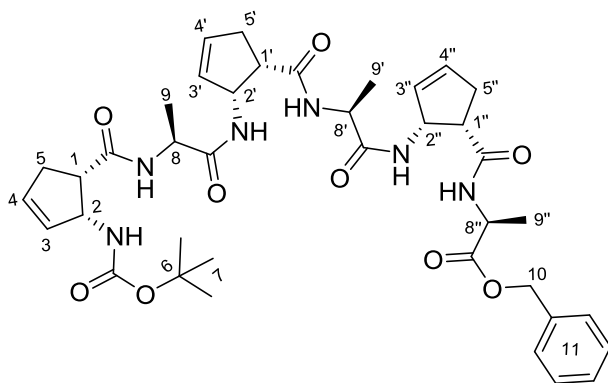droxycyclopentane-1-carbonyl)-*L*-alaninate (29b)**. **Yield** 74%. ^{1}**H NMR** (400 MHz, DMSO) δ rotamers 0.91-1.44 (m, 18H, H_7, H_9, $H_{9'}$ and $H_{9''}$), 1.55-2.09 (m, 6H, H_5, $H_{5'}$ and $H_{5''}$), 2.92-3.20 (m, 3H, H_1, $H_{1'}$ and $H_{1''}$), 3.64-4.39 (m, 12H, H_3, $H_{3'}$, $H_{3''}$, H_4, $H_{4'}$, $H_{4''}$, H_8, $H_{8'}$ and $H_{8''}$), 4.63 (s.br, 4H, OH), 5.08 (s.br, 2H, H_{10}), 6.12 (dd, J = 8.8 Hz, J = 8.4 Hz, 1H, NHCOOCCH$_3$), 7.26-7.40 (m, 5H, H_{11}), 7.50 (dd, J = 8.0 Hz, J = 8.0 Hz, 1H, CONH), 7.88 (ddd, J = 8.0 Hz, J = 7.2 Hz, J = 6.8 Hz, 2H, CONH), 8.40 (d, J = 6.8 Hz, 1H, CONH). **HRMS** (ESI, MeOH) calculated for $C_{39}H_{58}N_6O_{15}$: 850.9200, found M+Na: 873.3857.
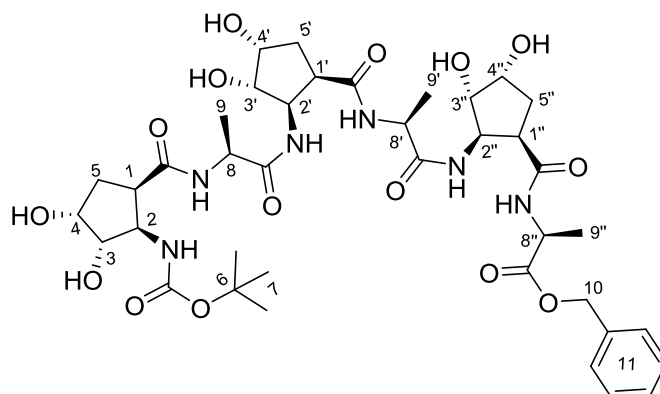
**Benzyl   ((1R,2R,3S,4R)-2-((S)-2-((1R,2R,3S,4R)-2-((S)-2-((1R,2R,3S,4R)-2-((tert-butoxycarbonyl)amino)-3,4-dihydroxycyclopentane-1-carboxamido)propanamido)-3,4-dihydroxycyclopentane-1-carboxamido)propanamido)-3,4-dihydroxycyclopentane-1-carbonyl)-L-alaninate (29c). Yield** 85%. **^{1}H NMR** (400 MHz, DMSO) δ rotamers 1.00-1.15 (m, 6H, H$_9$, and H$_{9'}$), 1.22 (d, J = 4.4 Hz, 1H, H$_{9''}$), 1.34 (s, 9H, H$_7$), 1.47-2.06 (m, 6H, H$_5$, H$_{5'}$ and H$_{5''}$), 2.95-3.13 (m, 3H, H$_1$, H$_{1'}$ and H$_{1''}$), 3.64-4.33 (m, 12H, H$_3$, H$_{3'}$, H$_{3''}$, H$_4$, H$_{4'}$, H$_{4''}$, H$_8$, H$_{8'}$ and H$_{8''}$), 4.53 (s.br, 6H, OH), 5.09 (dd, J = 32.0 Hz, J = 13.2 Hz, 2H, H$_{10}$), 6.09 (d, J = 7.2 Hz, 1H, NHCOOCCH$_3$), 7.22-7.44 (m, 6H, H$_{11}$ and CONH), 7.50 (d, J = 5.6 Hz, 1H, CONH), 7.75 (d, J = 7.2 Hz, 1H, CONH), 7.84 (d, J = 6.4, 1H, CONH), 8.27 (d, J = 3.6 Hz, 1H, CONH). **^{13}C NMR** (101 MHz, DMSO) 16.8 (C$_9$), 19.1 (C$_{9'}$ and C$_{9''}$), 28.5 (C$_7$), 33.3 (C$_5$, C$_{5'}$ and C$_{5''}$), 43.0 (C$_1$, C$_{1'}$ and C$_{1''}$), 48.3 (C$_8$, C$_{8'}$ and C$_{8''}$), 55.0 (C$_2$, C$_{2'}$ and C$_{2''}$), 56.9 (C$_4$, C$_{4'}$ and C$_{4''}$), 66.0 (C$_{10}$), 70.3 (C$_3$, C$_{3'}$ and C$_{3''}$), 128.6 (C$_{11}$), 173.2 (5xC=O,CONH).
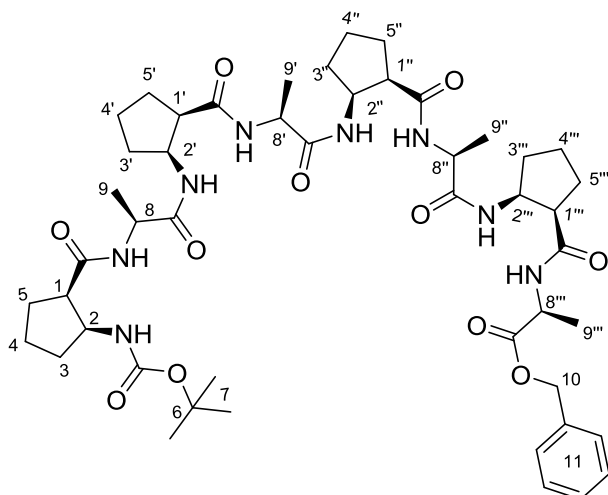
Benzyl ((1R,2S)-2-((S)-2-((1R,2S)-2-((S)-2-((1R,2S)-2-((S)-2-((1R,2S)-2-((tert-butoxycarbonyl)amino)cyclopentane-1-carboxamido)propanamido)cyclopentane-1-carboxamido)propanamido)cyclopentane-1-carboxamido)propanamido)cyclopentane-1-carbonyl)-L-alaninate (30c). Yield 77%. **^{1}H NMR** (400 MHz, DMSO) δ rotamers 1.01-1.20 (m, 9H, H_9, $H_{9'}$ and $H_{9''}$), 1.24 (d, J = 7.2 Hz, 3H, $H_{9'''}$), 1.34 (s, 9H, H_7), 1.38-1.93 (m, 24H, H_3, $H_{3'}$, $H_{3''}$,$H_{3'''}$, H_4, $H_{4'}$, $H_{4''}$, $H_{4'''}$, H_5, $H_{5'}$, $H_{5''}$ and $H_{5'''}$), 2.64-2.93 (m, 4H, H_1, $H_{1'}$, $H_{1''}$ and $H_{1'''}$), 3.93-4.36 (m, 8H, H_2, $H_{2'}$, $H_{2''}$, $H_{2'''}$, H_8, $H_{8'}$, $H_{8''}$ and $H_{8'''}$), 5.03-5.17 (m, 2H, H_{10}), 6.16-6.47 (m, 1H, N$\underline{H}$COOCCH$_3$), 7.27-7.40 (m, 5H, H_{11}), 7.41-7.64 (m, 2H, CONH$_{H1}$ and CONH$_{H2'}$), 7.65-7.96 (m, 4H, CONH$_{H1'}$, CONH$_{H2''}$, CONH$_{H1''}$, CONH$_{H2'''}$), 8.21 (dd, J = 6.4 Hz, J = 6.4 Hz, 1H, CONH$_{H1'''}$). **^{13}C NMR** (101 MHz, DMSO): 16.9 (C_9), 18.5 ($C_{9'}$, $C_{9''}$, $C_{9'''}$), 22.5 (C_4, $C_{4'}$, $C_{4''}$ and $C_{4'''}$), 27.3 (C_5, $C_{5'}$, $C_{5''}$ and $C_{5'''}$), 28.5 (C_7, $C_{7'}$, $C_{7''}$ and $C_{7'''}$), 32.5 (C_3, $C_{3'}$, $C_{3''}$, $C_{3'''}$) 47.2 (C_1, $C_{1'}$, $C_{1''}$ and $C_{1'''}$), 52.0 (C_8, $C_{8'}$, $C_{8''}$, and $C_{8'''}$), 54.4 (C_2, $C_{2'}$, $C_{2''}$ and $C_{2'''}$), 66.0 (C_{10}), 128.3 (C_{11}), 172.6 (6xC=O).

5.2.6 TETRAMERS, HEXAMERS AND OCTAMER CHARACTERISATION
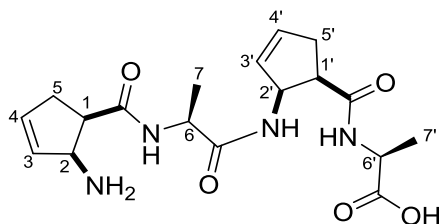
(2-((2*S*)-2-(2-aminocyclopent-3-ene-1-carboxamido)propanamido)cyclopent-3-ene-1-carbonyl)-*L*-alanine (TMU). Yield 49%. **mp** 168-176ºC. **^{1}H NMR** (400 MHz, D_2O) δ diastereomers 1.24-1.38 (m, 6H, H_7 and $H_{7'}$), 2.46-3.04 (m, 4H, H_5 and $H_{5'}$), 3.09-3.51 (m, 2H, H_1 and $H_{1'}$), 3.96-4.36 (m, 1H, H_6 and $H_{6'}$), 4.39-4.68 (m, 1H, H_2), 5.16 (br.s, 1H, $H_{2'}$), 5.49-5.87 (m, 2H, H_4 and $H_{4'}$), 5.92-6.33 (m, 2H, H_3 and $H_{3'}$). **^{13}C NMR** (101 MHz, D_2O) 16.7 (C_7 and $C_{7'}$), 30.5 (C_5), 34.0 ($C_{5'}$), 43.6 (C_1), 46.8 ($C_{1'}$), 49.8 (C_6), 50.1 ($C_{6'}$), 56.8 (C_2), 56.9 ($C_{2'}$), 125.9 (C_4), 128.0 ($C_{4'}$), 135.1 (C_3), 139.1 ($C_{3'}$), 173.2 (3xC=O, CONH), 180.3 (C=O, COOH). **HRMS** (ESI, H_2O) calculated for $C_{18}H_{26}N_4O_5$: 378.4290, found M+H 379.1977.
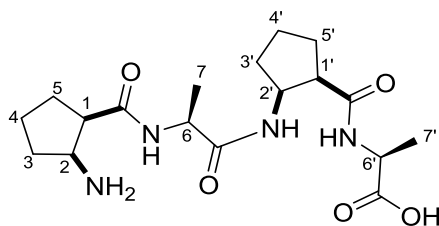
(2-((2*S*)-2-(2-aminocyclopentane-1-carboxamido)propanamido)cyclopentane-1-carbonyl)-*L*-alanine (TMS). Yield: 53%. **mp** 175-185ºC. **^{1}H NMR** (400 MHz, D_2O): δ diastereomers 1.22-1.31 (m, 6H, H_7 and $H_{7'}$), 1.54-2.12 (m, 12H, H_3, $H_{3'}$, H_4, $H_{4'}$, H_5 and $H_{5'}$), 2.86-3.02 (m, 2H, H_1 and $H_{1'}$), 3.73-3.83 (m, 1H, $H_{2'}$), 4.07 (q, $J = 7.2$ Hz, 1H, H_6), 4.12-4.23 (m, 1H, $H_{6'}$), 4.30 (ddd, $J = 20.8$ Hz, $J = 13.6$ Hz, $J = 6.8$ Hz, 1H, H_2).

^{13}**C NMR** (101 MHz, D$_2$O): 16.5 (C$_7$), 16.8 (C$_{7'}$), 21.5 (C$_3$), 22.0 (C$_5$), 28.2 (C$_4$ and C$_{4'}$), 30.3 (C$_{3'}$), 30.7 (C$_{5'}$), 45.5 (C$_1$), 47.9 (C$_{1'}$), 49.2 (C$_6$), 49.9 (C$_{6'}$), 53.6 (C$_2$), 53.7 (C$_{2'}$), 175.1 (3xC=O), 178.3 (C=O, COOH).
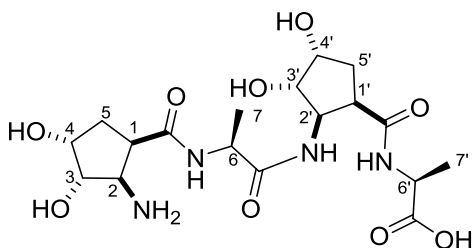
(2-((2S)-2-(2-amino-3,4-dihydroxycyclopentane-1-carboxamido)propanamido)-3,4-dihydroxycyclopentane-1-carbonyl)-*L*-alanine (TMH). Yield: 87%. **mp** 170-181 °C.

^{1}**H NMR** (400 MHz, D$_2$O): δ 1.25-1.43 (m, 6H, H$_7$ and H$_{7'}$), 1.89-2.31 (m, 4H, H$_5$ and H$_{5'}$), 3.10-3.45 (m, 2H, H$_1$ and H$_{1'}$), 3.65-3.80 (m, 1H, H$_2$), 3.97-4.46 (m, 7H, H$_{2'}$, H$_3$, H$_{3'}$, H$_4$, H$_{4'}$, H$_6$ and H$_{6'}$).
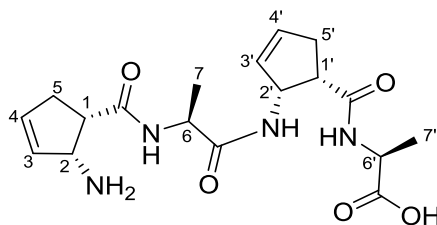
((1S,2R)-2-((S)-2((1S,2R)-2-aminocyclopent-3-ene-1-carboxamido)propanamido) cyclopent-3-ene-1-carbonyl)-*L*-alanine (TCDU). Yield: 33%. **mp** 195-205 °C.

Note: Compound **TCDU** was synthesised and characterised by NMR and the melting point measured. The NMR did not give a good reading, but some peaks were present, and a posterior analysis was to be run after further purification. When running it again the expected result was not achieved. Furthermore, the mass spectrometry did not

correspond to the expected molecular weight, so it was theorised that the compound degraded and due to time limitations and the fact that it was not of interest for further studies it was not synthesised again.
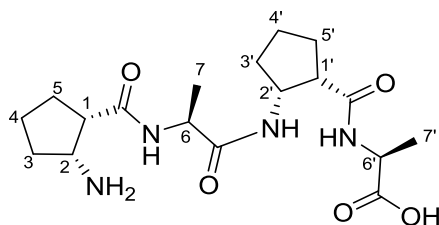
((1*S*,2*R*)-2-((*S*)-2((1*S*,2*R*)-2-aminocyclopentane-1-carboxamido)propanamido) cyclopentane-1-carbonyl)-*L*-alanine (TCDS). Yield: 86%. **mp** 190-205 °C. **^{1}H NMR** (400 MHz, D_2O): δ 1.28 (d, J = 7.2 Hz, 3H, H_7), 1.29 (d, J = 7.2 Hz, 3H, $H_{7'}$), 1.52-1.69 (m, 2H, H_3 and H_5), 1.70-2.04 (m, 8H, H_3, $H_{3'}$, $2xH_4$, $2xH_{4'}$, $H_{3'}$ and $H_{5'}$), 2.05-2.22 (m, 2H, $H_{3'}$ and $H_{5'}$), 2.91-3.05 (m, 2H, H_1 and $H_{1'}$), 3.82 (dt, J = 6.4 Hz, J = 4.0 Hz, 1H, $H_{2'}$), 4.10 (q, J = 7.2 Hz, 1H, H_6), 4.23 (q, J = 7.2 Hz, $H_{6'}$), 4.43 (dt, J = 14.8 Hz, J = 7.6 Hz, 1H, H_2). **^{13}C NMR** (101 MHz, D_2O): 16.9 (C_7), 17.8 ($C_{7'}$), 21.5 (C_3), 22.1 (C_5), 27.4 (C_4), 28.0 ($C_{4'}$), 30.2 ($C_{3'}$), 31.5 ($C_{5'}$), 45.6 (C_1), 47.1 ($C_{1'}$), 49.6 (C_6), 50.9 ($C_{6'}$), 53.0 (C_2), 53.5 ($C_{2'}$), 175.6 (3xC=O), 181.0 (C=O, COOH). **IR** (ν, cm^{-1}): 2924, 1548, 1451, 1393, 1359, 1307, 1269, 1237, 1136, 1051, 1020. **HRMS** (ESI, H_2O) calculated for $C_{18}H_{30}N_4O_5$: 382.4610, found M+H 383.2292.
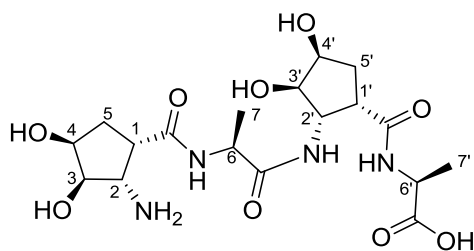
((1*S*,2*S*,3*R*,4*S*)-2((*S*)-2-((1S,2S,3*R*,4S)-2-amino-3,4-dihydroxycyclopentane-1-carboxamido)propanamido)-3,4-dihydroxycyclopentane-1-carbonyl)-*L*-alanine (TCDH): Yield: 45%. **mp** 174-182 ℃. **HRMS** (ESI, H_2O) calculated for $C_{18}H_{30}N_4O_9$: 446.4570, found M+Na: 469.1788.

Note: compound **TCDH** was synthesised and the NMR showed contamination with NMO from the previous step, further purification did not afford enough amount for a proper characterisation and mass spectrometry was performed to confirm the expected molecular weight. Due to time limitations and the fact that this compound was no longer needed, a second batch was not performed to fully characterise it.
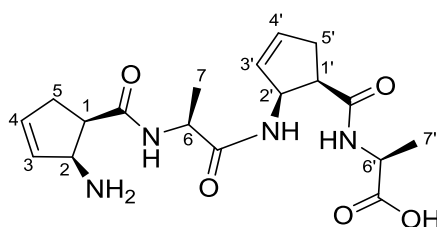
((1*R*,2*S*)-2-((*S*)-2((1*R*,2*S*)-2-aminocyclopent-3-ene-1-carboxamido)propanamido) cyclopent-3-ene-1-carbonyl)-*L*-alanine (TCUU). Yield 23%. **mp** 158-170 ℃. **^{1}H NMR** (400 MHz, D_2O): δ 1.32 (d, *J* = 7.2 Hz, 3H, H_7), 1.35 (d, *J* = 7.2 Hz, 3H, $H_{7'}$), 2.47-2.59 (m, 1H, H_5), 2.68-2.85 (m, 3H, H_5 and $2xH_{5'}$), 3.39 (dq, *J* = 8.4 Hz, *J* = 8.4 Hz, 2H, H_1 and $H_{1'}$), 4.15 (q, *J* = 7.2 Hz, 1H, H_6), 4.22 (q, *J* = 7.2 Hz, $H_{6'}$), 4.43 (d, *J* = 7.6 Hz, 1H, H_2), 5.17 (d, *J* = 7.6 Hz, 1H, $H_{2'}$), 5.61 (dd, *J* = 5.6 Hz, *J* = 2.4 Hz, 1H, H_4),

155

5.81 (dd, J = 5.6 Hz, J = 2.4 Hz, 1H, $H_{4'}$), 6.07 (dd, J = 5.6 Hz, J = 1.6 Hz, 1H, H_3),

6.29 (dd, J = 7.4 Hz, J = 3.2 Hz, 1H, $H_{3'}$). **^{13}C NMR** (101 MHz, D_2O): 16.5 (C_7), 16.8

($C_{7'}$), 33.8 (C_5), 35.3 ($C_{5'}$), 43.7 (C_1), 46.7 ($C_{1'}$), 49.6 (C_6), 49.7 ($C_{6'}$), 56.6 (C_2), 56.9

($C_{2'}$), 125.8 (C_4), 127.8 ($C_{4'}$), 135.2 (C_3), 138.9 ($C_{3'}$), 173.2 (C=O, $CONH_{H1}$), 173.7

(C=O, $CONH_{H1'}$), 174.1 (C=O, $CONH_{H2'}$), 178.4 (C=O, COOH). **IR** (ν, cm^{-1}): 2924,

1548, 1451, 1393, 1359, 1307, 1269, 1237, 1136, 1051, 1020. **HRMS** (ESI, H_2O)

calculated for $C_{18}H_{26}N_4O_5$: 378.4290, found M+H 379.1979.
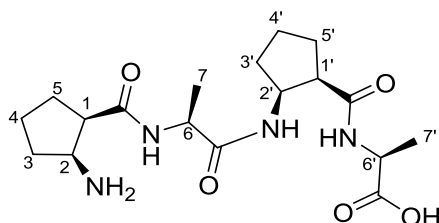
((1R,2S)-2-((S)-2((1R,2S)-2-aminocyclopentane-1-carboxamido)propanamido) cyclopentane-1-carbonyl)-L-alanine (TCUS). Yield: 56%. **mp** 180-194 °C. **^{1}H NMR**

(400 MHz, D_2O): δ 1.30 (d, J = 7.2 Hz, 3H, H_7), 1.31 (d, J = 7.2 Hz, 3H, $H_{7'}$), 1.57-2.21

(m, 12H, H_3, $H_{3'}$, H_4, $H_{4'}$, H_5 and $H_{5'}$), 2.95 (m, 2H, H_1 and $H_{1'}$), 3.80-3.89 (m, 1H, $H_{2'}$),

4.05 (q, J = 7.2 Hz, 1H, H_6), 4.24 (q, J = 7.2 Hz, $H_{6'}$), 4.39 (q, J = 7.2 Hz, 1H, H_2). **^{13}C**

NMR (101 MHz, D_2O): 16.8 (C_7), 17.0 ($C_{7'}$), 21.5 (C_3), 22.2 (C_5), 26.9 (C_4), 28.1 ($C_{4'}$),

30.2 ($C_{3'}$), 31.9 ($C_{5'}$), 45.5 (C_1), 48.0 ($C_{1'}$), 49.4 (C_6), 50.7 ($C_{6'}$), 52.9 (C_2), 53.5 ($C_{2'}$),

174.2 (C=O, $CONH_{H1}$), 174.3 (C=O, $CONH_{H1'}$), 174.5, (C=O, $CONH_{H2'}$), 180.0 (C=O,

COOH). **IR** (ν, cm^{-1}): 2924, 1548, 1451, 1393, 1359, 1307, 1269, 1237, 1136, 1051,

1020. **HRMS** (ESI, H_2O) calculated for $C_{18}H_{30}N_4O_5$: 382.4610, found M+H: 383.2290.
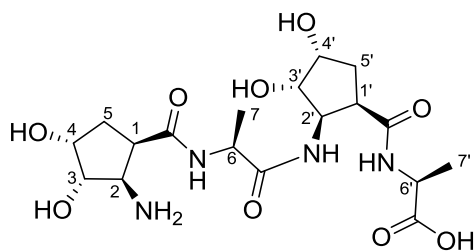
((1*R*,2*R*,3*S*,4*R*)-2((*S*)-2-((1R,2R,3S,4R)-2-amino-3,4-dihydroxycyclopentane-1-carboxamido)propanamido)-3,4-dihydroxycyclopentane-1-carbonyl)-*L*-alanine (TCUH): Yield: 67%. **mp** 148-156 °C. **^{1}H NMR** (400 MHz, D_2O): δ 1.25-1.41 (m, 6H, H_7 and $H_{7'}$), 1.92-2.08 (m, 1H, H_5), 2.13-2.28 (m, 3H, H_5 and 2x$H_{5'}$), 3.20-3.44 (m, 2H, H_1), 3.65-3.80 (m, 1H, H_2), 4.08-4.16 (m, 1H, H_6), 4.17-4.24 (m, 3H, $H_{2'}$, H_3 and H_4), 4.26-4.38 (m, 3H, $H_{1'}$, $H_{3'}$ and $H_{6'}$). **^{13}C NMR** (101 MHz, D_2O): 18.6 (C7 and C7'), 32.1 (C5), 34.6 (C5'), 39.2 (C_1), 42.6 (C1'), 49.5 (C4), 54.8 (C4'), 70.0 (C3 and C3'), 75.0 (C6), 76.0 (C6'), 175.0 (3xC=O), 180.3 (C=O, COOH). **HRMS** (ESI, H_2O) calculated for $C_{18}H_{30}N_4O_9$: 446.4570, found M+H: 447.2084.
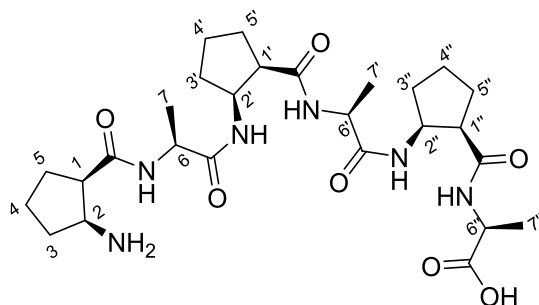
((1*R*,2*S*)-2-((*S*)-2-((1R,2S)-2-((*S*)-2-((1R,2S)-2-aminocyclopentane-1-carboxamido)propanamido)cyclopentane-1-carboxamido)propanamido)cyclopentane-1-carbonyl)-*L*-alanine (HCUS). Yield 76 %. **mp** 181-196°C. **^{1}H NMR** (400 MHz, D_2O): δ 1.22-1.37 (m, 9H, H_7, $H_{7'}$ and $H_{7''}$), 1.55-2.20 (m, 18H, H_3, $H_{3'}$, $H_{3''}$, H_4, $H_{4'}$, $H_{4''}$, H_5, $H_{5'}$ and $H_{5''}$), 2.87-3.07 (m, 3H, H_1, $H_{1'}$ and $H_{1''}$), 3.76-3.92 (m, 1H, H_2), 3.98-4.16 (m,

157

2H, H_6 and $H_{6'}$), 4.17-4.28 (m,1H, $H_{6''}$), 4.30-4.46 (m, 2H, $H_{2'}$ and $H_{2''}$). **^{13}C NMR** (101

MHz, D_2O): 16.8 (C_7 and $C_{7'}$), 21.9 (C_3, C_4 and C_5), 27.2 ($C_{3'}$, $C_{4'}$ and $C_{5'}$), 31.9 ($C_{3''}$,

$C_{4''}$ and $C_{5''}$), 45.4 (C_1), 47.9 ($C_{1'}$ and $C_{1''}$), 49.4 (C_6), 49.8 ($C_{6'}$), 50.2 ($C_{6''}$), 52.8 (C_2

and $C_{2'}$), 53.4 ($C_{2''}$), 174.4 (5xC=O, CONH), 180.4 (C=O, COOH). **HRMS** (ESI, H_2O)

calculated for $C_{27}H_{44}N_6O_7$: 564.6840, found M+H: 565.3342.
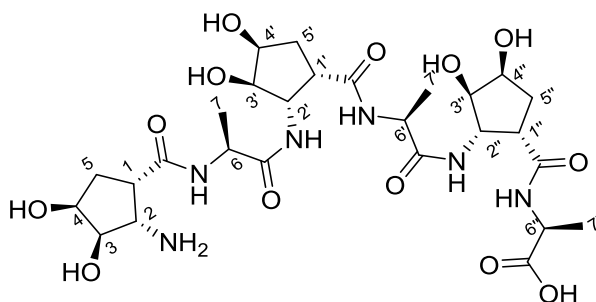
((1S,2S,3R,4S)-2-((S)-2-((1S,2S,3R,4S)-2-((S)-2-((1S,2S,3R,4S)-2-amino-3,4-dihydroxycyclopentane-1-carboxamido)propanamido)-3,4-dihydroxycyclopentane-1-carboxamido)propanamido)-3,4-dihydroxycyclopentane-1-carbonyl)-L-alanine (HCDH). Yield: 24%. **mp** 163-174 ℃. **^{1}H NMR** (400 MHz, D_2O): δ 1.10- 1.45 (m,

9H, H_7, $H_{7'}$ and $H_{7''}$), 1.80-2.36 (m, 6H, H_5, $H_{5'}$ and $H_{5''}$), 3.05-3.50 (m, 3H, H_1, $H_{1'}$ and

$H_{1''}$), 3.62-3.95 (m, 2H, H_6 and $H_{6'}$), 3.96-4.45 (m, 10H, H_2, $H_{2'}$, $H_{2''}$, H_3, $H_{3'}$, $H_{3''}$, H_4,

$H_{4'}$, $H_{4''}$ and $H_{6''}$). **^{13}C NMR** (101 MHz, D_2O): 17.7 (C_7), 23.7 ($C_{7'}$ and $C_{7''}$), 32.5 (C_5,

$C_{5'}$ and $C_{5''}$), 39.4 (C_1), 43.0 ($C_{1'}$ and $C_{1''}$), 49.6 (C_2, $C_{2'}$ and $C_{2''}$), 50.8 (C_6), 54.7 ($C_{6'}$

and $C_{6''}$), 70.1 (C_4 and $C_{4'}$ and $C_{4''}$), 75.6 ($C_{3'}$, $C_{3''}$), 76.0 (C_3), 175.6 (5xC=O, CONH),

180.4 (C=O, COOH). **HRMS** (ESI, H_2O) calculated for $C_{27}H_{44}N_6O_{13}$: 660.6780, found

M+H: 661.3049.
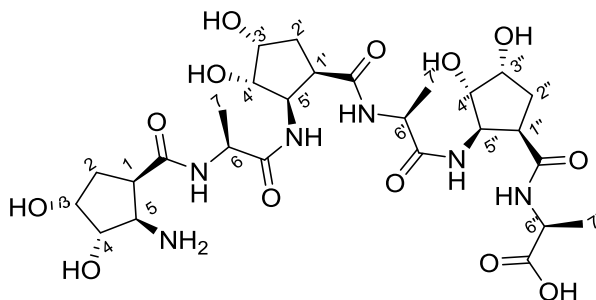
((1*R*,2*R*,3*S*,4*R*)-2-((*S*)-2-((1*R*,2*R*,3*S*,4*R*)-2-((*S*)-2-((1*R*,2*R*,3*S*,4*R*)-2-amino-3,4-dihydroxycyclopentane-1-carboxamido)propanamido)-3,4-dihydroxycyclopentane-1-carboxamido)propanamido)-3,4-dihydroxycyclopentane-1-carbonyl)-*L*-alanine

(HCUH). Yield: 33%. **mp** 163-190 ℃. ^{1}**H NMR** (400 MHz, D_2O): δ 1.25- 1.46 (m, 9H, H_7, $H_{7'}$ and $H_{7''}$), 1.89-2.22 (m, 6H, H_5, $H_{5'}$ and $H_{5''}$), 3.22-3.45 (m, 3H, H_1, $H_{1'}$ and $H_{1''}$), 3.51-3.79 (m, 2H, H_6 and $H_{6'}$), 4.02-4.43 (m, 10H, H_2, $H_{2'}$, $H_{2''}$, H_3, $H_{3'}$, $H_{3''}$, H_4, $H_{4'}$, $H_{4''}$ and $H_{6''}$). ^{13}**C NMR** (101 MHz, D_2O): 16.2 (C_7), 16.8 ($C_{7'}$ and $C_{7''}$), 30.5 (C_5), 32.4 ($C_{5'}$), 34.4 ($C_{5''}$), 39.2 (C_1), 42.7 ($C_{1'}$ and $C_{1''}$), 49.3 (C_2, $C_{2'}$ and $C_{2''}$), 54.8 (C_6), 55.2 ($C6'$ and $C6''$), 70.0 (C_4 and $C_{4'}$ and $C_{4''}$), 75.5 ($C_{3'}$, $C_{3''}$), 76.0 (C_3), 176.7 (6x C=O). **HRMS** (ESI, H_2O) calculated for $C_{27}H_{44}N_6O_{13}$: 660.6780, found M+Na: 683.2877.
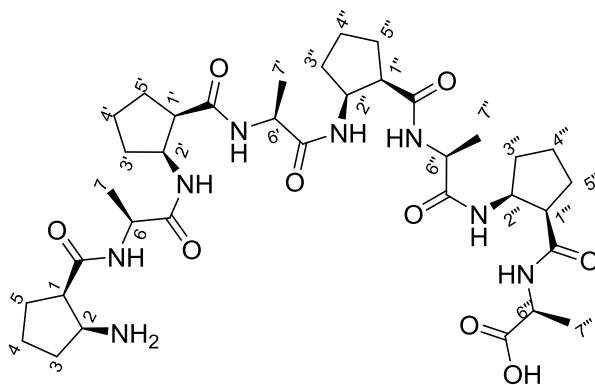
((1*R*,2*S*)-2-((*S*)-2-((1*R*,2*S*)-2-((*S*)-2-((1*R*,2*S*)-2-((*S*)-2-((1*R*,2*S*)-2-aminocyclopentane-1-carboxamido)propanamido)cyclopentane-1-carboxamido)propanamido)cyclopentane-1-carboxamido)propanamido)cyclopentane-1-carbonyl)-*L*-alanine

(OCUS). Yield: 67%. **mp** 195-215 ℃. **^{1}H NMR** (400 MHz, D$_2$O): δ 1.22-1.36 (m, 12H, H$_7$, H$_{7'}$, H$_{7''}$, H$_{7'''}$), 1.53-2.20 (m, 24H, H$_3$, H$_{3'}$, H$_{3''}$, H$_{3'''}$, H$_4$, H$_{4'}$, H$_{4''}$, H$_{4'''}$, H$_5$, H$_{5'}$, H$_{5''}$ and H$_{5'''}$), 2.86-3.07 (m, 4H, H$_1$, H$_{1'}$, H$_{1''}$ and H$_{1'''}$), 3.72-3.89 (m, 1H, H$_2$), 4.03-4.45 (m, 7H, H$_{2'}$, H$_{2''}$, H$_{2'''}$, H$_6$, H$_{6'}$, H$_{6''}$ and H$_{6'''}$). **^{13}C NMR** (101 MHz, D$_2$O): 16.8 (C$_7$, C$_{7'}$, C$_{7''}$ and C$_{7'''}$), 22.0 (C$_3$, C$_4$ and C$_5$), 27.0 (C$_{3'}$, C$_{4'}$ and C$_{5'}$), 30.0 (C$_{3''}$, C$_{4''}$ and C$_{5''}$), 31.9 (C$_{3'''}$, C$_{4'''}$ and C$_{5'''}$), 45.3 (C$_1$), 47.9 (C$_{1'}$, C$_{1''}$ and C$_{1'''}$), 49.3 (C$_6$), 49.3 (C$_{6'}$), 49.5 (C$_{6''}$ and C$_{6'''}$), 52.8 (C$_2$ and C$_{2'}$), 53.4 (C$_{2''}$ and C$_{2'''}$), 174.4 (7xC=O, CONH), 178.5 (C=O, COOH). **IR** (ν, cm^{-1}): 2924, 1548, 1451, 1393, 1359, 1307, 1269, 1237, 1136, 1051, 1020. **HRMS** (ESI, H$_2$O) calculated for C$_{36}$H$_{58}$N$_8$O$_9$: 746.9070, found M+H: 747.4404.

5.3 RESULTS AND DISCUSSION

5.3.1 SYNTHESIS OF THE UNSATURATED, SATURATED AND HYDROXYLATED FOLDAMERS

The synthetic steps to obtain the desired compounds, both as mixtures of the possible isomers and enantiomerically pure were, as in Chapter 4, reactions of deprotection, coupling and hydroxylation. Focus is given to details of the synthesis that differ from those discussed in Chapters 3 and 4. In this way, emphasis is given to the synthesis of the hydroxylated compounds. The unsaturated and saturated tetramers were obtained by deprotecting the amino and the acid groups in equal amounts of the corresponding dimer and coupling them together. This approach could not be followed for the hydroxylated compounds because the hydroxyl groups would compete with the acid group and condensate into an ester.

To avoid this competing reaction the hydroxyl groups had to be protected (Figure 5.2). The challenge was to find a protecting group (G) resistant to an acid moiety when deprotecting the amine group. The first attempt to protect the hydroxyl groups used the monomeric derivative **10a** (Scheme 5.2). Imidazole (Im) is often used as base to remove the HCl formed when the nucleophile (hydroxyl group) attacks the electrophile (TBSCl). Compound **31a** was successfully synthesised and the methodology was applied to compound **13c** with a 92% yield. The next step was to orthogonally deprotect compound **32a** (Scheme 5.3) and couple both products to obtain **26a-c**.
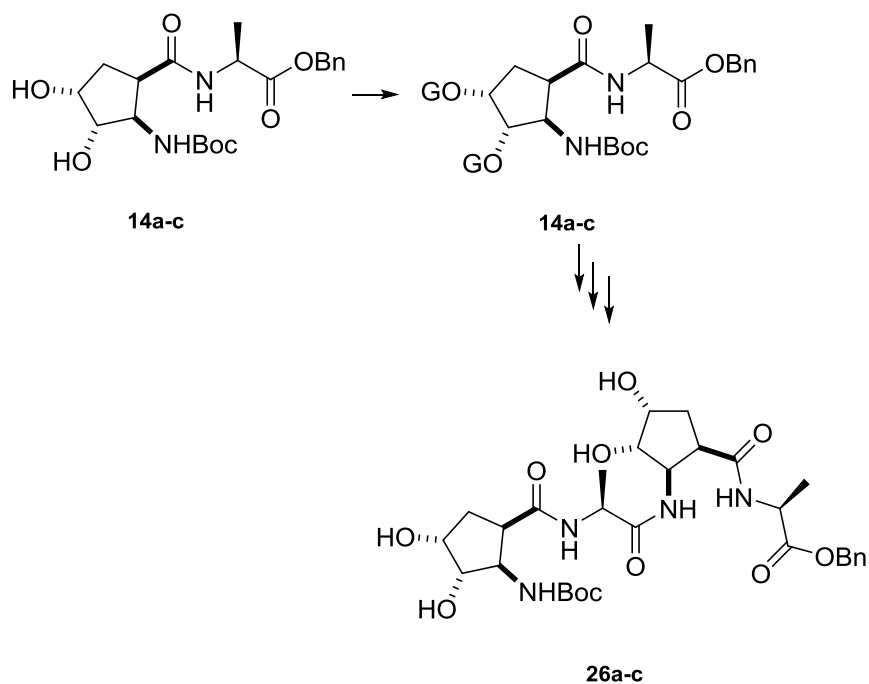
Figure 5.2 Representation of the synthetic strategy to obtain the hydroxylated tetrameric precursor.
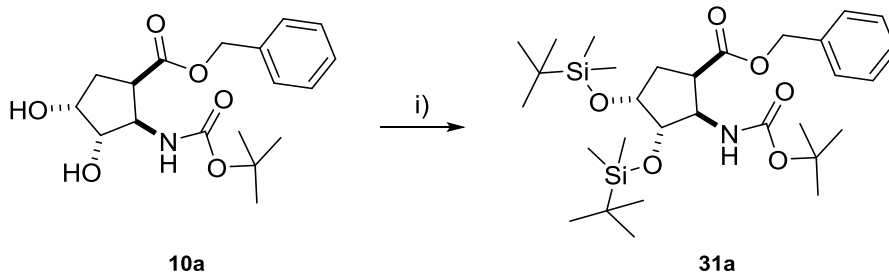
Scheme 5.2 Protection of the hydroxyl groups. i) TBSCl, Im, DMF, 0°C, O.N.

The expected result of the deprotection *via* hydrogenation was successful (compound

33a, Scheme 5.3) but the NMR analysis of the deprotection of the amine group *via* TFA

revealed the loss of the Boc group, as expected, and the loss of the TBS group as well

(Figure 5.3). The peaks at ~0.00 and ~1.00 ppm should integrate for 12 and 18 protons, respectively. This indicates that the protecting group is absent in the product.
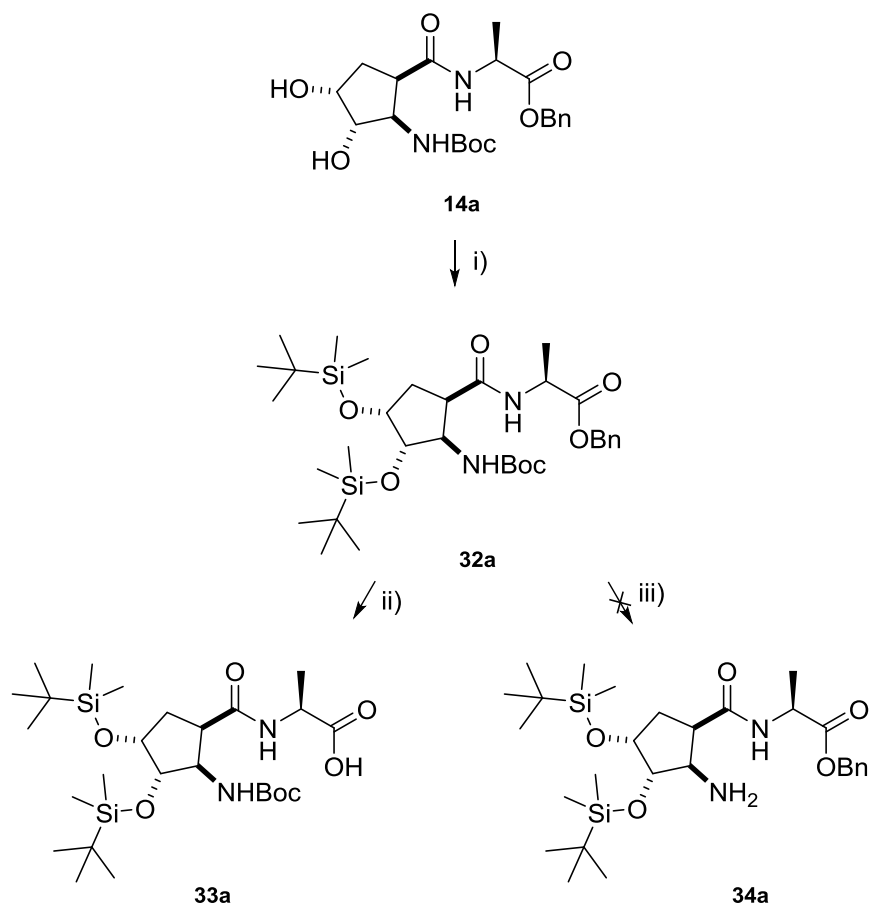
Scheme 5.3 i) TBSCl, Im, DMF; ii) H2 (1atm), Pd/C, MeOH; iii) TFA, DCM, 0°C.
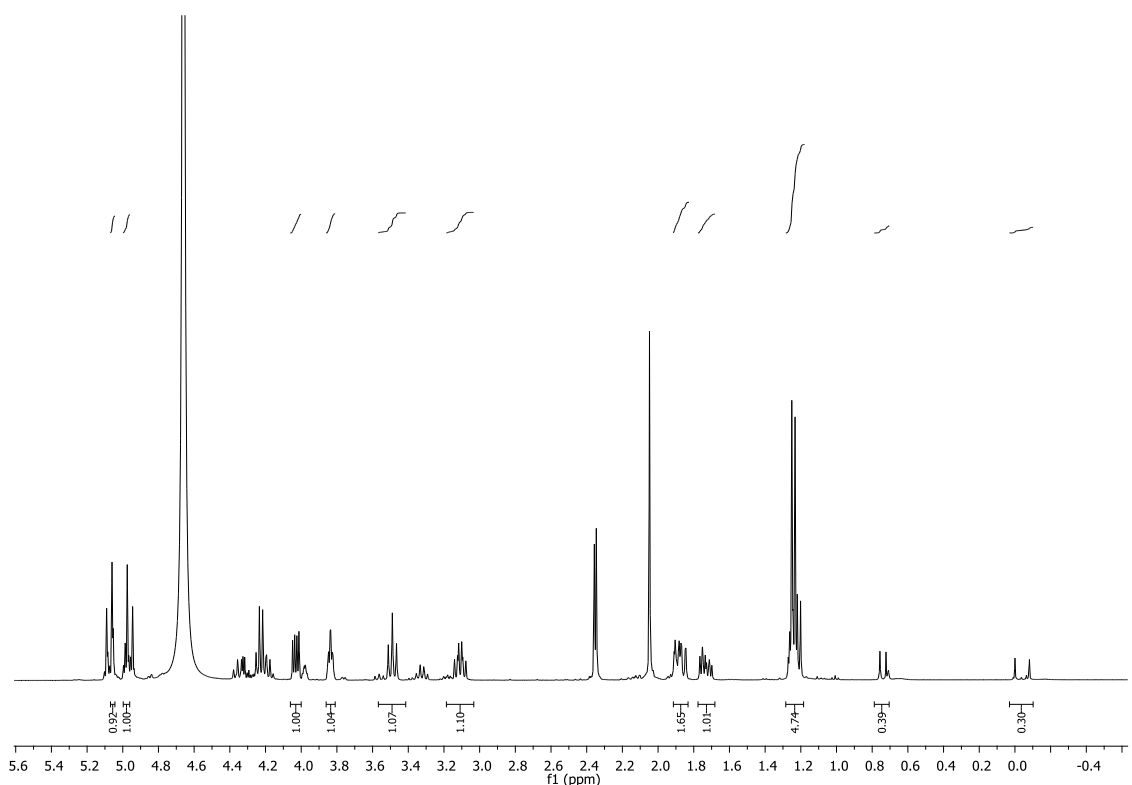
Figure 5.3 ^{1}H NMR spectrum of the deprotection product.

Scheme 5.4 illustrates two other attempts to protect the hydroxyl groups using *p*-Methoxybenzyl Chloride (PMBCl) following the procedure by Jenkins *et al.*[105] and 1,3-Dichloro-1,1,3,3-tetraisopropylsiloxane (TIPDSiCl$_2$). The reaction with PMBCl was not successful and the expected product using TIPDSiCl$_2$ was identified by NMR. The TIPDSiCl$_2$ protection was labile to an acidic moiety making it impracticable to use this methodology.
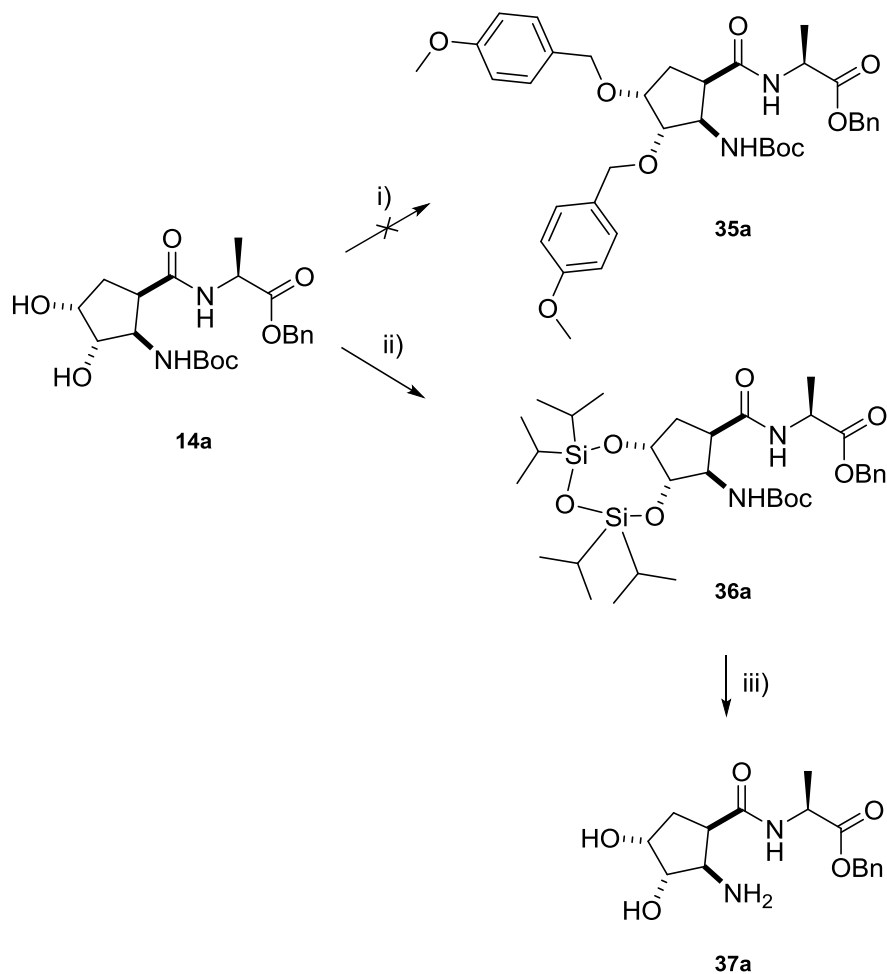
Scheme 5.4 i) PMBCl, NaH, DMF; ii) ,TIPDSiCl$_2$, Et$_3$N, DCM; iii) TFA, DCM, 0°C.

Compounds **26a-c** were successfully synthesised using the same methodology as for the dimers, i.e., hydroxylating the unsaturated tetramer as illustrated in figure 5.1.

5.3.2. WATER UPTAKE DETERMINATION

The thermogravimetric profiles of the compounds synthesised in this chapter is depicted in Figure 5.4 and Figure 5.5 with α-lactose behaving as before. The weight loss analysis shows that the compounds herein synthesised are hygroscopic and, after equilibration with water, they then lose weight as temperature rises. However, the number of waters (N_w) per molecule of compound (Figure 5.6) is relevant only for compound **TCUS** which is the compound with the lowest D/A (hydrogen bond donor/acceptor ratio) (Table 5.1). The hydroxylated series has a N_w of 1 or 2 except for compound **TCDH** which follows the trend of the previous compounds with lower molecular weight.
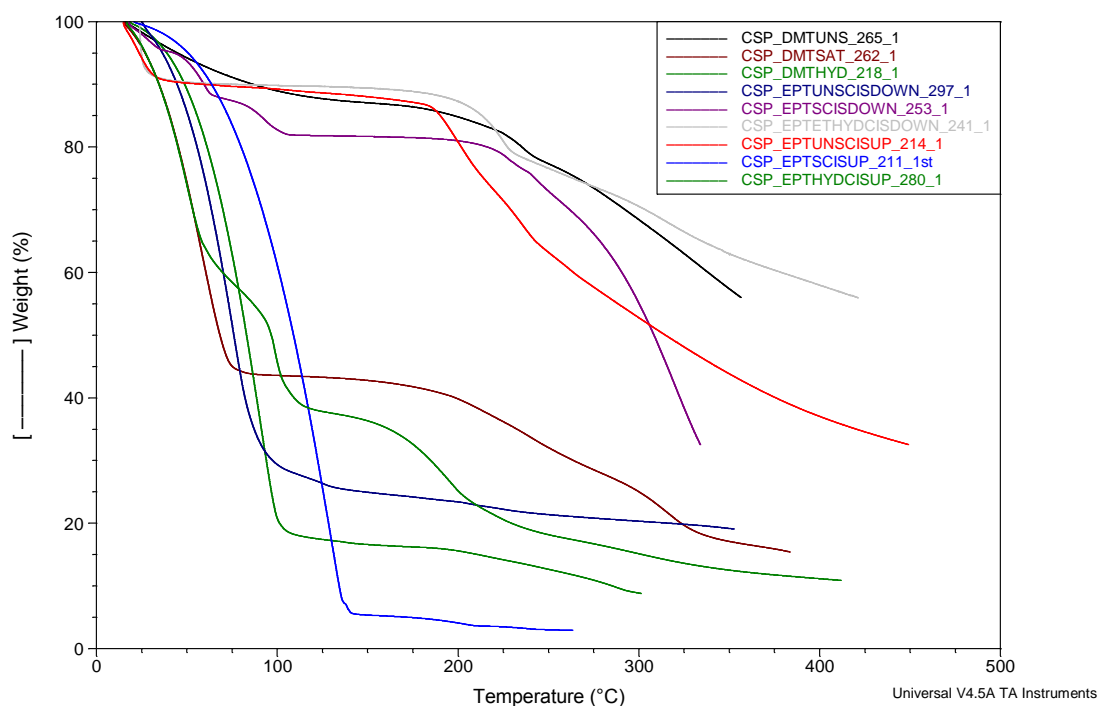
Figure 5.4 Thermogravimetric profiles for the tetrameric, hexameric and octameric structures. Sample codes, top to bottom: 265 – TMU, 262 – TMS, 218 – TMH, 297 – TCDU, 253 – TCDS, 241 – TCDH, 214 – TCUU, 211 – TCUS, 280 – TCUH.

166
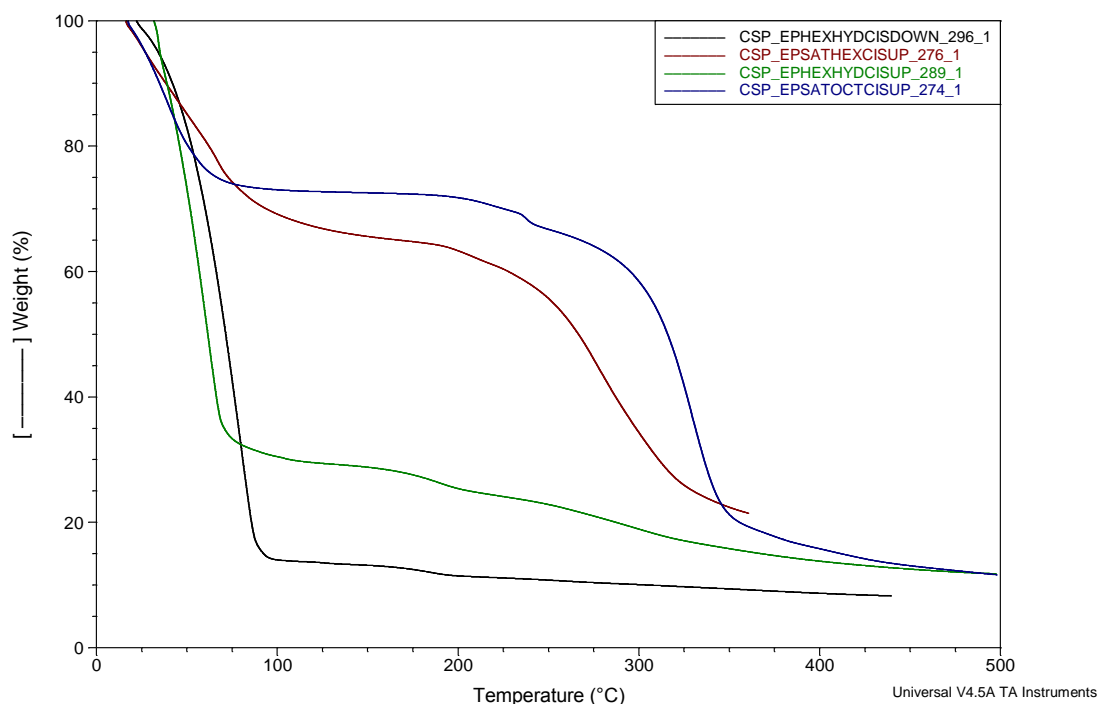
Figure 5.5 Thermogravimetric profiles for the hexamers and octamer. Sample codes, top to bottom: 296 – HCDH, 276 – HCUS, 289 – HCUH, 274 – OCUS.
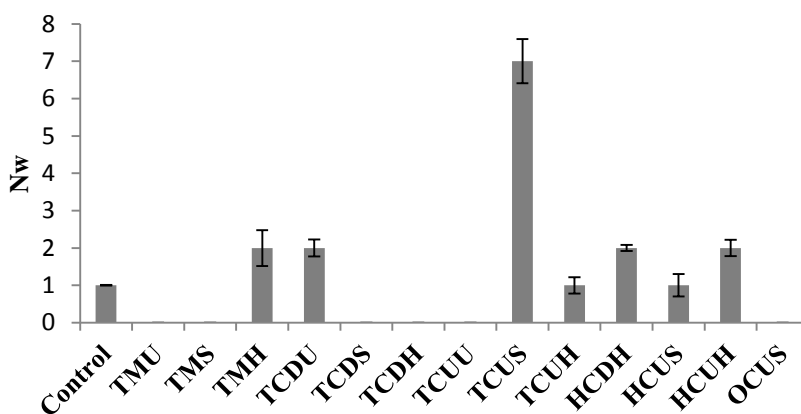
Figure 5.6 Water uptake of the higher molecular weight structures. Data are mean ± SD from n=3.

Thermograms for each compound can be found in Appendix A11.

167

Table 5.1 Physico chemical properties of the foldameric structures.

Compound	Mw	T/ºC	mp/ºC	D/A	D/A sites	N_w
TMU	378.43	120-150	168-176	5/9	6/14	0
TMS	382.46	113-150	175-185	5/9	6/14	0
TMH	446.46	115-149	170-181	9/13	10/22	2±0.48
TCDU	378.43	117-152	195-205	5/9	6/14	2±0.23
TCDS	382.46	110-155	190-205	5/9	6/14	0
TCDH	446.46	108-150	174-182	9/13	10/22	0
TCUU	378.43	115-150	158-170	5/9	6/14	0
TCUS	382.46	128-150	180-194	5/9	6/14	7±0.59
TCUH	446.46	120-150	148-156	9/13	10/22	1±0.22
HCDH	660.68	110-155	163-174	13/19	14/32	2±0.08
HCUS	564.68	115-152	181-196	7/13	8/20	1±0.30
HCUH	660.68	105-150	163-190	13/19	14/32	2±0.22
OCUS	746.91	110-155	195-215	9/17	10/26	0

The weight loss from the analysed compounds generally occurs at temperatures up to ~115°C (Figures 5.4 and 5.5). This correlated with "free" water and none or neglectable bound water which would be bound to the molecules and hence expected to be released at higher temperatures. As mentioned above, the outstanding compound is **TCUS** which has N_w of 7 molecules of water per molecule of compound. To better understand this behaviour, circular dichroism spectra were recorded for all compounds to investigate whether there was a specific folding shape that could explain these date, perhaps due to internal hydrogen bonding which would occupy the potential water binding sites and, in particular to determine if any of the compounds would fold into a α-helix. The results are depicted in figure 5.7. From the literature, it is well established that random coils give a CD profile with a maximum at 190 nm, β sheets at 200 nm and α-helices give two three maximums (at 210, 190 and an opposite at 185 nm). It can be seen that most of the structures fold into a random coil (with a negative maximum at ~190 nm) and 4 of the compounds (**TCDS**, **TCDH, HCUH** and **HCDH**) fold into a β sheet with a maximum at ~200 nm.
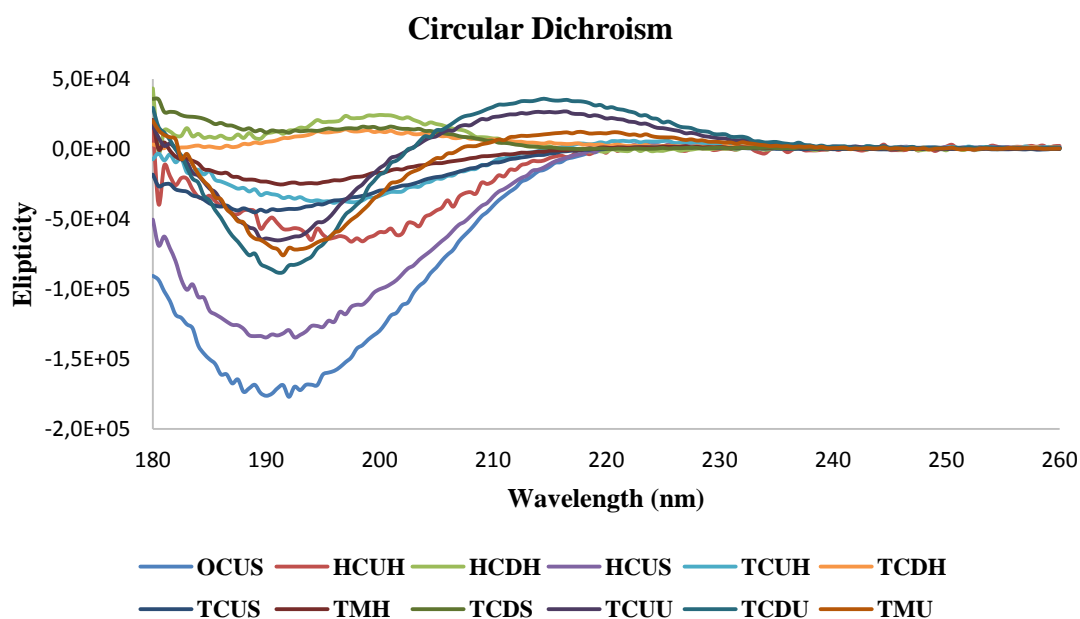
Figure 5.7 Circular dichroism spectra for the synthesised structures. Spectra were run in water between 2-6 mM.

5.3.3. DYNAMIC VAPOUR SORPTION

From the results above and previous chapters, the behaviour of the hydroxylated series differed to expectations. DVS experiments were run to further investigate on the hydroxylated series. The samples tested were **MMH**, **DMH** and **TMH** and the results are illustrated in Figure 5.8-11 using the same positive control as for the TGA experiments. The data for the DVS experiments can be consulted in Appendix A12.

The isothermal curves follow two typical patterns for sorption (Figure 5.12 a), i.e., type II (**MMH**) and type III (**DMH** and **TMH**), according to the classification by Brunauer et al.[106]

170
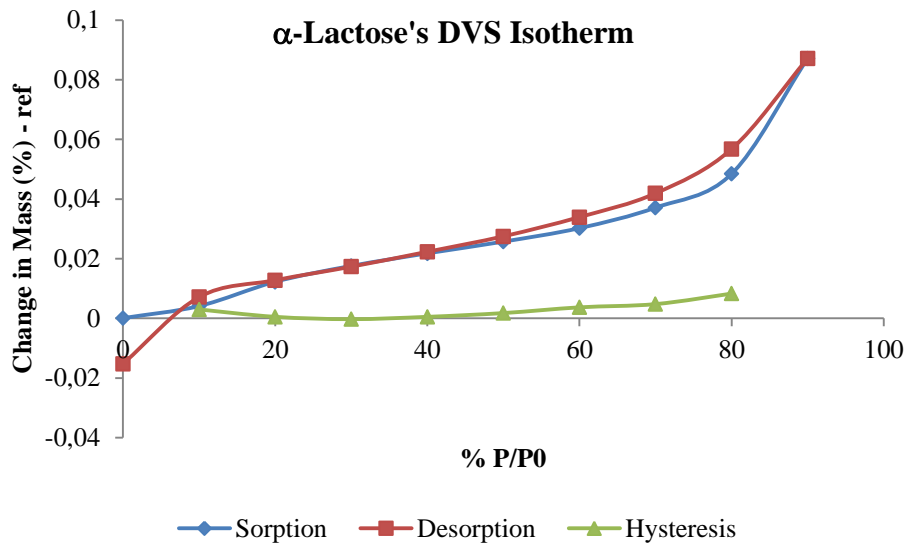
Figure 5.8 Sorption isotherm for α-lactose.
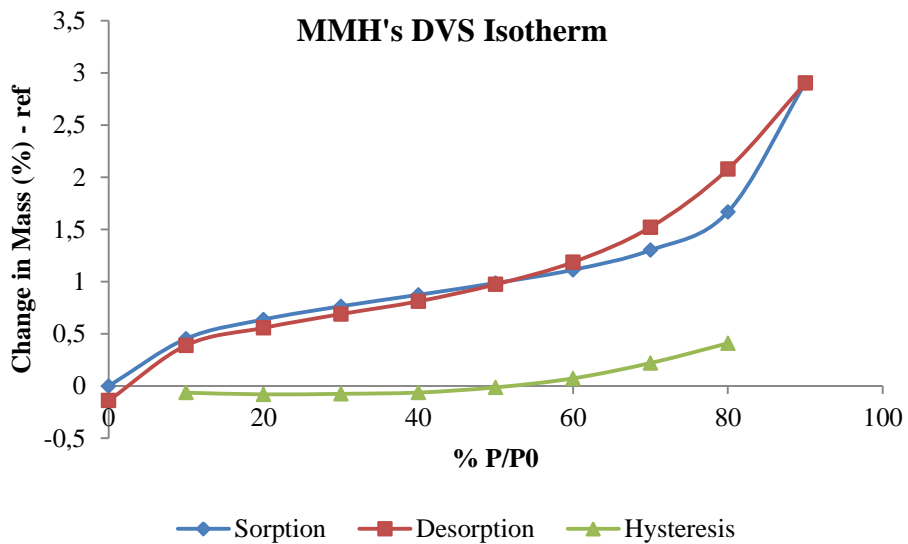
Figure 5.9 Sorption isotherm for compound MMH.
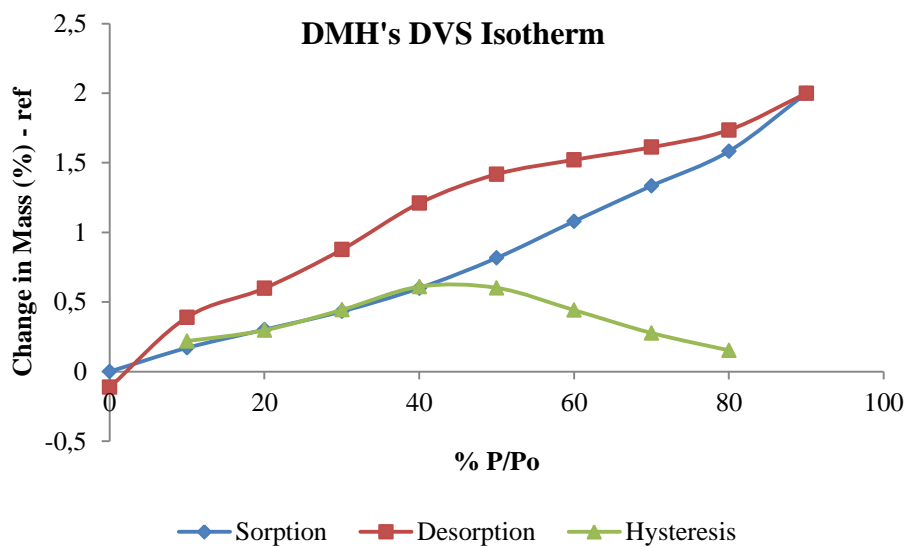
Figure 5.10 Sorption isotherm for compound DMH.
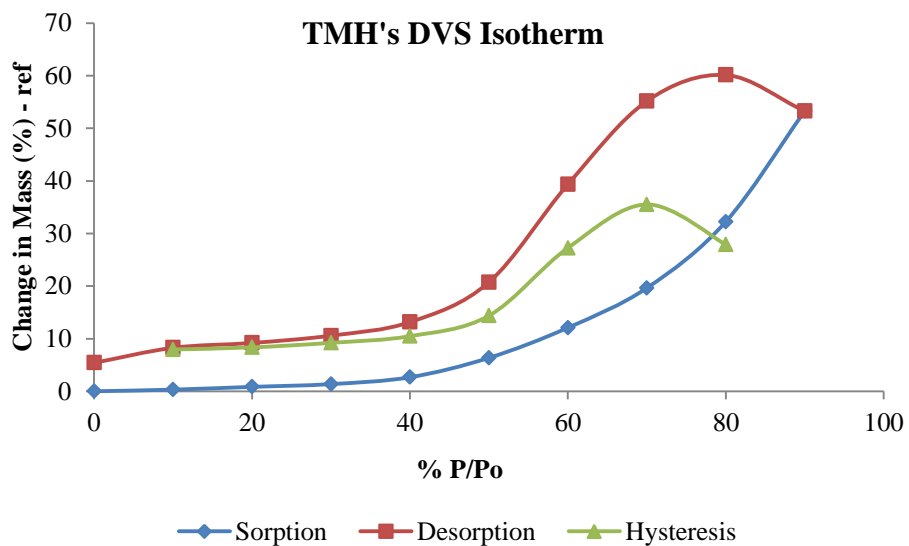
Figure 5.11 Sorption isotherm for compound TMH.

The typical shape of an isotherm reflects the way in which the water binds to a system. An isotherm can typically be divided into three regions (Figure 5.12 b); region I represents strongly bound water, in region II water molecules bind less firmly and region III represents free water. The difference between sorption and desorption curves is termed hysteresis.

The DVS experiments for compound **MMH** confirmed the result obtained from TGA, showing that any water adsorbed was free water (isotherm curve presents hysteresis at region III, Figure 5.9), and gave some insight into the behaviour of compounds **DMH** and **TMH**. Both compounds have marked hysteresis; **DMH**'s hysteresis has a maximum at region II (Figure 5.10), indicating weekly bound water, and **TMH**'s hysteresis infers the formation of a hydrate (region I of the desorption curve has 5% more weight than the starting amount of compound, Figure 5.11).
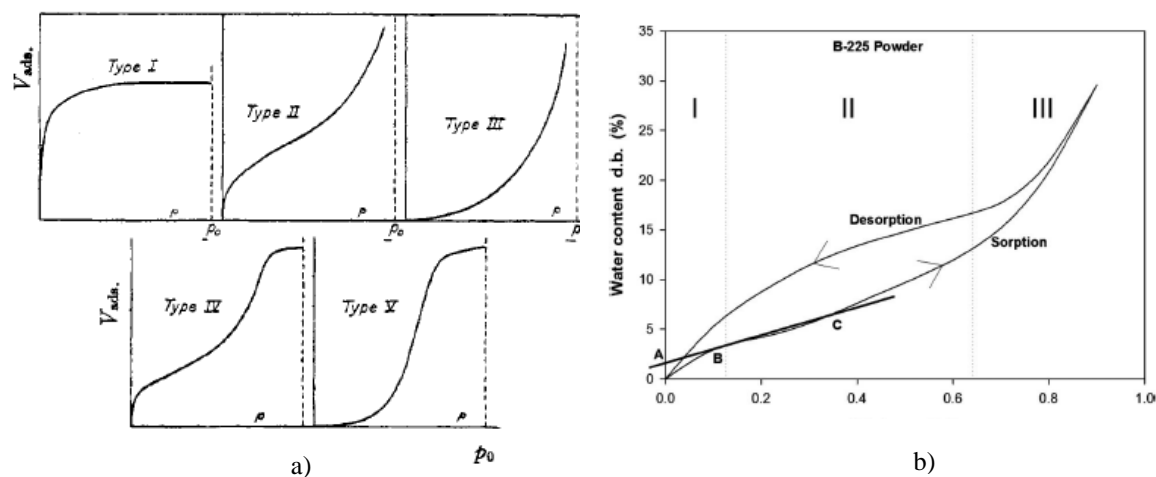
Figure 5.12 a) The five types of van der Waals adsorption isotherms.[106] b) Regions of a sorption isotherm.[107]

In order to understand if this could also be observed in the solid state, attempts to grow crystals of the tested compounds and their enantiomerically pure isomers were made. Several solvent systems were employed with no success. Three crystals grew in water at room temperature over a period of 7-10 days for compounds **MCUH** (Figure 5.13), **DCUH** (Figure 5.14) and **DCDH** (Figure 5.15).

The single crystal unit cell of compound **MCUH** revealed two different structural arrangements (Figure 5.13 a). The overlap of the two structures (Figure 5.13 b) shows that they differ in the orientation of the $-CH_2-$ bond of the pentacycle. Canfield et *al*[108] recently described a new type of conformational isomerism for two enantiomers not describable within existing IUPAC nomenclature. This type of conformational isomerism does not change the relative spatial orientation of the chiral centres and so, they are basically the same compound. Figure 5.13 c) illustrates the inter and intramolecular hydrogen bonds that leave no available sites for any water to bind to while in solution.
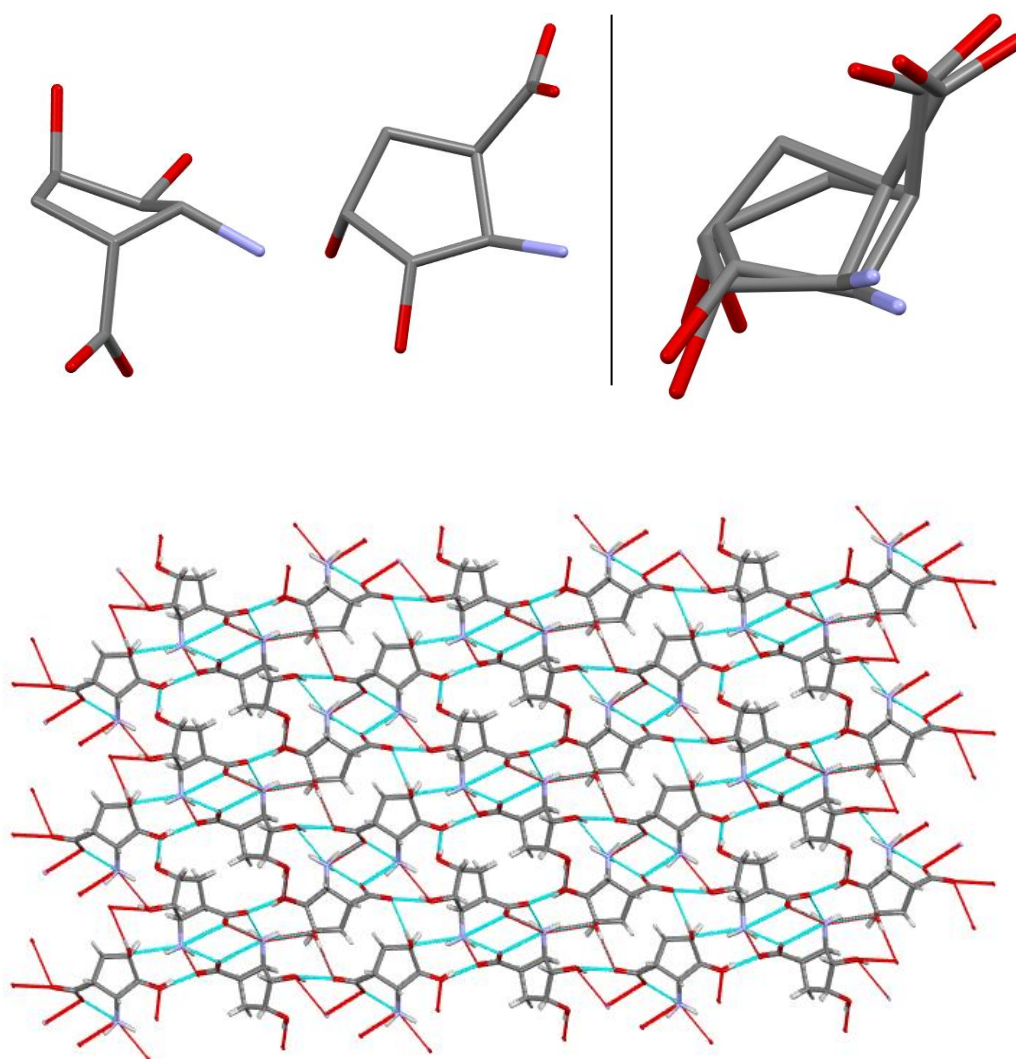
Figure 5.13 a) Structure determined from a single crystal of compound MCUH. b) Overlay of the two conformational isomers of compound MCUH. c) Packing pattern of the crystal structure.

The structure determined from a single crystal of compounds **DCUH** (Figure 5.14) and **DCDH** (Figure 5.15) drive to the same conclusion; inter and intramolecular hydrogen bonds occupy all the available binding sites.
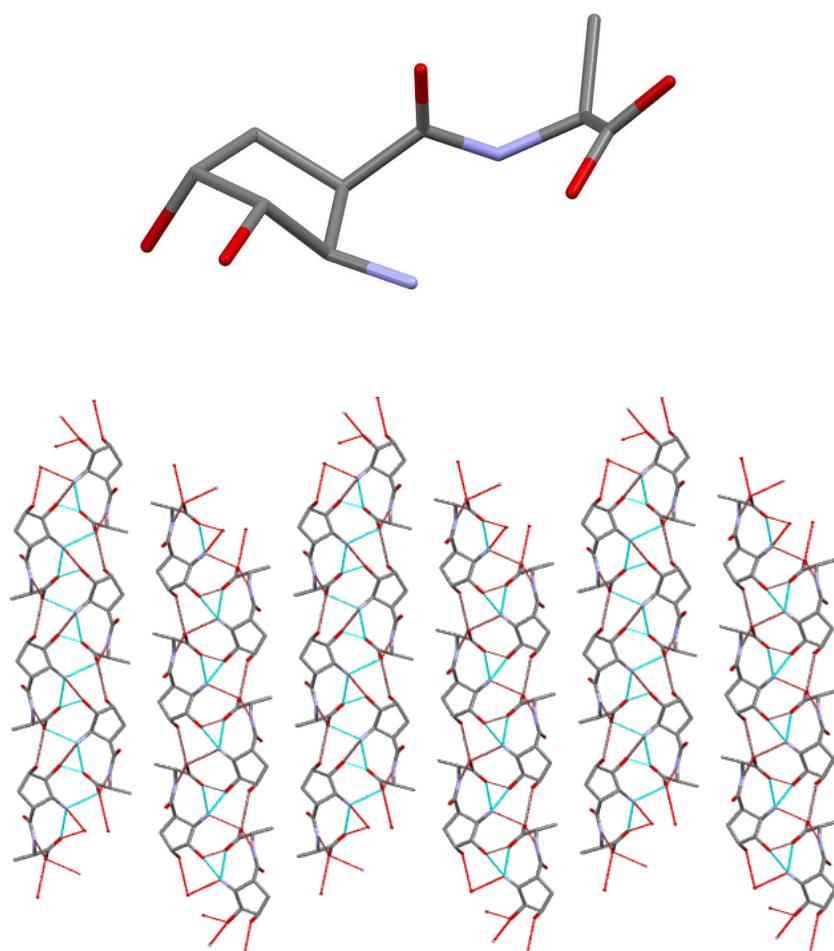
Figure 5.14 a) Structure determined from a single crystal of compound DCUH. b) Packing pattern of the crystal structure.

The packing pattern of both dimmers shows hydrophobic channels, which could contribute to the lack of dissolution of these compounds (recalling Figure 4.8, Chapter 4, Section 4.3.3) in a 100% RH environment.
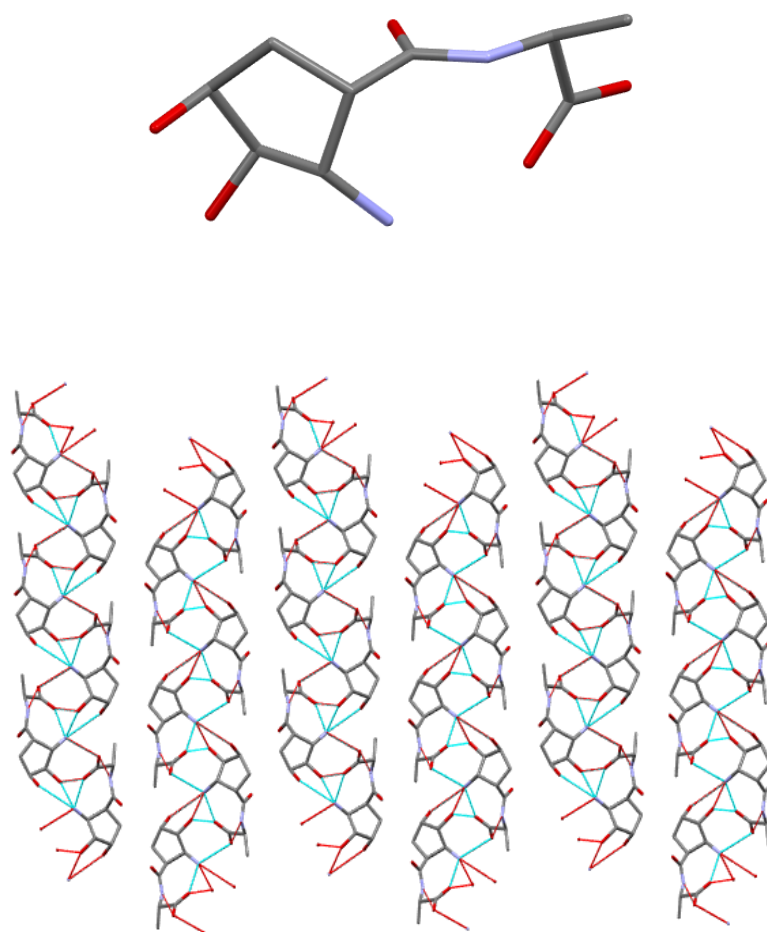
Figure 5.15 a) Structure determined from single crystal of compound DCDH. b) Packing pattern of the crystal structure.

5.4 CONCLUSIONS

A total of 13 compounds were successfully synthesised in reasonable to good yields though these were lower than previously obtained for similar couplings.

The increase of the molecular weight to ~2 and ~2.5 fold, from Chapter 4, had no significant difference in the water holding capacity. Compound **TCUS** follows the same trend as observed for **DCUS**, being the only compound with a significant N_w; though the D/A relationship is much higher for **TCUS**, both compounds bind to 7 water molecules per molecule of compound. The saturated hexamer and octamer do not follow the trend of the *cis* up configuration compounds binding to 1 (one) and 0 (zero) water molecules per molecule of compound. This observation suggests that the foldameric structures are binding intramolecularly with no specific folding shape as demonstrated by the CD spectra.

The hydroxylated series differs from the smaller molecules, binding to 2 molecules of water except for compound **TCDH**. The sorption isotherms indicate that the hydroxylated series could be forming hydrates as the peptide chain is increased. The structures determined from a single crystal explain the lack of water holding capacity of the hydroxylated series, showing that intra and intermolecular bonds occur in detriment of hydrogen bonding to water.

Chapter 6 will evaluate the *stratum corneum* uptake of the selected compounds from Chapter 3, 4 and 5.

CHAPTER 6

6. UPTAKE/DESORPTION STUDIES

This Chapter is organised in three Sections. Section 6.1 gives a brief overview of the skin models commonly used and the compounds selected for the uptake assays. Section 6.2 presents the methods used to assess the skin uptake of the selected compounds and the results obtained, and Section 6.3 shows the chapter's conclusions.

6.1 INTRODUCTION

Skin has long been used as an entry point for drug delivery and the first barrier to overcome is the SC. Ideally, the assay of a candidate would be run *in vivo*, accounting for all the dynamics of a biological system. This is obviously not feasible for a completely unknown new chemical entity (NCE); table 6.1 lists a range of appropriate skin models with their advantages and disadvantages.

Porcine skin has been frequently used as a surrogate for human skin due to its similarities. Its anatomy,[109] physiology[110,111] and immune system[112] have been shown to have similar components and function with human skin.[113] Table 6.2 and 6.3 illustrate the comparison of thickness between animal skins and human skin.

Table 6.1 Skin models.[114]

Model	Advantages	Disadvantages
Human skin		
In vivo	Gold standard	Often precluded for ethical reasons
Ex vivo	Best surrogate for in vivo humans	Not readily available, variability
Animal skin		
In vivo	Reasonably easy to obtain animals, can be scaled up to humans, hairless species available	Pigs: similar barrier to humans, but difficult to handle Rodents: different barrier properties from humans
In vivo chimeric model	Human skin xenografts on mice allows testing on living human skin	Technically difficult
Ex vivo	Easy to obtain	Different barrier properties, variability
Artificial membranes		
Simple polymeric models	Useful for studying basic diffusion mechanisms, consistent and homogenous	Not representative of human skin
Lipid-based models	Useful for screening	Not representative of human skin
Reconstructed skin models		
Reconstructed human epidermis	Built-in barrier properties	Usually more permeable than human skin
Living skin equivalents	Can be engineered to include a range of normal or disease features	Usually more permeable than human skin

Table 6.2 Thickness of skin layers of different species.[115]

Species, anatomic site	SC (μm)	Epidermis (μm)	Whole skin (mm)
Human, forearm	17	36	1.5
Pig, back	26	66	3.4
Pig, ear	10	50	1.3
Mouse, back	5	13	0.8

Table 6.3 Thickness of human and animal skin.[115]

Species	SC (μm)	Epidermis (μm)	Whole skin (mm)
Human	16.8	46.9	2.97
Pig	26.4	65.8	3.43
Rat	18	32	2.09
Mouse	9	29	0.10
Hairless mouse	8.9	28.6	0.70

Due to its similarities and ease of access, pig skin (isolated SC) from the flank was used in this project to assess the selected compounds in the uptake assays.

6.1.1 SELECTED COMPOUNDS AND SELECTION CRITERIA

From the TGA results, a screening was done based on the water holding capacity under the assumption that compounds that hydrogen bond to water will penetrate/permeate into/through the SC. The compounds with the higher N_w were chosen from the monomeric series (Chapter 3, Section 3.3.3). From the unsaturated and saturated series, the highest water holding compound were **MCUU** and **MCDS**. Their enantiomers were also assessed to evaluate the influence of chirality. From the library of compounds generated in Chapter 4, **DCUS** and **DCUU** were selected; **DCUS** holds 7 molecules of water per molecule of compound and **DCUU** holds 4. From Chapter 5, **TCUS**, **TCUU**, **HCUS** and **OCUS** were selected. Though **TCUU**, **HCUS** and **OCUS** do not hydrogen bond to water, inferences on other physical properties can be made. Also, the complete saturated series was assessed, allowing conclusions on molecular weight influence on uptake of a series. The summary of the selected compounds can be found in table 6.4 and the structures visualised in Figure 6.1.

Table 6.4 Water holding capacity of the selected compounds.

	Compound									
	MCDU	MCUU	MCDS	MCUS	DCUS	DCUU	TCUS	TCUU	HCUS	OCUS
N_w	2	3	2	1	7	4	7	0	1	0
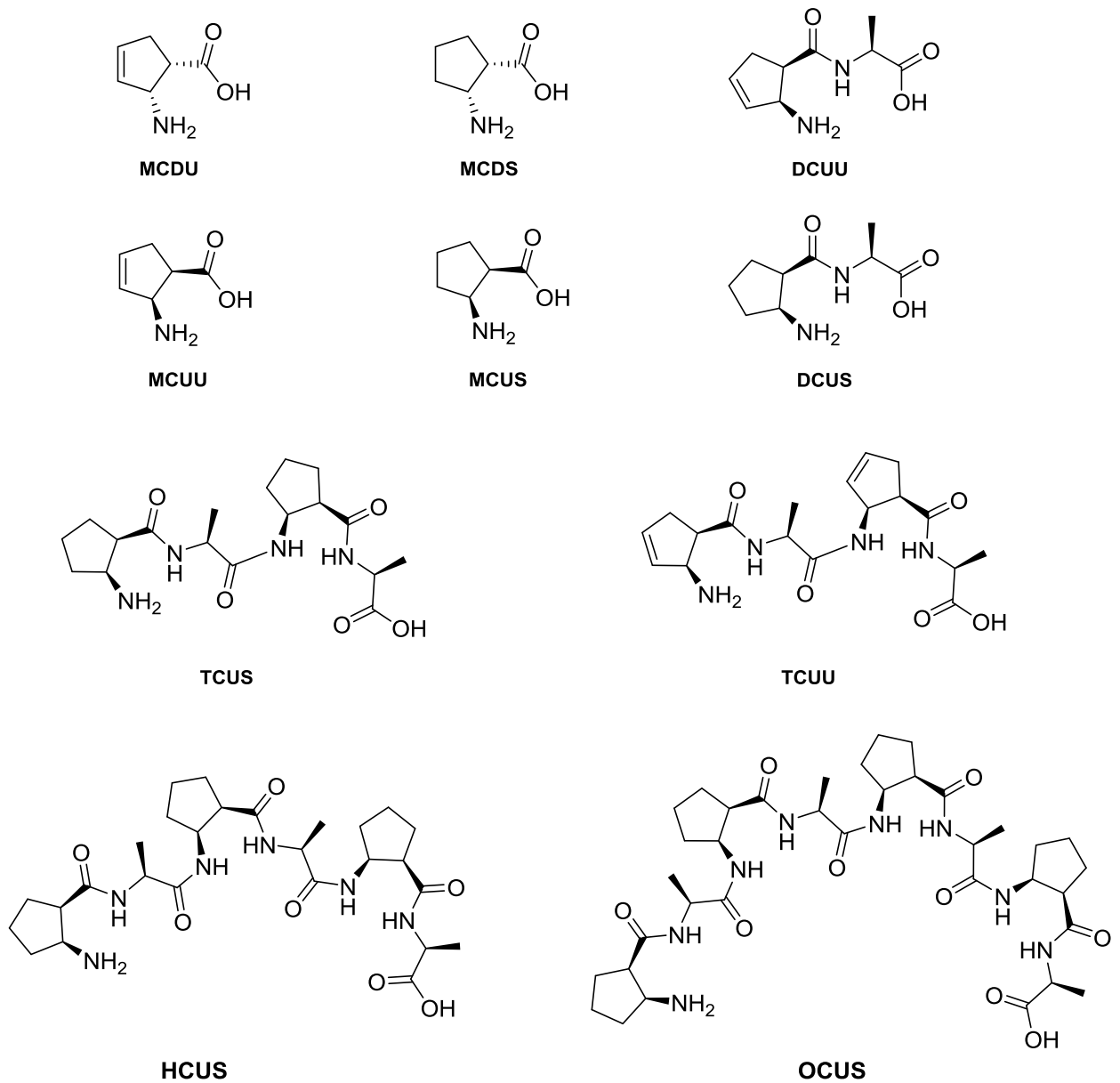
Figure 6.1 Selected compounds assessed for uptake into pig *stratum corneum.*

6.2 COMPOUND UPTAKE DETERMINATION

6.2.1 2,4,6-TRINITROBENZENE SULFONATE (TNBS) ASSAY

The TNBSA assay for primary amines, amino acids and peptides was first reported in 1960 by Satake *et al.*[116] and the method has evolved ever since. The reaction involved is illustrated in Figure 6.2.

Meisenheimer complex
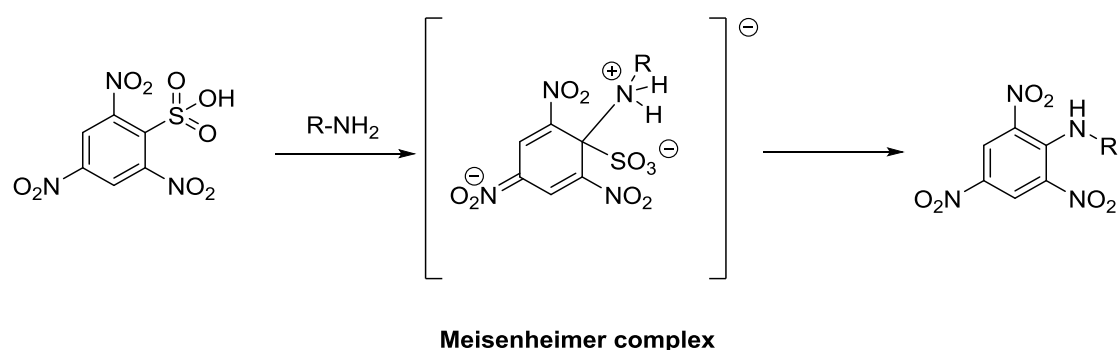
Figure 6.2 Derivatisation of a free amine with TNBSA.

The method is based on the chemical reaction between TNBSA and a free primary amine forming an intermediate chromophore (λ_{max} = 420 nm) known as Meisenheimer complex.

To test the method on the selected compounds, a preliminary assay was run using a commercially available dipeptide (Gly-Gly), following the procedure described by Snyder and Sobocinski.[117] The buffer used in this procedure (sodium tetraborate pH 9.3) was substituted by $NaHCO_3/Na_2CO_3$ buffer, pH 9.3, for readiness reasons. A good

linear correlation between concentration and absorbance was observed as can be seen in Figure 6.3.

Gly-Gly

$y = 0,0118x + 0,0218$
$R^2 = 0,9948$
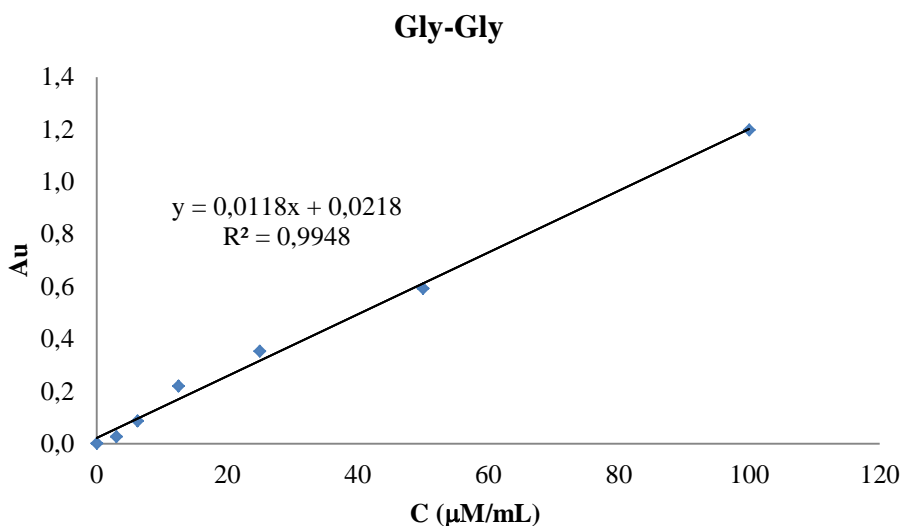
Figure 6.3 Calibration curve for peptide Gly-Gly.

The method was then applied to the monomer **MCUU**. A sample (1.27 mg) of SC was dipped in a saturated solution of **MCUU**, following the procedure described in Chapter 2. The SC was then removed, and the solution was freeze dried for 48 hours to afford a white solid (m < 0.1 mg). The solid was dissolved in 1 mL of buffer and 25 μL of TNBSA were added and left reacting at room temperature along with the standard solutions. The absorbance was read at 420 nm and the correlation between read absorbances and concentration is depicted in Figure 6.4. The LOD (limit of detection) was determined to be 3 μM for **MCUU**.

Dilution was required (1:16) to read the absorbance of the sample and the diluted solution gave 0.760 Au. Applying the calibration curve and considering the dilution factor, the sample had a concentration of 1200µM (9.4 µg, equivalent to 7.4µg/mg SC).
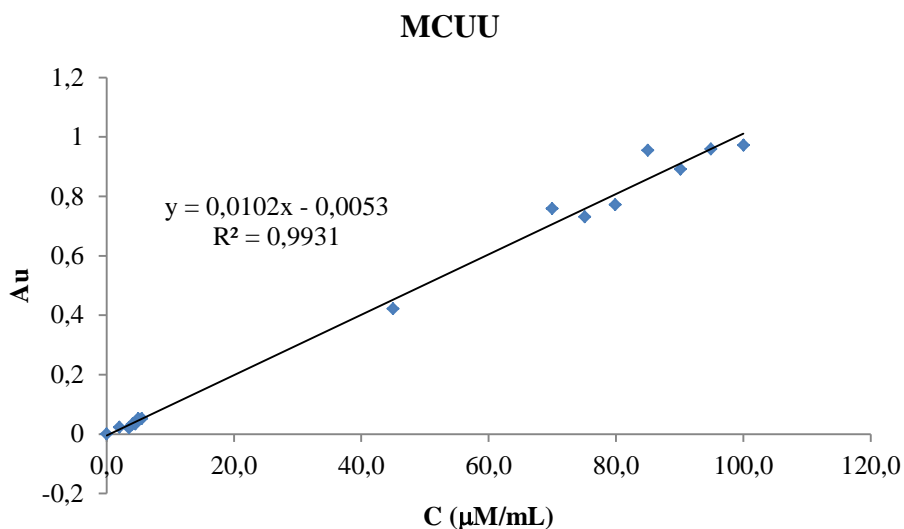
Figure 6.4 Calibration curve for compound MCUU.

From preparing a saturated solution to calculating the amount of compound absorbed by SC a period of time of 4-5 days was needed. In an attempt to reduce analysis time, a saturated solution of **MCUU** was prepared in pH 9.3 buffer and a sample of SC was dipped into it. After a period of 24 hours the integrity of the SC was compromised as stated by Ali *et al.*[118] and the sample degraded in solution.

During the execution of the method, a change in colour for the most concentrated solutions was observed. The absorbance was measured again after 2 hours (2.5 hours of reaction) and, in fact, the readings were different (Table 6.5).

Table 6.5 Absorbance of MCUU standard solutions after reaction time of 30 minutes and 2.5 hours.

	Concentration (μM)								
	100	45	95	90	75	4.5	5	70	80
Au (30 min)	0.972	0.421	0.959	0.891	0.731	0.034	0.052	0.759	0.771
Au (2.5 h)	1.369	0.480	1.077	0.961	0.814	0.056	0	0.819	0.908

Different TNBSA reaction times have been reported by Obi[119] (2 hours) and Cayot[120] (24 hours); Sarantonis *et al.*[121] reported that above pH 9.0 a parallel reaction occurs with HO⁻ and Grotzky and co-workers[122] state that the side product formed (picric acid, Figure 6.5) absorbs at 355 nm with a shoulder at approximately 430 nm.
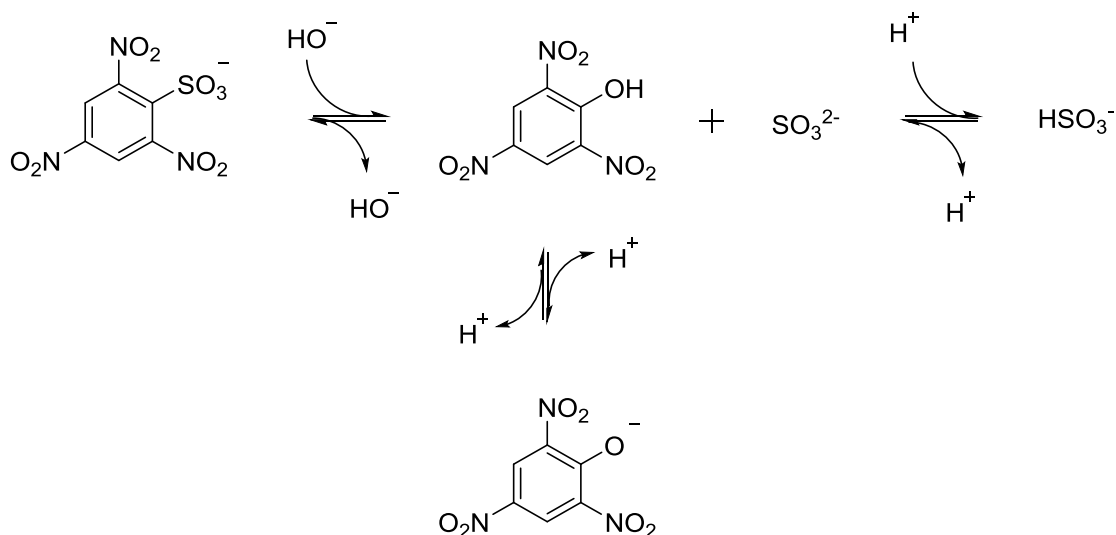
Figure 6.5 Side reaction of TNBSA forming picric acid.

Due to the unreliability of this method's results it was inappropriate to continue and so a new one was sought.

6.2.2 LC/MS METHOD

Method B, described in Chapter 2 (Section 2.16), was applied with the advantage of no requirement for derivatisation or labelling of the compounds. The concentration of each desorption solution was determined using the calibration curves depicted in Figures 6.6 to 6.15. To ensure that the readings were not masked by the release of any compound from the SC, a blank consisting of SC dipped into the sorption/desorption solution (water) was run. The EIC (Extracted Ion Chromatogram) gave a MS of 226.95 Da at 2.3 min, which represented no interference with the retention time of the analytes. The retention time (Rt) of each compound is listed in Table 6.6.

Table 6.6 Retention times of the selected compounds.

					Compound					
	MCDU	MCUU	MCDS	MCUS	DCUS	DCUU	TCUS	TCUU	HCUS	OCUS
Rt (min)	3.2	3.2	3.2	3.2	3.2	3.2	\4.1	4.1	3.3	4.2

MCUU

$$y = 20836x + 43757$$
$$R^2 = 0,9928$$
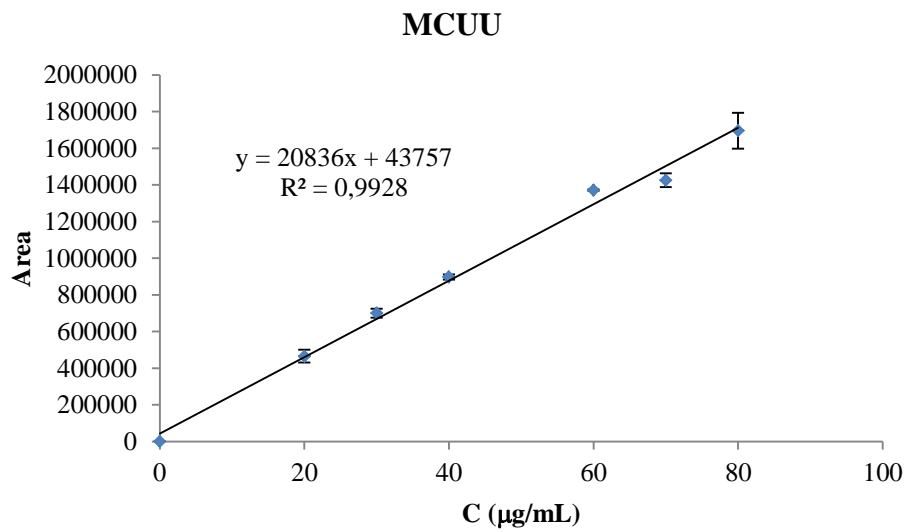
Figure 6.6 Calibration curve for compound MCUU. Data are mean ± SD from n=2.

MCDU

$$y = 18989x - 62493$$
$$R^2 = 0,9829$$
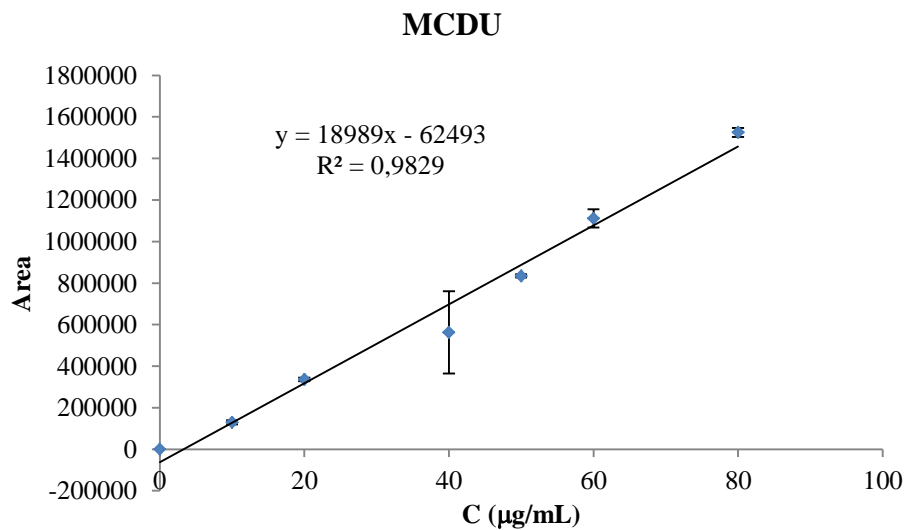
Figure 6.7 Calibration curve for compound MCDU. Data are mean ± SD from n=2.
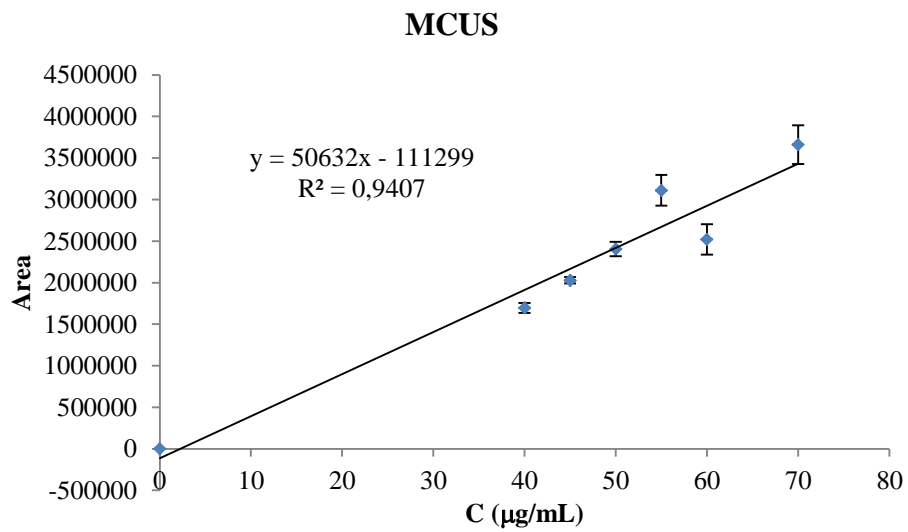
MCUS

Figure 6.8 Calibration curve for compound MCUS. Data are mean ± SD from n=3.
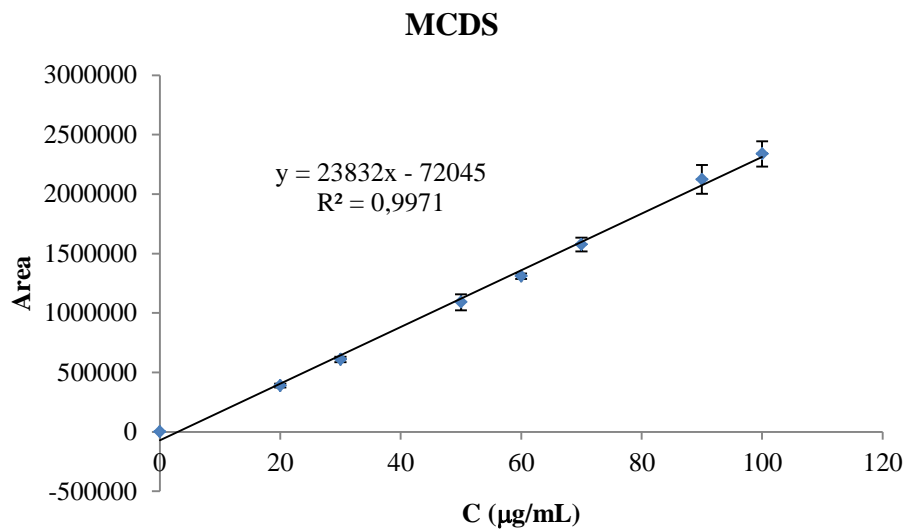
MCDS

Figure 6.9 Calibration curve for compound MCDS. Data are mean ± SD from n=3.

DCUU

y = 131079x + 267868
R² = 0,9885
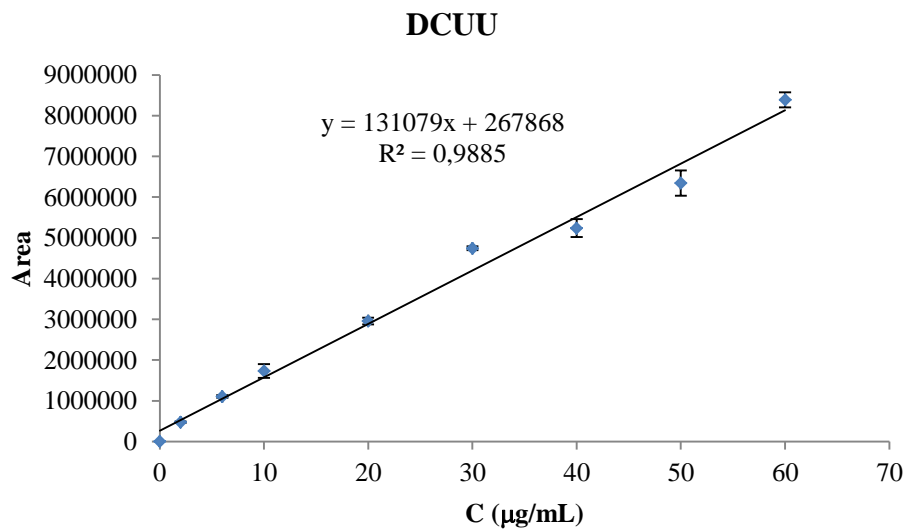
Figure 6.10 Calibration curve for compound DCUU. Data are mean ± SD from n=3.

DCUS

y = 789451x + 330562
R² = 0,9867
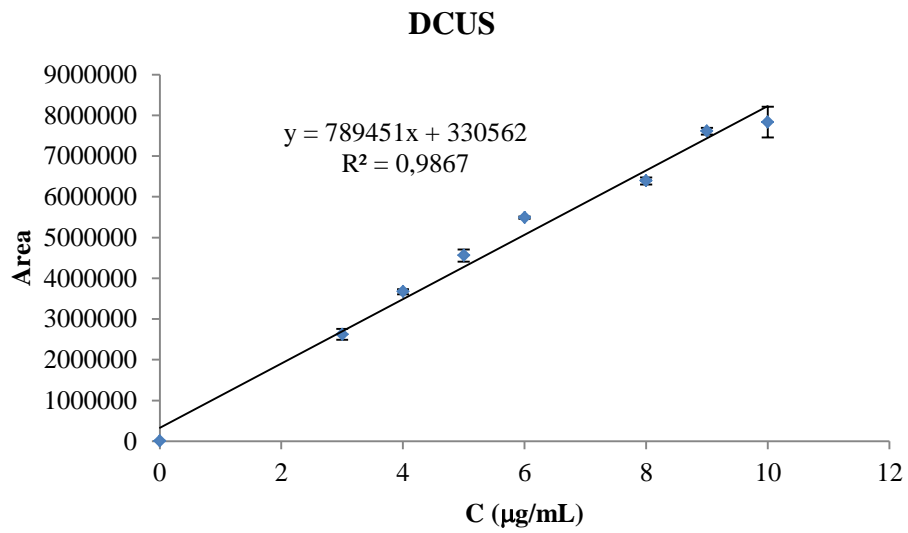
Figure 6.11 Calibration curve for compound DCUS. Data are mean ± SD from n=2.

TCUU

$y = 446364x + 800072$
$R^2 = 0{,}9947$
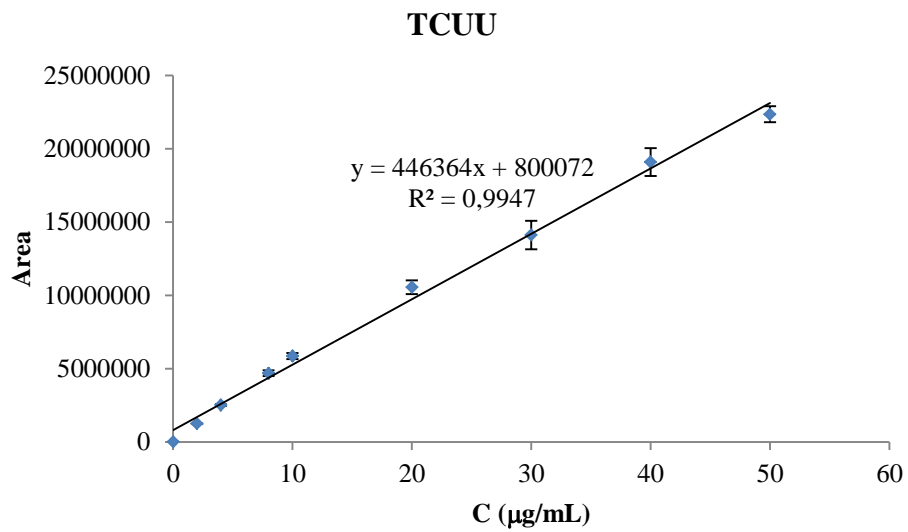
Figure 6.12 Calibration curve for compound TCUU. Data are mean ± SD from n=3.

TCUS

$y = 795930x + 86696$
$R^2 = 0{,}9999$
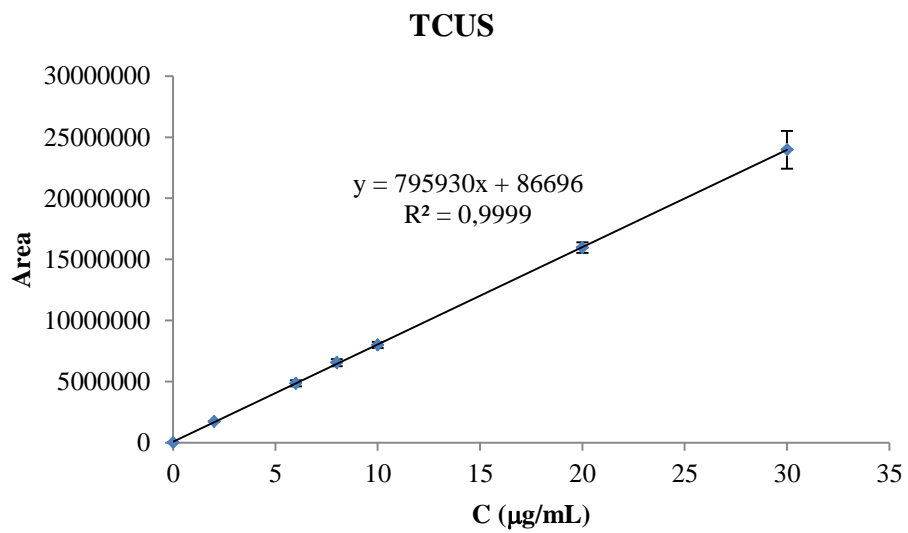
Figure 6.13 Calibration curve for compound TCUS. Data are mean ± SD from n=3.

HCUS

$y = 791143x + 307026$
$R^2 = 0,9671$
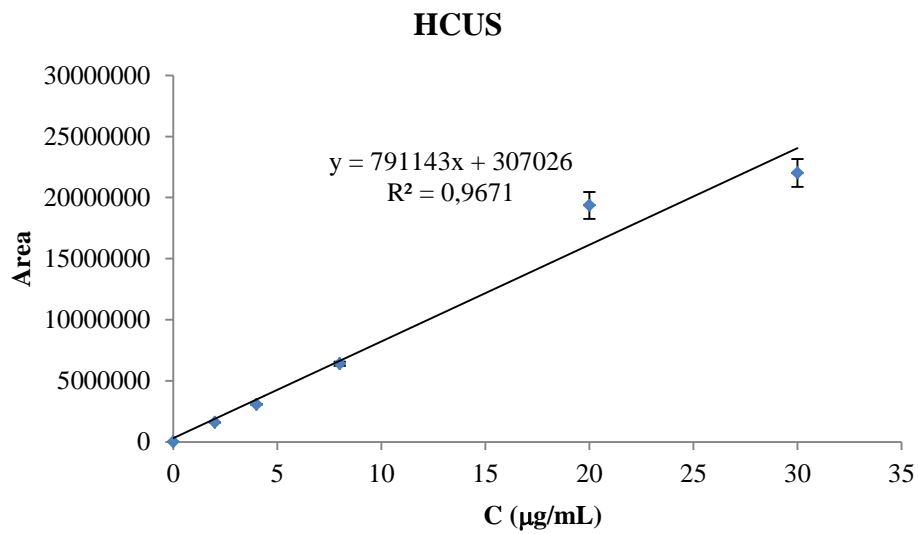
Figure 6.14 Calibration curve for compound HCUS. Data are mean ± SD from n=3.

OCUS

$y = 341709x + 57438$
$R^2 = 0,9798$
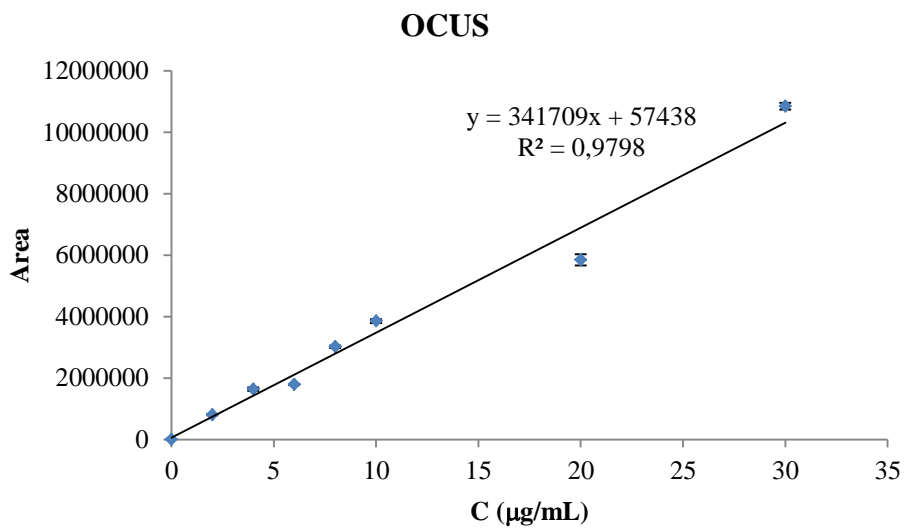
Figure 6.15 Calibration curve for compound OCUS. Data are mean ± SD from n=2.

Due to time restrains the LOD and LOQ (limit of quantification) was not experimentally determined and the values indicated in table 6.7 are calculated using the calibration curves. In this way LOD and LOQ were calculated according to the following equations:

$$LOD = \frac{3 \times SD}{slope}$$

$$LOQ = \frac{10 \times SD}{slope}$$

Where, SD is the standard deviation of the data set.

Due to time constraints and the large number of samples requiring analysis some of the analysed compounds only have 2 repeats. This was accepted because generally the calibration curves gave very good correlations, R^2, values and so n=2 was judged to be sufficiently reliable for the experiments.

Table 6.7 Limit of detection and limit of quantification calculated for each compound.

	Compound									
	MCUU	MCDU	MCUS	MCDS	DCUU	DCUS	TCUU	TCUS	HCUS	OCUS
LOD (µg/mL)	4.7	11.7	4.7	5.3	2.4	0.4	2.5	2.1	2.2	0.5
LOQ (µg/mL)	15.8	39.1	15.7	17.6	7.9	1.5	8.4	6.9	7.3	1.7

There is good correlation for every analysed compound. The LC/MS method allows the quantification of the analytes *via* LC and MS; some of the analysed compounds (smaller molecules) were not UV active and the calibration curves were obtained measuring the EIC areas of the protonated or/and the sodiated forms. Table 6.8 shows the detected mass *vs* the molecular weight of each compound.

Table 6.8 Calculated molecular weight (Mw) and detected mass units (EIC).

	Compound									
	MCUU	**MCDU**	**MCUS**	**MCDS**	**DCUU**	**DCUS**	**TCUU**	**TCUS**	**HCUS**	**OCUS**
Mw	127.06	127.06	129.08	129.08	198.10	200.24	378.43	382.46	564.68	746.91
EIC	128.07	128.07	130.08	130.09		201.24				
					182.09		379.20	383.24	565.34	747.45
(Da)	150.06	150.06	152.07	152.07		223.11				

Compound **DCUU** differed to the behaviour of the other compounds and an analysis of the possible fragments was done to understand the EIC of 182.09. A difference of 17 mass units corresponds to the loss of the hydroxyl group of the carboxylic acid (Figure 6.16). Fragmentation was also observed for the tetramers, hexamer and octamer; in which case all the area of the fragments was taken in account. Though the type of ionisation used (ESI) is adequate for large biological molecules, the temperature of the ionising source may have an influence in fragmentation.

Chemical Formula: $C_9H_{14}N_2O_2{}^\bullet$
Exact Mass: 182,1055

Chemical Formula: $HO^\bullet$
Exact Mass: 17,0027
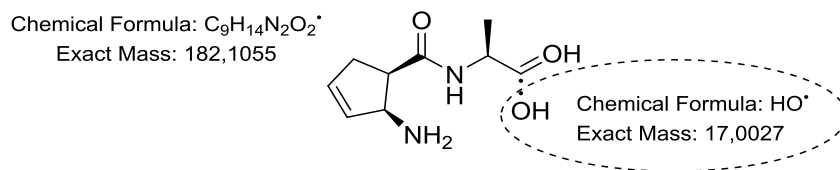
Figure 6.16 Proposed fragmentation for compound DCUU.

Using the calibration curves obtained for the analytes, the "solubility" of the analyte in the SC (S_{asc}), the partition coefficient between SC and water (K_{scw}) – presented as Log P_{scw}, ($P = K_{scw}$) – and the aqueous solubility (S) of each compound were determined and are listed in Table 6.9.

Table 6.9 Partition coefficient and solubility for the set of selected compounds.

	Compound									
	MCUU	**MCDU**	**MCUS**	**MCDS**	**DCUU**	**DCUS**	**TCUU**	**TCUS**	**HCUS**	**OCUS**
$S_{asc}\pm SD$ ($\mu g/mg$ SC)	297±0	150±2	42±4	131±0	5±1	18±2	18±1	15±1	17±2	22±1
$S\pm SD$ (mg/mL)	100±6	83±6	12±1	34±3	30±4	52±7	15±1	7±1	11±2	7±1
Log P_{scw}	-1.99	-2.06	-1.80	-1.90	-3.06	-2.74	-2.26	-2.07	-2.19	-1.83

The solubility decreases with the increase of the molecular size, with the monomers being the most soluble compounds followed by the dimer and tetramers. **TCUS, HCUS** and **OCUS** have no marked difference in their solubility. **HCUS** is slightly higher (11

197

mg/mL) than the other two (both with 7 mg/mL). The S_{asc} shows interesting behaviour along the saturated series, i.e., it decreases from monomer to dimer, with the same value for the tetramer and increases as the size of the peptide grows showing there is a non-obvious nor linear relationship between molecular weight and hydrophilicity/hydrophobicity.

6.3 CONCLUSIONS

Two quantification methods were tested: TNBSA and LC/MS. TNBSA, though giving good linearity, proved to be slow in execution time and gave unreliable results and it had the disadvantage of requiring derivatisation. The LC/MS method revealed more reliable results and lower execution time.

The aqueous solubility of the enantiomers **MCUU** (100 mg/mL) and **MCDU** (83 mg/mL) is significantly different and the same conclusion is drawn for enantiomers **MCUS** (12 mg/mL) and **MCDS** (34 mg/mL). The *cis* up configuration has higher S for the unsaturated monomer, but it behaves in the opposite manner in the saturated monomer. The same trend is observed for the partition coefficient (K_{scw}), i.e., a higher uptake for the *cis* up unsaturated monomer and the opposite trend for the saturated monomer.

Chapter 7 provides further critique of these data and aims to provide insight on the structure /activity relationships of the analysed compounds.

CHAPTER 7

7. GENERAL DISCUSSION AND SUGGESTIONS

This Chapter is divided in four Sections. Section 7.1 and 7.2 present relationships between the compounds' properties, Section 7.3 gives the Chapter's conclusions and Section 7.4 suggests future work in the field.

7.1 RELATIONSHIP OF THE PHYSICAL PROPERTIES FOR THE ALL DATA SET

Chapters 3, 4, 5 and 6 report and analyse data in a "separate" manner. However, it is the purpose of this project to try to observe trends in the collected data. The following sections will present data in totality. Figure 7.1 presents the melting point variation with the molecular weight and the molecular structure as enantiomerically pure compounds or as a mixture of two or more of the possible isomers.
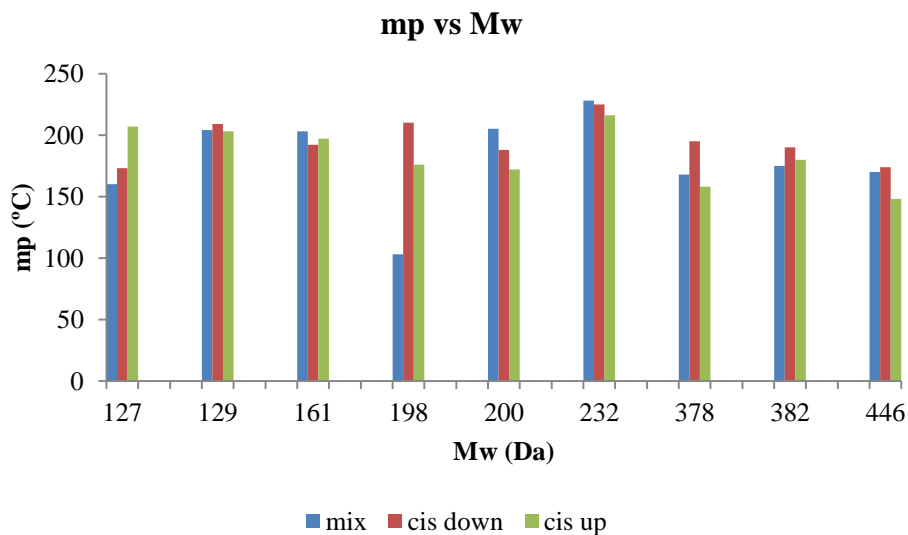
Figure 7.1 Influence of the structure and molecular weight in the melting point.

The melting point of the mixture of enantiomers/diastereomers (blue bar) is generally different from their isolated isomers (enantiomer/diastereomer). There is no clear simple relationship between configurations, i.e., the *cis* down configuration (red bar) is not always the enantiomer/diastereomer with higher or lower melting point than the *cis* up configuration isomer (green bar). The melting point as a function of the molecular weight for the mixture of compounds and their enantiomerically pure isomers is depicted in Figures 7.2-4.
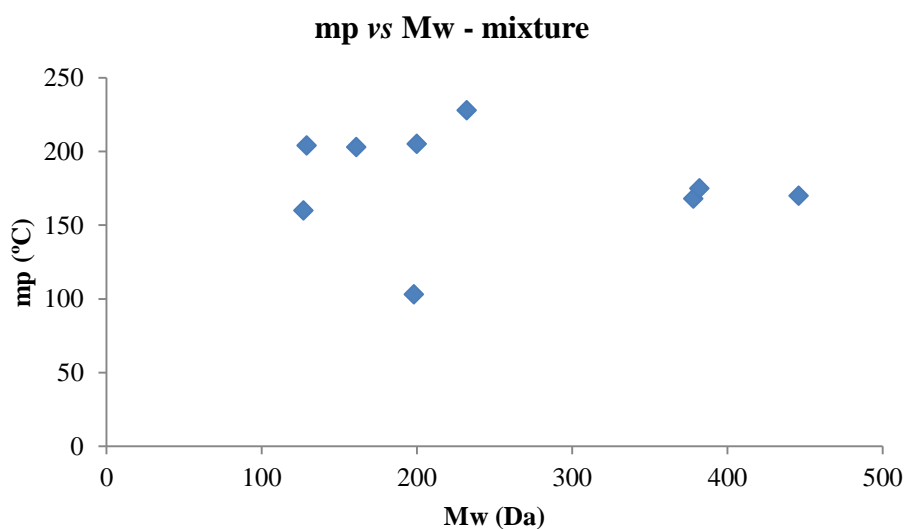
Figure 7.2 Relationship between mp and Mw for the library of compounds as a mixture of enantiomers/diastereomers.

The melting point of a mixture of enantiomers/diastereomers can be interpreted as the measure of the melting point of an impure sample; compounds **MMU**, **MMS**, **MMH**, **DMU**, **DMS** and **DMH** are a mixture of two enantiomers (monomeric series) and diastereomers (dimeric series); **TMU**, **TMS** and **TMH** are a mixture of four diastereomers. The *cis* down series of compounds (Figure 7.3) presents a linear trend for

lower Mw's (< 300 Da) but it changes for "heavier" molecules. The elaborated polynomial relationship in Figure 7.3 has an inflection ~600 Da with no experimental data and a poor correlation (the polynomial relationship has the sole purpose of trying to fit the data to a mathematical equation and express its complexity).

mp *vs* Mw - cis down

$$y = -2E\text{-}10x^5 + 4E\text{-}07x^4 - 0,0003x^3 + 0,0958x^2 - 13,393x + 867,75$$
$$R^2 = 0,6748$$
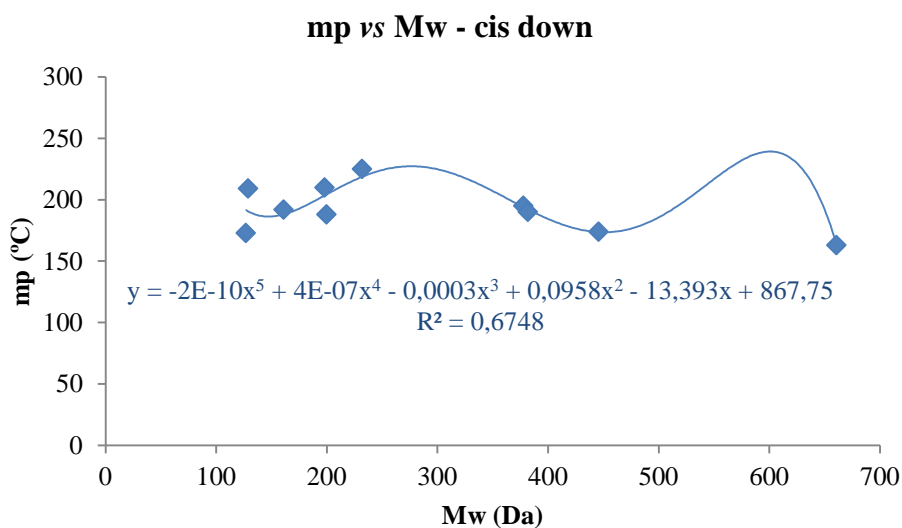
Figure 7.3 Relationship between mp and Mw for the library of compounds with *cis* down configuration.

The *cis* up series of compounds (Figure 7.4) also presents a complex relationship between the melting point and Mw. Up to ~500 Da, the relationship presents a slight decrease of the melting point with the increase of the molecular weight.

mp *vs* Mw - cis up

$$y = 7E\text{-}13x^6 - 2E\text{-}09x^5 + 2E\text{-}06x^4 - 0{,}0009x^3 + 0{,}2524x^2 - 33{,}497x + 1890{,}9$$
$$R^2 = 0{,}7451$$
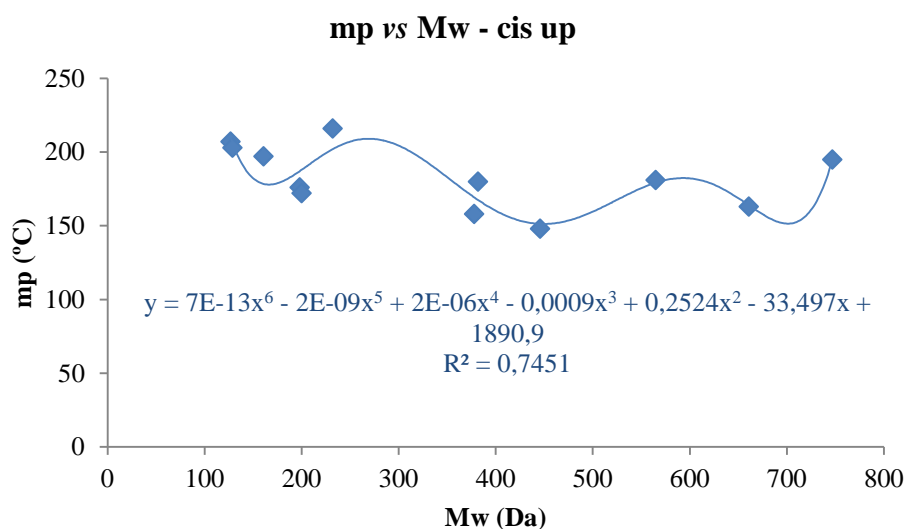
Figure 7.4 Relationship between mp and Mw for the library of compounds with *cis* up configuration.

Due to the nature of the compounds, D/A[d] (donor/acceptor ratio) is directly related with the molecular weight and therefore, to the number of hydrogen bonds that a compound can potentially form. It was theorised that this relationship would be measurable by the N_w absorbed by each compound, this assumption was already tested in previous chapters and it was seen that there is no direct relationship.

From Figure 7.5, showing the number of water molecules as a function of molecular weight of the different compounds, it can be concluded that, once again, chirality has an important role in the results. The behaviour of the synthesised compounds as a mixture or as enantiomerically pure is very different and so an analysis of $N_w = f(\text{D/A})$ is made separately.

---

[d] For ease of use, in this Chapter, D/A is the the sum of D and A previously determined.
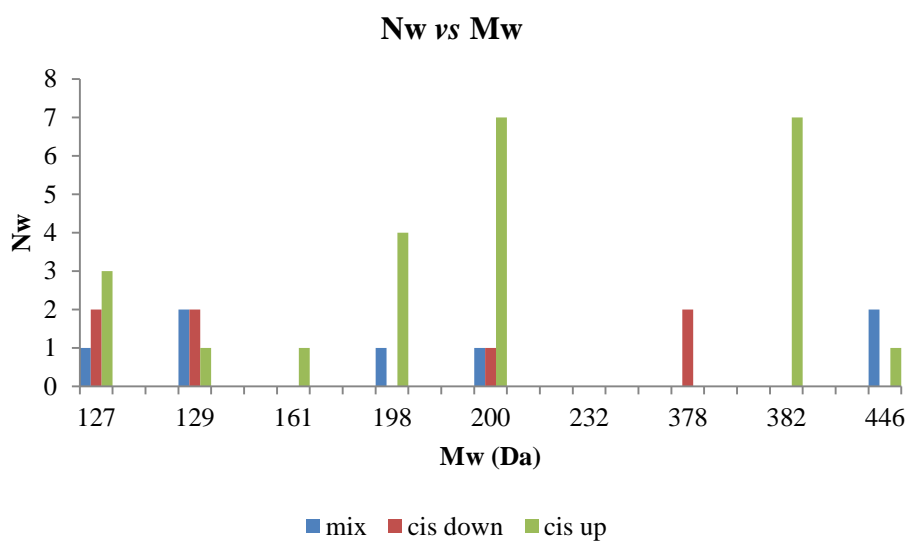
Figure 7.5 Variation of N_w with Mw of different isomers.

The scattered pattern illustrated in Figure 7.6 reinforced the need of a separate analysis by configuration. Figure 7.7 shows the pattern for the *cis* down configuration compounds and it can easily be noticed that more than half (5 out of 9) of the compounds do not bind to water when compared to the *cis* up configuration (Figure 7.8).

Nw *vs* D/A - mix
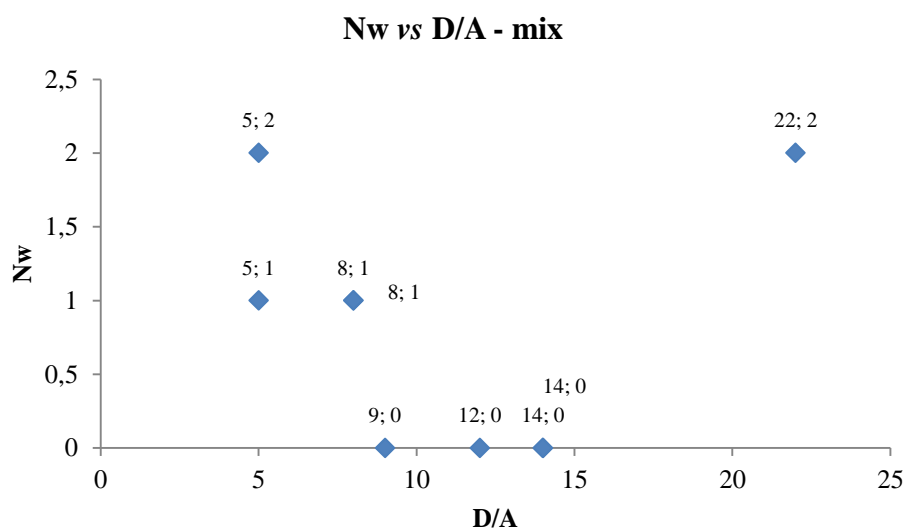
Figure 7.6 Number of water molecules per molecule of compound *vs* D/A for compounds as a mixture of enantiomers/diastereomers.

Nw *vs* D/A - *cis* down
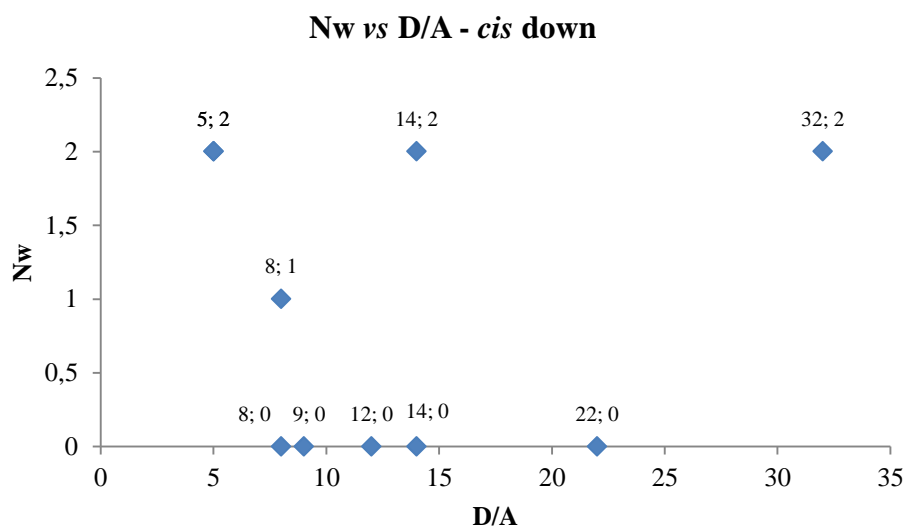
Figure 7.7 Number of water molecules per molecule of compound *vs* D/A for enantiomerically pure compounds with *cis* down configuration.

205

Nw *vs* D/A - *cis* up
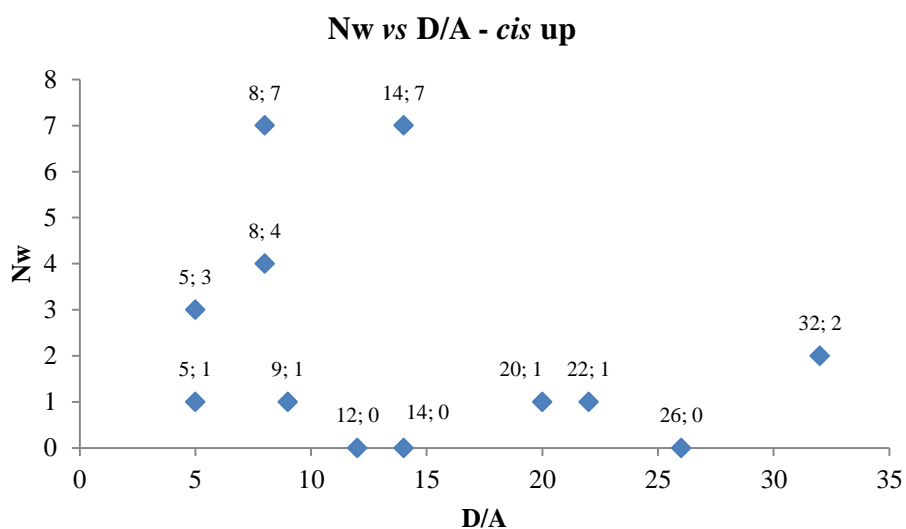
Figure 7.8 Number of water molecules per molecule of compound *vs* D/A for enantiomerically pure compounds with *cis* up configuration.

It is not easy to establish a reliable relationship between these properties when so many variables are involved. Adding diversity (different configurations) to one of the variables (Mw) increases the error's degree of freedom. To continue this study and with the purpose of finding SAR (structure activity relationships) between properties, the following analysis focusses on the compounds selected in Chapter 6 for which skin uptake data is also available.

7.2 RELATIONSHIP OF THE PHYSICAL PROPERTIES FOR THE SELECTED COMPOUNDS

The selection of compounds allows a qualitative analysis on the influence of the physical properties measured in this project as well as using properties that are predicted using known software packages. The influence of chirality will be analysed when possible or relevant.

Figure 7.9 illustrates N_w as a function of D/A for the selected compounds, where it is possible to see a linear dependence of the variables for some of the compounds (blue diamonds). This linearity is not straight forward though, there is an increase of the molecular weight, but the configuration of the cyclic amino acid varies. Three of the outliers (red diamonds) belong to the same series of compounds (saturated series), this series will be evaluated separately later.

Comparing the effect of different spatial arrangements, Figure 7.10 shows the influence of chirality for two pairs of enantiomers with the same D/A relationship (**MCDU**, **MCUU**, **MCDS** and **MCUS**) and approximately the same molecular weight (127 and 129 Da).

Nw *vs* D/A
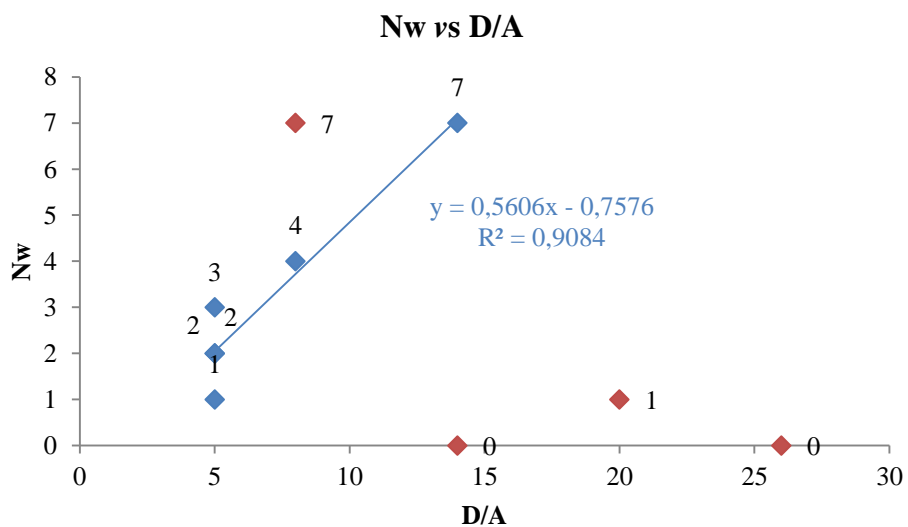
Figure 7.9 Number of water molecules per molecule of compound *vs* D/A for the selected compounds.

Solubility and uptake *vs* Nw
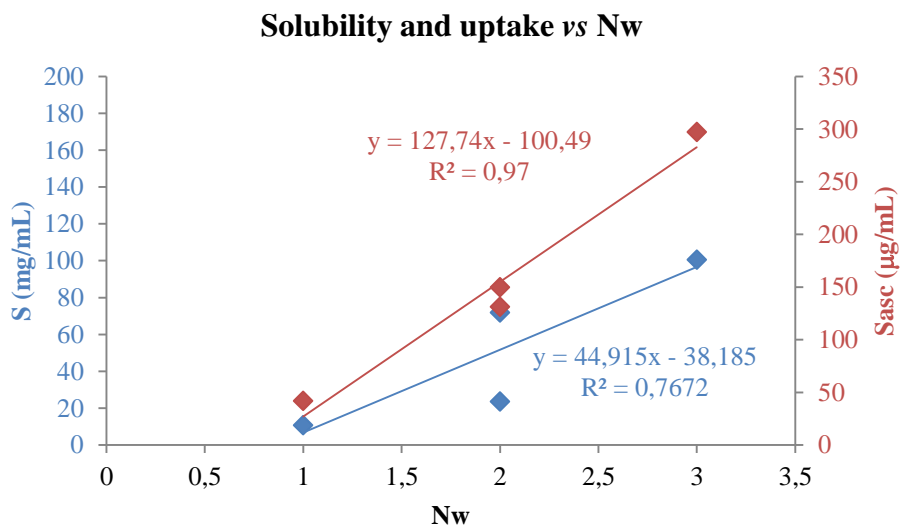
Figure 7.10 Aqueous solubility and uptake into the SC as a function of Nw for compounds with the same D/A relationship.

The two compounds that present a N_w of 2 (**MCDU** and **MCDS**) have very different behaviour in terms of aqueous solubility and uptake into the SC. **MCDU** (72 mg/mL) is 3 fold more soluble in water than **MCDS** (24 mg/mL) but their uptake into the SC is approximately of the same order, i.e., 150 µg/mL and 131 µg/mL, respectively. The behaviour of their enantiomers is even more dissonant. This can be seen as a reflection of chirality and also as a reflection of the structural change as they differ in a saturated/unsaturated bond. Figure 7.11 depicts the remining compounds analysed and it is evident that the trend is different from that previously observed. The solubility (blue diamonds) does tend to increase with the increase of N_w but the uptake (red diamonds) of these compounds suggests independence from N_w
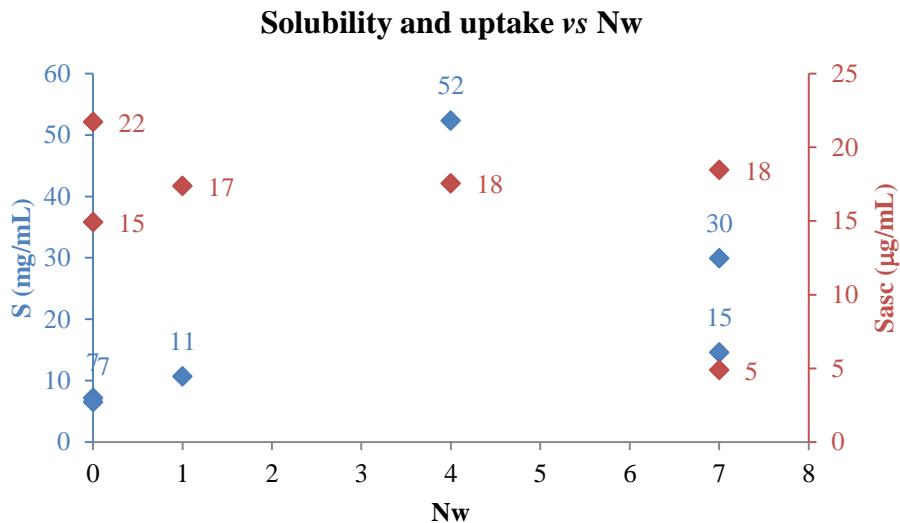
Figure 7.11 Solubility and uptake into the SC as a function of N_w for compounds with different D/A relationship.

Figure 7.12 shows the solubility and uptake as a function of the D/A relationship. For compounds with the same D/A relationship, the solubility and uptake differ significantly. As before, while discussing figure 7.10, four monomers have the same D/A (5) relationship as do two dimers (D/A = 8) and two tetramers (D/A = 14). These compounds are two sets of enantiomers (monomers) and two different compounds of the dimers and tetramers (saturated and unsaturated); the influence of the structural differences reduces as the size of the molecules increase. Analysing molecular size, it seems to dilute its influence on solubility and uptake as the molecules grow as they progress to the same value. Following this last observation, Figure 7.13 illustrates uptake as a function of aqueous solubility, where it can be seen that the solubility and the uptake are directly related, and one increase with the other (red diamond was considered an outlier). Figure 7.14 shows the same relationship but this time for the saturated series with *cis* up configuration, from monomer to octamer. The trend line observed is inconclusive (R^2 0.43) though generally it reverses, i.e., the compound with the higher solubility (**DCUS**) is the one with the lower uptake but it is not the compound with the lower or higher molecular weight. In fact, **DCUS** and **TCUS** are the compounds with the higher number of bound water (7), **TCUS** has almost twice the Mw of **DCUS**, half the solubility in water and three times the uptake; inferring that solubility and uptake are strongly related to spatial arrangement.
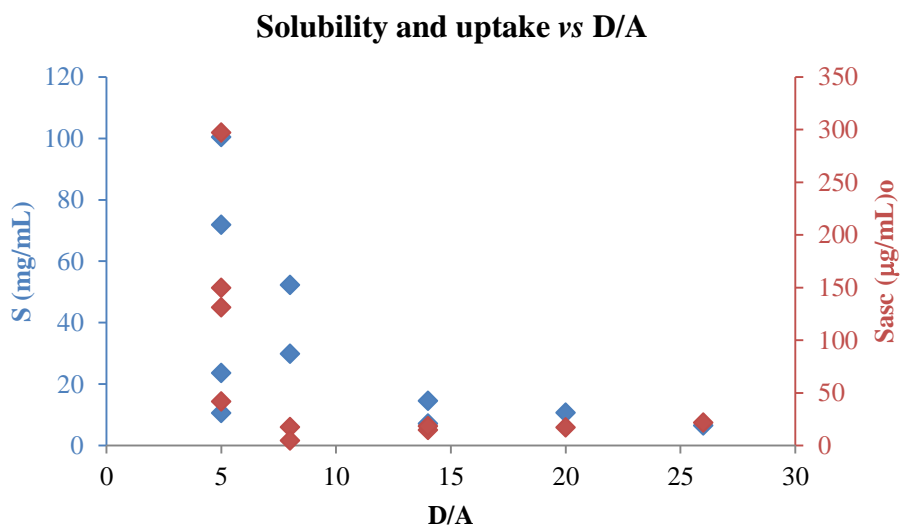
Figure 7.12 Solubility and uptake as a function of D/A for the selected compounds.
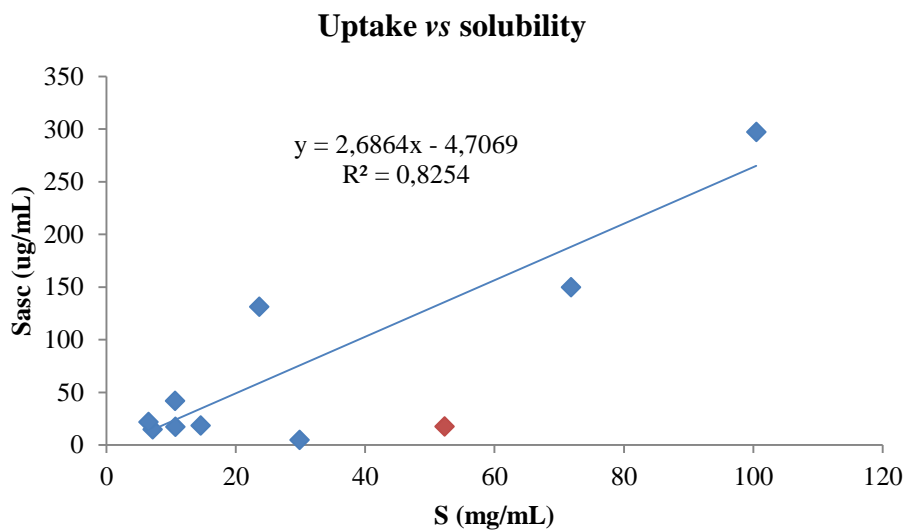
Figure 7.13 Uptake as a function of the solubility.

Uptake vs solubility - *cis* up saturated series

$$y = -0,9686x + 34,818$$
$$R^2 = 0,4362$$
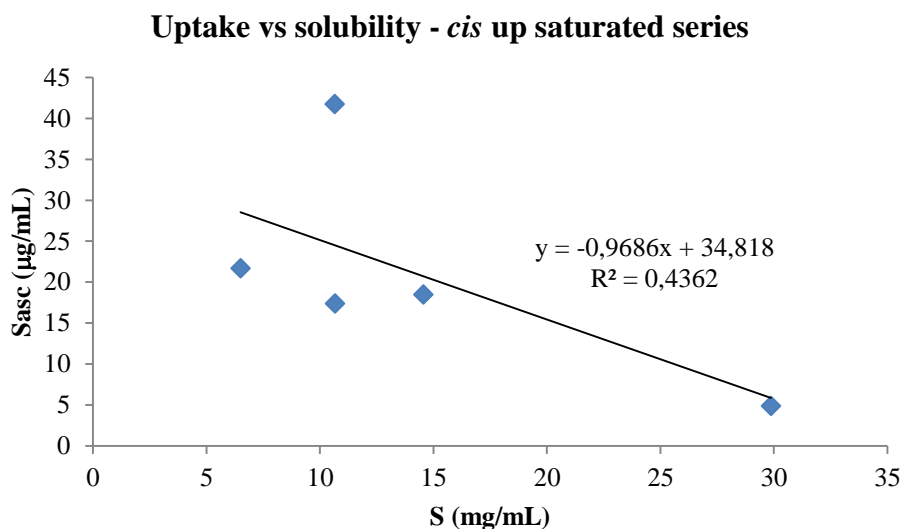
Figure 7.14 Uptake as a function of the solubility for the cis up configuration of the saturated series.

Several software packages are available to predict physical properties of compounds. In this project, Chemdraw, ALogP and Chemicalize were used to predict the LogP and the solubility of the selected compounds and these values were compared to experimental aqueous solubility and pig stratum corneum water LogP (Table 7.1, Figure 7.15 and 7.16).

Drug candidates are often screened according to LogP since the LogP value provides indications on whether a substance will be absorbed by a living tissue, or easily removed to the essentially aqueous plasma. It defines the ratio of its solubility in two immiscible solvents (usually, octanol and water) and it is an important measurement of the physical nature of a substance and thereby a predictor of its behaviour in different environments.

Table 7.1 LogP and LogS obtained experimentally and *via* algorithms.

	Chemdraw			ALogPS		Chemicalize		Experimental	
	LogP (Broto's Method)	CLogP	LogS	ALogP	LogS	LogP	LogS	LogP$_{asc}$	LogS
MCUU	-1.36	-2.58	-0.49	-2.51	0.12	-2.36	1.71	-1.99	2.00
MCDU	-1.36	-2.58	-0.49	-2.51	0.12	-2.36	1.71	-2.06	1.86
MCUS	-0.64	-2.30	-0.59	-2.45	0.22	-2.16	1.83	-1.80	1.03
MCDS	-0.64	-2.30	-0.59	-2.45	0.22	-2.16	1.83	-1.90	1.37
DCUU	-2.37	-2.56	-0.73	-2.23	-0.84	-2.90	1.14	-3.06	1.72
DCUS	-1.65	-2.28	-0.82	-2.07	-0.84	-2.69	1.26	-2.74	1.48
TCUU	-4.34	-2.62	-2.03	-0.63	-2.80	-3.49	-0.38	-2.26	0.85
TCUS	-1.65	-2.06	-2.21	-1.06	2.25	-3.08	-0.14	-2.07	1.16
HCUS	-0.86	-1.83	-3.60	-1.71	-3.41	-3.47	-1.12	-2.19	1.03
OCUS	*	-1.61	-4.99	-1.98	-3.82	-3.85	-1.64	-1.85	0.81

* The method did not predict a value for this molecule

The LogP prediction algorithms that best correlate with the experimental (pig SC/water LogP) data are LogP Chemicalize for monomers and dimers and ALogP and ClogP from Chemdraw for molecules with higher molecular weight, though neither predicts chirality effects.The LogS prediction is best fitted by LogS from Chemicalize.

Comparison of LogP's
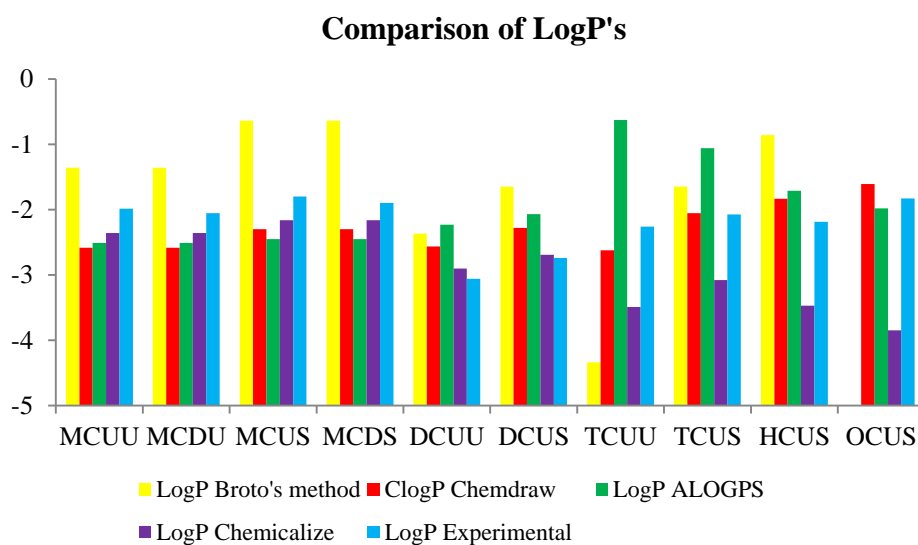
Figure 7.15 Comparison of predicted and experimentally obtained values of LogP.

Comparison of LogS's
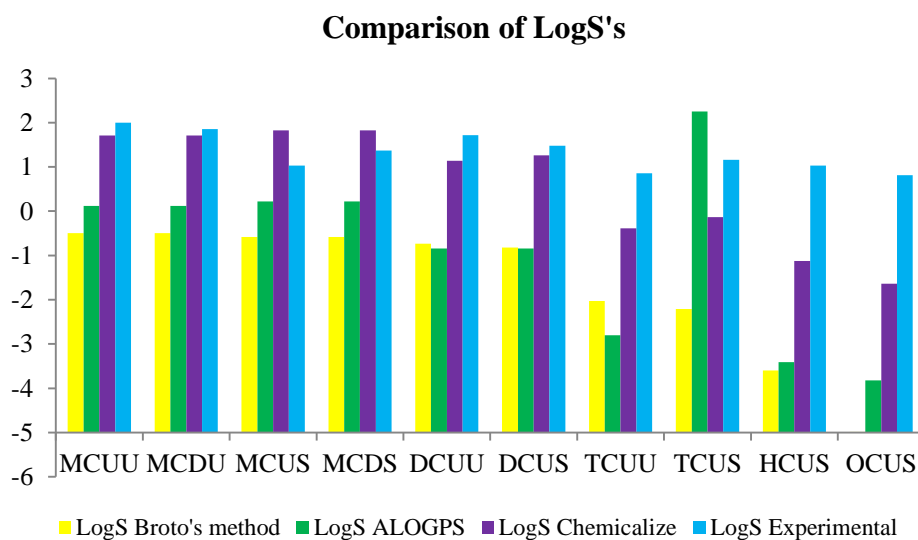
Figure 7.16 Comparison of predicted and experimentally obtained values of LogS.

7.3 CONCLUSIONS

The melting point of a mixture of enantiomers/diastereomers and its enantiomerically pure forms differ with no noticeable trend. This difference is at times greater than 20 ºC but it is not always the *cis* up or *cis* down configuration is the one with the higher or lower melting point. This has an influence on the solubility of the different enantiomers.

There is a linear relationship between N_w and D/A with no relation to chirality, i.e., the linearity is independent from the configuration. This trend holds for lower molecular weight compounds, but as the molecular size increases then the N_w absorbed tends to zero. However, the hydroxylated series starts to bind to water as the molecular weight increases suggesting that the internal arrangement and the side chain motifs of the molecules have great influence on their ability to hydrogen bond to water (and hence alters in their hydrophilicity/lipophilicity.

The solubility and the uptake of the analysed compounds have a linear relationship with N_w for molecules with lower Mw, but this relationship changes for larger molecules. The solubility, though lower, is directly related to the number of bound water molecules and the uptake shows N_w independence.

There is a linear and proportional correlation between solubility and uptake, this relationship is disturbed by the structural differences of the enantiomers/diastereomers, as the saturated series demonstrates. For this series (*cis* up), solubility and uptake are indirectly correlated.

LogP Chemicalize is the best theoretical prediction algorithm for smaller molecules and ALogP and ClogP from Chemdraw are more appropriate for molecules with higher

molecular weight. Chirality effects are not contemplated by the software used. On the other hand LogS prediction is roughly fitted by LogS from Chemicalize.

The physical properties have an influence in the solubility and uptake, their relationship is not always linear and other properties have to be taken in account. Chirality clearly plays a role since such molecules, with the same molecular weight, have different melting point, solubility and uptake.

In summary, the project began by designing a series of monomers that could be assembled into larger structures, to investigate the influence of chirality on molecular uptake into *stratum corneum*. In parallel the monomers were designed to have different hydrogen bonding capabilities which was expected to confer the ability to bind to water. In general terms, the addition of hydrogen bonding capabilities presented internal hydrogen bonding opportunities as the molecular weight was increased from monomer to dimer. The assemblies, or foldamers, clearly confounded the simple initial hypothesis and prevented simple hydrogen bond site-water binding correlations. The internal structures also confounded simple relationships between chirality and uptake (or other properties) since simple chemical representations of structures are not based in the reality of the molecular assembly – as shown by the X-ray diffraction results. One further key lesson is apparent. A large library of molecules was synthesised – an extensive series of monomers (e.g. unsaturated, saturated and hydroxylated) and these then built into their own series of "macromolecules" (monomer, dimer, tetramer, hexamer, octamer). From the critique above, some trends could be described within a subset of the data – for example trends in the monomers or trends across a macromolecule series, or trends in a particular *cis* up or down series. However, considering the data in total, such trends are not apparent in all series or classes and

216

indeed trends from one series reverse in another. This illustrates the importance of not selecting a narrow range of materials and the extrapolating findings more broadly; had a single series, for example the saturated ones, been used throughout but they could have erroneously then been extrapolated to other chemical series.

7.4 FUTURE WORK

From this project, a number of directions could be followed. Below is a list of some potential future work that could be further investigated.

- Firstly, the work could continue with diffusion studies of the selected compounds using Franz Cell equipment to provide a clearer insight on the dynamics of these compounds in a permeation process and would dissipate doughts about the SC permeability.

- Test the selected compounds in excised human skin. This would be firstly uptake studies into isolated sheets of human epidermal membranes to evaluate if human skin is chirally selective for these molecules. Molecules that enter the tissue could then be tested as permeation enhancers. An initial hypothesis was that the molecules would bind to water and so could have permeation enhancing properties.

- As an extension to the above, it would be feasible to conjugate the selected compounds with a drug and evaluate the influence of the conjugation on physical properties and uptake into SC.

- A more complete study would involve complete testing of all compounds synthesised, spatially the hydroxylated series. The small molecular weight hydroxylated compounds do not bind to water and the present study suggests no obvious relationship between N_w and uptake but it does suggest a linear relationship between solubility and uptake.

- A more powerful package for molecular dynamics would be advisable to predict N_w that theoretically bind to each compound and rationalise the design of new candidates.

- Explore the foldameric potential of the synthesised compounds varying concentration, temperature, pH and solvent systems in order to relate their characteristic folding to permeation.

REFERENCES

1. Jepps, O. G.; Dancik, Y.; Anissimov, Y. G.; Roberts, M. S., Modeling the Human Skin Barrier-Towards a Better Understanding of Dermal Absorption. *Advanced drug delivery reviews* **2013,** *65* (2), 152-168.

2. Williams, A. C., *Transdermal and Topical Drug Delivery*. Pharmaceutical Press: London, UK, 2003.

3. Cross, S. E.; Roberts, M. S., Subcutaneous Absorption Kinetics and Local Tissue Distribution of Interferon and Other Solutes. *J. Pharm. Pharmacol.* **1993,** *45*, 606-609.

4. Singh, S.; Singh, J., Transdermal Drug Delivery by Passive Diffusion and Iontophoresis: A Review. *Med Res Rev* **1993,** *13* (5), 569-621.

5. Montagna, W., *The Structure and Function of the Skin*. Academic Press Inc.: New York, 1956.

6. Burkitt, H. G.; Young, B.; Heath, J. W., *Wheater's Functional Histology: A Text Book and Colour Atlas*. 3rd ed.; Chirchill Livingstone: London, 1994.

7. Bouwstra, J. A.; Groenink, H. W. W.; Kempenaar, J. A.; Romeijn, S. G.; Ponec, M., Water Distribution and Natural Moisturizer Factor Content in Human Skin Equivalents Are Regulated by Environmental Relative Humidity. *J Invest Dermatol* **2008,** *128*, 378–388.

8. Silva, S. M.; Hu, L.; Sousa, J. J.; Pais, A. A.; Michniak-Kohn, B. B., A Combination of Nonionic Surfactants and Iontophoresis to Enhance the Transdermal Drug Delivery of Ondansetron HCl and Diltiazem HCl. *European journal of*

pharmaceutics and biopharmaceutics : official journal of Arbeitsgemeinschaft fur Pharmazeutische Verfahrenstechnik e.V **2012,** *80* (3), 663-73.

9.   El Maghraby, G. M.; Barry, B. W.; Williams, A. C., Liposomes and Skin: From Drug Delivery to Model Membranes. *European journal of pharmaceutical sciences : official journal of the European Federation for Pharmaceutical Sciences* **2008,** *34* (4-5), 203-22.

10.   Christophers, E.; Kligman, A. M., Visualization of the Cell Layers of the Stratum Corneum. *J Invest Dermatol* **1964,** *42*, 407–409.

11.   Christophers, E., Cellular Architecture of the Stratum Corneum. *J Invest Dermatol* **1971,** *56*, 165–169.

12.   Scheuplein, R. J., Mechanism of Percutaneous Absorption. *J Invest Dermatol* **1967,** *48* (1), 79–88.

13.   Elias, P. M., Stratum Corneum Architecture, Metabolic Activity and Interactivity with Subjacent Cell Layers. *Exp Dermatol* **1996,** *5*, 191-201.

14.   Elias, P. M.; Gruber, R.; Crumrine, D.; Menon, G.; Williams, M. L.; Wakesfield, J. S.; Holleran, W. M.; Uchida, Y., Formation and Functions of the Corneocyte Lipid Envelope (CLE). *Biochim. Biophys. Acta* **2014,** *1841*, 314-318.

15.   McGrath, J. A.; JUitto, J., The Filaggrin story: Novel Insights into Skin-Barrier Function and Disease. *Trends in molecular medicine* **2008,** *14* (1), 20-27.

16.   Scott, I. R.; Harding, C. R.; Barrett, J. G., Histidine-Rich Protein of the Keratohyslin Granules. Source of the Free Amino Acids, Urocanic Acid, and Pyrrolidone Carboxylic Acid in the Stratum Corneum. *Biochim. Biophys. Acta* **1982,** *719* (1), 110-117.

17.   Middleton, J. D., The Mechanism of Water Binding in Stratum Corneum. *Brit J Derm* **1986,** *80* (7), 437-450.

18.   Lodén, M.; Maibach, H. I., *Dry Skin and Moisturizers Chemistry and Function*. CRC Press: 2005.

19.   Imokawa, G.; Hiroshi, K.; Kawai, M., Stratum Corneum Lipids Serve as a Bound-Water Modulator. *J Invest Dermatol* **1990,** *96* (6), 845-851.

20.   Sakai, S.; Yasuda, R.; Sayo, T.; Ishihawa, O.; Inoue, S., Hyaluronic Acid Exists in the Stratum Corneum. *J Invest Dermatol* **2000,** *14* (16), 1184-1187.

21.   Hara, M.; Ma, T.; Verkman, A. S., Selectively Reduced Glycerol in Skin of Aquaporin-3-deficient Mice May Account for Impaired Skin Hydration, Elasticity, and Barrier Recovery. *J. Biol. Chem.* **2002,** *277* (48), 46616–46621.

22.   Arezki, N. R.; Williams, A. C.; Cobb, A. J.; Brown, M. B., Design, Synthesis and Characterization of Linear Unnatural Amino Acids for Skin Moisturization. *International journal of cosmetic science* **2017,** *39* (1), 72-82.

23.   Svensson, C. K., Biotransformation of Drugs in Human Skin. *Drug Metab Dispos* **2009,** *37* (2), 247-253.

24.   Oesch, F.; Fabian, E.; Oesch-Bartlomowicz, B.; Werner, C.; Landsiedel, R., Drug-Metabolizing Enzymes in the Skin of Man, Rat and Pig. *Drug Metab Rev* **2007,** *39*, 659–698.

25.   Zhang, Q.; Grice, J. E.; Wang, G.; Roberts, M. S., Cutaneous Metabolism in Transdermal Drug Delivery. *Curr Drug Metab* **2009,** *10*, 227-235.

26.   Baron, J. M.; Höller, D.; Schiffer, R.; Frankenberg, S.; Neis, M.; Merk, H. F.; Jugert, F. K., Expression of Multiple Cytochrome P450 Enzymes and Multidrug

Resistance-Associated Transport Proteins in Human Skin Keratinocytes. *J Invest Dermatol* **2001,** *116* (4), 541-548.

27.   Swanson, H. I., Cytochrome P450 Expression in Human Keratinocytes: an Aryl Hydrocarbon Receptor Perspective. *Chem. Biol. Interact.* **2004,** *149* (2), 69–79.

28.   Nacht, S.; Yeung, D.; Beasley Jr., J. N.; Anjo, M. D.; Maibach, H. I., Benzoyl Peroxide: Percutaneous Penetration and Metabolic Disposition. *Journal of the American Academy of Dermatology* **1981,** *4* (1), 31–37.

29.   Slominski, A.; Tobin, D. J.; Zmijewski, M. A.; Wortsman, J.; Paus, R., Melatonin in the Skin: Synthesis, Metabolism and Functions. *Trends Endocrin Met* **2007,** *19* (1), 17-24.

30.   Langer, R., Transdermal Drug Delivery: Past Progress, Current Status, and Future Prospects. *Advanced drug delivery reviews* **2004,** *56* (5), 557-8.

31.   Illel, B.; Schaefer, H.; Wepierre, J.; Doucet, O., Follicles Play an Important Role in Percutaneous Absorption. *Journal of pharmaceutical sciences* **1991,** *80* (5), 424-427.

32.   Siddiqui, O.; Roberts, M. S.; Polack, A. E., Percutaneous Absorption of Steroids: Relative Contributions of Epidermal Penetration and Dermal Clearance. *J Pharmacokinet Biop* **1989,** *17* (4), 405-424.

33.   Heisig, M.; Lieckfeldt, R.; Wittum, G.; Mazurkevich, G.; Lee, G., Non Steady-State Descriptions of Drug Permeation Through Stratum Corneum. I. The Biphasic Brick-and-Mortar Model. *Pharmaceutical research* **1996,** *13* (3), 421-426.

34.   Sznitowska, M.; Janicki, S.; Williams, A. C., Intracellular or Intercellular Localization of the Polar Pathway of Penetration Across Stratum Corneum. *Journal of pharmaceutical sciences* **1998,** *87* (9), 1109-1114.

35.   Roberts, M. S.; Pugh, W. J.; Hadgraft, J., Epidermal Permeability: Penetrant Structure Relationships. The Effect of H-Bonding Groups in Penetrants on their Diffusion Through the Stratum Corneum. *International journal of pharmaceutics* **1996,** *132* (1-2), 23-32.

36.   Forslind, B., A Domain Mosaic Model of the Skin Barrier. *Acta Derm Venereol* **1994,** *74* (1), 1-6.

37.   Tregear, R. T., *Physical Functions of the Skin*. Academic Press Inc.: London, 1966.

38.   Moriguchi, I.; Hoirono, S.; Liu, Q.; Nakagome, I.; Matsushita, Y., Simple Method of Calculating Octanol/Water Partition Coefficient. *Chem. Pharm. Bull.* **1992,** *40* (1), 127-130.

39.   Lenn, J. D.; Neil, J.; Donahue, C.; Demock, K.; Tibbetts, C. V.; Cote-Sierra, J.; Smith, S. H.; Rubenstein, D.; Therrien, J. P.; Pendergrast, P. S.; Killough, J.; Brown, M. B.; Williams, A. C., RNA Aptamer Delivery through Intact Human Skin. *J Invest Derm* **2018,** *138*, 282-290.

40.   Lipinski, C.; Lombardo, F.; Dominy, B. W.; Feeny, P. J., Experimental and Computational Approaches to Estimate Solubility and Permeability in Drug Discovery and Development Setting. *Adv Drug Deliver Rev* **2001,** *46*, 3-26.

41.   Krishnaiah, Y. S.; Nada, A., Enantioselective Penetration Enhancing Effect of Carvone on the In Vitro Transdermal Permeation of Nicorandil. *Pharm Dev Technol* **2012,** *17* (5), 574-582.

42.   Valentova, J.; Bauerova, K.; Farah, L.; Devinsky, F., Does Stereochemistry Influence Transdermal Permeation of Flurbiprofen Through the Rat Skin? *Archives of dermatological research* **2010,** *302* (8), 635-8.

43.   Cilurzo, F.; Minghetti, P.; Alberti, E.; Gennari, C. G.; Pallavicini, M.; Valoti, E.; Montanari, L., An Investigation into the Influence of Counterion on the RS-Propranolol and S-Propranolol Skin Permeability. *Journal of pharmaceutical sciences* **2010,** *99* (3), 1217-24.

44.   Reddy, I. K., *Chirality in Drug Design and Development*. Marcel Dekker, Inc.: New York, 2004.

45.   Hutt, A. J.; Tan, S. C., Drug Chirality and its Clinical Significance. *Drugs* **1996,** *52* (Suppl. 5), 1-12.

46.   Lu, H., Stereoselectivity in Drug Metabolism. *Expert Opin Drug Metab Toxicol* **2007,** *3* (2), 149-158.

47.   Smith, S. W., Chiral Toxicology: it's the same thing...only different. *Toxicol. Sci.* **2009,** *110* (1), 4-30.

48.   Afouna, M. I.; Fincher, T. K.; Khan, M. A.; Reddy, I. K., Percutaneous Permeation of Enantiomers and Racemates of Chiral Drugs and Prediction of Their Flux Ratios Using Thermal Data: A Pharmaceutical Perspective. *Chirality* **2003,** *15*, 456–465.

49.   Kommuru, T. R.; Mansoor, A. K.; Reddy, I. K., Racemate and Enantiomers of Ketoprofen: Phase Diagram, Thermodynamic Studies, Skin Permeability, and Use of Chiral Permeation Enhancers. *Journal of pharmaceutical sciences* **1998,** *87* (7), 833-840.

50.   Suedee, R.; Bodhibukkana, C.; Tangthong, N.; Amnuaikit, C.; Kaewnopparat, S.; Srichana, T., Development of a Reservoir-Type Transdermal Enantioselective-Controlled Delivery System for Racemic Propranolol using a Molecularly Imprinted

Polymer Composite Membrane. *Journal of controlled release : official journal of the Controlled Release Society* **2008,** *129* (3), 170-178.

51.   Suedee, R.; Brain, K. R.; Heard, C. M., Differential Permeation of Propranolol Enantiomers Across Human Skin in Vitro from Formulations Containing an Enantioselective Excipient. *Chirality* **1999,** *11*, 680-683.

52.   Heard, C. M.; Brain, K. R., Does Solute Stereochemistry Influence Percutaneous Penetration? *Chirality* **1995,** *7*, 305-309.

53.   Yuan, X.; Capomacchia, A. C., Influence of Physicochemical Properties on the In Vitro Skin Permeation of the Enantiomers, Racemate, and Eutectics of Ibuprofen for Enhanced Transdermal Drug Delivery. *Journal of pharmaceutical sciences* **2013,** *102* (6), 1957-1969.

54.   Katritzky, A. R.; Jain, R.; Lomaka, A.; Petrukhin, R.; Maran, U.; Karelson, M., Perspective on the Relationship between Melting Points and Chemical Structure. *Cryst. Growth Des.* **2001,** *1* (4), 261-265.

55.   Chu, K. A.; Yalkowsky, S. H., An Interesting Relationship between Drug Absorption and Melting Point. *International journal of pharmaceutics* **2009,** *373*, 24-40.

56.   Zeng, A.; Wang, C.; Yuan, B.; Yang, G.; Fu, Q., The Influence of Chirality, Physicochemical Properties, and Permeation Enhancers on the Transdermal Permeation of Amlodipine Across Rat Skin. *Drug Dev. Ind. Pharm.* **2010,** *36* (6), 724-734.

57.   Kommuru, T. R.; Khan, M. A.; Reddy, I. K., Effect of Chiral Enhancers on the Permeability of Optically Active and Racemic Metoprolol across Hairless Mouse Skin. *Chirality* **1999,** *11*, 536-540.

58.   Cilurzo, F.; Alberti, E.; Minghetti, P.; Gennari, C. G.; Casiraghi, A.; Montanari, L., Effect of Drug Chirality on the Skin Permeability of Ibuprofen. *International journal of pharmaceutics* **2010,** *386* (1-2), 71-76.

59.   Suedee, R.; Jantarat, C.; Lindner, W.; Viernstein, H.; Songkro, S.; Srichana, T., Development of a pH-Responsive Drug delivery System for Enantioselective-Controlled Delivery of Racemic Drugs. *Journal of controlled release : official journal of the Controlled Release Society* **2010,** *142* (1), 122-131.

60.   Nelson, D. L.; Cox, M. M., *Principles of Biochemistry.* 4th ed.; W H Freeman and Company: NY, USA, 2004.

61.   Gellman, S. H., Foldamers: A Manifesto. *Accounts Chem Res* **1998,** *31* (4), 173-180.

62.   Prausnitz, M. R.; Langer, R., Transdermal Drug Delivery. *Nat. Biotechnol.* **2008,** *26* (11), 1261-1268.

63.   Wiedersberg, S.; Guy, R. H., Transdermal Drug Delivery: 30+ Years of War and Still Fighting! *Journal of controlled release : official journal of the Controlled Release Society* **2014,** *190*, 150-6.

64.   Williams, A. C.; Barry, B. W., Penetration Enhancers. *Advanced drug delivery reviews* **2004,** *56* (5), 603-18.

65.   Kulkarni, V. S., *Handbook of Non-Invasive Drug Delivery Systems.* Elsevier: Oxford, UK, 2010.

66.   Cardoso, A. M.; Morais, C. M.; Cruz, A. R.; Silva, S. G.; Vale, M. L.; Marques, E. F.; Pedroso de Lima, M. C.; Jurado, A. S., New Serine-Derived Gemini Surfactants as Gene Delivery Systems. *European journal of pharmaceutics and biopharmaceutics :*

official journal of Arbeitsgemeinschaft fur Pharmazeutische Verfahrenstechnik e.V
2015, *89*, 347-356.

67.   Rennert, R.; Neundorf, I.; Beck-Sickinger, A. G., *Nucleic Acid and Peptide Aptamers*. Humana Press ed.; Totowa, NJ, 2009; Vol. 535, p 389-403.

68.   Janusova, B.; Skolova, B.; Tukorova, K.; Wojnarova, L.; Simunek, T.; Mladenka, P.; Filipsky, T.; Riha, M.; Roh, J.; Palat, K.; Hrabalek, A.; Vavrova, K., Amino Acid Derivatives as Transdermal Permeation Enhancers. *Journal of controlled release : official journal of the Controlled Release Society* **2013,** *165* (2), 91-100.

69.   Desai, P.; Patlolla, R. R.; Singh, M., Interaction of Nanoparticles and Cell-Penetrating Peptides with Skin for Transdermal Drug Delivery. *Molecular membrane biology* **2010,** *27* (7), 247-59.

70.   Namjoshi, S.; Toth, I.; Blanchfield, J. T.; Trotter, N.; Mancera, R. L.; Benson, H. A., Enhanced Transdermal Peptide Delivery and Stability by Lipid Conjugation: Epidermal Permeation, Stereoselectivity and Mechanistic Insights. *Pharmaceutical research* **2014,** *31* (12), 3304-3312.

71.   Chen, Y.; Shen, Y.; Guo, X.; Zhang, C.; Yang, W.; Ma, M.; Liu, S.; Zhang, M.; Wen, L. P., Transdermal Protein Delivery by a Coadministered Peptide Identified via Phage Display. *Nat. Biotechnol.* **2006,** *24* (4), 455-60.

72.   Kumar, S.; Sahdev, P.; Perumal, O.; Tummala, H., Identification of a Novel Skin Penetration Enhancement Peptide by Phage Display Peptide Library Screening. *Molecular pharmaceutics* **2012,** *9* (5), 1320-30.

73.   Kumar, S.; Zakrewsky, M.; Chen, M.; Menegatti, S.; Muraski, J. A.; Mitragotri, S., Peptides as Skin Penetration Enhancers: Mechanisms of Action. *Journal of*

controlled release : official journal of the Controlled Release Society **2015,** *199*, 168-78.

74.   Menegatti, S.; Zakrewsky, M.; Kumar, S.; De Oliveira, J. S.; Muraski, J. A.; Mitragotri, S., De Novo Design of Skin-Penetrating Peptides for Enhanced Transdermal Delivery of Peptide Drugs. *Advanced healthcare materials* **2016,** *5* (5), 602-609.

75.   Gennari, C. G.; Franze, S.; Pellegrino, S.; Corsini, E.; Vistoli, G.; Montanari, L.; Minghetti, P.; Cilurzo, F., Skin Penetrating Peptide as a Tool to Enhance the Permeation of Heparin through Human Epidermis. *Biomacromolecules* **2016,** *17* (1), 46-55.

76.   Gautam, A.; Nanda, J. S.; Samuel, J. S.; Kumari, M.; Priyanka, P.; Bedi, G.; Nath, S. K.; Mittal, G.; Khatri, N.; Raghava, G. P., Topical Delivery of Protein and Peptide Using Novel Cell Penetrating Peptide IMT-P8. *Scientific reports* **2016,** *6*, 26278.

77.   Fülöp, F.; Martinek, T. A.; Toth, G. K., Application of Alicyclic Beta-Amino Acids in Peptide Chemistry. *Chemical Society reviews* **2006,** *35* (4), 323-334.

78.   Mandity, I. M.; Weber, E.; Martinek, T. A.; Olajos, G.; Toth, G. K.; Vass, E.; Fulop, F., Design of peptidic foldamer helices: a stereochemical patterning approach. *Angewandte Chemie* **2009,** *48* (12), 2171-2175.

79.   Sheldrick, G. M., SHELXT – Integrated Space-Group and Crystal-Structure Determination. *Acta Crystallogr. Sect. A: Found. Crystallogr.* **2015,** (A71), 3-8.

80.   Sheldrick, G. M., Crystal Structure Refinement with SHELXL. *Acta Crystallogr. Sect. C: Cryst. Struct. Commun.* **2015,** (C51), 3-8.

81.   Dolomanov, O. V.; Bourhis, L. J.; Gildea, R. J.; Howard, J. A. K.; Puschmann, H., OLEX2: a complete structure solution, refinement and analysis program. *J. Appl. Crystallogr.* **2009,** *42*, 339-341.

82. Boultif, A.; Louër, D., Powder Pattern Indexing with the Dichotomy Method. *J Appl Cryst* **2004,** *37*, 724-731.

83. David, W. I. F.; Shankland, K.; Streek, J.; Pidcock, E.; Motherwellb, W. D. S.; Cole, J. C., DASH: A Program for Crystal Structure Determination from Powder Diffraction Data. *J. Appl. Crystallogr.* **2006,** *39*, 910-915.

84. Kligman, A. M.; Christophers, E., Preparation of Isolated Sheets of Human Stratum Corneum. *Arch Derm* **1963,** *88*, 702.

85. Forró, E.; Fulöp, F., Advanced Procedure for the Enzymatic Ring Opening of Unsaturated Alicyclic β-Lactams. *Tetrahedron-Asymmetr* **2004,** *15* (18), 2875-2880.

86. Kiss, L. F., E.; Sillanpää, R. and Fülöp, F., Diastereo- and Enantioselective Synthesis of Orthogonally Protected 2,4-Diaminocyclopentanecarboxylates: A Flip from b-Amino- to b,γ-Diaminocarboxylates. *J. Org. Chem.* **2007,** *72* (23), 8786-8790.

87. Benedek, G.; Palkó, M.; Wéber, E.; Martinek, T. A.; Forró, E.; Fülöp, F., Efficient Synthesis of Hydroxy-Substituted Cispentacin Derivatives. *Eur. J. Org. Chem.* **2008,** (21), 3724-3730.

88. Malpass, J. R.; Tweddle, N. J., Reaction of Chlorosulphonyl Isocyanate with 1,3-Dienes. Control of 1,2-and 1,4-Addition Pathways and the Synthesis of Aza-and Oxa-bicyclic Systems. *J Chem Soc Perk T 1* **1976**, 874-884.

89. Griffiths, G. J.; Previdoli, F. E., Diels-Alder Reaction of Methanesulfonyl Cyanide with Cyclopentadiene. Industrial Synthesis of 2-Azabicyclo[2.2.1] hept-5-en-3-one. *J. Org. Chem.* **1993,** *58*, 6129-6131.

90. Boyle, G. A.; Edlin, C. D.; Li, Y.; Liotta, D. C.; Morgans, G. L.; Musonda, C. C., Enantioselective Synthesis of the Carbocyclic Nucleoside (-)-Abacavir. *Organic & biomolecular chemistry* **2012,** *10* (9), 1870-1876.

91.   Singh, R.; Vince, R., 2-Azabicyclo[2.2.1]hept-5-en-3-one: Chemical Profile of a Versatile Synthetic Building Block and its Impact on the Development of Therapeutics. *Chemical reviews* **2012,** *112*, 4642-4686.

92.   Durst, T.; O'Sullivan, M. J., Reduction of N-Chlorosulfonyl b-Lactams to Beta-Lactams with Sodium Sulfite. *J. Org. Chem.* **1970,** *35* (6), 2043-2044.

93.   Frau, J.; Coll, M.; Donoso, J.; Muñoz, F.; Vilanova, B.; Garcia-Blanco, F., Alkaline and Acidic Hydrolysis of the β-Lactam Ring. *Electron J Theor Ch* **1997,** *2*, 56-65.

94.   Coste, J.; LeNguyen, D.; Castro, B., PyBOP: A New Peptide Coupling Reagent Devoid of Toxic By-product. *Tetrahedron Lett.* **1990,** *31* (2), 205-208.

95.   VanRheenen, V.; Kelly, R. C.; Cha, D. Y., An Improved Catalytic OsO4 Oxidation of Olefins to E-1,2-Glycols using Tertiary Amine Oxides as the Oxidant. *Tetrahedron Lett.* **1976,** *23*, 1973-1976.

96.   Tao, J.; Kazlauskas, R., *Biocatalysis for Green Chemistry and Chemical Process Development*. John Wiley & Sons, INC., Publication: Hoboken, New Jersey, 2011.

97.   Clouthier, C. M.; Pelletier, J. N., Expanding the Organic Toolbox: a Guide to Integrating Biocatalysis in Synthesis. *Chemical Society reviews* **2012,** *41* (4), 1585-605.

98.   Davis, B. G.; Boyer, V., Biocatalysis and Enzymes in Organic Synthesis. *Nat. Prod. Rep.* **2001,** *18* (6), 618-640.

99.   Forró, E.; Fulöp, F., Lipase-Catalyzed Enantioselective Ring Opening of Unactivated Alicyclic-Fused b-Lactams in an Organic Solvent. *Org. Lett.* **2003,** *5* (8), 1209-1212.

100.   Li, C.; Tan, T.; Zhang, H.; Feng, W., Analysis of the Conformational Stability and Activity of Candida antarctica Lipase B in Organic Solvents. Insight from

Molecular Dinamycs and Quantum Mechanics/Simulations. *J. Biol. Chem.* **2010,** *285* (37), 28434-28441.

101.   Pinck, L. A.; Kelly, M. A., The Solubility of Urea in Water. *J. Am. Chem. Soc.* **1925,** *47* (8), 2170-2172.

102.   Rezus, Y. L. A.; Bakker, H. J., Effect of urea on the structural dynamics of water. *Proceedings of the National Academy of Sciences of the United States of America* **2006,** *103* (49), 18417-18420.

103.   Giuliano, M. W.; Maynard, S. J.; Almeida, A. M.; Reidenbach, A. G.; Guo, L.; Ulrich, E. C.; Guzei, I. A.; Gellman, S. H., Evaluation of a cyclopentane-based gamma-amino acid for the ability to promote alpha/gamma-peptide secondary structure. *J. Org. Chem.* **2013,** *78* (24), 12351-61.

104.   Kaul, R.; Brouillette, Y.; Sajjadi, Z.; Hansford, K. A.; Lubell, W. D., Selective tert-Butyl Ester Deprotection in the Presence of Acid Labile Protecting Groups with Use of ZnBr2. *J. Org. Chem.* **2004,** *69* (18), 6131–6133.

105.   Jenkins, D. J.; Riley, A. M.; Potter, B. V. L., Chiral Cyclopentane-Based Mimics of D-myo-Inositol 1,4,5-Trisphosphate from D-Glucose. *J. Org. Chem.* **1996,** *61* (22), 7719-7726.

106.   Brunauer, S.; Deming, L. S.; Deming, W. E.; Teller, E., On a Theory of the van der Waals Adsorption of Gases. *J. Am. Chem. Soc.* **1940,** *62* (7), 1723-1732.

107.   Aguirre-Álvarez , G.; Foster, T.; Hill, S. E., Modelling of Isotherms and their Hysteresis Analysis in Gelatin from Different Sources. *CyTA – Journal of Food* **2013,** *11* (1), 68-74.

108.   Canfield, P. J.; Blake, I. M.; Cai, Z.-L.; Luck, I. J.; Krausz, E.; Kobayashi, R.; Reimers, J. R.; Crossley, M. J., A New Fundamental Type of Conformational Isomerism. *Nature Chemistry* **2018,** *10*, 615-624.

109.   Debeer, S.; Le Luduec, J.; Kaiserlian, D.; Laurent, P.; Nicolas, J.; Dubois, B.; Kanitakis, J., Comparative Histology and Immunohistochemistry of Porcine Versus Human Skin. *Eur J Dermatol* **2013,** *23* (4), 456-466.

110.   Montagna, W., Comparative Anatomy and Physiology of the Skin. *Arch Derm* **1967,** *96*, 357-363.

111.   Montagna, W.; Yen, J. S., The Skin of the Domestic Pig. *The Journal of Investigative Dermatology* **1963**, 11-21.

112.   Wilson, H. L.; Obradovic, M. R., Evidence for a Common Mucosal Immune System in the Pig. *Molecular Immunology* **2015,** *66*, 22-34.

113.   Summerfield, A.; Meurens, F.; Ricklin, M. E., The Immunology of the Porcine Skin and its Value as a Model for Human Skin. *Molecular Immunology* **2015,** *66*, 14-21.

114.   Abd, E.; Yousef, S. A.; Pastore, M. N.; Telaprolu, K.; Mohammed, Y. H.; Namjoshi, S.; Grice, J. E.; Roberts, M. S., Skin Models for the Testing of Transdermal Drugs. *Clin Pharmacol* **2016,** *8*, 163-176.

115.   Shah, V.; Maibach, H. I.; Jenner, J., *Topical Drug Bioavailability, Bioequivajence and Penetration*. 2nd ed.; 2014.

116.   Satake, K.; Okuyama, T.; Ohashi, M.; Shinoda, T., The Spectrophotometric Determination of Amine, Amino Acid and Peptide with 2,4,6-Trinitrobenzene 1-Sulfonic Acid. *J. Biochem.* **1960,** *47* (5), 654-660.

117.   Snyder, S. L.; Sobocinski, P. Z., An Improved 2,4,6-Trinitrobenzenesulfonic Acid Method for the Determination of Amines. *Anal. Biochem.* **1975,** *64* (1), 284-288.

118.   Ali, S. M.; Yosipovitch, G., Skin pH: From Basic Science to Basic Skin Care. *Acta Derm Venereol* **2013,** *93* (3), 261-267.

119.   Obi, I. U., Application of the 2,4,6-Trinitrobenzene-l -Sulfonic Acid (TNBS) Method for Determination of Available Lysine in Maize Seed. *Agric Biol Chem* **1982,** *46*, 15-20.

120.   Cayot, P.; Tainturier, G., The Quantification of Protein Amino Groups by the Trinitrobenzenesulfonic Acid Method: A Reexamination. *Anal. Biochem.* **1997,** *249*, 184-200.

121.   Sarantonis, E. G.; Karayannis, M. I., Construction and Analytical Applications of Liquid Membrane Electrode for Trinitrobenzenesulfonic Acid (TNBS). *Anal. Biochem.* **1983,** *130* (1), 177-184.

122.   Grotzky, A.; Manaka, Y.; Fornera, S.; Willeke, M.; Walde, P., Quantification of a-Polylysine: a Comparison of four UV/Vis Spectrophotometric Methods. *Anal Methods* **2010,** *2*, 1448-1455.